Modelling, Experimental Validation and Evaluation of a Parallel Hybrid-Electric Propulsion System for Small-Scale UAVs

Jamal Wilson

December 20, 2024

B.Sc Engineering, University of Victoria, 2021
A Thesis Submitted in Partial Fulfillment of the Requirements for the Degree of

Master of Applied Science

in the Department of Mechanical Engineering

University of Victoria

Modelling, Experimental Validation and Evaluation of a Parallel Hybrid-Electric Propulsion System for Small-Scale UAVs

by

Jamal Wilson
B.Sc Engineering, University of Victoria, 2021

Supervisory Committee

Dr. Afzal Suleman, Supervisor
Department of Mechanical Engineering

Dr. Zuomin Dong, Departmental Member
Department of Mechanical Engineering

Dr. Pan Agathoklis, Outside Member
Department of Electrical Engineering

Abstract

The aviation industry is currently focused on research and development of propulsion systems that produce less emissions, are more efficient, and can provide better range/endurance. Hybrid-electric systems have shown promising potential in reducing emissions. Current battery technologies do not have the energy density required to meet most application requirements. While combustion technology has improved in efficiency over the decades; hybrid technology is required to take the next big step. In addition to the environmental benefits parallel hybrid technology provides other benefits such as operating mode variety, redundancy, and higher endurance.

In this thesis research, the primary goal is to model, evaluate and validate a mathematical model developed for a parallel hybrid-electric propulsion system. This model will be used in Model Based Design (MBD) to predict system performance, improve component selection, and optimize operation. For this thesis the modelling and design was completed for small-scale unmanned aerial vehicles (UAVs). A test bench was redesigned to handle the power produced by the combustion engine and electric motor (EM). For the experimental configuration a 50cc Corvid-50 combustion engine was used which produces 2.8kW at 7000RPM. This engine was combined with a SKP 6485 electric motor capable of 4.12kW continuously with a maximum speed of 8364RPM. Both power units are coupled together with a Mayr 500.301.0 type 4 electromagnetic clutch rated for 40Nm at 7000RPM. The propulsion system is connected to an electric dynamometer with programmable load capable of simulating any power profile. Telemetry for the system is collected through National Instruments hardware, electronic speed controller, and engine control unit.

During operation the test bench is able to operate in five different modes. Combustion and electric-only operation are capable by disabling the clutch for electric-only and running the electric motor at zero current for combustion. When running the system in a hybrid configuration there are three command modes: dual speed, throttle and speed, speed and current. Each of these command modes dictate which power unit governs speed while the other has direct torque control. Each of these hybrid modes provides the opportunity for regeneration and boost modes when requested. The test bench generates the experimental data required to model the propulsion system with accuracy. Using datasheets, unloaded runs, governing equations, and controller values component level models were created to complete initial simulations. The model and test iterative process repeated until the system level model responded well. To further develop the simulation model a virtual flight mission was created.

The test bench and Simulink model ran the virtual flight mission in combustion, electric, and hybrid modes. These different runs provided the data required to assess the model's accuracy and demonstrate the difference between each propulsion technology. For these tests the simulation was able to predict speed and torque within a range of 1-12% for steady-state operation between flight segments. The starting torque of the electric motor to initiate combustion was modelled to represent cold starts where the torque range was between 2-3Nm. Over the length of the fifteen-minute flight mission run the simulation predicted battery charge and fuel consumption within 5%. Energy density of each propulsion type was analyzed for the components used on the test bench. This showed that combustion power has the highest available energy density at 1.17MJ/kg; electric power is substantially lower at 0.35MJ/kg. The initial energy density of the hybrid system is 0.71MJ/kg but can be further optimized. By optimizing the energy masses for the hybrid-electric system an energy density equal to the combustion engine was accomplished with a 0.77kg mass

reduction. This optimization process can be taken further by improving the command sequence of the system to incorporate regeneration, clutch disengagement, and throttle curve modification to reduce fuel flow.

The results of this research project created a simulation model and test bench capable of high-power flight tests. Both the model and test bench will continue to develop; further increasing the ability to design, optimize, and test parallel hybrid systems. This will provide the experience and knowledge to design, build, and integrate a power unit ready for flight testing.

Table of Contents

List of Figures

List of Tables

Acknowledgments

I would like to express my gratitude to the Center for Aerospace Research (CfAR) for both funding this project and providing the facilities necessary for its development. Their support has been critical in enabling me to pursue and complete this research, and I am grateful for the resources they made available to me.

This achievement would no be possible without Dr.Suleman, whose trust and support over the past eight years have been invaluable. The opportunities he has provided me have been fundamental to my growth as a student and aspiring engineer. He has always provided an open door for me and made my professional development a great experience. His insights and encouragement have been key to helping me navigate the challenges of my studies and career.

I also wish to thank Jay Matlock for his expert guidance during my master's program, especially in relation to the parallel hybrid project. His support and confidence in my ability to manage the project allowed me to explore new ideas and take ownership of the work. I am grateful for the autonomy he allowed me and the constructive feedback throughout the process.

Thank you to my girlfriend for making life outside of my studies much easier during this busy time. She made the long hours much more bearable. I appreciate the support you provided without hesitation. To my dad, I give you all the credit for teaching me to problem solve, think independently, and work hard since I was a young boy. To my mom, I appreciate you encouraging me to take breaks and prioritize my health while working endless hours.

Glossary

AC Alternating Current, an electric current that reverses direction periodically.

BLDC Brushless Direct Current, a type of electric motor that operates without brushes.

BSFC Brake Specific Fuel Consumption, a measure of the fuel efficiency of an engine.

CAN Controller Area Network, a robust vehicle bus standard for connecting microcontrollers and devices.

CHT Cylinder Head Temperature, an important parameter in engine management.

CI Compression Ignition, a type of internal combustion engine that uses compression to ignite the fuel.

CNC Computer Numerical Control, a method for automating machine tools via computer programming.

CSV Comma-Separated Values, a file format used for data storage.

CVT Continuously Variable Transmission, a type of automatic transmission that can change seamlessly through a range of gear ratios.

DC Direct Current, an electric current that flows in one direction steadily.

DCT Dual-Clutch Transmission, a type of transmission that uses two separate clutches for odd and even gear shifts.

Direct-Axis The axis aligned with the magnetic field in synchronous machines.

Dynamometer An instrument used to measure force, torque, or power.

ECU Electronic Control Unit, a device that controls one or more electrical systems in a vehicle.

EFI Electronic Fuel Injection, a system that delivers fuel to the engine in a controlled manner.

EM Electric Motor, a device that converts electrical energy into mechanical energy.

EMF Electromotive Force, the electric potential generated by a battery or generator.

Energy Density The amount of energy stored in a given system per unit mass.

ESC Electronic Speed Controller, a device used to control the speed of an electric motor.

FOC Field-Oriented Control, a method for controlling motors.

GPID General Purpose Interface Bus, a short range digital protocol for communication.

GUI Graphical User Interface, a visual way of interacting with a computer or electronic device.

Hall Effect Sensor A sensor that detects the presence of a magnetic field and converts it into an electrical signal.

Hybrid-Electric A vehicle that combines an internal combustion engine with an electric propulsion system.

ICE Internal Combustion Engine, a type of engine that generates power through the combustion of fuel.

IDE Integrated Development Environment, software that provides comprehensive facilities to programmers.

Inertia The resistance of any physical object to the change in its velocity.

LiPo Lithium Polymer battery, a type of rechargeable battery commonly used in UAVs and other devices.

Load Cell A transducer that converts a force into an electrical signal.

MAP Manifold Absolute Pressure, a sensor that measures the pressure within the intake manifold.

Map A representation of data points in a defined space, often used in performance tuning.

MAT Manifold Air Temperature, temperature of the air in a combustion engines intake manifold.

MBD Model Based Design, the use of complex models throughout the design process to reduce development time.

MCU Microcontroller Unit, a compact integrated circuit designed to govern a specific operation in an embedded system.

MGU Motor Generator Unit, a component used in hybrid and electric vehicles to convert energy.

MGU-H Motor Generator Unit Heat, used to convert heat energy into electrical energy in hybrid systems.

MGU-K Motor Generator Unit Kinetic, used to recover energy during braking in hybrid systems.

MOSFET Metal-Oxide-Semiconductor Field-Effect Transistor, used for switching and amplifying electronic signals.

OAT Outside Air Temperature, the ambient temperature outside a vehicle.

PHTB Parallel Hybrid Test Bench.

PID Proportional-Integral-Derivative controller, a control loop feedback mechanism widely used in industrial control systems.

PMSM Permanent Magnet Synchronous Motor, an electric motor that uses permanent magnets for its operation.

PWM Pulse Width Modulation, a technique used to control the power delivered to electrical devices.

Quadrature-Axis The axis perpendicular to the direct axis in synchronous machines.

RMS Root Mean Square, a statistical measure used to relate AC power to DC equivalent.

RS232 A standard for serial communication transmission of data.

S-rating A measure of the discharge rating of LiPo batteries, indicating their ability to deliver current.

SCPI Standard Commands for Programmable Instruments, a standard for communication with test and measurement devices.

Serial A method of data transmission in which data is sent sequentially over a communication channel.

SI Spark Ignition, a type of internal combustion engine that uses a spark plug to ignite the fuel-air mixture.

SOC State of Charge, a measurement of the current charge level of a battery.

Static Friction The force that resists the start of sliding motion between two surfaces in contact.

Telemetry The process of recording and transmitting the readings of an instrument.

Thermal Efficiency A measure of the efficiency of a heat engine, defined as the ratio of useful work output to heat input.

TPS Throttle Position Sensor, a sensor that monitors the position of the throttle valve.

UART Universal Asynchronous Receiver-Transmitter, a hardware communication protocol.

UAS Unmanned Aerial System, encompasses the UAV and the ground control system.

UAV Unmanned Aerial Vehicle, commonly referred to as a drone.

VESC Vedder Electronic Speed Controller, an open-source speed controller for brushless motors.

Viscous Damping A force that opposes the motion of an object through proportional to its velocity.

1 Introduction

1.1 Motivation

Hybrid-electric powertrains have existed since the late nineteenth century with the first hybrid car built by Ferdinand Porsche in 1900 [1]. The vehicle used a combustion engine to extend the range via a generator, making it a series hybrid system. With the increased focus to reduce emissions hybrid vehicles have become more popular. For example, Toyota offers nineteen hybrid models in North America, accounting for 44.3% of all sales in February 2024 [2]. Additionally, Formula 1 has been hybrid powered since 2014 [3] and is considered the pinnacle of motorsport. The automotive industry has embraced the hybrid-electric powertrain, benefiting from higher efficiency, lower emissions, and more power. The aerospace sector on the other hand does not have a single hybrid-electric aircraft commercially available for purchase, with U.S National Renewable Energy Lab not expecting aircraft until after 2030 [4].

This thesis research aims to further the understanding of parallel hybrid-electric propulsion systems. In general, aerospace technology is studied and tested at a small-scale for proof of concept before further development. The propulsion system covered here is designed for Unmanned Aerial Vehicles (UAVs) with a power requirement of under seven kilowatts.

Hybrid-electric propulsion systems have many benefits over conventional configurations including reduced emissions, longer endurance, and higher redundancy. Many aerospace sectors could apply hybrid technology to improve their diversity and capabilities. The UAV sector is currently valued at $31.70 billion and expected to reach $92.13 billion by 2030 [5]. This provides ample opportunity for hybrid-electric testing on small-scale aircraft to verify the propulsion systems before full-scale research. UAVs are used in multiple sectors such as agriculture, military, commercial, and recreational. The introduction of hybrid-electric propulsion into these sectors could provide consumers with their delivery packages faster, farmers with better yields, reduced risk for infantry, and unique perspectives for videography, photography, and surveying.

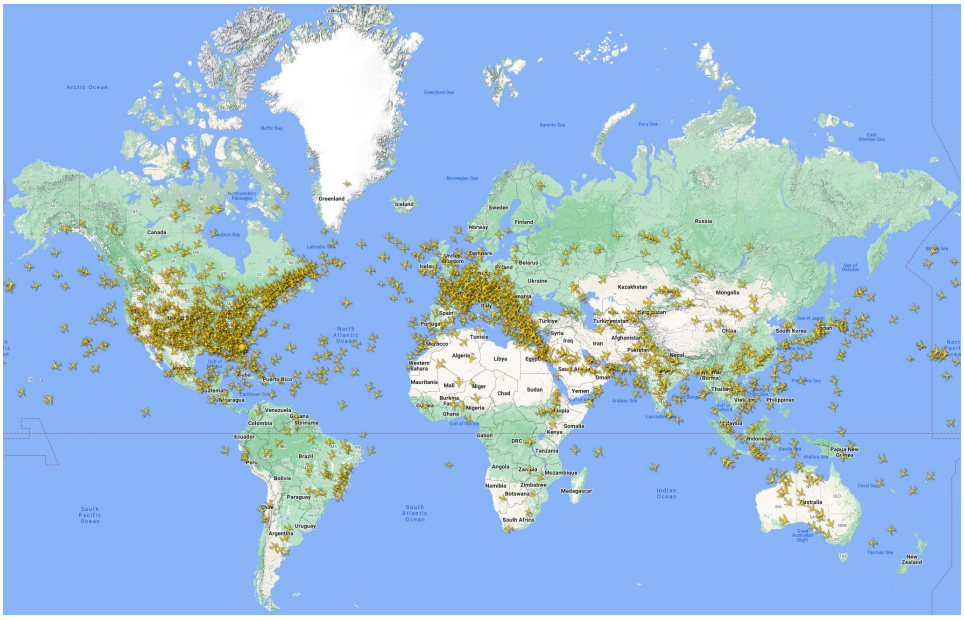

Figure 1: Global flight traffic averaging 250,000 flights per day [6]

The UAV sector is a steppingstone in developing more efficient and climate friendly full-size aircraft. Aviation contributes 2% of CO_2 emissions globally while the industry is responsible for 4% of global warming contributions by humans [7]. From 1990 to 2019 passenger demand has increased 337.73% [7]. Fortunately, aviation has become increasingly more efficient reducing the energy required to fly one passenger-kilometer by 1.6 megajoules since 1990 [7]. This has been achieved by using lighter materials, more efficient engines, and better aerodynamics. The next step in improving flight emission aside from electrification is the development of Sustainable Aviation Fuels (SAFs), which aims to help the sector meet its net-zero CO_2 emissions by 2050 [8]. SAFs are derived synthetically or from waste such as cooking oils, agricultural residue, or landfill trash. They can also be made from biological sources such as corn, palm trees, or switch grass. These sources are refined into a carbon-rich fuel which is the primary part of jet fuel. Not all SAFs are the same and many of them reduce CO_2 emissions by 70-80% [8]. Combining research in sustainable fuels and hybridization could provide a large shift in aviation technology that pushes it into a modern era of propulsion.

1.2 Problem

The benefits of hybrid-electric systems are well known in the industry. These systems provide reduced emissions by supplementing power with electrification. Hybrid power also extends the range and endurance of an aircraft by charging onboard batteries with a generator. High demand segments of a mission profile such as take-off can be done with pure electric power, saving fuel for more power efficient segments like cruise.

However, modelling of parallel hybrid-electric propulsion systems has not been investigated in enough depth compared to hybridized aircraft performance. Hybrid research often compares the new system to conventional combustion power demonstrating the well-known benefits of the technology. To understand the propulsion system more completely mathematical models, simulation, and experimental testing must be conducted. The research discussed in this paper does exactly that by using a dual shaft hybrid-electric propulsion system designed for small UAV platforms. The work completed creates a strong baseline for understanding system response, mode switching, limitations, and performance. These aspects are studied in theoretical models and experimental testing in which they serve as validation for each other. With this research further hybrid-electric development can continue with a stronger prediction of system response and component requirements.

1.3 Current Technology

As stated previously, hybrid-electric systems were first developed by Porsche in 1899 and shown to the public in 1900 [1]. Since then, the technology has grown and matured with the first successful mass-produced hybrid being the Toyota Prius in 1999 [9]. The Prius continues to be a popular hybrid choice for consumers; however, many manufacturers now offer hybrid vehicles in their lineup. This movement has been fueled by the need for greener, more fuel-efficient vehicles. These modern hybrid systems now offer plug-in charging and longer electric-only ranges because of the rapidly growing all-electric sector.

The aviation sector has not put significant resources into all-electric or hybrid propulsion until recently. The new technology has proven difficult to implement, manufacturer Lilium recently announced it is facing bankruptcy after spending $1 billion on developing an eVTOL aircraft for

urban applications [10]. Currently there are no publicly available full size all-electric or hybrid aircraft, with experts not expecting any until 2030 at the earliest [4]. With these predictions it appears that the industry is focusing on all-electric systems despite its shortcoming in range and weight, both of which are remedied with hybrid technologies.

1.3.1 Automotive

Parallel hybrid technology has been used in automotive applications for years and can now be considered in its mature phase. Thanks to the increase in all-electric vehicle development the electric technology of hybrid systems has greatly improved in the last ten years. Most hybrid vehicles are parallel because the flexibility of such a system allows the vehicle to operate in either electric, combustion, or hybrid mode.

Toyota currently has one of the most diverse hybrid lineups in the automotive sector with their hybrid technology being used in hatchbacks, sedans, and SUVs. This enables the cars to run in electric-only modes for low speeds and in traffic, while the combustion engine allows the vehicle to drive long distances without worrying about electric charge while also having regenerative braking. These systems have the ability to run in hybrid mode where the electric power and combustion power is combined, this can increase acceleration thanks to the electric motor providing instant torque. When electric motors and combustion engines are on separate axles the car is capable of all-wheel drive and better traction thanks to electric traction control. Hybrid vehicles are currently one of the best options for a greener solution to fossil fuels without the challenges of all-electric technologies.

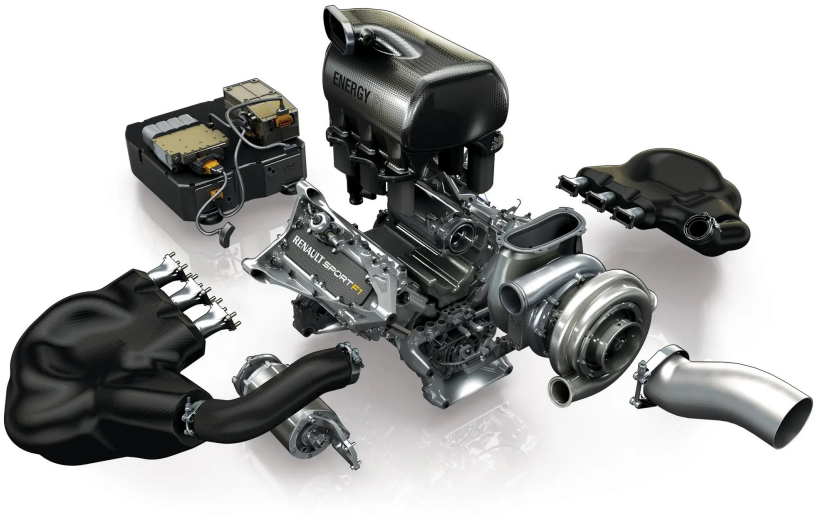

Figure 2: Formula 1 powertrain showing major components [11]

However, the most advanced hybrid-electric technology in automotive isn't from Toyota, it is in Formula 1. The FIA introduced in 2014 that the motorsport would be hybrid powered, using 1.6 liter 90 degree V6s that produce 850 horsepower (1000 horsepower with electric boost) [3]. The hybrid technology includes two Motor Generator Units (MGUs), one that harnesses kinetic energy (MGU-K) and the other thermal energy (MGU-H). The kinetic generator harnesses energy from the crankshaft under braking and can also add power to the crankshaft when requested,

allowing the driver to add 120kW of power at the press of a button. The thermal generator unit collects energy from the exhaust by being attached to the turbocharger, between the compressor and turbine. Since it is directly connected to the turbocharger it can also spin the turbocharger when required, eliminating turbo lag. Both the MGU-H and MHU-K charge the onboard battery that is located behind the driver under the fuel tank to lower the center of gravity. On top of the hybrid system Formula 1 engines have reached over 50% thermal efficiency, whereas road cars are between 20-40% [12]. With the advances in this thermal efficiency and the introduction of hybrid technology the current generation of F1 car has 20% more power and produce 26% less CO_2 emissions compared to the previous generation [3].

The development of automotive hybrid technology has been prevalent for over a decade and now benefits the environment, consumers, and motorsport in many ways. This technology is transferable into the aviation sector; unfortunately, it seems that its implementation is far from a reality for commercial uses and is just now being developed at a smaller scale.

1.3.2 Aerospace

Looking at UAV applications there are currently a few hybrid propulsion systems on the market for series hybrid. The systems use a combustion engine to extend range with a generator permanently coupled to the internal combustion engine (ICE). Looking at some of the current hybrid propulsion systems shows a gap in the market for parallel technology and its benefits.

Currawong is an engineering firm based in Australia that delivers a strong catalogue of high-end components for small-scale UAVs. They currently provide the Cortex-50 series hybrid engine which is a 50 cubic centimeter engine paired to a T-Motor U13II motor-generator. This unit is capable of 2.1kW of power at 7500RPM while weighing 4.7kg. The hybridization of the DA-50 core increased the fuel efficiency, range, endurance, and reduced battery requirements [13]. The typical configuration for this technology is using the combustion engine to recharge the battery, essentially making it a gasoline generator. This power unit can also send electrical power directly to the motors via the transmuter. The Cortex-50 is instrumented with numerous sensors that allow for precise data collection of the electronic fuel injection (EFI), generator, and electric systems. The software and instrumentation from Currawong make it a unique company in the sector compared to other small-scale UAV systems.

Figure 3: Currawong Cortex series hybrid power unit [13]

Pegasus Aeronautics also provides series hybrid units for small-scale UAVs both a 35cc and 70cc variant [14]. Their systems are a simple generator unit mounted to the crankshaft of the combustion engine. This allows for engine starting and generation making it a simple range extending unit, not a fully instrumented unit like the Cortex. The GE35 is capable of 2kW from a 35cc engine weighing 2.6kg, excluding required electronics. The Pegasus package does not provide as much telemetry nor a transmuter making it a less complete package.

Löweheiser is a company in Spain that provides EFI systems for small-scale UAVs and recently provides a hybrid generator [15]. This package is a unit between the Currawong and Pegasus in terms of features, it has enough instrumentation to monitor the EFI and generator system and includes the required electronics to get it running. This unit is capable of 2.4kW from a 32cc engine with no information on the fuel consumption of the ICE. This is a system that provides less data collection and system monitoring than the Currawong unit but has not been on the market long enough to have the same reputation.

There are many other products on the market for series hybrid generator systems, all of which operate in the same manner as the ones discussed above. Parallel hybrid UAV systems are far more difficult to find and in a much earlier stage of development.

Parallel Flight Technologies is currently developing an unmanned aircraft system (UAS) in a unique configuration that is not the conventional series or parallel configuration. This vehicle uses four separate combustion engines with propeller and ducted fan combination. This system is described as fully redundant and their own proprietary system [16]. This project is still in development and no details are provided on how the system operates making it difficult to classify.

Figure 4: Parallel Flight Technologies UAS power unit located in each boom [16]

Research projects exist for parallel hybrid UAV systems at various universities in the US, Australia, and other countries [17][18]. Government agencies are also running their own programs to further progress in the sector. However, as it exists right now there are no readily available parallel hybrid power units for UAVs.

Current full-scale aircraft projects are in the process of testing and developing platforms for all-electric and hybrid systems. Ampaire is leading the charge with their EEL demonstrator aircraft based on a Cessna 208B Grand Caravan [19]. This platform has the lowest emissions in its class with fuel savings between 50-70% depending on the flight plan [20]. The EEL has completed over 27,000 miles and has set the hybrid record for longest non-stop flight at 1135 nautical miles and longest endurance at 12 hours with two hours of fuel remaining [20].

In Canada there has been work done by the National Research Council (NRC) and Pratt & Whitney to push the agenda for hybrid propulsion. NRC successfully completed test flights on its Cessna 337 Skymaster platform which replaced the 400 pound pusher engine with an 88 pound parallel hybrid-electric motor [21]. NRC has also partner with Pratt & Whitney to develop a hybrid-electric version of the De Havilland Dash 8-100 which will be used for regional flights [21]. Commercial airliner Air Canada has agreed to buy a small fleet of hybrid-electric aircraft from Swedish company Heart Aerospace which expect to deliver said aircraft in 2028 [22].

Figure 5: NRC HEAT test aircraft in flight in 2022 [23]

Various manufactures have been working on hybrid aircraft and propulsion systems for a lower emissions future. General Electric (GE) produces many aircraft engines and power many popular commercial jets [24]. NASA has partnered with GE to help develop and test a new hybrid-electric propulsion system. GE tested its megawatt class hybrid propulsion system at NASAs Neil A.Armstrong Flight Research Center which has the capability of simulating high altitude tests, marking a big milestone for the GE hybrid project [25]. Other initiatives are being led by Airbus which has been pushing for decarbonization for numerous years and currently run development programs for hybrid-electric, fuel cell, and all-electric aircraft [26]. Airbus' EcoPulse, based on a Daher TBM 900, completed its first flight on November 29 2023 [27]. This flight was a short 100-minute mission to test the high voltage battery, flight computer, electric propulsion, and hybrid-electric turbogenerator.

1.4 Research and Academia

Hybrid-electric propulsion is an increasingly popular topic in research and academia because of the developing requirements for more ecological modes of transportation. Numerous papers have completed studies on energy systems, aircraft performance, airframe design, operation strategies, and feasibility for hybrid-electric technology.

Energy system studies aim to select and optimize fuel/battery parameters to improve the ecological performance of hybrid systems to meet specific goals. A research group at the University of

Warsaw developed a case study comparing various hybrid technologies with the goal to reduce pollutants to meet the objective goal of the European Green Deal [28]. The research conducted compares turboelectric, full-electric, solar, hybrid-hydrogen, and hybrid-electric aircraft. For these systems energy management is a critical design aspect that can improve the performance of these hybrid aircraft. Leite and Voskuiji's paper on energy management demonstrates an approach in determining when to use combustion power versus stored electric energy [29]. For this research the authors used dynamic programming and a specific aircraft model to optimize energy management control. A more specific study on energy management for plug-in hybrid electric vehicles by Martinez et.al [30] outlines the currently available optimization algorithms. This case study demonstrates the benefits and shortcomings of each algorithm without a clear best method. Combining this case study with research from Lei [31] and Xie [32] shows an agreement on the topic in which there is no best method. A more complex paper by Tyler Wall shows a control method that aims to optimize switching and operation of two common operating modes: battery discharging and battery charging [33]. All groups show that the energy management optimization problem is case dependent and must be thoroughly tested for the application.

A group from the Universidade de Lisboa conducted a research paper on the ecological outcomes of all-electric and hybrid aircraft [34]. This paper used a multi-disciplinary approach to reducing the environmental footprint of aircraft. The researchers assessed the environmental impact of production, future battery technology, material selection, propulsion system emissions, and life-cycle analysis. This research provides insights into the lesser assessed effects that aviation has on the environment and can be used to further improve cleaner flight. Building on this theme a recent study by Thonemann et.al in the Journal of Cleaner Production attempted to determine the life cycle inventory of future hybrid-electric aircraft [35]. Using primary sources, industry expertise, and scientific literature the team developed inventory datasets for the years spanning 2030, 2040, and 2050. The aircraft footprint study was based on 200-600 nautical mile missions for 50 passenger aircraft. It was found that there was a high level of uncertainty in the predicted life cycle environmental impact but the life cycle assessment should continue to develop as end-of-life information becomes available.

Conceptual design research is a heavily populated topic in hybrid propulsion. These projects create theoretical aircraft designs to demonstrate the validity of hybrid propulsion for various applications. A group from Germany published a paper studying the performance of a narrow-body transport aircraft with dual turbofans and electric fans mounted under the wing [36]. This research looked into the effects of aircraft performance with the increase in useful power. It was concluded that this configuration was best suited for short-range/regional flights. This area of research also includes sizing exercises to determine an aircraft design for specific mission profiles. A paper by Trainelli et.al provides a guide into sizing a propeller-driven, fixed-wing hybrid electric aircraft [37]. This research creates an iterative process that provides a design envelope for a specific set of requirements for aircraft and mission profile. Two papers on aircraft sizing by Riboldi describe a more complex procedure that uses historical data and sizing-matrix plots [38][39]. These papers combine conventional historical ICE data and sizing-matrices to create a procedure for sizing hybrid-electric aircraft. There are different methods to aircraft sizing for hybrid propulsion that follow the same conceptual principles. A group of researchers from Germany and Australia provide a detailed report on sizing an aircraft for minimal installed power and optimal degree of hybridization [40]. This paper uses conventional power-to-weight ratio and wing-loading to determine the design envelope, but adds a degree of hybridization optimization requirement to

further constrain the sizing exercise. The outcome of this paper demonstrates that conventional sizing methods are not appropriate for hybrid aircraft and that there is not a singular favored method [41]. Using their proposed sizing method Finger et.al were able to increase wing and power loading to improve cruise performance without effecting take-off performance.

There are many theoretical papers on the operation and optimization of hybrid aircraft. For example, a paper by Reynard et.al derive a range equation for hybrid-electric aircraft using the equations for combustion aircraft [42]. This study showed that the range prediction for the hybrid aircraft can be determined using a power split ratio between the two power units. This derived equation can predict range with relatively little knowledge of the aircraft configuration. Another group from the University of Malta performed the same exercise to derive an endurance equation [43]. This equation uses a power split in the same manner as Reynard et.al to determine the endurance of a hybrid-electric aircraft. There are numerous papers on exercises such as these that approach hybrid design as mathematical problem that can be derived from conventional methods. One paper demonstrates that using conventional design methods is not the ideal path for hybrid electric propulsion. A research team from the University of Salento developed a synergy model for hybrid aircraft [44]. The authors created relationships between the power system, mission, architecture, energy management, and other subsystems in the aircraft. They used this model to demonstrate that designing the propulsion system and aircraft together improved payload weight and increased cruise time compared to separately designed systems. This paper showed that retrofitting existing aircraft or modifying models developed for non-hybrid aircraft was suboptimal.

A paper published by the American Institute of Aeronautics and Astronautics studied which aircraft configurations benefit from parallel hybrid-electric power [45]. This paper by Finger et.al further substantiates the claims by Donateo showing that conventional aircraft are unlikely to benefit from the technology. It was shown that short-range, high-power aircraft with fluctuating power requirements are best suited for hybrid technology. Conventional aircraft with constant power flight missions do not benefit from the addition of electric power and converge to a combustion solution. With these findings the authors suggest that hybrid technology should be used in vertical take-off and landing (VTOL) applications where the performance benefits are substantial. Using a hybrid-electric power plant for a VTOL air taxi concept showed a reduction of more than 30% in MTOM and up to 65% in energy consumption when the hybridization was greater than 70%.

In the space of UAVs there is less research on hybrid-electric aircraft. The sizing exercises and energy management papers favor full-scale aircraft because of the availability of historical data, larger commercialization opportunities, and motivation to reduce emissions for commercial flight. Looking into the UAV and small-aircraft space there are a few papers that execute similar research to that discussed in this thesis.

A research project from Glassock et.al developed a parallel small-scale hybrid propulsion system with the intention to model and measure its performance [18]. The experimental setup for the project used a Mutunic 10cc engine, Plettenberg 220 electric motor, and a 20"x6" propeller (Figure 6). The research found that the electric motor power improves the climb rate of the aircraft, but the project was still in its early stages.

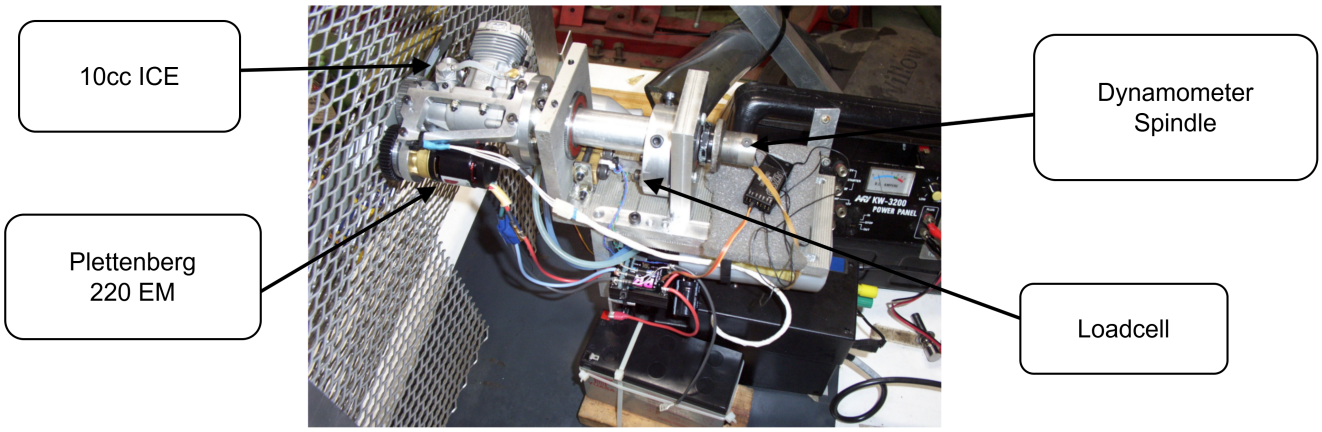

Figure 6: Experimental UAS created by Glassock et.al [18]

A more extensive study on the integration, testing, and validation of small-scale hybrid-electric UAVs comes from the Air Force Institute of Technology in Ohio [46]. Joseph Ausserer's research outlines component selection, control method, integration, experimental testing, and validation for a test bench which uses a Honda GX25 engine capable of 750W at 7000RPM and produces 1Nm of torque at 5000RPM. This combustion engine is coupled to an AXI 4130/20 which produces 1.75kW with a maximum speed of 16000RPM. This system was integrated into an airframe and flight ready at the end of the project. They were able to operate the propulsion system in electric, combustion, dual, and regeneration modes. This system claimed to be the first functional parallel hybrid prototype at the time. Another Air Force project using the same system underwent similar testing but successfully completed flight testing which demonstrated that the hybrid powerplant could run in every mode including dual and regenerative mode during flight [17]. This research provides a strong demonstration on how to design, integrate, and test a hybrid-electric system while also improving understanding of the underlying mechanics that govern hybrid operation.

A project at Queensland University of Technology is very similar in scale to the Air Force, with an OS fx-61 engine which produces 1.4kW of power at 16000RPM combined with a Plettenberg 220 BLDC with a maximum power of 1.5kW [18]. This research provides details on individual component testing, how to create a dynamometer for full system tests, and insight into power-plant efficiencies. Unlike the previous project this group decided to model and compare the bench test results to the predicted values from simulation. These simulations look at different propeller selection, fuel fractions, mission profiles, and optimization power demands. The research provides more detail on the dynamics of the simulated aircraft and how the propulsion systems specifications are affected by the requirements of the airframe and mission profile.

A theoretically heavy research project by Joachim Schoemann and Mirko Hornung developed a procedure that creates a theoretically accurate, computationally light model for small-scale hybrid propulsion systems [47]. This process included developing theoretical models of each component and mapping important parameters to determine operating ranges. This paper provides insights into the benefits of hybrid-electric propulsion systems compared to conventional configurations. This research provides good references to nominal values and parameters for common component configurations in the small-scale range.

Looking at the small-scale UAV landscape shows that there are not any commercially available options, however a collaborative group of researchers completed an extensive survey [48]. The

survey looks into both VTOL and fixed-wing UAVs that are currently in development, used for research, and will potentially be available to the public once fully developed. They found that many of the projects were canceled because of control algorithm development challenges and/or airframe controllability problems. One issue that was persistent through all the projects was the simplified models used to develop the aircraft and control design. These simplified models were not accurate enough for real-world testing and were often the cause for failure. Additionally, system identification was rarely used for these small-scale applications, which reduced the accuracy and fidelity of the dynamic models. The lack of validation for the UAVs was universal across all the explored projects, with all groups following the same process. The authors express that all these projects lack real-world validation, complex controller methods, and do not have extensive testing to determine the robustness of the systems.

A more unique research project from the Politecnico di Torino aimed to approach the problem of hybrid-electric propulsion from a purely virtual approach [49]. The authors developed a virtual test bench for UAVs using Matlab/Simulink by deriving and implementing the mathematical models of the various components. This paper shows the process of developing the models and the tools required to test via simulation. The models created are from a pure theoretical standpoint using the methods learned in mechanics, controls, and electronic textbooks. Despite the theoretical approach to the problem the paper outlines how the system works fundamentally and provides simulations results that can guide experimental applications.

At the University of Victoria Center for Aerospace Research (CfAR) hybrid research has caught traction since its inception in 2016. The program began with a simple parallel setup involving an AXI 4130/20 1.65kW electric motor coupled via a one way bearing to a 2.34kW DA-35 combustion engine [50]. This setup allowed for the collection of data in electric, combustion, regeneration, and boost mode, demonstrating the validity of the system. This first revision had many operational shortcomings which included: lack of flexibility with the one-way bearing, poor gearing, and limited data collection.

In 2019 a student group took over the development of the platform to further its capabilities. This group changed the platform to a modular post and plate design which allowed for the components in the system to be swapped more easily. An electromagnetic clutch was added to the system with a nominal rating of 5Nm. A second electric motor replaced the combustion engine for easier control and testing to validate the new design.

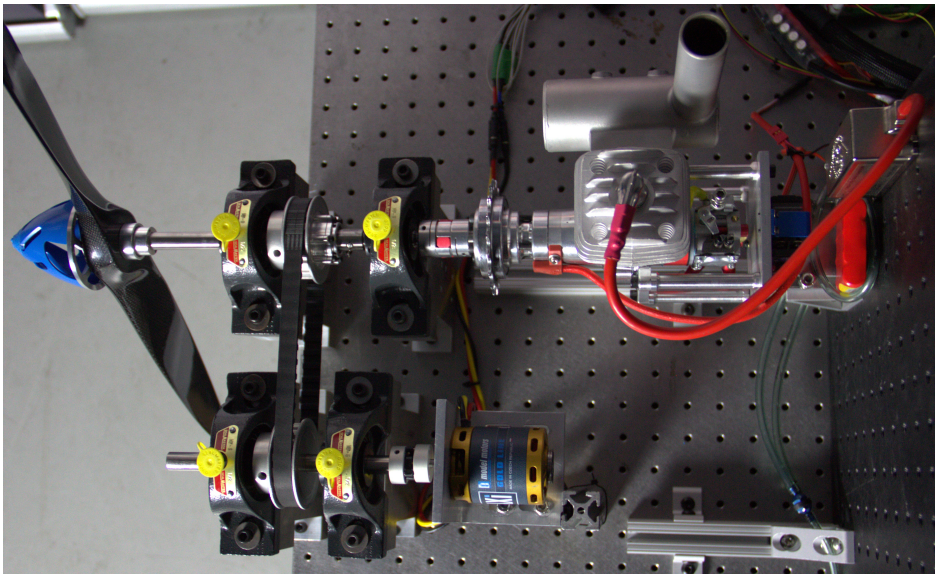

Figure 7: CfAR 2016 test bench configuration

The next large upgrade for the platform was to remove the propeller from the system, allowing for more diverse and controllable loading of the system. In 2021 another student group developed a dynamometer system for the test bench. This system uses a T-Motor U15II KV100 which is capable of 17.8Nm, this acts as an electromagnetic brake on the system. The case of the motor is connected to a pair of load cells which provide the torque moment that occurs around the axis of rotation. The torque reading of the load cells were coupled with a hall effect sensor for speed sensing which provides the mechanical power of the output shaft. Unfortunately, with the addition of the dynamometer the system can be sufficiently loaded to cause the clutch, belts, and pulleys to slip, creating a need for further upgrades. Since then, the test bench has been developed for better torque capability, better data acquisition, and more diverse mission profiles. Many of the upgrades on this test bench are part of the research in this paper and will be discussed in later sections.

1.5 Methodology

The research outlined in this paper studies the fundamentals of parallel hybrid-electric propulsion systems for small-scale UAVs from two directions: experimental and theoretical. Understanding the propulsion system from both perspectives provides a well-rounded definition of what is required for specific systems to operate both transiently and in steady-state. The goal of this research is to provide a method in predicting the behavior of a physical system before it is developed. This in turn can lower cost of development, reduce trial and error, increase design accuracy, and provide an overall better propulsion system.

The theoretical aspect of the project entails three key aspects: modelling, simulation, and validation. Using Matlab/Simulink the various components of the system will be modelled mathematically using methods learned in literature and with models created by Mathworks. This aspect of the project requires a keen understanding of how the hybrid system works, specifically power flow and how physical parameters affect the operation of the system. In order to understand if the modelling is correct simulations must be executed to visualize the system response. This will

require definition of the system inputs and boundary conditions. Once simulation results yield responses that appear plausible, they must be verified via testing.

The experimental side of the research entails the design, integration, and testing of a parallel hybrid test bench (PHTB). This system is a physical representation of the models created in Matlab/Simulink, with every component characterized in as much detail as possible to reduce the number of unknowns in the system. This test bench will be used to verify the results of the simulations and to find/derive certain parameters of the models that are difficult to calculate. Using the same inputs and boundary conditions as in the simulations, data will be collected from the experimental setup allowing for a strong understanding of the system response. An iterative process will occur where data and simulation will be compared, either outlining an error in understanding, modelling, or instrumentation. As the project progresses both the experimental and theoretical components will evolve and become more accurate. The results of this process provide a theoretical model and experimental test bench that can improve the development of current and future hybrid projects.

1.6 Objectives

The overarching objective of this thesis is to better understand how the hybrid-electric propulsion system at UVic CfAR works. This research will provide metrics representing the benefits of hybrid-electric propulsion that are well documented in industry and literature. More importantly, this project hopes to uncover knowledge of how the system operates from three perspectives: electrical, mechanical, and software. These domains dictate the system response of the test bench and require proper understanding in order to model the propulsion system correctly. The knowledge gained from this research can then be used to develop a wide range of hybrid systems that are efficient, powerful, and ready for small-scale UAV integration.

Objective 1: How is a small-scale parallel hybrid-electric test bench designed and what challenges are encountered? The hybrid test bench is not only a proof-of-concept platform but also a knowledge verification tool. This system allows for the testing of operational hypothesis, as well as basic mission profile runs to better understand how hybrid propulsion operates with physical visualization. This goal will provide a general guideline in how to approach designing a test bench, hopefully inspiring other institutions to build their own. Importantly, the key challenges and delays in the development process will be disclosed to improve success for projects and improve results for other researchers.

Objective 2: How does a small-scale dual shaft parallel hybrid-electric propulsion system operate and what limitations are there? Deriving equations provides a fundamental theoretical understanding of how hybrid-electric systems work, but real-world implementation requires a deeper knowledge of multiple disciplines. The objective explains the operation of the test bench at CfAR with a deeper explanation. This will provide the details required to select components, operate power systems, and collect data. Component selection is important in delivering the required power and system dynamics for a given airframe and/or mission. Yet, the components of the system must also fall within an operational range where power transmission is feasible at this scale. Power management systems allow the combustion and electric motor to operate in safer ranges, understanding the fundamentals of the management conditions is needed to properly command and engage the test bench. With a working system it is important to instrument the test bench correctly to collect data accurately and with purpose. The information collected from sensors on

the hybrid system provides safety and knowledge into the system's operation allowing researchers to make conclusions on its effectiveness as a technology.

Objective 3: Can the system be modelled to predict system response? The Matlab/Simulink model created for this thesis will provide a robust theoretical framework for understanding and predicting system responses based on the components on the current test bench. Steady-state responses of the simulations will provide data for standard operating ranges of the hybrid-electric propulsion system. While transient responses such as start-up and clutch engagement will indicate edge case scenarios that components must be able to handle but not necessarily sustain. Ideally, this model will have the capability of providing parametric studies to determine ideal operating conditions and parameters. The accuracy of the model's response will need to be determined and justified since the response of the physical system always has deviations and operation is never identical from one test to another.

Objective 4: What are the key parameters for component models and what do they represent? To create accurate and representative models of the components in the hybrid system it is imperative that the importance of the component with respect to its effect on system response is known. Deriving the models of specific components will inherently expose the importance of certain parameters and how they make the component behave. Running simulations with parameters that are out of range or sync may cause a system response that is unrepresentative. Understanding how such parameters affect the component output, and the system response not only increases the understanding of how the component works but can also help troubleshoot why a certain system response is occurring. Going through each component model learning the significance and effect of each parameter also provides insight into how to design an optimized hybrid propulsion system.

Objective 5: How do these key parameters affect the response of the system and how sensitive is this response? With a strong understanding of the parameters in each component it becomes intuitive which variables have a large effect on the components response. Realizing and understanding what parameters have a large effect on system performance is key to running parametric studies. Using such parameters as a test variable can demonstrate the limitations and strengths of the component. This in turn can sway the decision-making process for component selection and matching. When a system is sensitive to a given variable/parameter it is critical that said value is studied, specified, and selected correctly for experimental applications.

Objective 6: Can component specifications be determined in simulation to improve the design process? The Matlab/Simulink model aims to provide insight into how components pair and what specifications must be in place to guarantee smooth operation. The model hopes to provide a tool to test different component specifications, enabling CfAR to test the dynamics in simulation before purchase. This will optimize the component selection process reducing the need for component testing and trial methods. The model will also reduce the number of unknowns when entering the design phase since simulations will predict operation ranges for all components in the system.

Objective 7: What are the key benefits of the small-scale hybrid-electric propulsion system? Designing, building, modelling, testing, and analyzing the hybrid-electric test bench used at CfAR creates a well-rounded approach to characterizing the system. This will provide the knowledge and confidence to summarize the benefits and shortcomings of the technology. The completed research will outline how hybrid-electric propulsion can expand small-scale UAV applications by drawing comparisons to conventional configurations that are currently used in the sector.

1.7 Thesis Outline

The introduction provides a brief history of hybrid-electric systems and their uses. This is further expanded on by looking into the technology that is currently being used. The automotive sector currently has the most diverse applications of hybrid technology with cars from companies like Toyota taking the lead in reducing emissions by using hybrid-electric platforms. At the pinnacle of motorsport Formula 1 uses an advanced hybrid-electric system that harnesses both kinetic and thermal energy to charge the battery, leading to reduced fuel consumption and increased performance. Various projects have researched small-scale UAV hybrid propulsion and have laid strong frameworks for future work. Unfortunately, commercial aviation is well behind the automotive sector with large manufacturers still developing the technology. In recent years smaller research and aviation companies have successfully flown full scale aircraft with hybrid propulsion systems. With a strong understanding of the current state of the technology a set of objectives was outlined. The research in this project aims to contribute new information and insight into the development, modelling and understanding of small-scale hybrid-electric propulsion systems for UAVs.

A technical overview will cover the theoretical principles of hybrid-electric systems and their various architectures. Understanding the difference between these configurations and how they operate will explain why the parallel configuration was selected for this project. A top-level explanation on how dual shaft parallel systems operate will follow, providing a fundamental knowledge base required for the following sections of the research paper. This overview will include the components in the system, their purpose, effect on the system, and a short description of how they are controlled.

The design of the test bench is critical in verifying the validity of hybrid propulsion as well as providing a means of comparing results from simulations. This section will outline the mechanical design of the test bench, going into the failure points of old iterations and how they were mitigated. Component selection will be discussed to outline the specifications, features, and purpose with respect to the overall system operation. The nuances of building a system at this scale will be the key take away since there are few examples currently operating in the field. The principles and methodology of designing the system can scale with the application but new criteria will need to be considered when moving to larger higher-powered applications. This section should prove to be a helpful reference for other researchers as it covers the challenges of designing a novel propulsion system.

Creating a Matlab/Simulink model of the hybrid test bench is the main objective for this thesis work. The majority of knowledge gain occurs in the modelling process and the experimental testing which combine for the bulk of the research project. This section outlines the process of creating a component model and integration at a system level. This process has three main components: understanding of the component fundamentals, collection and/or derivation of governing equations, and model validation. The first step, understanding component fundamentals, is arguably the most important part. Knowing how the component works and what parameters drive the response are key in deriving an accurate model. Without this understanding a model can be created that has little to no resemblance to the real world but seems correct due to lack of knowledge.

The second step is where the fundamental knowledge on the subject is tested and is critical in creating a functioning model. Collecting and deriving the governing equations for a given component or system is where a model gains its function and resolution. The complexity of the model is directly related to the equations used to describe the component/system.

The last part of modelling is validating the model that was created, this can be done in multiple ways. Validation can be as simple as using a known input with a known output, this does not verify how the model works but does validate the results. A more robust way of testing the model involves hardware in the loop methods and/or experimental testing. These two methods can provide information on what responses the model produces and how they are produced, reducing the amount of operational unknown in the model.

The simulation and experimental testing section discusses the process of running theoretical mission profiles in Simulink and Matlab. This includes what parameters are required inputs and how they affect the system response. Various operating points are selected for simulation to see how the system performs in different instances. These simulations are later compared to experimental results to determine the validity of the model. With acceptable results these findings can then be compared to traditional systems.

The experimental part of the research covers how the test bench is operated and the results from test runs. Various test scenarios will be executed which include the required inputs, loading, commands, and the resulting telemetry. These results give a good understanding of how the propulsion system behaves and which operation modes are needed for certain demands. In addition to the system response, limitations and errors in the data collection will be discussed to provide an indication of the system's accuracy.

The data from the experimental results will be analyzed from the testing section. This will make the information easier to interpret and provide better understanding of what the data represents. Simulation data will also be discussed in a similar manner, providing understanding of what the system response expresses. These two different sets of data are then compared to outline the efficacy of the model and simulation environment. This section will provide a well-rounded summary of how effective the system model is at predicting system response and how robust the test bench is for propulsion testing. These results from the two environments will then be directly compared to conventional propulsion systems. This will provide a strong summary of the benefits and disadvantages of hybrid-electric propulsion for the small UAV class.

The conclusion section will combine all findings from the research into a condensed summary. This will include how this research failed or completed the objectives set at the beginning of the thesis. These accomplishments will also be defined on their accuracy and implications to real world applications. This section will also outline the usability of the test bench and simulation environment to disclose guidelines for operation and data analysis. Future research goals on the topic will also disclosed to improve the performance of both the test bench and system model.

2 Technical Overview

This section of the paper covers the fundamental configurations of hybrid-electric systems and the components used to make them. The three main categories of hybrid configurations are explained in terms of principles, components, and operation. This provides a basic understanding of the systems and creates a baseline for explaining the components in each system. The most common component variants of hybrid-electric systems are discussed at a fundamental level to give more detail on the system configurations. This information will be expanded on in the modelling section where mathematical models will be found and/or derived.

2.1 Hybrid Configurations

There are several different configurations for hybrid-electric systems with three overarching classifications: series, parallel, and series-parallel. The fundamental architecture for these categories will be explained, with more detail being disclosed for the various types of parallel systems since that is the focus of this research. Furthermore, the energy modes and operation of the systems will be explained to provide the required knowledge to understand how to model these systems.

2.1.1 Series Hybrid

Series hybrid-electric systems are the simplest configuration for hybrid technology. The main characteristic of these systems is that the electric motor is the only power unit connected to the output. For land vehicles the electric motor drives the wheels, and for UAVs the electric motor drives the output shaft directly. This type of system can be considered a range extender where the battery is charged via a combustion engine. The reduced complexity of this system makes it easy to control, simplifies the design, and reduces the cost.

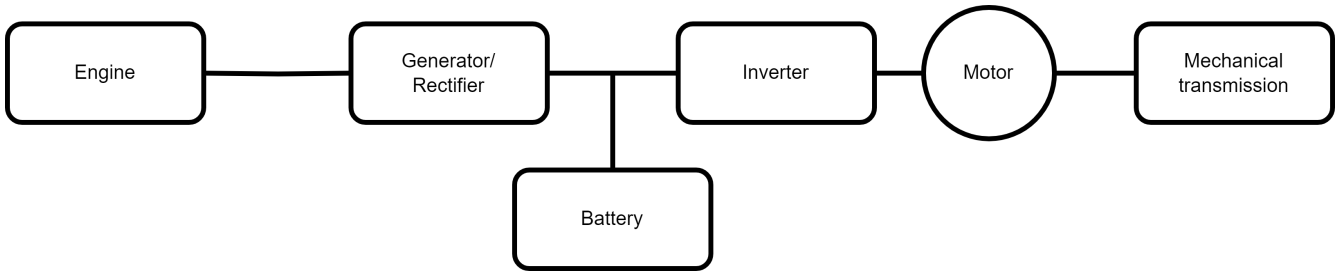

Figure 8: Series hybrid configuration [51]

2.1.1.1 Component Layout

The minimum selection of components for a series hybrid system are as follows:

- Gas turbine/Combustion engine/Fuel cell
- Generator
- Inverter
- Power converter(s)
- Battery
- Gearbox (optional)
- Controllers

The electric motor is connected to the output shaft of the aircraft, or in the case of a ground vehicle to the wheels. A gearbox may be required if the speed of the propeller/wheels is not correct for the

applications requirement or to increase efficiency. The generator converts the rotational speed of the combustion power unit into electrical power. In the case of a hydrogen fuel cell the generator is built into the power unit. A power converter is used to transform the generated power into the right voltage and current for the system electronics. This usually includes converting alternating current (AC) power into direct current (DC) and dropping the voltage to the required voltage of the battery and/or electric motor. Lower voltage systems will draw power from the battery which will also require converters to obtain the correct voltage range. The two power units and the converters require controllers to handle operational logic and to keep the system running as requested.

2.1.1.2 Operation

The way series hybrid systems operate depends on the demands of the specific scenario and the state of current components. There are four basic modes for these kinds of systems when the vehicle is in motion.

- Battery only: This is used when the battery has enough charge, and the power requirement is low for the discharge rate. In this mode the output is powered directly from the battery through the electric motor.
- Dual power: This occurs when the power demand is too high for the battery alone. The combustion engine is turned on and the power is delivered by both the generator and the battery.
- Combustion: When the power demand is high and it is not feasible to use battery only mode. This often occurs when the battery is neither full nor empty and power is required from the system.
- Power split: In this mode there is a power demand and the battery has low charge. When this occurs power from the combustion engine is sent through the generator. This electrical power is then sent to the electric motor and the battery. This allows the battery to charge while the vehicle is in motion and still meets the power demands of motion.

2.1.2 Parallel Hybrid

Parallel hybrid systems have more variability in their configurations compared to series systems. This means that the selection of architecture is customized to the application more so than a series project. Many of the component principles from series applications transfer to these parallel drivetrains. The main reason for using a parallel system instead of series is to have the ability to drive the output with either power unit or both.

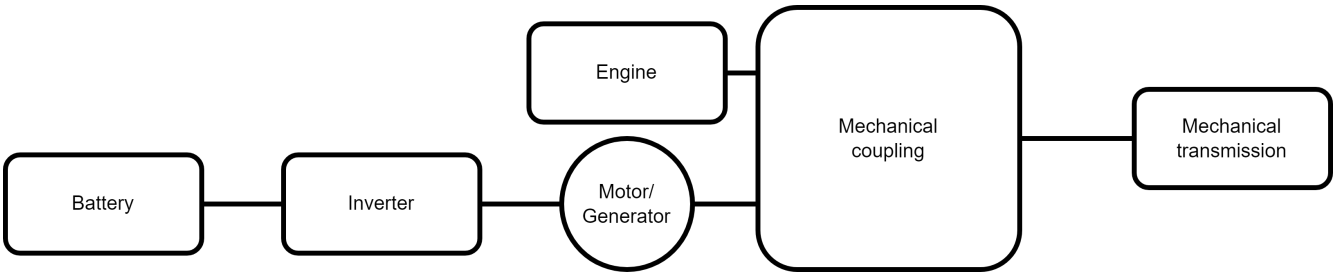

Figure 9: Parallel hybrid configuration [51]

2.1.2.1 Component Layout

A parallel system usually contains the following components, with some being required for certain architectures and others not:

- Gas Turbine,Combustion Engine
- Electric Machine
- Power Converter(s)
- Battery
- Gearbox (optional)
- Belts/Pulleys/Gears/Clutches
- Controllers

These components are similar to a series system, with the main difference being the drivetrain and electric motor. Unlike a series configuration where the system is only driven by the electric motor a parallel system can choose between electric, combustion, or combined power. This is achieved in a couple of different ways depending on the specific configuration. One common method is by adding a single clutch after the combustion engine. This allows the output to be powered with just the electric motor with the clutch open. With the clutch engaged the combustion engine can drive the output by itself with the electric motor rotating passively or generating electricity. Another capability with the clutch engaged is that both power units can provide energy and drive the output together. Some other coupling methods used in automotive are a dual-clutch transmission (DCT) or a continuous variable transmission (CVT). For simpler or lower power applications gears, belts, one-way couplers, and pulleys can be used for the mechanical coupling of the two power units.

2.1.2.2 Operation

Parallel systems have similar operating modes to series systems, but with more versatility. These modes are as follows:

- Electric only: This mode is possible when the battery has enough charge and the electric motor output is high enough to meet the demand. This allows the combustion engine to be turned off and saves fuel.
- Combined power: When power demand is high both the electric motor and combustion engine supply power to the output.
- Combustion-only: If power demands are too high for the electric motor and combined power is not ideal this mode is required. The combustion engine provides all the power and if the battery charge level is high enough then charging is not required.
- Power split: For parallel systems combustion power is sent directly to the output with some of the power being sent through the electric motor. This means that the motor is capable of charging the battery via an inverter or rectifier.

These modes for parallel systems allow for flexibility in choosing which power unit directly drives the output. Additionally, the parallel hybrid systems can be more efficient because combustion power can directly drive the output which reduces losses. The direct-drive of both power units allows for the system to be tuned more dynamically, improving the system response and performance.

2.1.3 Series-Parallel Hybrid

The last category of hybrid-electric systems is the series-parallel configuration. This takes the features of both system types and combines them. This means the system is capable of operating in all the modes of each system. Unlike a series system it has a direct connection between output and combustion engine. A dedicated generator is added to the system to charge the battery without affecting the power of the electric motor.

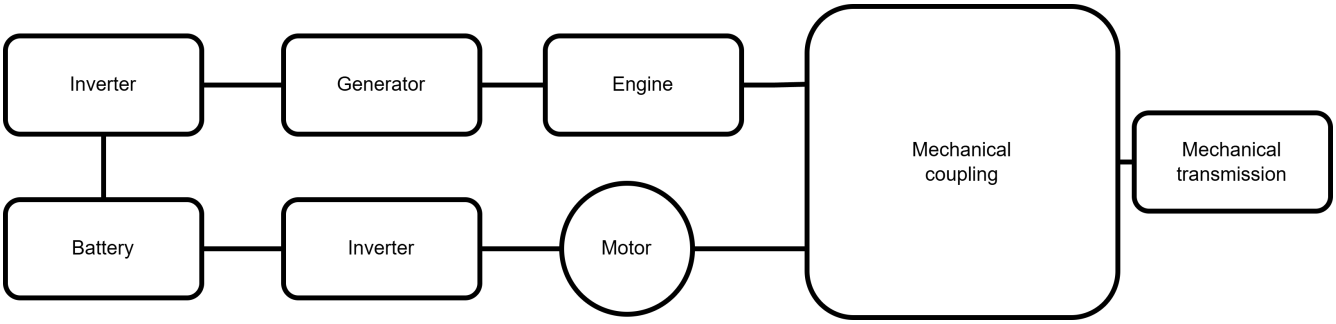

Figure 10: Series-Parallel hybrid configuration [51]

2.1.3.1 Component Layout

The minimum selection of components for a series-parallel hybrid system are as follows:

- Gas Turbine,Combustion Engine
- Electric Machines
- Power Converter(s)
- Battery
- Gearbox (optional)
- Controllers

The components of this final system type are a combination of series and parallel systems. This is required to allow the powertrain to operate in both series and parallel modes.

2.1.3.2 Operation

The operation of series-parallel systems is a summation of the two previously discussed types. However, because of this versatility in operating modes the fuel efficiency and system response can be optimized further than parallel and series configurations. The main disadvantage of this system is the complexity and cost of the system.

2.2 Components

The common components for each architecture were listed in the configuration section with minimal explanation. The following subsections describe the components in more detail as well as the variants that exist which affect their characteristics. Additionally, the basic operation, advantages, disadvantages, and common applications of these components will be disclosed. Mathematical models and detailed information for certain components will follow in the modelling section of this paper.

2.2.1 Internal Combustion Engines

Internal combustion engines are robust and durable power units that operate on the principle of burning fuel. There are two kinds of combustion engines that exist, spark ignition and compression ignition, both of which have their advantages and disadvantages. Compression ignition (CI) engines use compression to cause the fuel to combust in the engine, however this kind of power unit is not commonly used in aerospace applications so it will not be discussed. Spark ignition (SI) combustion engines are the most common type of engine and are used in motorcycles, cars, trucks, aircraft, and smaller applications such as lawnmowers. These types of engines are selected for hybrid-electric powertrains and will be the focus of this research.

2.2.1.1 Construction

SI engines are built on the same fundamental principles no matter the size or power of the unit. There are two main variants of these standard SI engines, two stroke and four stroke, this refers to the number of strokes the engine requires to produce power. The typical construction of each type is shown in the diagrams below. A two-stroke engine contains the following components, and the diagram below shows how they are configured.

- Cylinder head: This part contains the combustion that occurs and is where the spark plug is often installed.
- Piston: The pistons' main job is to keep the cylinder sealed and allows for expansion and compression.
- Crankshaft: This component connects to the piston and converts the translational movement into rotation.
- Connecting Rod: This part is responsible for connecting the piston to the crankshaft allowing for the translation of movement.
- Crank Case: This block holds the crankshaft and allows for oil circulation for most engines.
- Spark Plug: This unit is responsible for creating a spark that burns the fuel when the piston has reached the top of the cylinder.

All the components that exist in a two-stroke engine are also used in a four stroke engine. The components listed below are added and the diagram below shows how they are configured.

- Head: This part sits above the cylinder, houses the intake port, exhaust port, cam(s), and spark plug.
- Intake Valve(s): These components sit in the intake port and allows air to enter the cylinder when required.
- Exhaust Valve(s): These behaves the same as the intake but allows exhaust to escape the cylinder when required.
- Camshaft(s): The camshaft is a lobed shaft that tells the intake and exhaust valves when to open and close. In modern engines there are multiple camshafts for more flexibility with timing.
- Valve Cover: This is used to seal the camshafts and valves from the environment.
- Oil Pan: The pan holds oil which is circulated throughout the engine. This is required for four stroke engines because oil is not mixed into the fuel like two stroke applications.

2.2.1.2 Engine Cycles

These two different engine configurations operate with some differences, the main being the engine cycle. The engine cycle dictates the components required and the performance of the engine, these stroke types are as follows for the two different variants:

Two-Stroke:

1. Air/fuel enters the cylinder while exhaust exits.
2. Air/fuel is compressed and combusted.

Four-Stroke:

1. Air/fuel is drawn in by pulling the piston down.
2. Air/fuel is compressed by the piston pushing up.
3. Mixture is combusted via spark, pushing the piston down.
4. Exhaust is pushed out by the piston.

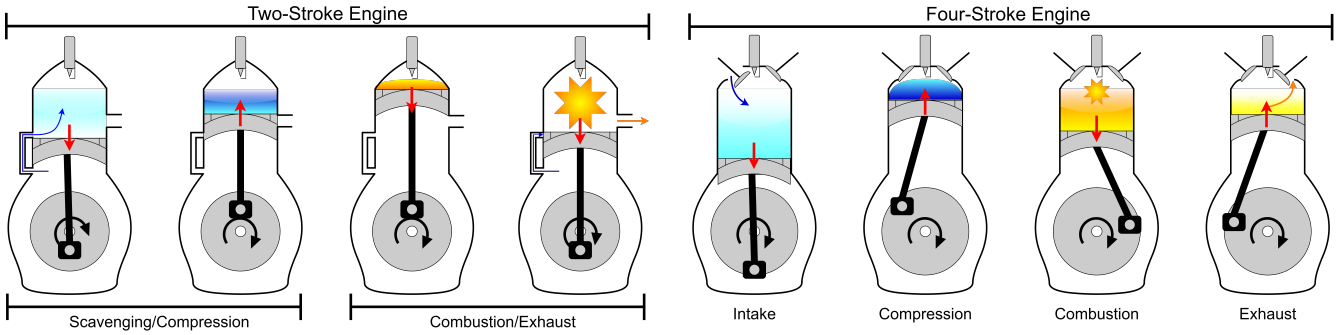

Figure 11: Two and four stroke engine cycles

With combustion engines there is a specific amount of fuel and air required for the system to become self-sustaining. The cycles shown in Figure 11 demonstrate that the inlet and exhaust are connected to the movement of the piston. If the air-fuel mixture is drastically off the system can stall because of failed combustion, or it can run inconsistently if the mixture is out of the acceptable range.

2.2.1.3 Air-Fuel Systems

The air-fuel mixture of a combustion engine is the most critical part of operation. This mixture has a direct effect on the fuel efficiency, combustibility, reliability, power, and longevity of the power unit. There are two air-fuel system types; carburetted and electric fuel injection, with both having variations in how fuel and air enters the cylinder.

2.2.1.4 Carburetors

Carbureted fuel systems were the main fueling system for consumer cars up until 1991 [52], which was then replaced with the more efficient EFI. Many aircraft still in operation today use carburetors because of prolonged ownership and longevity compared to consumer automobiles. Carburetors are non-electric systems that operate on Bernoulli's principles, making them fairly simple compared to EFI.

The basic operation is fundamentally a fluid dynamics system with air and gasoline. Carburetors are designed to control the air to fuel mixture of the system which is critical for healthy engine operation. This is accomplished by using the air intake pressure to draw fuel into an air stream creating a certain mixture ratio. As stated by Bernoulli; static pressure reduces with increased velocity, meaning that when the throttle is opened further more fuel is mixed in. This allows the carburetor to maintain the correct fuel mixture at various speeds and demands. The mechanical design of a carburetor varies substantially on the application, some require more precise fueling than others. A common carburetor is shown in the Figure 12 below.

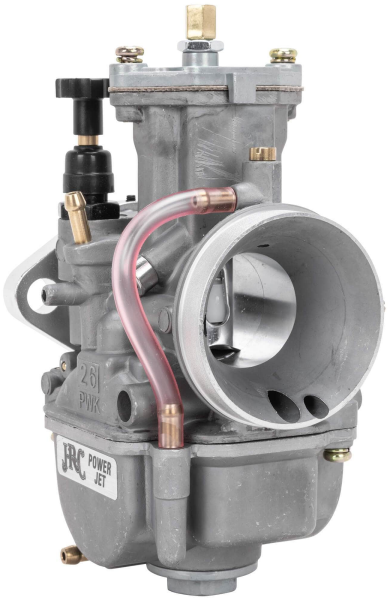

Figure 12: JRC 26mm carburetor [53]

There are a few components that should be explained for a better understanding of how the system works. Fuel is stored in the float chamber; this allows for a reserve amount of fuel to be available immediately. If fuel was drawn directly from the tank or fuel lines, the system would not be responsive and may even have pressure challenges. The pilot jet handles operation under low throttle conditions, such as idle. This jet is also combined with the main jet when the throttle is opened further, one of the most important parts of carburetor design is sizing the jets correctly.

The diaphragm moves with the pressure caused by the intake of air. This in turn moves the jet needle allowing more or less fuel flow from the main jet. These components work to create the amount of fuel and air that is pulled into the venturi, which atomizes the mixture and passes it into the combustion chamber. This fuel system was used to control fueling since 1888 and was used exclusively until the late 1980s [52]. Compared to modern EFI systems it is inaccurate and does not have any telemetry, which is why electric fuel injection systems are more favorable today.

2.2.1.5 Electric Fuel Injection

Modern fuel systems now use processors and sensors to control the air to fuel ratio for combustion engines. This new approach to fueling allows for more accurate control, better efficiency, and robust telemetry. Unlike the carbureted system it is a simpler mechanical design but requires better understanding of instrumentation and software. To control the fuel amount in the system EFI uses a component called an injector. These use a pulse-width modulation (PWM) signal to adjust how much fuel is injected into the air stream. This allows for more adaptability compared to the diaphragm and screw adjustments used in carburetors. The injectors in modern vehicles have multiple possible locations where they inject the fuel. The earliest type of fueling is port injection, this is where fuel is injected prior to the intake valve and mixed with air before entering the cylinder. The other type of fuel injection is direct, where fuel is sprayed into the cylinder. Direct injection is more efficient, provides a cleaner burn, and better performance. However, the technology is more expensive because of firing directly into the combustion chamber. There are also engines that use both forms of injection, allowing for the system to benefit from both sets of advantages.

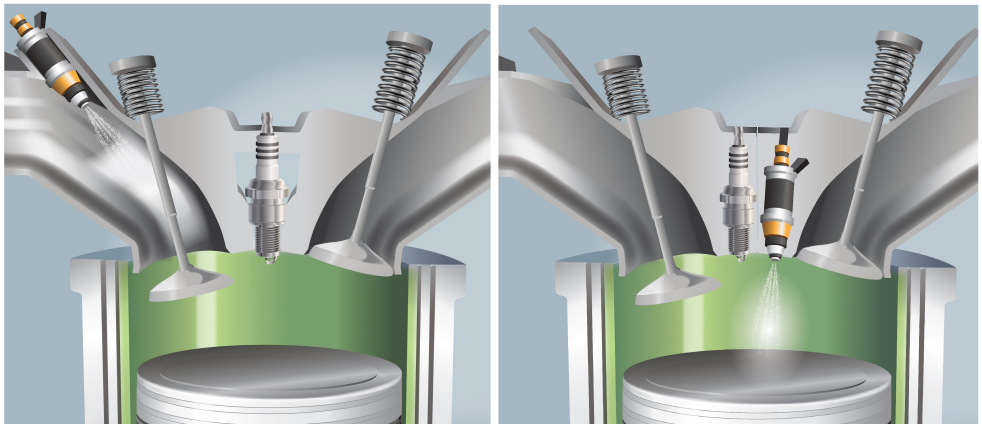

Figure 13: Port vs direct injection [54]

To use electronic fuel injection systems sensors must be present to monitor some key parameters. The carburetor system uses pressure and valves to accomplish air-fuel mixing, however EFI needs electronic feedback. The following electronics are required at a minimum to accomplish EFI:

- Engine Control Unit: This is a processor that controls all the electronics in a modern fuel system. For engine control this unit governs fuel ratios, throttle curve (if available), timing, modes, forced induction control, etc.
- Manifold Absolute Pressure (MAP) Sensor: This provides the pressure in the intake manifold which the ECU uses to determine fuel injection combined with the MAF.

- Mass Air Flow (MAF) Sensor: This reads the flow rate of the intake air and allows the ECU to predict fueling combined with the MAP.
- Throttle Position Sensor (TPS): The position of the throttle is required to determine load input, deceleration cut, transient throttle, etc.
- Oxygen (O2) Sensor: This is located after combustion on the exhaust to determine the efficiency of the burn.
- Other Sensors: There are numerous other accessory sensors such as oil pressure, fuel pressure, intake temperature, and coolant sensor. These provide feedback to the ECU which aims to operate the engine in a safe and efficient method.

This modern fueling system provides efficient, accurate and tunable control of the air-fuel mixture for combustion engines. For this reason, it is the fuel control method of choice for all cars today and many aircraft. This system is used for the research in this paper since it provides better data compared to carbureted systems and is more representative of current UAV applications.

2.2.2 Electric Motors

Electric motors convert electrical energy into rotational mechanical energy. There are different categories of electric motors that all operate on the same principle. The interaction that causes the energy conversion is electromagnetism. These motors create mechanical energy by having a shaft interact with a magnetic field which is created by an electric current through wire windings. Some common, noticeably different types of electric motors are discussed below, focusing on their applications and differences.

2.2.2.1 DC Series Motors

This architecture is a self-excited direct current (DC) motor that has the field windings in series with the armature windings [55]. This configuration means there are fewer turns in the field windings because of the armature current flowing through them. These wires also have a larger diameter to reduce resistance, creating a heavier motor. The performance of this motor is unaffected by the heavier construction thanks to the strong magnetic field created by the higher current. The torque is also linear and directly proportional to the field current. The high starting torque of this type of motor means it has many applications that require power at relatively low speeds. This means DC series motors are used in cranes, air compressors, lifts, winches, power tools, and many other common devices.

2.2.2.2 Brushless DC Motors

Known as a BLDC motor, this type of electric motor's key feature is that they do not have brushes. Brushes are used to swap the polarity of the poles in a motor to maintain the rotation of the armature. Going brushless increases the efficiency, life span, and performance of the DC motor. Thus, a BLDC can change the polarity without anything contacting both the rotor and stator which reduces electromagnetic interference. This motor class can have two different configurations, one where the rotor is in the center of the motor and the other where the rotor is mounted along the perimeter [56]. The speed of these motors is controlled by the frequency at which the current is supplied and can operate at very high speeds with low noise. Additionally, BLDCs can have increased position accuracy by adding more electromagnets. However, high current should not be supplied for long periods of time because the heat generated can weaken the magnets and

damage the windings. BLDCs are often used for high-speed applications such as drones, industrial automation, and robotics.

2.2.2.3 Permanent Magnet Synchronous Motors

This motor follows the same type of brushless construction as the BLDC which means that the permanent magnet synchronous motor (PMSM) shares the main advantages of a brushless DC motor. The main difference for a PMSM is the structure of the stator and windings which is configured to produce a sinusoidal back-electromagnetic field (EMF), compared to the BLDCs trapezoidal [57]. This motor is also capable of producing more torque at low speeds compared to BLDCs. The main disadvantage of this architecture is that they are expensive and difficult to spin initially because they are not self-starting. PMSMs are used in many common items such as AC units, refrigerators, compressors, washer machines, etc.

2.2.2.4 Induction Motors

There are numerous different induction motors that require AC to operate, with the most basic one being the squirrel cage induction motor. This type of EM operates with a magnetic field that is created in the stator windings which causes the shaft to rotate. The rotor in these motors does not require any electrical connections, which makes it simpler and more reliable. Compared to an AC PMSM these induction motors are cheaper, simpler but are less efficient and have a lower power density.

2.2.3 Energy Storage

For hybrid and all-electric systems energy storage is an important part of using the technology to its full potential. The energy density challenge of electric cars and aircraft today is caused by the energy storage requirements of these new technologies. Modern batteries currently do not have energy density required to replace gasoline without significant weight penalty [58]. There are many different compositions of batteries that are available and two of them are discussed below. There are also supercapacitors that vary significantly from batteries and have not been used as extensively as batteries.

2.2.3.1 Lithium-ion Batteries

This battery technology is the most used type of energy storage in electronic devices today. The basic composition of these batteries are as follows:

- Electrodes: These are the positively and negatively charged parts of the battery that are connected to the current collectors.
- Anode and Cathode: Are the negative and positive charged electrodes respectively.
- Current Collectors: These are foils that are connected to the electrodes and terminals. The foils transmit the current to terminals which connect to the electric device that uses the battery.
- Separator: This part of the battery separates the electrodes but allows lithium ions to travel from anode to cathode.

This battery technology is used extensively because of its numerous improvements over older battery technologies. Some common lithium-ion battery types are listed in Table 1.Some advantages for this battery technology include low weight, long lifespan, fast charging, and high energy density. Unfortunately, there are some challenges with repair because of the advanced construction and safety standards. One variant of a lithium-ion battery called lithium-polymer (LiPo) uses a polymer electrolyte instead of liquid. This type of battery is an extreme fire hazard when the pack is punctured or damaged. Different lithium-ion batteries are used in hybrid-electric vehicles such as cars and UAVs.

	Specific Energy $[Wh/kg]$	Cycle Life
Lithium Cobalt Oxide	150-200	500-1000
Lithium Manganese Oxide	100-150	300-700
Lithium Nickel Manganese Cobalt Oxide	150-220	1000-2000
Lithium Iron Phosphate	90-120	2000+
Lithium Nickel Cobalt Aluminum Oxide	200-260	500
Lithium Titanate	50-80	3000-7000

Table 1: Common lithium ion battery types [59]

2.2.3.2 Nickel-Metal Hydride Batteries

The battery construction is similar between chemical variants and Nickel-Metal Hydride (Ni-MH) batteries have the same anode/cathode construction as lithium-ion. The cathode contains nickel hydroxide as its principle active material, the anode uses hydrogen-absorbing alloys. This includes NiFe, MgNi, and $LaNi_5$ which are the commonly used materials for the anode. The main benefits of this technology compared to lithium-ion is that it has high device compatibility, safer to use, can be fully discharged without concern, and is cheaper. These come at the cost of self-discharge issues, slower charging, and lower energy density. This battery technology is often used for lower power and less demanding applications.

2.2.3.3 Super Capacitors

Supercapacitors are double layer capacitors that have much higher capacitance compared to regular capacitors. The construction of a classic capacitor is simple, there are two conductive parallel plates separated by a dielectric gap. These two plates have a voltage differential applied to them which creates static charge. This charge is stored and can be discharged when required, supercapacitors are built differently and are more complex due to the demand for high capacitance.

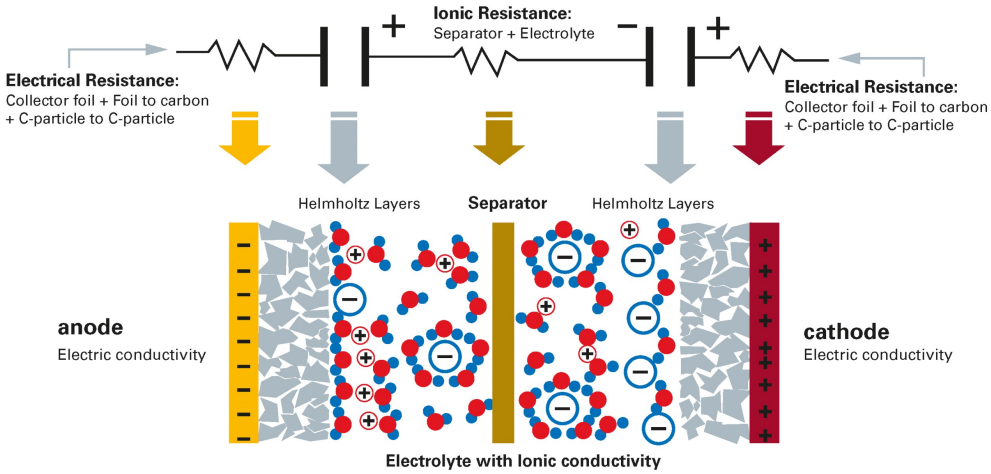

Figure 14: Dual layer supercapacitor construction [60]

Supercapacitors use cylindrical or flat layers of activated carbon for the active construction material. The dielectric gap between layers is replaced with dilute sulfuric acid, contact between these materials creates a double layer. These pairs are then separated by porous organic film to prevent short-circuiting [60]. This chemical enhancement of the capacitor increases it ability to store energy. Supercapacitors charge significantly faster, have a much larger cycle rating, and can deliver power much quicker. However, lithium-ion batteries have a higher energy density, are much cheaper, and provide a higher voltage.

2.2.4 Gearboxes and Transmissions

Gearboxes and transmissions provide speed and torque control to the system via gears, clutches, and/or pulleys. This allows for input devices to run in efficient ranges and creates a wider operation window compared to direct-drive methods. One thing to note is that transmissions are used by many vehicles, but not often by aircraft, which use gearboxes or direct-drive. Both these types of systems are governed by conservation of power to transmit rotation; meaning that an increase in torque reduces speed and vice versa.

2.2.4.1 Gearboxes

There are numerous compound gearboxes that are all designed for their own operating conditions and applications. These are sets of gears that transfer power from the input to the output, with some aiming to increase torque and others to reduce it. The main difference in these gearboxes is the gear profile and configuration that dictates how the load is handled.

- Spur Gears: The conventional gear profile where the teeth are cut as a two dimension profile
- Helical Gears: These gears have teeth that are orientated at an angle to the shaft's rotational axis. This allows for multiple teeth to be engaged at once which increases the load rating. This operates smoother and quieter compared to spur gears.
- Double Helical Gears: This incorporates two sets of helical gears located next to each other with a gap. These pairs have opposite helix angles which eliminate thrust loads and provides better tooth overlap.

- Herringbone Gears: These are similar to double helical variants but without the gap between gears. This makes them more compact and are often used for high shock applications.

Figure 15: Common gear types [61]

Various gearbox types can be built with multiple gears of any ratio to meet the demands of an application. A more complex gearbox type that uses any of the gear profiles above is a planetary gearbox. This type of gearbox is used for large torque low volume applications; they are much more compact compared to their compound equivalent geartrain. This configuration includes a minimum of 3 gears: a planetary gear, sun gear, and internal gear (ring gear). The planetary and sun gear are standard external gears of any profile, which can be sized to dictate ratios. The internal gear is a ring-shaped gear with internal teeth which interfaces with the two other gears and keeps them inside the ring. The planetary gears rotate around the sun gear, this can create multiple different gearbox behaviors which are tabulated in Table 2 below along with a diagram of a planetary gearbox.

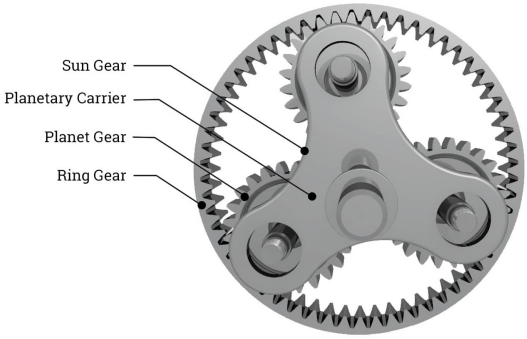

Figure 16: Simple planetary gear system [62]

Driver	Hold	Driven	Result
Input Shaft	Ring Gear	Output Shaft	Reduction
Input Shaft	Output Shaft	Ring Gear	Reverse+Delay
Output Shaft	Input Shaft	Ring Gear	Delay
Output Shaft	Ring Gear	Input Shaft	Acceleration
Ring Gear	Output Shaft	Input Shaft	Reverse+Acceleration
Ring Gear	Input Shaft	Output Shaft	Delay
Input and Output Shaft	NA	Ring Gear	1:1

Table 2: Results of various operating modes of a planetary gear [63]

These gear profiles and geartrain types are the most common variants used for power transmission in vehicles, there are others used for robotics and automation. These include bevel gears, worm gear set, and hypoid gears which are used in steering racks and differentials in vehicles. Compound and planetary gearboxes are commonly found in hybrid-electric vehicle transmissions.

2.2.4.2 Manual Transmissions

The manual transmission was the first type of transmission used in consumer vehicles and the simplest example. These transmissions contain parallel shafts with multiple gears mounted to them. There are three shafts: the input shaft, countershaft, and output shaft. There are also shift shafts that allow for the transmission to change gears, and the number of shafts depends on the number of gears available.

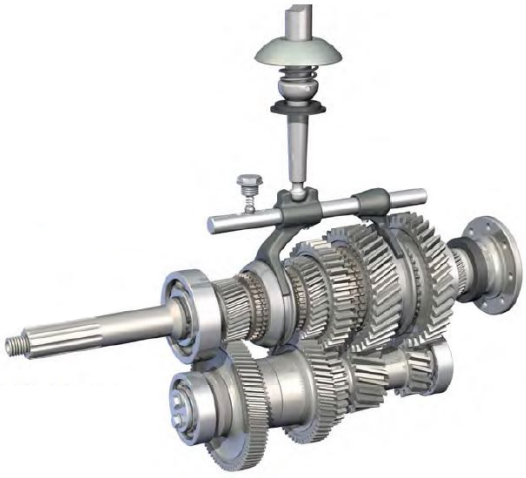

Figure 17: Manual transmission diagram [64]

Figure 18: Standard synchronizer [65]

The shift shafts slide parallel with the countershaft which allows them to engage and disengage the output shaft from the countershaft. The input shaft always spins with the countershaft because the gears are meshed, the engagement of the output shaft is accomplished by synchronizers. Synchronizers are coned friction assemblies that are located between gear pairs. The synchronizers use friction to make both gears spin at the same speed before it fully engages the gear pair with the shift fork. This synchronization is required for smoother shifting, easier operation, and to reduce transmission damage.

The process of changing gears in this transmission is operated by the user and has no automation. When changing gears, the clutch is disengaged from the engine to reduce the load and speed on the input shaft. The shift fork then pushes the shift shaft which is connected to a synchronizer. The synchronizer matches the speeds of the two gears that are to be selected and then slides into place engaging the gears. This engagement causes the output shaft to spin which is connected to a differential which sends power to the wheels.

2.2.4.3 Automatic Transmissions

The automatic transmission removes the need for operators to change gears themselves and allows for more control over fuel efficiency. This type of transmission uses a compound planetary gearset which operates like two planetary gearsets combined. Automatic transmissions use a torque converter instead of a clutch to decouple the transmission from the engine. This device is a fluid coupler that uses an impeller, turbine, stator, and transmission fluid to transfer rotation from the engine to the input shaft. The impeller is connected to the engine, as the impeller speed increases more fluid is transferred into the turbine which is connected to the transmission. This means at idle speed there is not enough fluid rotation to rotate the turbine, essentially disconnecting the transmission from the engine.

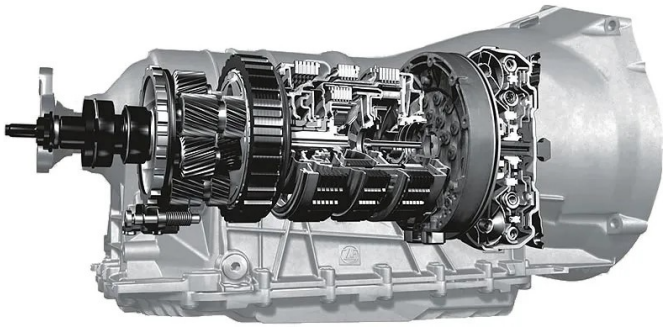

Figure 19: Automatic transmission cross section [66]

The compound gearset in an automatic transmission has multiple engagement configurations that are accomplished with a one-way clutch that prevents the carrier from spinning in both directions. Changing gears is accomplished in a few different ways and is quite complex. Gear changes occur by either making the suns or the ring gears inputs. Any combination of the two scenarios creates various gear ratios which allow for it to have the same range of gears in a smaller package compared to the manual transmission.

2.2.4.4 Dual-Clutch Transmissions

The dual-clutch transmission (DCT) is one of the most modern types of transmissions that improves automatic transmissions substantially. The DCT as the name implies uses two clutches to improve shifting and response time. The torque converter and planetary gearset in an automatic transmission cause the transmission to be slow at shifting and less responsive compared to a manual transmission. A DCT has more in common with a manual transmission than an automatic because of the use of synchronizers and parallel compound gearsets. The operation of the transmission is the same as the manual transmission, however it acts like two manual transmissions at once. This is accomplished by splitting the single input shaft into two, separating the even and odd

gears. This is why two clutches are required in the transmission, one for each input shaft which are housed in the clutch case. The transmission electronics predict which gear the user wants next and engages the unused clutch accordingly. When the operator requests a gear change it happens almost immediately because the next gear is already engaged.

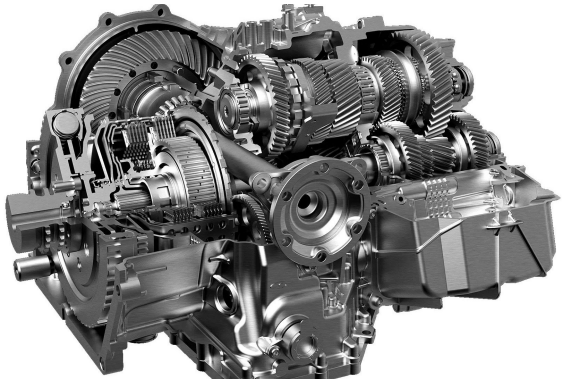

Figure 20: A dual-clutch transmission used in the Audi R8 [67]

The dual-clutch transmission includes the convenience of an automatic transmission but improves on shift time and response. With the removal of planetary gearsets and the torque converter the gears engage and feel like a manual transmission but shifts faster. These DCTs are paired with paddle shifters on the steering wheel to allow the user to select gears individually like a manual transmission but without a shifter. DCTs are more expensive compared to the two conventional configurations but provide a much better experience when an automatic transmission is required, such as with hybrid vehicles.

2.2.4.5 Continuous Variable Transmissions

This is another automatic transmission version which aims to increase fuel efficiency and reduce shift shock on the drivetrain. The operating principle for these transmissions is that the planetary gearsets are replaced with a pulley system. This pulley system uses variable-diameter pulleys that allow for the pulley to increase or decrease speed without disengagement from the engine [68]. These pulleys are usually two 20-degree cones facing each other, the distance between the two cones dictate the diameter and speed ratio. The driven pulley is a conventional v-belt pulley that is often connected to the output shaft.

There are also Toroidal continuous variable transmissions (CVT) which use discs and power rollers. This works on the same principle as the belt CVT but instead of a variable-diameter pulley it uses rollers. The rollers rotate between the two cone shaped discs to change the ratio between the input and output discs.

Both these CVT systems allow for nearly infinite number of gear ratios between the two maximum and minimum diameters. This means that vehicles can pick the most ideal ratio and change it continuously while being driven. The main operational characteristic of these transmissions is that there is no gear change feel and an increase in fuel efficiency.

2.2.5 Clutches

One of the characteristic features of a parallel hybrid-electric system is the ability to separate electric and combustion power. This is often accomplished by using a clutch which can connect and disconnect the coupled power unit from its output. Most clutches have two bodies, one connected to the input and the other the output. These two bodies are connected and disconnected in a few different ways depending on the clutch type.

2.2.5.1 Centrifugal Clutch

This type of clutch is considered an automatic clutch because it does not require an external input to activate. The basic configuration of a centrifugal clutch includes a housing, shoes, spider, and springs which are arranged to engage with rotational speed. The input shaft is connected to the spider which houses the springs and keeps the shoes aligned in the correct orientation. As the input shaft spins faster the radial forces cause the springs to extend and the clutch shoes to contact the housing.

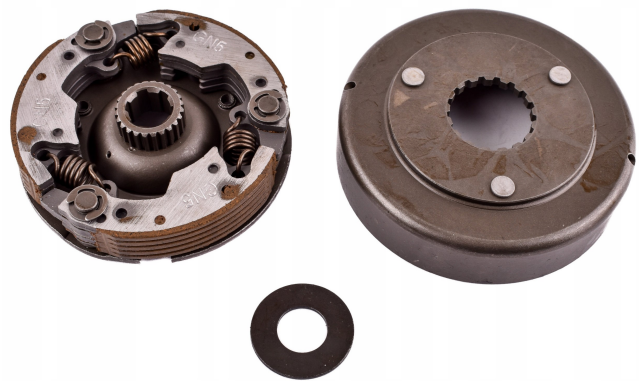

Figure 21: Centrifugal clutch with the internals removed from the housing [69]

With the output being connected to the housing this means that the two are now connected and rotating together. This simple centrifugal design means that at low speeds the clutch is disengaged allowing the engine to idle. Once the rotational speed is increased the clutch begins to engage and rotate the output as desired. This clutch type is used in compact applications with low power that do not require control separate from speed such as lawnmowers and scooters.

2.2.5.2 Hydraulic Clutch

The hydraulic clutch is one of the most common configurations and is used in consumer vehicles. This type of clutch has a more complex assembly compared to other clutches but can transfer much higher torque levels without requiring electricity like an electromagnetic system. The main components for the hydraulic clutch system are as follows:

- Diaphragm spring: This keeps the clutch and pressure plate engaged during rotation.
- Clutch disc: Is connected to the input and makes contact with the pressure plate while the clutch is engaged.
- Pressure plate: The pressure plate is connected to the output and makes contact with the clutch disc when engaged.

- Clutch fork: Actuated axially with the clutch to separate the pressure plate from the clutch disc.
- Throw-out bearing: Allows the clutch fork to compress the diaphragm spring during operation enabling the clutch to disengage.
- Master cylinder: Houses the hydraulic fluid and is actuated by the input device (pedal, actuator, etc).
- Slave cylinder: This is connected to and moves the clutch fork to engage and disengage the clutch.

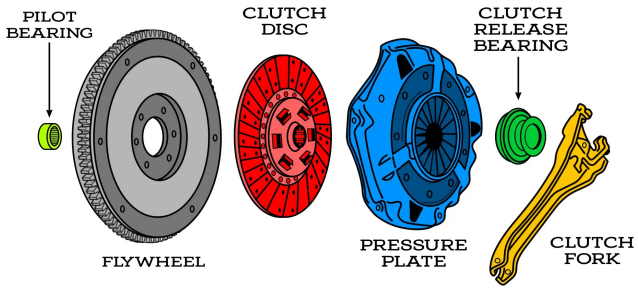

Figure 22: Hydraulic clutch main components [70]

This system uses hydraulic power to control the state of the clutch assembly by separating the pressure plate from the clutch disc. Looking at the clutch assembly when the clutch is engaged the pressure plate is in contact with the clutch disc, making the input and output rotate together. To disengage the clutch the fork activates the through-out bearing which puts pressure on the spring diaphragm releasing the pressure plate from the clutch disc.

2.2.5.3 Electromagnetic Clutch

The electromagnetic clutch is a much simpler assembly compared to the two mechanically oriented forms discussed thus far. This type of clutch has 3 main parts; the armature, rotor, and coil which are similar to electric motor architectures. The input and output of the clutch can be connected to either the armature or rotor. These two components rotate freely and are separated when the clutch is disengaged. The main difference between the armature and rotor is that the latter rotates around the field coil. This makes the rotor stationary axially and is only free to rotate.

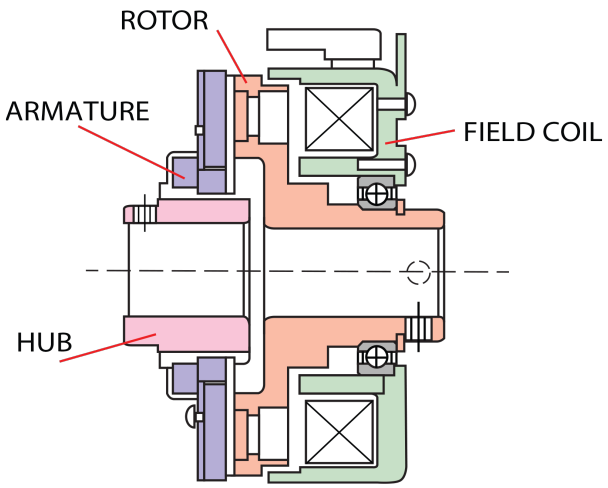

Figure 23: Basic electromagnetic clutch configuration [71]

To engage the clutch current is sent through the field coil which causes it to create a magnetic field. This electromagnetic force pulls the armature into the rotor and the two rotate together because of frictional forces. These clutches are well suited for remote operation but can be overheated since the electric energy is dissipated as heat.

2.2.6 Energy Conversion

In multidisciplinary applications it is often required that energy is converted since most components in the system run with different power systems. For electrical systems there are four main types of converters that are discussed below, these are required to make sure all components have the power required without risk of damage or malfunction.

2.2.6.1 Inverters

For converting DC power to AC an inverter is used, which uses a diode array and microcontroller for conversion. These are often used for controlling rotational speed of AC and brushless motors because of the input voltage and output frequency being decoupled. For how these systems work and how they are configured see the electronic speed controller (ESC) section below.

2.2.6.2 Rectifiers

Rectifiers accomplish the opposite function of an inverter which is converting three phase or AC power into DC. This is done with diodes that switch the negative portion of the AC wave positive, creating a pulsating positive wave form. There are many different rectifier configurations that are briefly described below:

- Half-Wave Rectification: This configuration is used for simple applications where the rectification output does not need to be accurate. This type of rectification uses only half of the AC power every cycle. Common applications for this type of circuit are pulse generator circuits, firing circuits, and low power charging circuits.
- Full-Wave rectification: Building on the principles of the half-wave configuration a full-wave circuit allows for full power from the AC power source by using the negative half of the

sine wave. This type of circuit is used in modern electronics such as cell phones, UPSs, car alternators, and audio amplifiers.

- Others: The two fundamental rectifier circuits listed above can be combined and tweaked to make numerous other types of rectifiers. These are used for specific applications and improve some of the challenges found with the full and half-wave circuits. Some configurations include uncontrolled, positive half, negative half, bridge, center tap, and N-phase rectifiers.

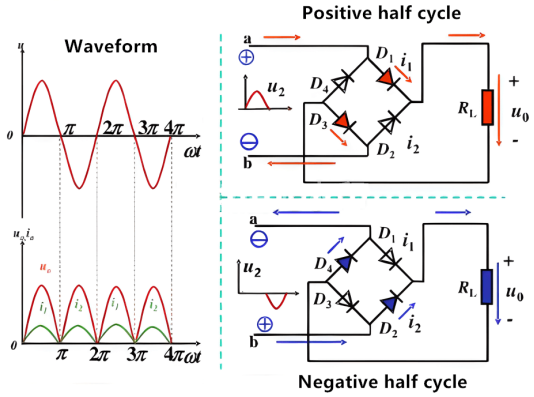

Figure 24: Full-wave rectifier circuit and resulting waveforms [72]

The circuits described above convert the sine wave into a pulsating signal that is often unusable and requires some manipulation after the conversion. The most common requirement is to smooth the pulsating signal with a capacitor. Once the signal is smoothed adequately it can be treated as DC power by many different components.

2.2.6.3 DC-DC Converters

Electronic devices rarely require the same voltage for an entire electromechanical system especially in high power applications. This is where DC-DC converters are used, this allows for fewer input voltages and a simpler system. There is a large range of voltages between 1.2 and 48 volts that are common in DC electronic components. It is important to select a converter that has the voltage range, noise level, and precision required for the components in the system. The most common converter types are described below and help narrow down the right converter for the application:

- Buck Converter: This takes a higher voltage and drops it to a desired value by using Metal Oxide Semiconductor Field Effect Transistors (MOSFETs), diodes, inductors, and capacitors. These components work together to switch, store, and regulate the duty cycle of the circuit effectively reducing the output voltage proportionally to the input.

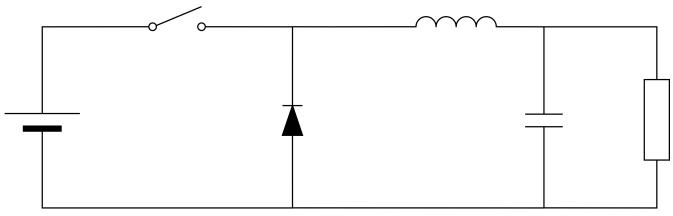

Figure 25: Buck converter circuit [73]

- Boost Converter: This converter is the opposite of a buck converter; it steps up the voltage input to a higher voltage. This circuit uses the same components but in a different configuration where the switch, diode and inductor changing positions counterclockwise.

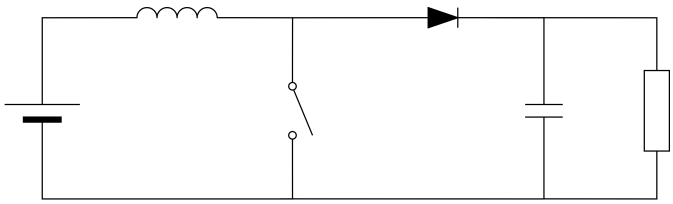

Figure 26: Boost converter circuit [74]

- Buck-boost Converter: As the name suggests the converter combines the operation of both the previous types of converters. This circuit can step a voltage up or down depending on the request.

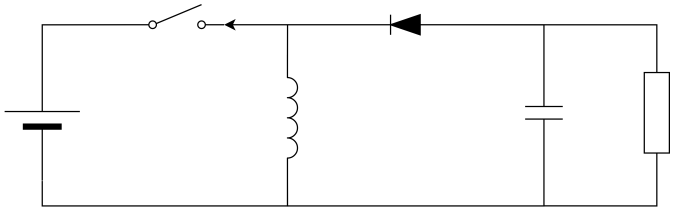

Figure 27: Buck-Boost converter circuit [75]

- Cuk Converter: The Cuk converter is effectively a buck-boost circuit with two inductors and capacitors. The main advantage of this configuration over conventional ones is that it produces a smoother output and is more efficient. These improvements come at the cost of more components, higher current stress on the switches, and requires an inverting component on the output or input.

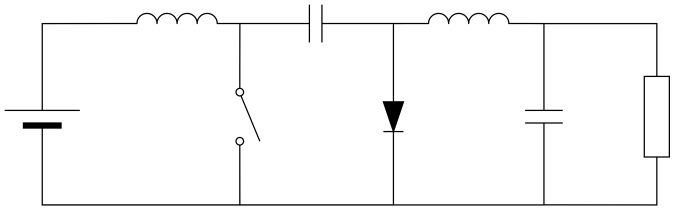

Figure 28: Cuk converter circuit [76]

Choosing from these types of converters is the first step in conditioning the power in a hybrid system. Power requirements for a device can vary substantially, for example a sensor could require only 5 volts to operate correctly whereas a DC motor could need 48 volts to spin at full power. However, when selected correctly a hybrid system can operate with one or two high voltage batteries that operate even the lowest power components.

2.2.6.4 AC-AC Converters

Unlike DC-DC converters, AC-AC converters do not simply increase or decrease the voltage, their job is more complicated. AC-AC converters are used to regulate root mean square (RMS) current and/or frequency of the AC output which improves the power quality and compatibility with various load types. There are multiple different AC-AC converter classifications which are as follows:

- Single-phase converters: These are used to control the RMS voltage and frequency for single phase AC systems which require relatively low power.
  - Phase-controlled: TRIACS or thyristors are used to adjust the phase angle and are often used for resistive or inductive loads.
  - Pulse-width modulated: The RMS output voltage is regulated via high frequency switching; this is often accomplished with IGBTs or MOSFETs.
- Three-phase converters: Often used in industrial or high-power applications, this converter regulates the RMS and frequency for three-phase AC systems.
  - Phase-controlled: These operate the same as single-phase phase-controlled converters.
  - Matrix: This type uses bidirectional switches and DC links to regulate the AC power. Matrix converters are compact, efficient, and more flexible compared to the phase control units.
- Cycloconverters: These are systems that convert the frequency to a lower output while maintaining the same RMS voltage. Cycloconverters are used in high power low frequency applications that require precise control such as induction and synchronous motor drives.

These types of converters are not often used in hybrid-electric vehicles and therefor will not be discussed in further detail.

2.2.7 Controllers

With complex electromechanical systems there is an inherent need for more control and telemetry. This is where controllers are required which are often embedded systems that use signals to command various components. In modern vehicles there can be more than 70 controllers that are used to monitor and control the vehicle [77]. The two main controllers for the hybrid-electric test bench at CfAR are discussed below as well as a brief overview of some common other controllers used in hybrid vehicles.

2.2.7.1 Electronic Speed Controllers

An electric speed controller is used with electric motors to command speed based on the data signals received as input. The ESC is connected between the battery and EM providing control over numerous parameters. For PMSM/BLDC applications the electronic speed controller converts direct current from the battery to the required three-phase power the motor needs based on the requested command. The conversion of DC to three-phase with modulation is accomplished using three main components in the ESC.

- Microcontroller (MCU): This component interprets the signal from the command input, keeps track of the motors position, and sends pulses to the gate driver.

- Gate Driver: Converts the low voltage signal from the MCU to a higher voltage for the MOSFETS.
- Metal Oxide Semiconductor Field Effect Transistors (MOSFET): These are switches that create a three-phase signal and control coil activation in the motor.

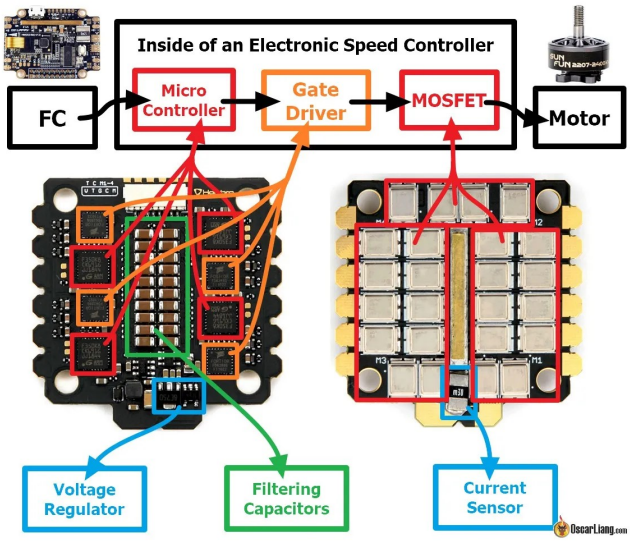

Figure 29: Basic operation of an ESC [78]

There are other smaller components in an ESC that perform other tasks such as a Battery Eliminator Circuit (BEC) that acts as a voltage regulator. An electronic speed controller can also have features such as hall effect sensor support, CAN, UART, various inputs, and safety limits. An effective ESC is able to control a specified motor with enough telemetry for the given task. Understanding how an ESC works and it's limitations is essential for effective motor control in hybrid systems.

2.2.7.2 Engine Control Units

An Engine Control Unit (ECU) in its most basic form is a computer that controls the ignition and injection for combustion engines. ECUs have inputs and outputs for multiple sensors to control the EFI system, while modern cars may even use the ECU to control other modules outside of the EFI system. The basic sensors for an ECU are similar to the required sensors for the EFI system:

- Air temperature
- Coolant temperature
- Throttle position
- Manifold pressure
- Engine speed

A basic ECU outputs are the fuel injectors, throttle position, and ignition coils, which are activated based on the input sensors and ECU settings. The logic used by an engine control unit is often in the form of lookup tables to command the optimal output values for the current operating state. An ECU is required when electronic fuel injection is present, this system provides control and telemetry that is needed for hybrid systems.

2.2.7.3 Other Controllers

In the current modern era of vehicles and aircraft there are countless digital interfaces that need to be controlled. This means that there are numerous controllers on top of the ECU, some examples are as follows:

- Transmission Control Unit (TCU)
- Anti-lock Braking System (ABS) Control Unit
- Electronic Stability Control (ESC) Control Unit
- Airbag Control Unit
- Body Control Module (BCM)
- Instrument Cluster Control Unit
- Infotainment Control unit
- Tire Pressure Monitoring System (TPMS) Control unit
- Battery Management System (BMS)
- Power Management Unit (PMU)
- Hybrid Control Unit (HCU)
- Vehicle Control Unit (VCU)

The name of a controller and how it works varies by manufacturer but the overall requirement to control all the complexities of modern propulsion systems remains the same. Hybrid systems have added requirements compared to conventional systems since there are two power plants that must communicate with each other.

3 Test Bench Design

Hybrid-electric propulsion systems contain numerous components that are required to operate as mentioned in the previous sections. One of the main challenges for hybrid technology is selecting the right components for a given application and assessing their capabilities. This is where a test bench becomes a valuable tool for designing and testing potential components and/or configurations. In this research project a modular test bench was developed for this exact purpose, to test components in specific configurations before integrated design. This section describes the current configuration of the test bench which is used for experimental testing during this thesis.

3.1 System Layout

The fundamental test bench design is a post and plate configuration that allows for the test apparatus to have distinct sections that are simple to disassemble. There are eight segments in the current system configuration, these sections include: power units, couplers, clutch, timing belt system, parallel to dynamometer coupler, timing belt system, and dynamometer.

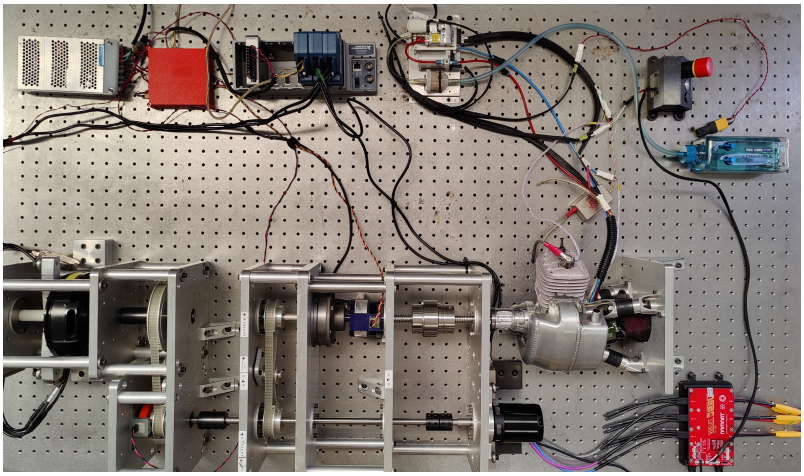

Figure 30: Hybrid-electric test bench 2024

The power unit section of the test bench contains the PMSM and ICE with their own shafts and bearings. With the current configuration these two components are mounted separately since they use substantially different mounting methods. The PMSM is a shaft side mounting system which allows the coil portion of the motor to spin freely. The combustion engine has motor mounts that must be connected to a rigid plate which supports a portion of the engine weight but are primarily used to reduce the vibrations that transfer from the engine into the system.

To connect the power units to their respective shaft couplers are required to maintain the desired modularity. The PMSM has a smooth torque output which allows for a simple steel rigid coupler to be used for connection. However, the combustion engine has significant vibration and torque spikes because of the reciprocating piston inside the cylinder. To properly transfer power into the shaft a flexible torque coupler was used. This coupler has a polyurethane core between two steel halves, this allows for vibration and misalignment to occur while transferring significantly less noise to the system compared to a rigid coupler. The polyurethane core is designed to shear at a specific torque value which protects the components in the drivetrain from damage.

The next section of the test bench is where the clutch and ICE speed sensor are located. The rotational speed sensor in this segment is responsible for measuring the output speed of the combustion engine. The clutch is also in this segment and allows both power units to run separately or synchronously depending on the clutch state.

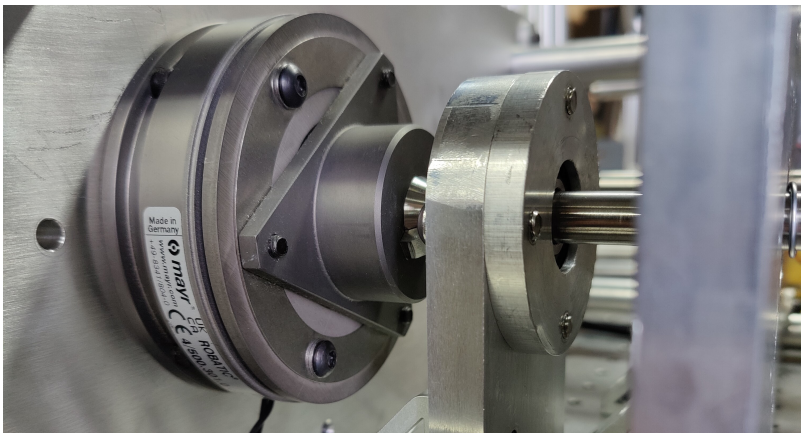

Figure 31: Mayr ROBATIC Type 4/500.301.0 electromagnetic clutch

The final segment of the hybrid propulsion system in the test bench is the timing belt system. This allows for the pulley ratio between the combustion engine and electric motor to be modified. The ratio is particularly important when the power units have substantially different speeds. The flexibility of various pulley sizes can also be used to dictate the operating ranges of the ICE and/or PMSM to optimize the power, speed, or energy consumption of the coupled system.

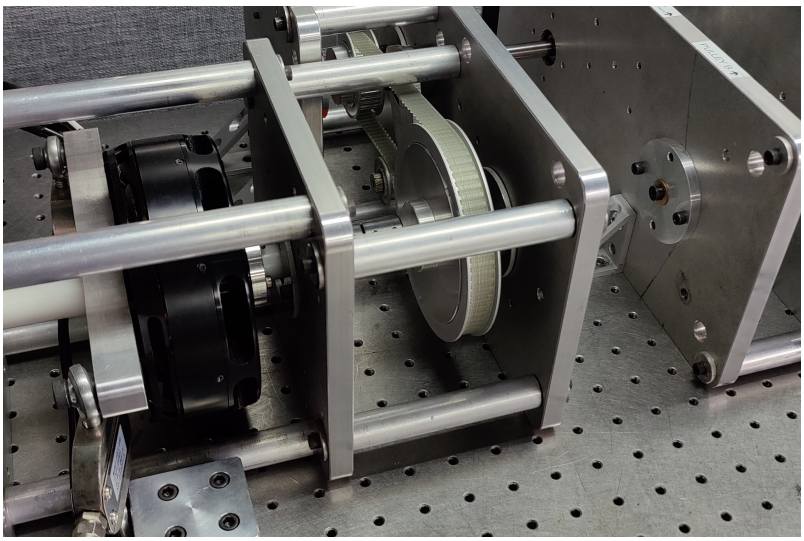

Figure 32: Dynamometer section of the parallel hybrid test bench

The hybrid system is connected to a dynamometer which consists of three sections. The first being a simple rigid coupler that connects the output shaft of the hybrid system to the dynamometer input shaft. The second section is another timing pulley system with rotational speed sensing. The pulley ratio here is required to decrease the input speed because the electric motor used for braking is substantially larger/slower than the PMSM and ICE. The final segment of the dynamometer is the electric motor and rectifier, which are used to apply electrical load to the hybrid system which simulates a mission profile without the need for a propeller and airframe.

3.2 Components

Component selection begins with predefined design goals set early on in the project but often changes as challenges occur and goals shift. The latest parallel hybrid test bench configuration shares no components in common with the first design, a shift that has occurred over the last seven years as challenges and scope requirements changed. The current components have the capability that current research projects require and will be used for the foreseeable future. The specifications, features, and justifications for each component are discussed in this section.

3.2.1 Permanent Magnet Synchronous Motor

The electric motor for the parallel hybrid test bench is responsible for electronic starting of the combustion engine, producing power, and charging the battery. These three tasks determine certain features and specifications that the motor must have to meet operational requirements.

Electronic starting of the ICE requires high torque at low speed due to the compression created in the cylinder while turning the engine over. This means that the electric motor requires a minimum torque rating but more importantly has position sensors. Sensorless control uses the back electromotive force to estimate pole location which only works at higher speeds. That is why sensorless motors cannot start under high load and often become unstable at low speed. Under these strenuous scenarios sensorless control loses pole angle and starts to energize the poles out of sync from the shaft causing the motor to oscillate between positions (referred to as cogging) or even stall. Conversely, position sensors allow the electronic speed controller to know exactly what state the poles are in at all times. A sensored control scheme knows exactly what pole to energize and when; allowing for maximum torque at nearly zero speed.

The speed range for the selected electric motor is less important than torque because of the belt systems incorporated into the test bench. However, it was convenient to select a motor that had a similar maximum speed as the combustion engine which is 8000 rotations per minute. This allows for simple pulley ratios and full use of the power range for both the combustion engine and the PMSM. The full specifications of the electric motor are tabulated below:

Parameter	Value
Voltage	48 V
RPM/V	205
Maximum Power	6336 W
Rated Power	4118 W
Maximum Torque	5.53 Nm
Rated Torque	3.76 Nm
No Load Speed	9840 RPM
Rate Speed	8364 RPM
Maximum Current (15 sec)	132 A
Continuous Current	86 A
Construction	12N14P

Table 3: Key specifications for the SKP 6485

The SKP 6485 is a medium size outrunner motor that is capable of producing good power while not being too large and heavy. It is capable of 5.53 newton meters of torque and 6.34 kilowatts of

power while weighing 1.1 kilograms. This is packaged into a 64 millimeter diameter housing that is 85 millimeters long, which can fit into small-scale UAV airframes without modifications. The hall sensors provide sensored control for high torque applications while also having a temperature sensor to provide safety limits for operating temperature. This motor paired with the correct electronic speed controller is capable of starting the combustion engine consistently and producing substantial power during boost/regeneration.

3.2.2 Electronic Speed Controller

The ESC for the test bench needs to have the ability to control the electric motor under a variety of load scenarios. For combustion starting the speed controller must be able to read the position sensors and provide enough current to overcome ICE compression. Additionally, the speed rating and telemetry capability of the ESC must meet the operation range of the SKP 6485 and test bench requirements.

	Value	Unit		Features
Voltage Range	6-75	V		CAN,USB,UART communication
Current (Continuous,Burst)	300,450	A		Sensored/Sensorless control
External Electronics	3.3-12	V		Analog/Digital inputs and outputs
External Electronics	0.5-1	A		Regenerative braking

Table 4: Vedder Electronic Speed Controller (VESC) 75/300 specifications and features

This ESC is capable of 75 volts at 300 amps continuous which is well above the PMSMs capability but future-proofs the test bench for high power applications. Most importantly this electronic speed controller supports hall and temperature sensors while also using various versions of CAN which are in many UAVs at CfAR. The software (discussed later in this section) that comes with the VESC 75/300 also provides many features that increase telemetry collection, precise control, and increased safety.

3.2.3 Internal Combustion Engine

Small-scale combustion engines for UAVs are often two stroke engines that use a carburetor for fuel management. Unfortunately, carburetors do not provide telemetry or precise control over the combustion engine operation. This means that electronic fuel injection is required from the small-scale ICE to be viable for the hybrid test bench. The Corvid-50 from Currawong Engineering offers a two-stroke engine with electronic fuel injection and a small generator (not used for the test bench application). As per most two stroke engines this unit requires 91 octane fuel with a 50:1 fuel oil mixture. The specifications and features of the engine are shown in Table 5 below.

	Value	Unit		Features
Power	2.8	kW		Air cooled
Displacement	50	cc		Electronic fuel injection
Max. Speed	8000	RPM		Full telemetry suite
Weight	3.89	kg		Reduced BSFC vs Carbureted

Table 5: Corvid-50 specifications and features

The combustion engine comes as a ready to install package that includes everything needed to mount and run the power unit. There is an ECU included with the package called the IntelliJect

(discussed in a later section) which controls the EFI and timing of the two-stroke engine. The EFI system is fed by a self-priming fuel pump design by Power4Flight which operates between 250 and 350 kilopascals. To prevent engine damage, cylinder head and manifold temperature sensors are installed which control the active cooling cowl to open or close the inlet flap.

The mounting system for the Corvid-50 is a three-post configuration that connects directly to the block of the engine. Each post consists of two rubber mounts, one at the block and another at the chassis mounting location. These mounts are designed to cantilever off a bulkhead with a propeller on the crankshaft; this setup does not work for the test bench. These motor mounts were upgraded to stiffer solid rubber cylinders to better stabilize the motor since the crankshaft is more constrained than intended by the manufacture.

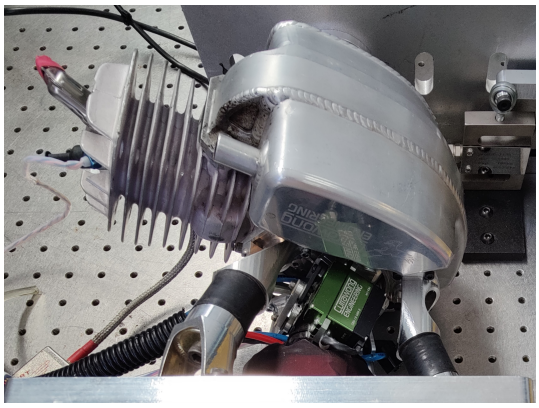

Figure 33: Corvid-50 engine with updated mounts.

This combustion engine package is ideal for the test bench application because it is purpose built for small-scale UAV applications. The collection of sensors allows for extensive telemetry and personalized control over engine operation. The ECU (discussed in the next subsection) allows for full tuning, limiting, and data collection of the engine operation which is required when designing hybrid-electric propulsion systems. The features from this engine package allow for no gaps in information and provides all the data required to design, tweak, and optimize the hybrid system.

3.2.4 Engine Control Unit

The IntelliJect engine control unit is responsible for controlling every part of the combustion engine system. This means it dictates software limits, uses lookup tables, reads sensor values, and displays real time data. The following sensors are supported by the ECU:

- Input voltage
- Manifold air temperature (MAT)
- Cylinder head temperature (CHT)
- Manifold air pressure (MAP)
- Fuel pressure
- Analog throttle position sensor (TPS)
- CPU temperature
- Humidity
- Digital barometer
- Outside temperature (OAT)
- Input current
- Analog barometer

These sensors are used to calculate and command the inputs/outputs of the ECU to control the speed, torque, and throttle of the combustion engine. This is accomplished using governors, lookup

tables, and curves in the IntelliJect software (discussed at the end of this section). This control unit has onboard power conditioning allowing for an input rating between 8-30 volts. The ECU is packaged into a 71.3 gram case measuring 54.4 millimeters by 80.4 millimeters which is ideal for small-scale UAV applications where both weight and envelope are restricted.

3.2.5 Clutch

The electromagnetic clutch used in the hybrid system is responsible for connecting/disconnecting the combustion engine from the electric side, making it a parallel system. Selecting a clutch requires a specification that satisfies the rotational speed of the system and the torque that needs to be transferred through the clutch. Size and weight can also be a factor when selecting a clutch that will be installed in an aircraft, though there may not be many options depending on the speed and torque requirements.

The first electromagnetic clutch selected for the hybrid test bench in 2020 was a Miki 101-06-11G-24V small-scale unit. The clutch was rated for 8000 rotations per minute and 5 newton meters of torque, the maximum nominal torque from the combustion engine is 4.06 newton meters. Unfortunately, once load was applied to the hybrid test bench the clutch slipped continuously at any speed and throttle. This was caused by the torque spikes generated during the combustion cycle, which are not taken into account when looking at nominal torque values for the engine.

Looking at the combustion data and talking with another hybrid development it was agreed that torque spikes can reach up to ten times that of the nominal value. Using this value, it was important to select a new clutch that was capable of 40 newton meters of torque, Table 6 below shows the specifications of the chosen Mayr ROBATIC Type 4/500.301.0.

	Value	Unit
Nominal Torque	40	Nm
Diameter	100	mm
Voltage	24	V
Max. Speed	7000	RPM
Weight	1.5	kg

Table 6: Mayr 500.301.0 Type 4 specifications

Finding an electromagnetic clutch that meets the 7500 RPM limit of the Corvid-50 and the 40Nm torque spike values was very difficult and Mayr is the only company which supplies clutches that closely matches these requirements. The clutch is more than capable of handling the torque of the system; tests have been run where it has experiences twice the load of the previous clutch without slipping. The clutch is relatively large for small-scale UAVs with a weight of 1.5 kilograms and a diameter of 100 millimeters but has been the most reliable clutch thus far. Engineers at Mayr clarified that the maximum speed is at maximum sustained torque, meaning it can be run at higher speeds with lower loads. With the clutch specified and working well the next step was the test bench design is to improve the performance of the belts and pulleys.

3.3 Belt System

Similar to the clutch requirements the belts and pulleys must be speed and torque rated for the power running through the system. Early iterations of the belt system used aluminum timing pulleys that were held onto the shaft via set screws. During operation these pulleys would slip and rotate on the shafts because of the high combustion torque. The torque spikes from the combustion engine would also cause the belt tensioners to loosen and snap.

The timing pulleys were upgraded to aluminum timing pulleys with keyways, these keyed features stop the pulley from rotating on the shaft improving the torque capacity. The new pulleys also allow for a wider timing belt increasing from 9.5 to 12.7 millimeters, the increased surface area provides more torque/power capabilities. The current ratio between the combustion engine and electric motor is one to one since they share almost identical speed ranges. The belt system in the dynamometer however is a 2.25:1 ratio because the much large BLDC for braking has a maximum speed that is near half of the two power units in the hybrid system.

A belt tensioner is required for multiple reasons when designing a belt system. The first being that finding a belt that is the exact required length for the application is often difficult. Another reason is for assembly and maintenance, buying a belt that is longer than required makes it easier to service the belt without removing the pulleys from the system. The last cause for a belt tensioner is to allow the belt to flex while still maintaining enough tension to engage the pulley and rotate without slippage.

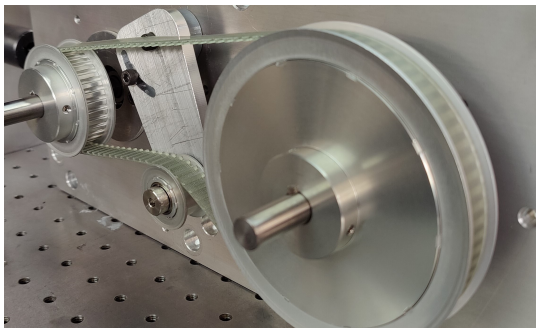

Figure 34: Upgraded belt system with keyways and tensioner.

The tensioner design is fundamentally the same as most off the shelf options but smaller in scale. An aluminum plate with a pivot bolt and slide groove is connected to one of the system plates. An idler pulley is connected to the end of the tensioner plate via a shoulder screw; allowing smooth rotation and minimal wear. When the pivot bolt and groove bolt are loose the tensioner is free to pivot increasing or decreasing the tension applied to the belt by the idler. The adjustment range was calculated to allow for a variety of pulley ratios which changes the location of the belt line substantially. This belt tensioner holds tension on any belt and pulley combination on the test bench and does not loosen after prolonged use and high load.

3.4 Torque Sensors

Knowing the power of the hybrid system at different points of interest is key to designing, optimizing, and controlling the system. One of the fundamental ways to find mechanical power is to collect the speed and torque at a given location. There are two key locations where this data should be collected, at the output of the PMSM and at the input of the dynamometer generator.

To find the torque at these locations load cells are used to measure the tangential force being exerted by the motor. A torque arm is connected to the motors mounting bolts which creates a known distance from the rotational axis and the mounting points for the load cells. Two load cells are mounted to the torque arm using shoulder screws and heim joints. The joints allow for misalignment and rotational freedom to reduce binding which guarantees the force being read is linear with the load cell axis.

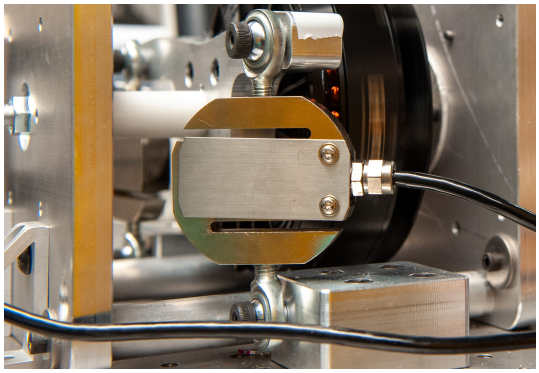

Figure 35: Dynamometer load cell mounting solution

The calculation of torque is simple once the force reading is collected from the load cells. The force at the load cell is multiplied by the distance from the rotational axis to the mounting hole. This provides a torque value whose accuracy is dictated by the load cells and CNC machining used to create the torque arm. Having these two torque arm setups on the PMSM and dynamometer provides the input and output torque of the electric side of the system. For the combustion engine torque, the ECU calculates the value generated by the combustion engine using the speed sensor and power map. These torque measurements are then combined with speed readings to calculate the power of the hybrid system.

3.5 Rotational Speed Sensors

Two locations on the test bench have rotational speed sensors; one attached to the output shaft of the combustion engine before the clutch disc and the other on the input shaft of the dynamometer. The speed is measured via a hall effect sensor circuit mounted to the plates near the shafts. Hall sensors react to a magnetic field and are often used to detect proximity, position, speed, and current.

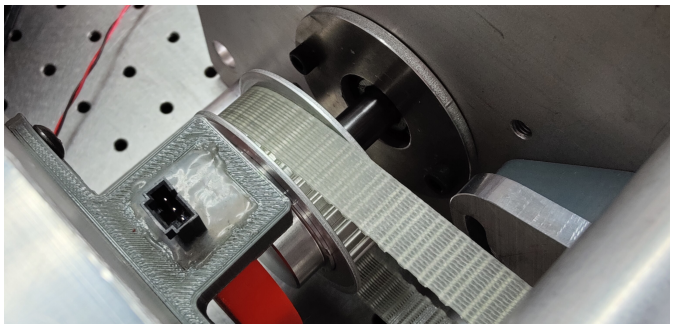

Figure 36: Potted hall effect sensors with orange magnet disc housing

For speed detection the hall effect circuit is mounted near the rotating shaft which has a disc attached to it. In the disc is a single neodymium magnet, when the magnet passes by the hall effect sensor a voltage is generated. This magnet passes the sensor more frequently as the shaft rotates faster, creating a square wave signal when connected to an oscilloscope.

To calculate the speed from the signal generated by the hall effect sensor the frequency of the square wave must be found. In theory this is accomplished by inverting the period, however for experimental signals it also requires some filtering to reduce noise and errors. This frequency can then be converted to any speed unit such as radians per second or rotations per minute. With the torque and speed sensors installed the power of the system can be measured at the two locations allowing for a better understanding of how power is split between the power units as well as the losses through the drivetrain. These power values paired with the ones provided by the VESC, ECU, and programmable load provides all the input/output information required to control the hybrid test bench effectively.

3.6 Dynamometer

The hybrid test bench requires a load be applied to properly test the operation of the clutch, combustion engine, and electric motor. Small-scale UAVs often use propellers and this is how load was applied for earlier versions of the test bench. This provides predictable and smooth torque load on the system since the torque created by the propeller is directly connected to its speed.

Using a propeller has two major drawbacks; it cannot induce a rapid torque change or simulate a variety of flight scenarios. Using a dynamometer removes both of these challenges while also increasing the safety of the test bench by removing an exposed spinning object. The dynamometer on the test bench acts as an electric brake only which is able to apply torque almost instantly and can simulate every segment of a mission profile. This means the load can be increased to simulate the climb segment of a mission then reduced to reflect the transition to cruise or any other scenarios possible. The power from the output of the parallel system is measured by the torque and rotational speed sensors discussed early that are installed in the dynamometer.

3.6.1 Electric Brake

To apply load to the propulsion system a T-Motor U15II KV100 brushless DC motor is used. The specifications of the motor can be found in Table 7 below. This motor is geared down by a 2.25:1 pulley ratio due to its lower maximum speed compared to the propulsion system.

Parameter	Value
Voltage	48 V
RPM/V	100
Maximum Power	9942 W
Rated Torque	17.8 Nm
Rate Speed	4328 RPM
Continuous Current	171 A
Construction	36N42P

Table 7: Key specifications for the TMotor U15II

The three-phase power generated by the motor spinning passively is rectified to create a DC voltage and current. Connecting the programmable load to the rectifier applies a current that can be set by the test bench operator. The current applied by the programmable load creates a mechanical torque on the propulsion system which can be calculated using the T-Motor's torque constant. This resists the rotation of the hybrid output shaft and represents the loads that could be experienced during flight.

3.6.2 Rectifier

Similar to the ESC which uses MOSFETs and an MCU to convert DC power to controllable three phase power a rectifier converts three-phase into DC passively. The rectifier is connected to the brake in the dynamometer which creates three-phase power when spun by the hybrid-electric system. The rectifier allows the programmable load to apply mechanical resistance to the system via a DC load.

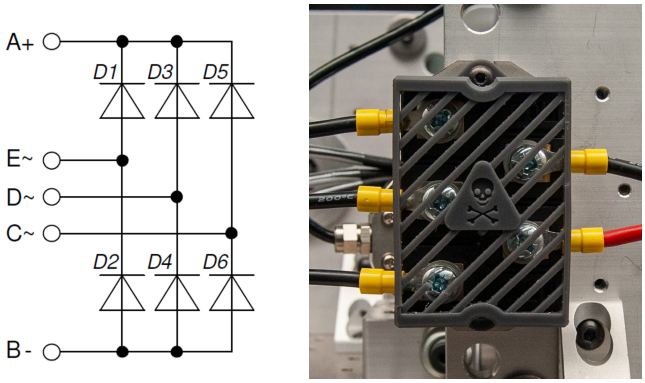

Figure 37: Rectifier circuit and unit

This converts the generator to a fully adjustable electronic brake with continuous control over the amount of torque being applied to the hybrid system. The rectifier used on the test bench is a IXYS VUO190-18NO7 which is rated for 250 amps RMS and 1800 volts. This rectification unit is robust and provides enough overhead for future iterations of the propulsion system with larger power units and higher conversion demands.

3.6.3 Programmable Load

The programmable load on the test bench is an Array 3756A electronic programmable load which is capable of 5 kilowatts, with a combination maximum of 240 volts and 260 amps. The unit can be manually programmed via the front panel applying multiple different types of signals. There are four main modes for the electronic load: constant voltage, constant current, constant resistance, and constant power. Constant current mode is used for the test bench as this generates a constant torque when connected to the dynamometer.

Figure 38: Array 3756A programmable load

While using the front panel inputs it is possible to toggle the load, input a single command, or apply a table-based sequence of loads. This manual mode is particularly useful for quick tests and simple load testing. Using the remote operation mode allows for more complex signal commands via the serial, RS232, and GPID ports on the rear of the 3756A. The commands are sent via Standard Commands for Programmable Instruments (SCPI) protocol and allow for more complex and dynamic signals to be loaded which is ideal for simulating a full mission profile on the test bench. Using the communication ports also allows for the programmable load to synchronize with the LabVIEW data collection which is required for controlling components on the test bench.

3.7 Software

The components and controllers used in the hybrid test bench require software to adjust settings and write configurations to run the system. Once the configurations are written to the controllers it is possible to run the system without active software. However, when operating the test bench, the software is left open to monitor live telemetry and send/check commands that are being sent to the electric and combustion system. The software used for the VESC, IntelliJect, and external sensors on the test bench are discussed in the sections below.

3.7.1 VESC Tool

The electronic speed controller is responsible for running the SKP 6485 and does so via the VESC Tool software. The software has an array of settings, features, and a graphic user interface (GUI) that allows for a high-level of control over the PMSM. The software has four key sections that are used consistently for the test bench and are explained below.

The setup section of the software is used to characterize the motor connected to the ESC and to generate initial settings. Once the motor is fully connected a setup wizard is used, in this window it will ask for the motor type, number of poles, approximate size, and battery specifications. The software will spin the motor through a range of speeds and ramps, once complete the software will display the motor parameters.

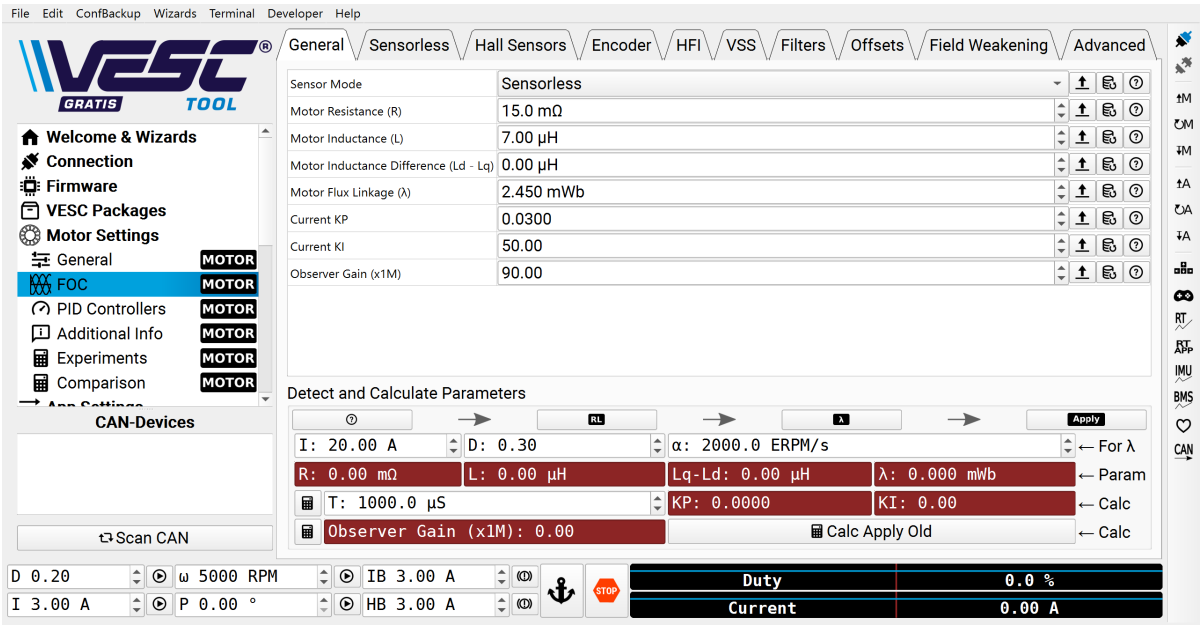

Figure 39: VESC software showing field-oriented control (FOC) control setting

Once this setup is completed the VESC tool then configures the software settings to represent the ideal operation for the PMSM. This includes setting the proportional, integral, and derivative (PID) gains, voltage and current limits, ramp speeds, and sensor calibrations. If the values are not what the operator wants, they can be modified and written to the ESC configuration.

The motor setup section of the software has a collection of settings to dictate how the motor is controlled, when to limit operation, and the response of the motor. Some note worth settings are:

- Control type – trapezoidal, DC, FOC, and GPD
- Sensor mode – hall sensors, encoder, resolver, custom
- Current values – motor, brake, battery, regeneration maximum
- Voltage values – start and end cutoff voltage
- RPM – maximum speed forward and reverse
- Temperature – safety limits for MOSFET and motor temperature
- Control type setting – sets PID gains, ramp speeds, motor parameters, sensor settings, and filters

Adjusting these parameters allows the motor to operate in any state other than what is limited by the physical PMSM. Once setup correctly the settings are written to the electronic speed controller configuration. This ensures that the configuration file is stored on the ESC which provides the option to operate the PMSM without being connected to the software.

In the VESC tool there are options that dictate which communication and input pins are used by the ESC. The application has the following settings that are part of the microcontroller operation:

- Communication – PPM, UART, ADC, NRF, PAS, and combinations
- Baud Rate for CAN
- CAN mode – VESC, UAVCAN, Comm bridge
- Kill switch mode – PPM low/high, ADC low/high

The communication settings allow for the selection of what inputs are being used on the VESC which includes: throttle inputs, data logging, external sensors, and multi-ESC linking. An analog or wireless throttle input device such as a potentiometer can be selected and mapped in this section by using the input wizard. The kill switch feature looks for a voltage change on the analog or PPM pins; this is used on the test bench for an emergency stop button. These settings are saved to a configuration file that can be loaded at any time.

The telemetry capabilities of the VESC are substantial and there are numerous ways to visualize and modify the data. In the VESC tool it is possible to activate real time data which shows graphs of currents, temperatures, RPM, rotor position, and control mode states. This provides a quick and seamless opportunity to see the current operating state of the PMSM. If having the software running is not wanted or required, the data can be logged to a comma-separated values (CSV) file to be later analyzed. This data logging can also occur while using the software and looking at real-time graphs during operation. There is also the option to log and view data from a GPS, gyroscope, and accelerometer which is particularly useful for mobile applications. Compared to other ESC software the VESC tool provides more than enough settings and data collection to develop/characterize the hybrid propulsion system.

3.7.2 IntelliJect

The Corvid-50 combustion engine uses electronic fuel injection and therefore also needs software to modify, monitor, and control the ECU. The IntelliJect software is responsible for keeping the timing, fuel ratio, and operation of the combustion engine in a safe, stable range. This software primarily uses lookup tables and limits to dictate if the current operating state is acceptable.

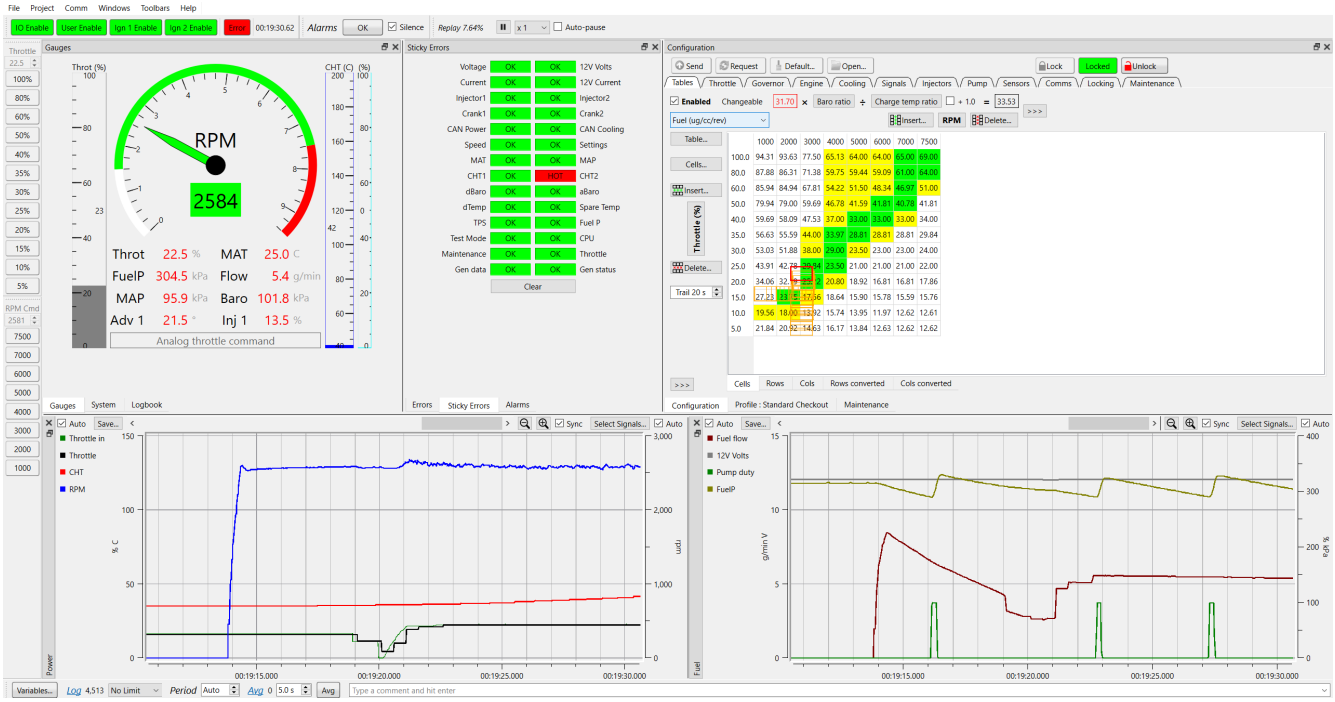

Figure 40: IntelliJect software user interface with live telemetry

There are two control inputs for the combustion engine in the software that are user operated: throttle and speed. The functionality of the ECU is fundamentally the same with either input mode, throttle maintains a specified throttle position while speed uses PID to maintain the requested value. There are numerous settings and lookup tables in the software that can be modified, some include:

- Power map – A two-dimensional table that relates throttle position, speed, and power. Depending on the input mode speed or throttle is determined by the power required by the system
- Manifold pressure map – A two-dimensional table to determine speed or throttle based on the manifold pressure
- Air flow map – Lookup table relating the speed, throttle, and air flow rate for combustion
- Fuel flow map – Same as the air flow map but for fuel
- Throttle curve – Used to map the throttle input and output
- Governor – This feature is used with PID to maintain throttle and/or speed set points
- Engine setting – This section is used to set rev limits, adjust crank angle sensors, and set ambient temperature
- Injector settings – Used to calibrate the ECU for specific injectors, this includes flow rate, minimum pulse time, pressure, and puddle time
- Pump settings – The pump uses PID to maintain an operating pressure, these settings adjust the gains, setpoint, prime time, and allowable error
- Sensor settings – These settings adjust which sensors are active and their required calibration parameters
- Communication settings – Set the baud rates, ports, and telemetry frequency for UART, CAN, and serial

These settings and maps can be modified to increase efficiency, power, timing, and smoothness of the combustion engine. This software can be used with any combustion engine that has the required sensors once the tables are properly tuned for the engine. The IntelliJect software displays any telemetry that is desired in real time while automatically logging the data to a CSV file. Similar to the VESC, once the software configuration is written to the ECU the combustion engine can operate without software and can take command from wireless or wired inputs. The software provides a full suite of sensor and control data to analyze the combustion engines operation during experimental testing on the test bench.

3.7.3 LabVIEW

The final piece of software used for the parallel test bench is LabVIEW by National Instruments. Unlike the other two software LabVIEW is a graphical integrated development environment (IDE) used for data acquisition, instrument control, and automation. The programming and GUI used in LabVIEW was created in house and used exclusively for the current test bench configuration.

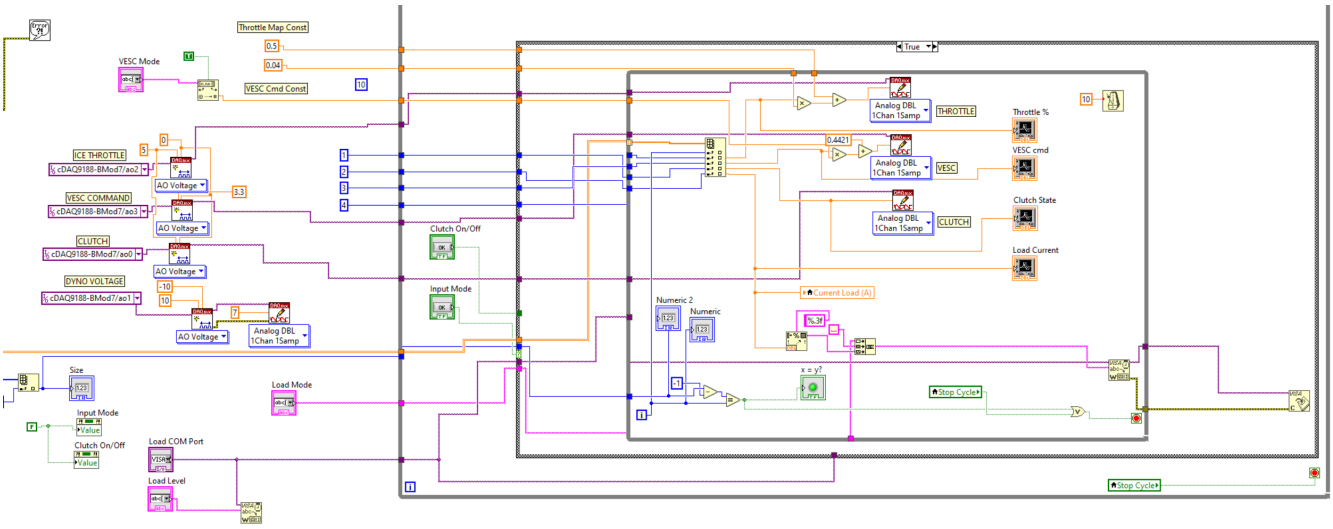

Figure 41: Visual programming used in the Labview software

This software is used to read, log, and filter data from the hall effect sensors and loads cells: while also executing the mathematics to find the speed and torque discussed in the components section. A GUI was created to show live data from these sensors, zeroing values, activating the clutch, and initiating logging. There are also multiple warning indicators in the GUI to indicate high voltage, clutch slip, and other errors.

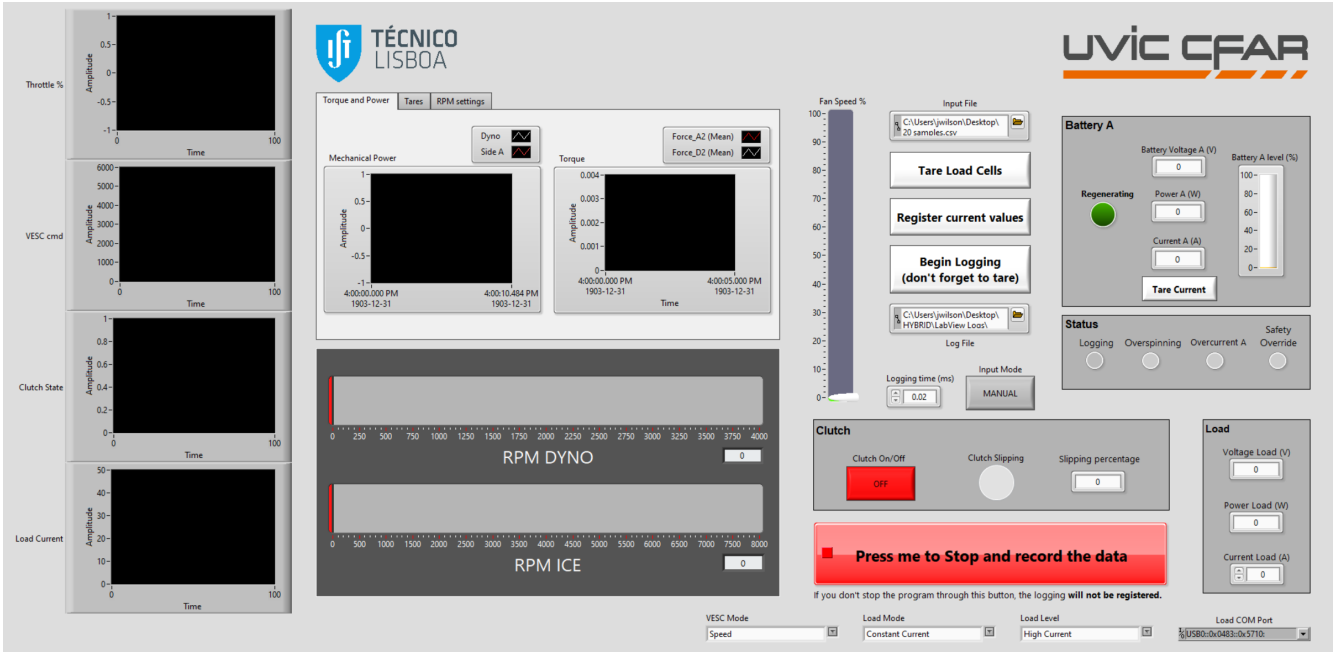

Figure 42: GUI created in house for test bench control

LabView from National Instruments holds complete control over the data acquisition modules connected to the hall sensors, strain gauges, and voltage regulators on the test bench. This means that the number of samples and frequency at which those samples are recorded is adjustable by the user. Additionally, the LabView software sends commands to the programmable load, ECU, and ESC. The data from this software is sampled at the same frequency as the VESC and IntelliJect software so that all data has similar resolution. The LabVIEW data combined with that of the ECU and VESC creates a complete characterization of the hybrid test bench. The telemetry provides the ability to compare power, speed, and torque both electrically and mechanically from input to output. This generates the data required from experimental testing to validate the propulsion system for any mission profile and/or airframe.

4 Computational Model

The main goal for this thesis work is to create a mathematical model of the parallel hybrid-electric propulsion test bench for use in Model Based Design (MBD). A mathematical model can provide prediction of the systems response, capabilities, and performance metrics without running a physical system. Experimental data is equally important and should always be collected when possible but having a simulation model in addition provides great benefit.

An accurate model of the system increases the opportunity to test components before they are purchased or installed into the test bench. Collecting the required parameters of a given component and adding it to the model allows for virtual component testing without investing money and time in experimental testing. This process can be used to choose between multiple component options based on their performance in simulation.

Additionally, having a mathematical model of the hybrid propulsion system is a useful tool for model based aircraft development. A model of the propulsion system can be used to run specific mission profiles and load scenarios that a future aircraft is expected to experience. This will provide information on whether the current propulsion system is viable for the aircraft or what components need to be upgraded before design and integration. This can increase the production speed of the aircraft while reducing the amount of time required to characterize and test the propulsion system. More importantly having a model allows for better optimization since the system is characterized before design: reducing the need for over specify components due to uncertainty.

This section discusses the process of creating a mathematical model of the hybrid propulsion system using MATLAB/Simulink. This includes component level modelling to represent the parts used on the test bench. Operating mode logic is described to characterize the different modes that the propulsion system operates in depending on the commands sent. Lastly the logic used to determine the speed and torque of the two power units depending on the state of the system was created.

4.1 Components

The fundamental level for modelling begins with each individual component in the system. This often includes finding or deriving the governing equations for the component. Once these equations are found the required parameters must be collected from a specification sheet, calculated, or found via experimental testing. Once all parameters are quantified testing the component model separately from the full system allows for better verification of the model.

If possible, running experimental testing on the component can provide data to further validate the model created. Using the same inputs in simulation as the experimental test is required to ensure that the comparison is legitimate. Any assumptions and simplifications made in the modelling process should be stated to provide understanding of the accuracy and what scenarios the model is designed for. This section covers the process of modelling each individual component in the propulsion system using these methods.

4.1.1 Electric Motor

The SKP 6485 is a surface mounted permanent magnet synchronous motor (PMSM), this means it uses three-phase input voltage to control phase currents, speed, and torque. Two important parameters can be calculated from the specifications found in Table 3: the motor back-electromotive force (EMF) constant (K_e) and torque constant (K_T). The motor back-EMF constant is the relationship between the reactive EMF and the speed of the motor (Equation 2); the faster the motor spins the higher the back-EMF and vice versa. The motor torque constant is directly related to the motor's design and indicates the amount of current for a given torque output, shown in Equation 1. Using Kirchoff's Voltage Law proves that both constants are equal when using the correct SI units. The two constants were calculated using the maximum values shown in Table 3 above.

$$T = IK_T \tag{1}$$

$$\omega = \frac{V_E}{K_E} \tag{2}$$

These two equations provide a simple electromechanical model of the PMSM motor, which is acceptable for rudimentary applications. These equations only show the current and voltage required for a specific torque and speed. For the hybrid propulsion system, a far more complex model was required to show transient responses, spin up speed, phase values, power, etc. This more complex model could be derived using various electric and mechanical laws which require extensive knowledge on the inner workings of a PMSM motor. MATLAB contains models for various motor types and are well documented which provides confidence in the model's capabilities.

The Surface Mount PMSM model by Mathworks [79] provides a detailed model that fits the specifications of the SKP 6485 used on the test bench. This model was built for a specific type of motor configuration, Table 8 below compares the model and SKP 6485 profiles.

	PMSM Model	SKP 6485
Input Voltage	Three-phase	Three-phase
Magnet Configuration	Surface Mounted	Surface Mounted
Back-EMF	Sinusoidal	Sinusoidal
Control Method	Field-Oriented Control	Field-Oriented Control
		Six-Sector Commutation

Table 8: Comparing the PMSM Simulink model and the electric motor

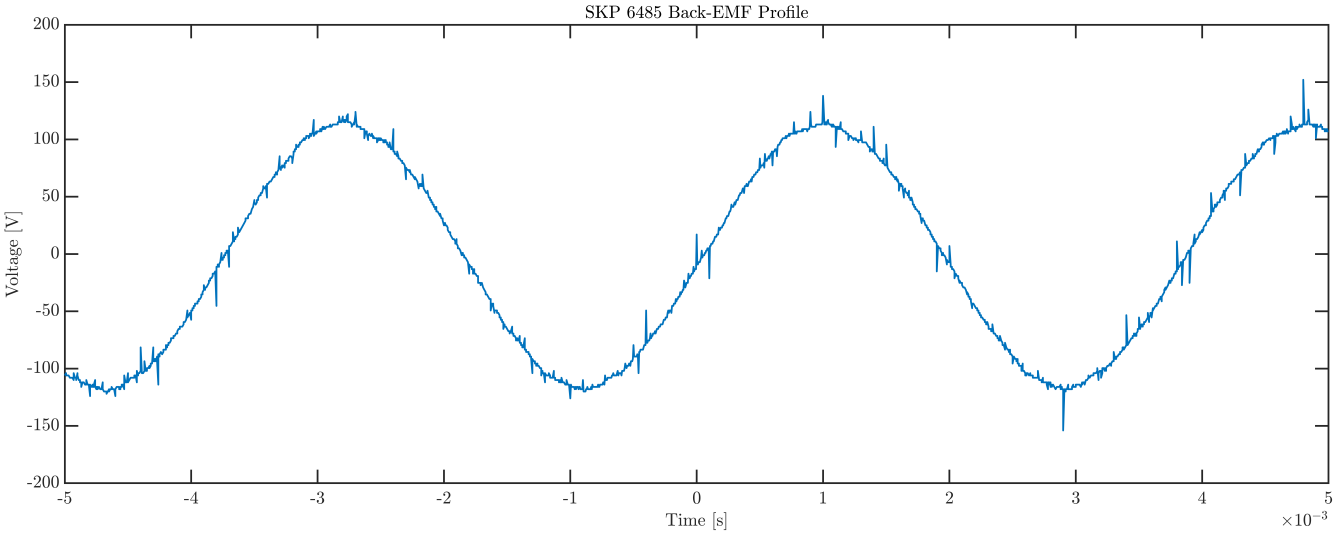

Figure 43: Measured back-EMF profile of the SKP 6485

There are four main motor parameters that are needed in the following equations to characterize the electric motor response. These include motor winding resistance, inductance, quadrature direct inductance difference, and flux linkage constant. These values need to be measured or found in the specification sheet. These values were measured using the VESC tool software for the electronic speed controller (ESC).

Parameter	Value
Winding Resistance	10.20 mΩ
Motor Inductance	11.39 μH
L_q-L_d	4.31 μH
Motor Flux Linkage	3.88 mWb

Table 9: SKP 6485 electrical properties from VESC software

Resistance and inductance are easily measured with an oscilloscope, multi meter, and LCM multimeter. The flux linkage constant is much more difficult to obtain but can be calculated using the following equations where P is the number of poles.

$$\lambda_{pm} = \frac{1}{\sqrt{3}} \frac{K_e}{1000P} \frac{60}{2\pi} \tag{3}$$

$$\lambda_{pm} = \frac{2}{3} \frac{K_t}{P} \tag{4}$$

The electric motor block provides a well detailed model that calculates numerous parameters that are required for a strong understanding of the motor response. The mechanical system of the motor is governed by Equations 5 and 6.

$$\frac{d}{dt}\omega_m = \frac{1}{J}(T_e - T_f - F\omega_m - T_m) \tag{5}$$

$$\frac{d\theta_m}{dt} = \omega_m \tag{6}$$

J	Combined inertia of motor and load	kgm^2
F	Combined viscous friction of the motor and load	$Nm/rad/s$
ω_m	Motor mechanical angular position	rad
T_m	Motor shaft torque	Nm
T_e	Electromagnetic torque	Nm
T_f	Motor shaft static friction torque	Nm
ω_m	Angular mechanical velocity of the motor	rad/s

Table 10: Variable definitions for mechanical governing equations for the PMSM

Equation 5 uses Newton's Second Law for rotation, the mechanical acceleration of the electric motor is found using the sum of torques divided by the second polar moment of inertia. The torque sum takes into account the load on the shaft, electrical torque, and the losses due to friction. To find the mechanical speed of the motor, use the derivative of the position with respect to time.

Finding the mechanical dynamics of the electric motor is far simpler than the electric properties of the PMSM. The first section of the electric model is the three-phase system which uses the speed, current, and voltage to characterize the motor. These equations have two reference frames: the motor flux frame and stator axis. In the motor flux frame there are two axes, the direct axis is aligned with the rotor magnetic axis while the quadrature axis is perpendicular to the direct axis [80]. These two axes are denoted with the subscript d and q respectively and are shown in Figure 44. Equations 8 through 10 characterize the dynamics of the electric motor using the electrical domain:

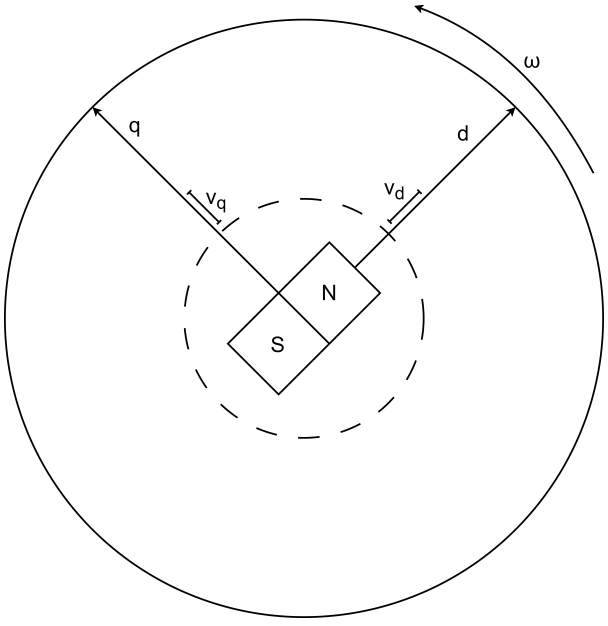

Figure 44: Axis orientation for PMSM

$$\omega_e = P\omega m \tag{7}$$

$$\frac{d}{dt}i_d = \frac{1}{L_d}v_d - \frac{R}{L_d}i_d + \frac{L_q}{L_d}P\omega_m i_q \tag{8}$$

$$\frac{d}{dt}i_q = \frac{1}{L_q}v_q - \frac{R}{L_q}i_q + \frac{L_d}{L_q}P\omega_m i_d - \frac{\lambda_{pm}P\omega_m}{L_q} \tag{9}$$

$$T_e = 1.5P[\lambda_{pm}i_q + (L_d - L_q)i_d i_q] \tag{10}$$

L_q, L_d	q- and d-axis inductances	H
R	Stator winding resistance	Ω
i_q, i_d	q- and d-axis current	A
v_q, v_d	q- and d-axis voltage	V
ω_e	Angular electrical velocity	rad/s
θ_e	Electrical angle	rad

Table 11: Variable definitions for electrical governing equations for the PMSM

The multiple power values of the PMSM are required to realize the efficiency of the system, what power is being transmitted, and which parameters influence power. The equations below calculate power values using stator and mechanical parameters which are the two domains responsible for rotating the PMSM. Mechanical power uses speed and torque to calculate the rotational power of the PMSM. The bus power is found using the sum of the products for each phase of the input. Mechanical power loss is related to the viscous and load frictions of the PMSM which resist rotation. Electrical losses are caused by resistance in the stator for both the direct and quadrature current. The last calculated power value is the stored power which represents the summation of the previous four powers.

$$P_{motor} = -\omega_m T_e \tag{11}$$

$$P_{bus} = v_{an}i_a + v_{bn}i_b + v_{cn}i_c \tag{12}$$

$$P_{elec} = -\frac{3}{2}(R^2 +_s i_q^2) \tag{13}$$

$$P_{mech} = -(\omega_m^2 F + |\omega_m|T_f) \tag{14}$$

$$P_{store} = P_{bus} + P_{motor} + P_{elec} + P_{mech} \tag{15}$$

i_a, i_b, i_c	Stator phase currents	A
v_{an}, v_{bn}, v_{cn}	Stator phase voltages	V

Table 12: Variable definitions for power governing equations for the PMSM

These governing equations build the model block for the PMSM which requires two inputs: load torque and phase voltage. For the hybrid system this represents the rotational load from the test bench and voltage from the electronic speed controller. In order to generate the outputs, the following parameters are required:

- Number of poles
- Stator resistance
- d-axis inductance
- Flux linkage constant
- Back-EMF constant
- Torque constant
- Load inertia
- Load viscous damping
- Load static friction

These parameters combined with the governing equations and inputs generate the model outputs which include the phase current, motor torque, and motor speed. Additionally, there is an information bus which outputs all the variables used in the governing equations. This model has enough complexity and flexibility to create a PMSM response that represents what occurs on the physical test bench.

4.1.2 Electronic Speed Controller

As seen in the PMSM model the electric motor requires a three-phase input in order to spin. While Simulink has multiple three-phase generators that could work with the PMSM model; this would create an open-loop control scheme that performs poorly. This is why the surface mount PMSM controller [81] is used to represent the electronic speed controller.

There are two main control schemes for a PMSM/BLDC: Six-Sector Commutation and FOC. Six-Sector Commutation is the most common control method which commutates ever 60 mechanical degrees and only energizes two phases at a time. This scheme requires one PID controller and is much simpler because it does not require electrical transforms. This method is used for trapezoidal back-EMF BLDCs since those configurations do not benefit from FOC and the back-EMF waveform matches the control profile. The SKP motor produces a sinusoidal back-EMF (shown in Figure 43) and the VESC supports FOC; therefore field-oriented control is used on the test bench. FOC commutates every 30 mechanical degrees and requires two PID controllers which produces a more sophisticated control scheme. A comparison of the two control modes is shown in Table 13 below.

	Advantages	Disadvantages
Six-Step Commutation	Simple control Low cost higher speed	High torque fluctuation Current noise Lower efficiency
FOC	Low torque fluctuation High efficiency Low noise Fast dynamic response	High cost Matching motor parameters Complex control

Table 13: Comparison of Six-step and FOC electric motor control methods

The model from Simulink provides closed-loop control with numerous inputs and parameters. The control scheme is shown in Figure 45, which uses feedback for speed, position, and current to control the speed of the electric motor.

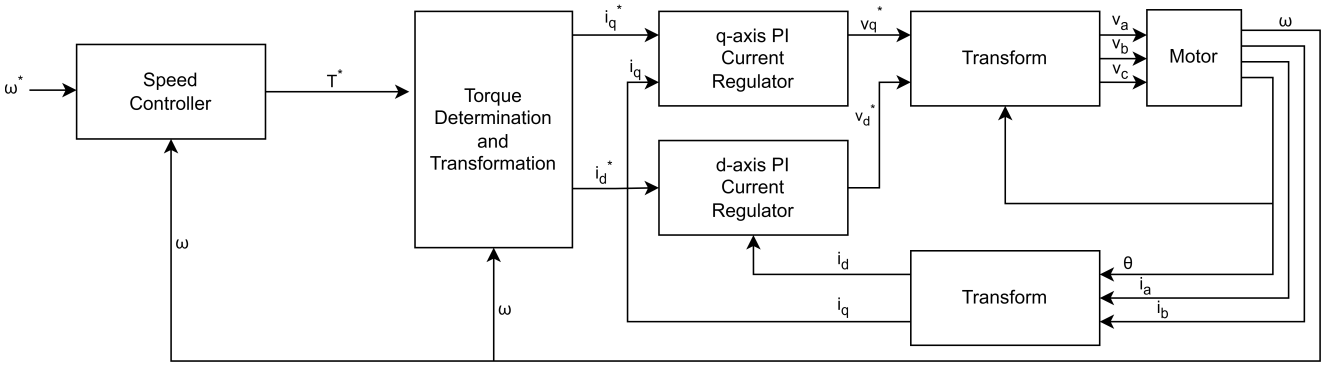

Figure 45: PMSM controller used for FOC control [82]

FOC control is accomplished by using PI control for both speed and current control. The proportional, angular, and rotational gains are calculated using the following equations:

$$z^3 + \frac{-3J_p + T_s b_a + T_s^2 K_{sa} + T_s^3 K_{isa}}{J_p} z^2 + \frac{(3J_p - 2T_s b_a - T_s^2 K_{sa})}{J_p} z + \frac{-J_p + T_s b_a}{J_p} \tag{16}$$

$$(z - p_1)(z - p_s)(z - p_3) = z^3 + (p_1 + p_2 + p_3)z^2 + (p_1 p_2 + p_s p_3 + p_1 p_3)z^2 - p_1 p_2 p_3 \tag{17}$$

$$b_a = \frac{J_p - J_p p_1 p_2 p_3}{T_{sm}} \tag{18}$$

$$k_{sa} = \frac{J_p(p_1 p_2 + p_s p_3 + p_1 p_3) - 3J_p + 2b_a T_{sm}}{T_{sm}^2} \tag{19}$$

$$K_{isa} = \frac{-J_p(p_1 + p_2 + p_3) + 3J_p - b_a T_{sm} - K_{sa} T_{sm}^2}{T_{sm}^3} \tag{20}$$

b_a	Speed regulator proportional gain
K_{sa}	Speed regulator integral gain
K_{isa}	Speed regulator double integral gain
T_{sm}	Motion controller sample time

Table 14: PMSM speed controller gain equation variable definitions

The model requires the physical parameters of the motor to determine the gains above as well as the feed-forward torque. This variable is required for torque determination and electric transforms, the equation below calculates this torque value.

$$T_{cmd\_ff} = J_p \dot{\omega}_m + F_v \omega_m + F_s \frac{\omega_m}{|\omega_m|} \tag{21}$$

Similar to the electric motor model this controller uses the two-axis approach to determine the base speed and current commands for the specified motors. The direct and quadrature frames are used to determine the following limits and variables:

$$T_{max} = \frac{3}{2} P(\lambda_{pm} i_q + (L_d - L_q) i_d i_q) \tag{22}$$

$$i_{q\_max} = \frac{v_m ax}{\frac{3}{2} P \lambda_{pm}} \tag{23}$$

$$\omega_{base} = \frac{v_{max}}{\sqrt{(L - q i_q)^2 + (\lambda_{pm})^2}} \tag{24}$$

$$v_d = -\omega_e L_q i_{q\_max} \tag{25}$$

$$v_q = \omega_e \lambda_{pm} \tag{26}$$

$$i_{max} = |i_{q\_max}| \tag{27}$$

$$v_{max} = \frac{v_{bus}}{\sqrt{3}} \tag{28}$$

i_{max}	Maximum phase current
v_{max}	Maximum line to neutral voltage
v_{bus}	DC bus voltage
T_{max}	Maximum motor torque
T_{cmd}	Commanded motor maximum torque

Table 15: Variable definitions for speed and current commands

The controller also implements current regulation with anti-windup, this varies from conventional PI current regulators because it takes into account the direct/quadrature force coupling. This increases transient response accuracy in the system, which is ideal for the test bench system which has many switching modes. As per many electronic applications transforms are required, the controller uses Clarke and Park transforms to find the voltages and currents in the three-phase signal.

These governing equations for the closed-loop control scheme of the PMSM controller create a system response that represents the VESC on the test bench. The parameters for the controller contain the same variables as the electric motor with the addition of maximum motor torque. Gains for both the speed and current controller can be modified but the model block calculates these values from the motor parameters. These automatic gain calculations perform well and are relatively close to the gains found on the ESC which also automatically populates the same values. This controller, like the VESC on the test bench, generates a three-phase voltage for the PMSM that changes based on the motor speed command, torque load, and motor position. The control mode, feedback, and performance closely match the real-world application providing confidence in the model's capability.

4.1.3 Dynamometer

To represent the load experienced by the propulsion system during flight a dynamometer is connected to the hybrid-electric system. The dynamometer creates a loading profile by electrically braking the system with a T-Motor U15II KV100 which is rectified and connected to the programmable load. The motor specifications provided by the manufacturer are shown in Table 7 and are used to calculate the back-EMF and torque constant.

As explained in the test bench design section the programmable load applies a current to the electric brake (T-Motor) which results in a mechanical torque. The model for this setup is relatively simple because the motor is passive. The equations below represent the torque applied by the break and the voltage produced by the rotating speed.

$$T_{dyno} = K_t I \tag{29}$$

$$v_{rms} = K_e \omega_{in} \tag{30}$$

$$v_{dc} = \frac{1}{N_{pulley}} \frac{3\sqrt{3}}{\pi} v_{rms} \tag{31}$$

$$v_{rms} = \frac{v_{avg}}{\sqrt{3}} \tag{32}$$

v_{dc} is the rectified voltage from the electric brake that connects to the programmable load. The pulley ratio for the dynamometer is included because having the transformation in this model simplifies many other parts of the system model and reduces the number of times the ratio is applied. This simple model represents the parameters required to find the load and power that is applied by the dynamometer onto the parallel system.

4.1.4 Combustion Engine

The Corvid-50 combustion engine is a mechanical thermal system that uses combustion to create rotational motion. There are many complex models that derive the governing equations for the thermal, chemical, and mechanical processes. These models have incredible detail to determine what is occurring internally with accuracy. For the hybrid-electric system application, the resolution that is required from the ICE model is the same information that is available to the engine control unit on the test bench. In Simulink there are two categories of combustion engine models available (for both spark and compression ignition), these include the following:

- Core Engines: These models incorporate everything in a spark ignition engine from the intake to the exhaust port. This requires all inputs that an ECU needs to run and a separate engine controller model must be used.
- Mapped Engines: These engines combine the core and controller into a single model. This model uses lookup tables (maps) and engine parameters to determine the operating point.

As the descriptions show, the core engines provide more flexibility but the mapped engine models represent the same level of control that the Corvid-50 offers and simplifies the modelling process. The spark ignition mapped engine model from Simulink [83] is incorporated into the hybrid propulsion model for its close resemblance to the test bench application. The first set of parameters to be populated in the combustion engine model are the engine characteristics. These values represent the size, cycle type, fuel type, and environmental specifics, these values are shown below.

Characteristic	Value	Units
Number of Cylinders	1	—
Crank revolutions per power stroke	1	-
Total displace volume	5×10^{-5}	m^3
Fuel lower heating limit	46×10^6	J/kg
Fuel specific gravity	0.745	-
Ideal gas constant air	287	J/kgK
Air standard pressure	101325	Pa
Air standard temperature	293.15	K

Table 16: Combustion engine characteristics

With the engine controller built into the model the number of inputs is much lower than a separate controller configuration. The inputs required are the engine speed and torque load, with these commands the engine model will determine all required variables to output the operating state. This is determined with the following lookup tables, much like a car, which uses the governing equations to create the engine outputs.

The ICE governing equations start with the normalized and nominal air mass of the engine, which is determined at bottom dead center under environmental standard temperature and pressure.

This parameter is important for determining the amount of fuel required for specific air-fuel ratios which must stay in a certain range to create healthy engine operation.

$$M_{Nom} = \frac{P_{std} V_d}{N_{cyl} R_{air} T_{std}} \tag{33}$$

$$L = \frac{(\frac{60s}{min}) Cps \dot{m}_{intk}}{(\frac{1000g}{kg}) N_{cyl} N M_{Nom}} \tag{34}$$

L	Normalized cylinder air mas	-
M_{Nom}	Nominal engine cylinder air mass at STP, bottom dead center	kg
Cps	Crankshaft revolutions per power stroke	$rev/stroke$
P_{std}	Standard pressure	Pa
T_{std}	Standard temperature	K
R_{air}	Ideal gas constant for air and burned gas mixture	-
V_d	Displaced volume	m^3
N_{cyl}	Number of engine cylinders	-
N	Engine Speed	RPM
$\dot{m}_{intk}$	Engine air mass flow	g/s

Table 17: Variables definitions for air mass calculation

The fuel flow must also be calculated in conjunction with the air mass, this is accomplished using the characteristics of the fuel and the required mass flow rate for the specific air-fuel ratio.

$$Q_{fuel} = \frac{\dot{m}_{fuel}}{(\frac{1000kg}{m^3}) Sg_{fuel}} \tag{35}$$

$\dot{m}_{fuel}$	Fuel mass flow	kg/s
Sg_{fuel}	Specific gravity of fuel	kg/m^3
Q_{fuel}	Volumetric fuel flow	m^3/s

Table 18: Parameter definitions for fuel flow calculation

There are three power equations for this model that use the fuel rate, engine speed, and fuel lower heating value. Some of the values in these equations are determined using the lookup tables that are discussed later in this section.

$$P_{crank} = -\tau \omega \tag{36}$$

$$P_{fuel} = \dot{m}_{fuel} LHV \tag{37}$$

$$P_{loss} = P_{crank} - P_{fuel} \tag{38}$$

The first parameters that are required for all lookup tables in the controller section of the model are the speed and torque breakpoints. These breakpoints determine the operating range of the engine and must be the same across all tables to properly calculate operating points. The breakpoint arrays must also be monotonically increasing or decreasing because the model interpolates between

points to determine values. The breakpoints for the combustion engine on the test bench are as follows:

$$\tau_{BP} = [0\ 0.4059\ 0.6089\ 0.8118\ 1.0148\ 1.2177\ 1.4207\ 1.6236\ 2.0295\ 2.4355\ 3.2473\ 4.0591]\ (Nm)$$

$$\omega_{BP} = [0\ 2000\ 3000\ 4000\ 5000\ 6000\ 7500]\ (RPM)$$

Using these breakpoints all tables are populated with the map values found in the IntelliJect ECU and converted when required. The first lookup table is the power map which determines the power output of the engine based on the commanded torque and speed. The IntelliJect provides a power map in watts that requests speed and throttle. This map was converted to the desired torque map with torque command and speed, the conversion is shown below in the final map.

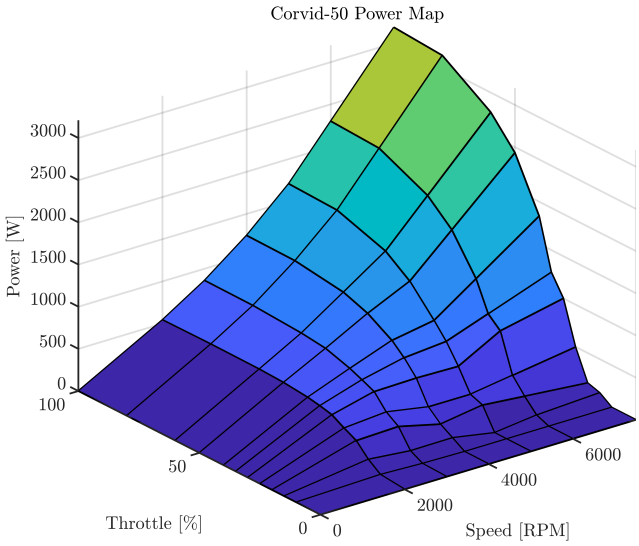

Figure 46: Corvid-50 power map

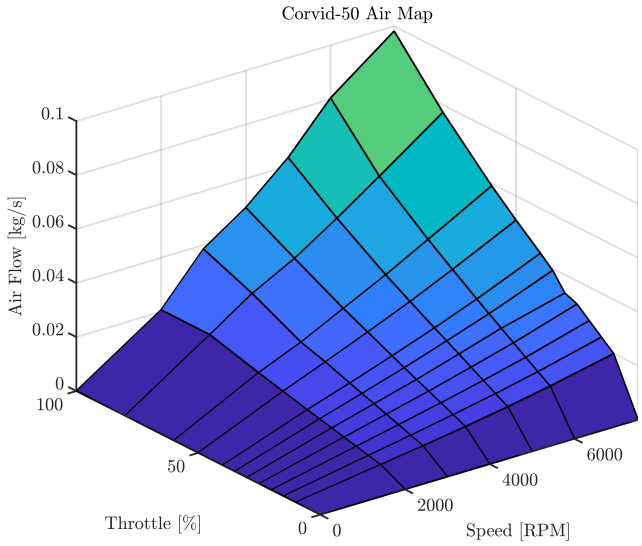

Figure 47: Corvid-50 air flow map

The conversion is based on one assumption; the throttle can be remapped as a percentage of maximum torque output. With this logic if the engine is sufficiently loaded adding throttle increases the commanded torque at a locked speed. Also, at a locked throttle if the load is increased the engine will reduce speed until stall or increase if load is reduced. The next map required for the combustion engine is the mass air flow in kilograms per second. Unlike the power map the air flow map is in the same units as the IntelliJect and only needs the throttle command changed to percent of maximum torque; the final map is shown in Figure 47.

The air flow map is followed by the fuel flow of the ECU map which requires its units converted. The ECU uses a fuel map which is a function of engine displacement and speed which allows it to scale across different engines. To convert the IntelliJect map in μg/cc/rev to kg/s the following equation was used to create the resulting table.

$$\dot{m}_{ice} = \frac{\dot{m}_{ECU} V_d \omega \times 10^{-9}}{60} \tag{39}$$

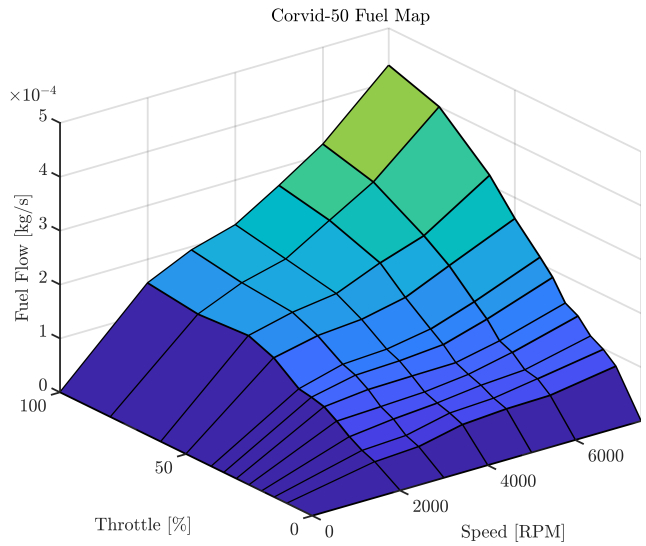

Figure 48: Corvid-50 fuel flow map

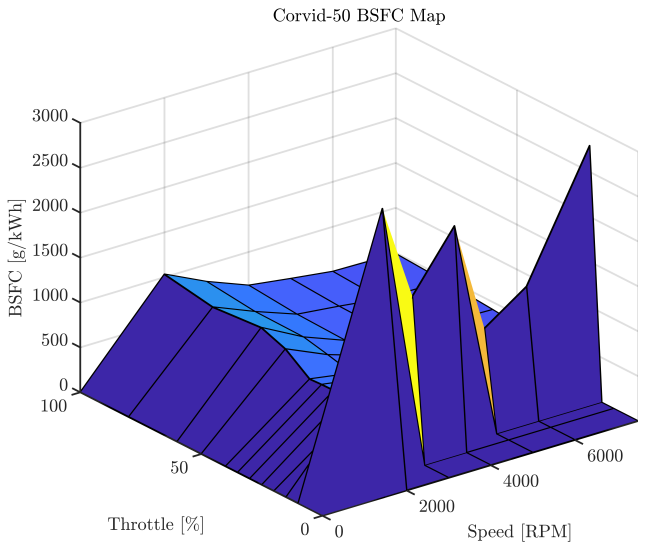

Figure 49: Corvid-50 BSFC map

The next table uses the fuel flow and power maps to determine the efficiency of the engine in terms of the brake specific fuel consumption (BSFC). This parameter represents the amount of fuel consumed per power unit created which is expressed in grams per kilowatt hour. BSFC is often used to compare engines that have significantly different characteristics; the conversion and resulting table are shown in Figure 49.

The remaining maps for exhaust temperature, hydrocarbons, carbon monoxide, nitrous oxides, carbon dioxide, and particulate matter are not provided by the IntelliJect ECU. To populate these tables the default maps from Simulink were scaled within the operating range of the Corvid-50. The emissions of this engine will be studied in the near future and the model will be updated when that data is available.

Since there is no additional controller for the combustion engine the full suite of inputs for an ECU is not required, this means there is no sensor array to model. The downside for not having a dedicated controller is that there is no telemetry for the following detailed parameters:

- Cam angle
- Spark advance
- Idle speed
- Air temperature and pressure

The parameters listed above during experimental testing are relatively constant because of its configuration. The main short coming of this model is that it is not capable of modelling engine start and stop. While the model lacks these features the shutdown process is not of particular interest and the PMSM is the primary component for startup and is modelled in detail. Therefore, this mapped ICE setup provides a great system response that closely represents the Corvid-50 and simulates the data that is needed for hybrid performance analysis.

4.1.5 Battery

The batteries used for the hybrid system are lithium polymer batteries from Gens Ace designed for hobby aircraft applications. There are three batteries in total for the experimental setup; two 25.8 volt (6S) in parallel which create a 51.6 volt (12S) battery with a 4000mAh capacity and a single 12.9 volt (3S) battery with 2200mAh capacity for powering the ECU.

Parameter	Value	Units
Capacity	4000	mAh
Voltage	22.2	V
Max discharge	90	C
Max continuous discharge	45	C

Table 19: Electric motor battery specifications

There are a couple ways to model a LiPo with the simplest being a static voltage with a capacity that depletes as current is drawn from the battery. There are three main disadvantages to a simple model like this; it does not adjust battery voltage with temperature, model voltage sag under load, and model the individual cells found in LiPo batteries. Fortunately, Simulink provides a specification sheet based battery model [84] that has great detail and adjustability. The model incorporates the following parameters:

- The rated capacity at nominal temperature
- Open circuit voltage
- Internal resistance
- Battery temperature
- Number of cells in series and parallel
- Initial voltage and output time constant

The model uses numerous equations to determine the performance of the battery, the first being the cell voltage which is calculated using the energy of the battery, current, and resistance. The current of the battery is determined by the current flow required by the pack and the number of cells in parallel, shown in the Equation 41.

$$v_T = E_m - i_{batt} R_{int} \tag{40}$$

$$i_{batt} = \frac{i_{in}}{N_p} \tag{41}$$

The output voltage of the battery is found using two equations, the first is the cell voltage multiplied by the number of cells in series. This is the unfiltered scenario where the voltage is instantaneous, the filtered configuration takes into account the voltage time constant and provides a more detailed voltage model shown in Equation 42.

$$v_{out} = \frac{v_{out}}{\tau s + 1} \tag{42}$$

One of the more important parameters to calculate in the battery model is the state of charge (SOC). The current state of charge is found using the initial state of charge and subtracting the total amount of current draw over time. This is represented as a percentage therefore the total current drawn overtime needs to be divided by the battery capacity.

$$SOC = SOC_o - \frac{1}{Cap_{batt}} \int i_{batt} dt \tag{43}$$

The energy of the battery can also be found by taking the integral of the current draw with respect to time.

$$Ld_{AmpHr} = \int i_{batt} dt \tag{44}$$

Power transfer of the battery, power loss, and stored energy are found by using basic electrical equations and conservation of energy laws. These provide the required parameters to account for power flow into and out of the battery.

$$P_{batt} = -v_{batt} i_{batt} \tag{45}$$

$$P_{loss} = -N_p N_s i_{batt}^2 R_{int} \tag{46}$$

$$P_{stored} = P_{batt} + P_{loss} \tag{47}$$

E_m	Battery open circuit voltage	V
v_T	Per module battery voltage	V
N_s	Number of cells in series	-
N_p	Number of cells in parallel	-
Cap_{batt}	Battery capacity	Ah
Ld_{AmpHr}	Battery energy	Ah

Table 20: Variable definitions for datasheet battery equations

This battery model creates a power response that is accurate to what is experienced during testing. The voltage of the battery drops when high power is demanded rapidly which occurs during startup. Using a voltage table allows for the cell voltage to deplete in the S shape that is found in LiPo batteries. Overall, the battery model provides more than enough detail to represent the Gens Ace batteries used to power the PMSM.

4.1.6 Clutch

For the test bench an electromagnetic clutch is used to couple the combustion engine to the rest of the drivetrain including the electric motor. The clutch is actuated by a 24-volt signal from the test bench power supply. Simulink has some clutch models that were used in early iterations of the model:

- Disc Clutch: This is part of the powertrain blockset and represents a hydraulic actuated pressure clutch which are often used in automotive applications.

- Cone Clutch: These are used as synchronizers for transmissions and clutched limited slip differentials.
- Dog Clutch: A dog clutch has teeth to stop clutch slipping but can only be actuated when speed is near zero.
- Logic-Controlled Clutch: This clutch transmits power via friction with a logic block that engages and disengages based on a signal port.

The models work in conventional setups where there is one power input and output, however when trying to implement these models with the parallel setup there were numerous challenges. Another reason these models were difficult to implement is that they use Simscape, which requires signal conversion from the rest of the Simulink model.

With these challenges a simplified clutch logic block was created using some of the principles from Simulinks models but with more equations to handle the parallel setup. The fundamental purpose of the clutch model is to transfer power when engaged. There are three states for the clutch; engaged with torque being transferred in the rated region, clutch engaged with torque greater than the clutch rating, and the clutch disengaged.

$$\tau_{out} = \begin{cases} \tau_{ICE} + \tau_{EM}, & \text{if } \tau_{ICE} + \tau_{EM} \leq \tau_{rated} \text{ \& clutch engaged} \\ f(\tau_s), & \text{if } \tau_{ICE} + \tau_{EM} \geq \tau_{rated} \text{ \& clutch engaged} \\ 0, & \text{if clutch disengaged} \end{cases} \tag{48}$$

$$\omega_{out} = \begin{cases} \max(\omega_{ICE}, \omega_{EM}), & \text{if } \tau_{ICE} + \tau_{EM} \leq \tau_{rated} \text{ \& clutch engaged} \\ f(\omega_s), & \text{if } \tau_{ICE} + \tau_{EM} \geq \tau_{rated} \text{ \& clutch engaged} \\ \omega_{EM}, & \text{if clutch disengaged} \end{cases} \tag{49}$$

$$f(\tau_s) = \frac{F_{clamp} R_{eff}}{2} \left[(\mu_k - \mu_s) sawtooth(\omega) + (\mu_s + \mu_k) \right] \tag{50}$$

$$f(\omega_s) = \omega[(\mu_k - \mu_s) sawtooth(\omega) + (\mu_s + \mu_k)] \tag{51}$$

R_{eff}	Effective radius	m
F_{clamp}	Clutch clamping force	N
τ_{out}	Clutch output torque	Nm
τ_{ICE}	ICE torque	Nm
τ_{EM}	Electric motor torque	Nm
τ_{rated}	Clutch torque rating	Nm
ω	Clutch output speed	rad/s
ω_{ICE}	Clutch plate speed	rad/s
ω_{EM}	Clutch rotor speed	rad/s
μ_k	Kinetic friction constant	-
μ_s	Kinetic friction constant during slippage	-

Table 21: Variable definitions for clutch model

When the clutch is engaged in the rated region the torque from both the electric motor and combustion engine are transferred through the driveline to the dynamometer. This state also means that the rotor and plate of the electromagnetic clutch are synchronized. This specific scenario is simplified compared to Simulink's friction disc clutch because it does not model the friction.

There is another engaged state that needs to be modelled: when the clutch is operating outside of its rated torque region. For this clutch state the rotor and plate are not synchronized due to the clutch slipping under torque load. This slipping mode exists when the clutch experiences torque that is higher than the nominal rating. A simplified friction model is used to give a visual indication of slip but is not currently used to characterize the dynamics of the system. The visual indication of slip is a sawtooth profile ($f(\tau_s)$,$f(\omega_s)$) that represents the slip stick phenomenon [85].

The final state of the clutch is when it is disengaged, where the rotor and plate do not make contact. In this stage the plate spins at the speed of the combustion engine and the rotor at the speed of the electric motor. There is no torque transfer in this state which means that all load from the dynamometer is handled by the PMSM which is directly connected.

This clutch model, while not as complex as the friction model from Simulink, represents the operation of the electromagnetic clutch on the test bench. The telemetry for the electromagnetic clutch is the signal, rotor speed, and plate speed. The designed model represents these three known parameters and gives indication of slipping when operating over its rated torque. Future clutch dynamics will be developed with working friction models once the Mayr clutch is characterized fully.

4.1.7 Drivetrain

Unlike the previously discussed models the drivetrain is a passive element that varies drastically based on the design. This aspect of the test bench can be calculated theoretically and measured during experimental testing. There are three parameters that are required to accurately model the drivetrain; the inertia, viscous damping, and static friction torque.

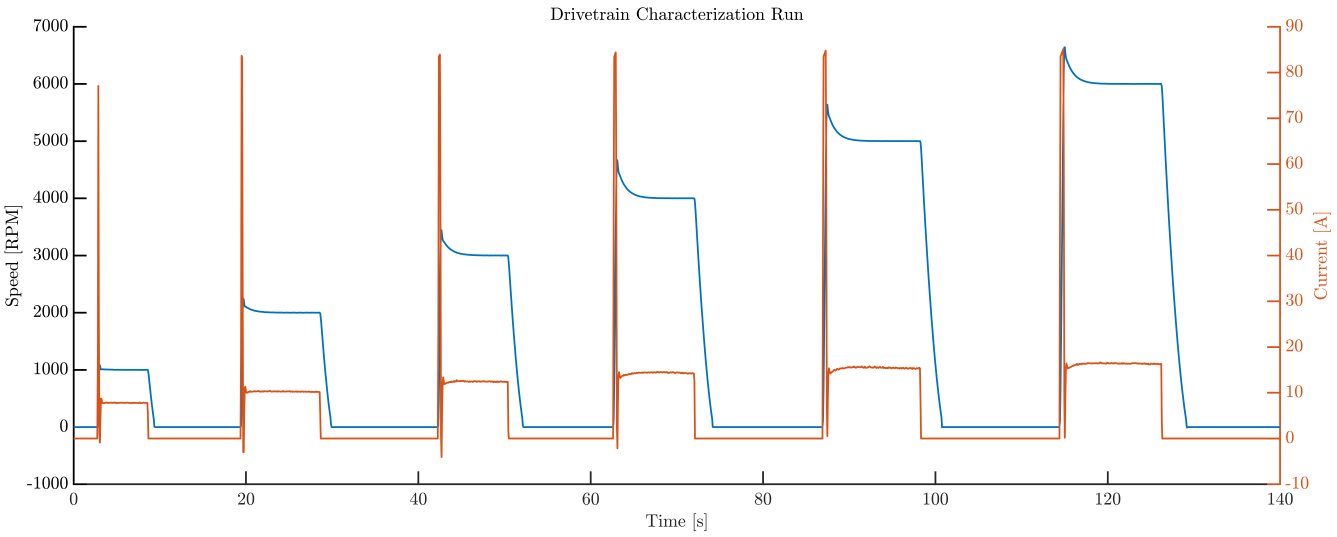

Figure 50: Speed and current values for drivetrain inertia, viscous damping, and static friction

Starting with inertia the masses and geometry of the individual components were collected via Solidworks, specification sheets, and real-world measurements. Using the appropriate inertia equations and parallel axis theorem the total inertia of the drivetrain was found and compared to the values determined in Solidworks with updated masses.

Another method to find the inertia of the drivetrain is using the electric motor to rotate the drivetrain. One important aspect of this experimental method is to set the ramp speed of the PMSM to zero. This means that when a speed is commanded by the ESC the motor attempts to reach the setpoint as fast as possible. With this setting applied the system was commanded, shown in Figure 50, from stationary to multiple speeds in increments of 1000 RPM. To find the inertia from this data acceleration and deceleration for each set point was calculated. The maximum torque for both cases is then divided by the acceleration and deceleration respectively. The data below represents the values used to find the experimental inertia values.

Speed $[rad/s]$	Torque $[Nm]$	Acceleration $[rad/s^2]$	Deceleration $[rad/s^2]$	Inertia $[kgm^2]$
104.84	0.287	453.23	119.73	0.0027
209.99	0.378	752.83	151.96	0.0028
314.73	0.458	962.71	173.60	0.0030
420.33	0.529	1116.91	186.17	0.0032
522.40	0.569	1044.90	204.74	0.0031
627.88	0.604	1110.94	209.65	0.0032

Table 22: Test data for drivetrain characterization

Comparing the values from Solidworks and the experimental results show that the inertia is within the 0.002-0.0032kgm^2 range. The final value for the model was determined to be 0.0023kgm^2, this value created torque spikes that were the most representative of the experimental test bench response.

Viscous damping is the resistive torque that is proportional to velocity, this determines the steady-state load of the drivetrain at a specific speed. To find this value the same data from the inertia testing was used. For viscous damping the steady-state torque and speed was required to calculate its value. The torque and speed can be found by averaging their values across the entire steady-state operating window. The torque and speed are then plotted against each other which produces a linear plot. A linear regression is then used to generate a governing equation; the slope represents the viscous damping in units of Nm per rad per second.

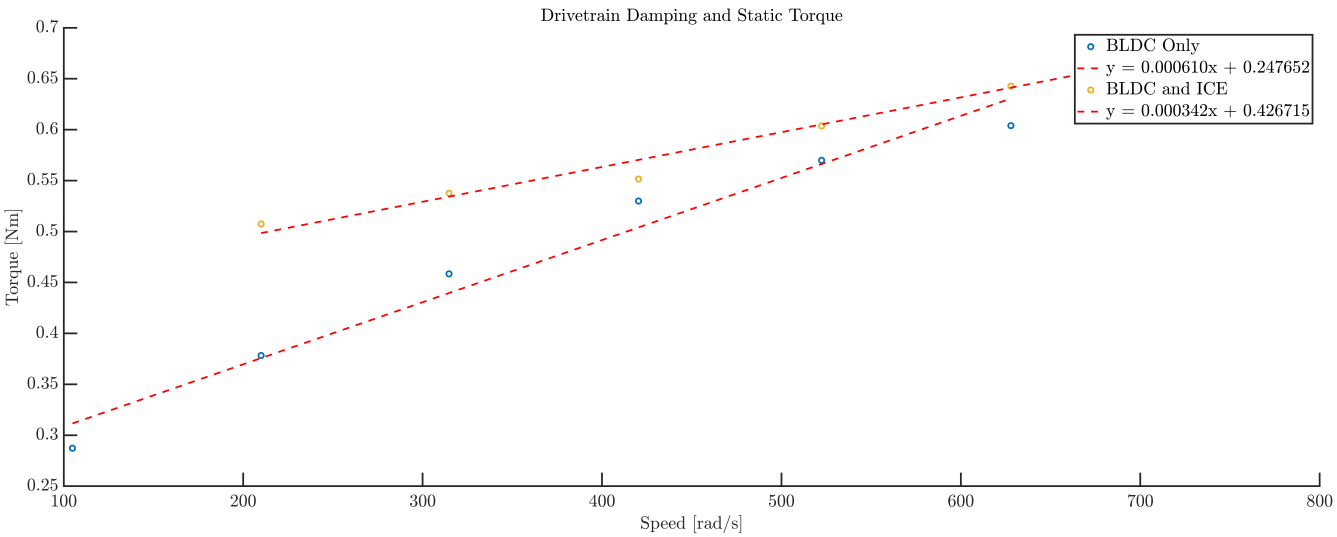

Figure 51: Drivetrain viscous damping curve based on experimental data

Figure 51 also includes when the clutch is engaged; this creates a scenario where the PMSM regulates the combustion engine spikes at the same speed. This results in less viscous damping for the PMSM to overcome since the combustion helps spin the drivetrain. The linear regression on the graph also provides the static friction torque value as well which is the y-intercept of the resulting equation. The values of the inertia, viscous damping, and static friction are tabulated below for both scenarios.

	Inertia $[kgm^2]$	Viscous Damping $[Nm/rad/s]$	Static Friction $[Nm]$
EM Only	0.0023	0.000610	0.2477
EM and ICE	0.0023	0.000342	0.4270

Table 23: Drivetrain dynamics characterization

The methods discussed in this section were used to model each component of the test bench with the complexity required to create system responses that represent what is experienced on the test bench. Physical connection between the components exist and must be modelled to create the parallel hybrid system. How these components interact with each other is derived in the next section using different mode scenarios which represent the three basic input combinations for electric and combustion power.

4.2 Hybrid Operating Modes

With component models created the inputs and how the system behaves needs to be defined. The two power units are active components that accept different input parameters to create power. How the system responds depends on the combination of these inputs. There are three main command combinations when the clutch is engaged that dictates the speed of the system and the torque being transmitted.

The first scenario is when both power units are commanded a speed (referred to as Mode 1). When this occurs both controllers have a speed setpoint to maintain via PID control. This command scheme does not provide control over the torque output of the power units. In this configuration whichever power unit has the higher available power at the commanded speed increases its torque

output to handle the load of the system. If the PMSM has the higher power ceiling in this mode, the combustion engine cuts fuel because the electric motor is carrying the system load. If the combustion engine is 'in charge' the electric motor drops current and maintains the minimum amount to maintain the commanded speed at smooth operation. The dual speed command configuration does not provide the control needed to exploit the advantages of a hybrid-electric system.

To remedy the shortcomings of the dual speed operating mode the PMSM has a commanded speed while the combustion engine receives a throttle command (Mode 2). This configuration allows for individual torque and speed control which is ideal for efficient power splitting. In this state the electric motor governs the speed of the system while the throttle command dictates the torque output of the ICE. The torque of the combustion engine and the electric motor are inversely proportional. When the throttle command increases the current output of the electric motor drops. The amount of torque produced by the ICE is determined by the power map which predicts how much torque is created at the given throttle and speed value. The amount of torque that the PMSM delivers is the difference between the system torque load and the amount created by the ICE. These roles can be reversed where the ICE dictates speed and the EM torque, this is referred to as Mode 3.

In both speed and torque commanded modes the electric motor can enter regeneration mode at any time to charge the LiPo batteries. When this occurs the combustion engine will be responsible for the full system load plus the added power requirement of the PMSM braking the system for regeneration.

In addition to the operating modes stated above there are a few others that exist. The test bench can operate in combustion-only mode as well as electric-only. These configurations are good for collecting data on conventional propulsion systems. There is also another hybrid command mode that can be used but requires constant input control. This mode is when the combustion engine is commanded throttle and the PMSM current. When in this configuration the speed of the system is not directly governed, instead it is dictated by the individual power and load of each power unit. This means that the speed value can fluctuate easily and is much harder to control. This method is not used in experimental testing or simulation because of its difficulty to control, potential for over-spinning, and stalling.

These various command modes provide a dynamic understanding of how the hybrid system works and the effects of the controllers based on command parameters. With these modes the logic on how speed and torque is determined can be examined and modelled in the next section.

4.3 Logic

In the various operating modes, the speed and torque of the two power units change based on the current state of the system. The speed and torque are determined not only by the dynamics of the system but also the controllers. This means that both controller logic must be modelled in addition to the mechanical component dynamics that have been discussed. This is accomplished using decision-based Simulink blocks to determine the speed and torque commands for each power unit.

4.3.1 Speed

The first and simplest operating mode in terms of speed control is Mode 1. In this scenario each controller receives a speed command and uses PID to maintain the requested speed. The ECU and ESC constantly adjust the required inputs to the power units to maintain the commanded setpoint as close as possible using the available feedback sensors.

When in Mode 1 both speed commands are matched, which simplifies determining the speed of the entire system. When the clutch is engaged the electric motor smooths the speed of the combustion engine by damping the torque spikes. This means that the PMSM draws more current when engaged with the combustion engine even though it is commanded the same speed. If the speed commands are not matched the system may stall or use significantly more power than intended.

$$\omega_{EM} = \begin{cases} \max(\omega_{ICE}, \omega_{EM}), & \text{if clutch is engaged} \\ \omega_{EM}, & \text{if clutch is disengaged} \end{cases} \tag{52}$$

$$\omega_{ICE} = \begin{cases} \max(\omega_{ICE}, \omega_{EM}), & \text{if clutch is engaged} \\ \omega_{ICE}, & \text{if clutch is disengaged} \end{cases} \tag{53}$$

In control Mode 2 when the PMSM is commanded a specific speed and the combustion engine a throttle value the speed is determined by the PMSM command when the clutch is engaged. The electric motor still smooths the combustion operation in this mode which increases the current use. When the clutch is open the PMSM runs at the commanded RPM while the combustion engine runs at its own speed. The combustion rotational speed is dependent on multiple factors in this mode when the clutch is not engaged. The throttle command means that the ICE could operate at any RPM along the commanded row of the power map. The speed at which it runs for a given throttle value varies with temperature and load; for example, when the ICE first starts it has a lower speed at a specific throttle than once the cylinder head warms up. The speed at a given throttle command also depends on the load of the shaft and can be determined by looking at the torque map.

$$\omega_{EM} = \omega_{EM} \tag{54}$$

$$\omega_{ICE} = \begin{cases} \omega_{EM}, & \text{if clutch is engaged} \\ f(\tau_{ICE}, throttle, T), & \text{if clutch is disengaged} \end{cases} \tag{55}$$

For Mode 3 in which the combustion engine is commanded a speed and the electric motor a current the speed determination is similar to the second scenario. The combustion engine maintains the speed command using its PID control scheme which has a governor curve to determine throttle for the specific speed. The electric motor speed is determined by the current being requested and the load on the output shaft. This behaves similarly to the combustion engine with a throttle command, but more consistent since the PMSM is less thermally sensitive.

$$\omega_{EM} = \begin{cases} \omega_{ICE}, & \text{if clutch is engaged} \\ \dfrac{i_{EM}K_t - f_E - \tau_{load}}{b_E}, & \text{if clutch is disengaged} \end{cases} \tag{56}$$

$$\omega_{ICE} = \omega_{ICE} \tag{57}$$

f_E	Static friction of the drivetrain without ICE	Nm
τ_{load}	Load torque from the dynamometer	Nm
b_E	Viscous damping of the drivetrain without ICE	$Nm/rad/s$

Table 24: Speed determination variables for Mode 3

With all of the scenarios mentioned the speed determination is based on a commanded speed and torque load that each power unit is capable of handling. If a speed is requested that the PMSM or ICE cannot produce under the current load, then the power unit will not reach the commanded speed. The torque demand for each power unit will depend on the command scenario which are discussed in the next section.

4.3.2 Torque

In a similar fashion to the speed logic, determining the torque command for each power unit is determined by the operating mode. The overall torque demand on the system is determined by the resistance of the rotating system and the load created by the dynamometer. This torque combined with the speed of the system can then be used to determine the power of the propulsion system.

$$\tau_{EM} = \begin{cases} \omega_{out}b_{EI} + \tau_{dyno}, & \text{if clutch is engaged} \\ \omega_E b_E + \tau_{dyno}, & \text{if clutch is disengaged} \end{cases} \tag{58}$$

$$\tau_{ICE} = \begin{cases} \tau_{dyno} - \tau_{EM}, & \text{if clutch is engaged} \\ f(\omega, throttle, T), & \text{if clutch is disengaged} \end{cases} \tag{59}$$

When the clutch is engaged in Mode 1 (Equations 58 and 59), the torque from the spinning system and the dynamometer is taken by whichever power unit has a greater power capacity at that speed. In this scenario when the EM is governing power the gas engine produces enough torque to maintain combustion at the operating speed. If the torque load of the system exceeds the capabilities of the electric motor the combustion engine throttle increases to supplement the torque output. If the torque load is greater than the sum of what both power units are capable of the system will slow until one or each power unit stalls. In the clutch disengaged state the PMSM is loaded by the dynamometer and the drivetrain. While the combustion engine is required to overcome the inertia it is connected to.

$$\tau_{EM} = \begin{cases} \tau_{dyno} - \tau_{ICE}, & \text{if clutch is engaged} \\ \omega_E b_E + \tau_{dyno}, & \text{if clutch is disengaged} \end{cases} \tag{60}$$

$$\tau_{ICE} = \begin{cases} f(\omega, throttle, T), & \text{if clutch is engaged} \\ f(\omega, throttle, T), & \text{if clutch is disengaged} \end{cases} \tag{61}$$

Equations 60 and 61 represent Mode 2 where the torque production of the combustion engine is directly controlled. When the clutch is engaged the electric motor governs the speed. As always, the torque sum of both power units combines to the dynamometer load plus the drivetrain requirements. The torque produced by the combustion engine is determined by the throttle value at the specific speed. If this ICE torque value is lower than the demand by the system, the electric motor supplements the requirement. As the throttle command increases the torque rises, and the torque produced by the PMSM decreases. The torque values are inversely proportional and sum to the load demand of the system at any given point in operation.

$$\tau_{EM} = \begin{cases} i_{EM} K_t, & \text{if clutch is engaged} \\ i_{EM} K_t, & \text{if clutch is disengaged} \end{cases} \tag{62}$$

$$\tau_{ICE} = \begin{cases} \tau_{dyno} - \tau_{EM}, & \text{if clutch is engaged} \\ f(\omega, throttle, T), & \text{if clutch is disengaged} \end{cases} \tag{63}$$

The torque production from each power unit in Mode 3 (Equations 62 and 63) operates similar to the throttle speed scenario. However, in this mode the torque of the electric motor is directly controlled and not limited by the speed of the system since torque is proportional to current. Again, the torques of the ICE and PMSM are inversely proportional while summing to meet to torque demand of the system. With the speed and torque logic determined it is possible to provide the required inputs for both the combustion engine and electric motor models.

All logic discussed this far represents the torque of each power unit once the system is rotating. To determine the starting torque of the system the following equations are used.

$$\tau_{EM} = \begin{cases} I_{EI} \dfrac{d\omega}{dt} + \tau_{comp} + \tau_{load}, & \text{if clutch is engaged} \\ I_E \dfrac{d\omega}{dt} + \tau_{load}, & \text{if clutch is disengaged} \end{cases} \tag{64}$$

$$\tau_{ICE} = \begin{cases} \dfrac{P_{EFI}}{\omega_{ICE}}, & \text{if clutch is engaged} \\ Not\ Possible, & \text{if clutch is disengaged} \end{cases} \tag{65}$$

b_{EI}	Viscous damping of the system with clutch engaged	$Nm/rad/s$
b_E	Viscous damping of the system with clutch disengaged	$Nm/rad/s$
I_{EI}	Inertia of the system with clutch engaged	kgm^2
I_E	Inertia of the system with clutch disengaged	kgm^2
τ_{dyno}	Load torque applied by the dynamometer at the output shaft	Nm
τ_{comp}	Torque to overcome ICE compression on startup	Nm
f_{EI}	Static friction of system with clutch engaged	Nm
f_E	Static friction of system with clutch disengaged	Nm
P_{EFI}	ECU predicted power based on fuel injection	Nm

Table 25: Torque logic variable definitions

The component and logic models from this section combine to create a complete representation of the parallel hybrid-electric test bench. These models were derived using theoretical methods when acceptable. The experimental data collected to determine component characteristics provided the parameters required to create a system that responds accurately when compared to real-world applications.

5 Simulation and Experimental Testing

The modelled components represent each critical individual part of the hybrid-electric propulsion system. In order to create a system model these components were connected using the drivetrain characteristics and the operational logic blocks. With a complete system model various test scenarios were run to determine the validity of the model. The following six tests were run to determine that the model correctly responds to the three operating modes and has the capability to run a successful flight mission.

5.1 Dual Speed Command (Mode 1)

The first operating mode tested was when both the electric motor and combustion engine were commanded the same speed. The test began with the combustion engine enabled and speed command set, with the clutch engaged the electric motor spun the ICE until combustion was self-sustaining. With the clutch open the combustion engine ran at 2500 RPM until the cylinder head reached the operational temperature of 100°C. Once up to temperature the electric motor was sent the combustion speed command so that both shafts had matching speeds, once synchronized the clutch was engaged.

With both shafts connected mechanically the operating speed was increased to 3000RPM, once stable the dynamometer was activated via the programmable load at 30A. This was a simple test where both power units stay at a constant speed while the load is applied, this helped determine how the torque is split between the EM and ICE. The test was relatively low power and speed for the overall test bench capacity but was sufficient in characterizing the bench is Mode 1 without significant risk.

5.1.1 Inputs

In order to run the test, there were four required inputs that were used for both simulation and experimental testing. These inputs included the ICE and PMSM speed, clutch state, and programmable load value, which are shown in Figure 52:

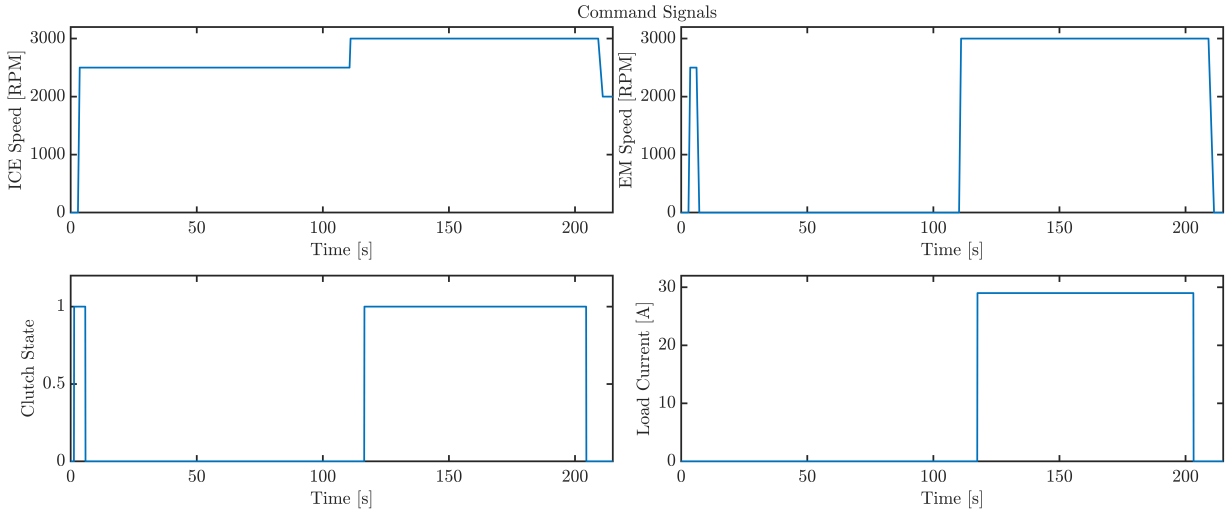

Figure 52: Input signals for Mode 1 low power test

These are commanded inputs that the operator has control over which vary based on the operating mode. In addition, the ECU and ESC have inputs and outputs that are not directly controlled by the user but are required for proper system operation. The combination of commanded and passive inputs drives the propulsion system and creates a specific system response.

5.1.2 System Response

The startup sequence of the test created a torque spike from the electric motor which was required to overcome the combustion engine compression. This torque spike varies depending on the engine fuel injection, temperature, and initial crank angle. The range for the starting torque of the EM was generally between two and three newton meters. The combustion engine and electric motor continued to spin until the combustion was stable. Unfortunately, the simulation does not have the ability to model the starting sequence of a combustion engine. Despite this limitation the torque response of the electric motor was modelled with the inertia, damping, and static friction found via experimental testing. The simulation responds to the starting sequence with a similar starting torque.

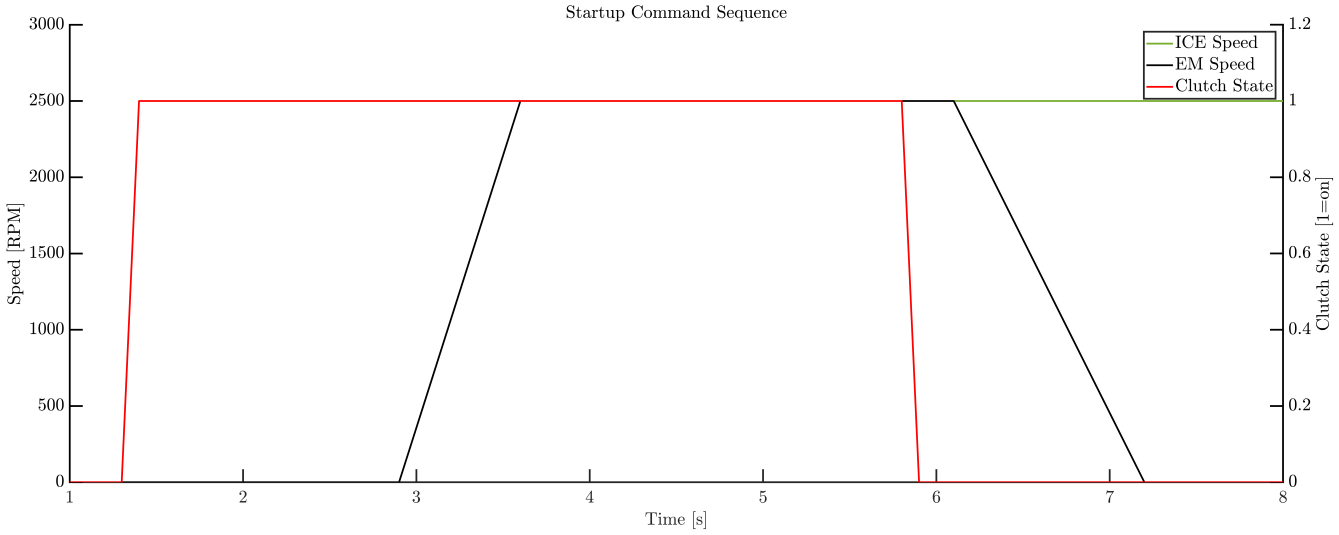

Figure 53: Input sequence to start combustion

When the combustion became stable the clutch was disengaged, this caused the combustion engine to accelerate to just over 5000RPM. The drastic speed increase was caused by the throttle command and accumulated fuel during the startup sequence. Since the electric motor was governing the speed during start up the combustion engine had not found steady-state under its own operation. In addition to these factors the ECUs PID control is designed for propeller load profiles, this means it is not aggressive enough to control rapid load changes. The speed of the combustion engine stabilized within a second of clutch release and ran at its commanded value until it reached operating temperature.

At operating temperature both power units were commanded to 3000RPM and then connected via the clutch once synchronized. Having the speeds matched reduces the torque load on the clutch and makes it easier to maintain commanded speeds for the ICE. Once the operating speed was stable the load was applied at 30A, this caused a 500RPM reduction on engagement that recovered within a second but overshot and maintained a speed slightly above 3000 rotations per minute.

This again was caused by the ECUs poor PID design for this specific application. This loaded scenario was held for a hundred seconds to see the system's steady-state response. The simulation response for this segment closely matched the experimental results without the speed variations caused by the ECU. This stable model response was caused by the mapped ICE model being much less sensitive to load and speed change.

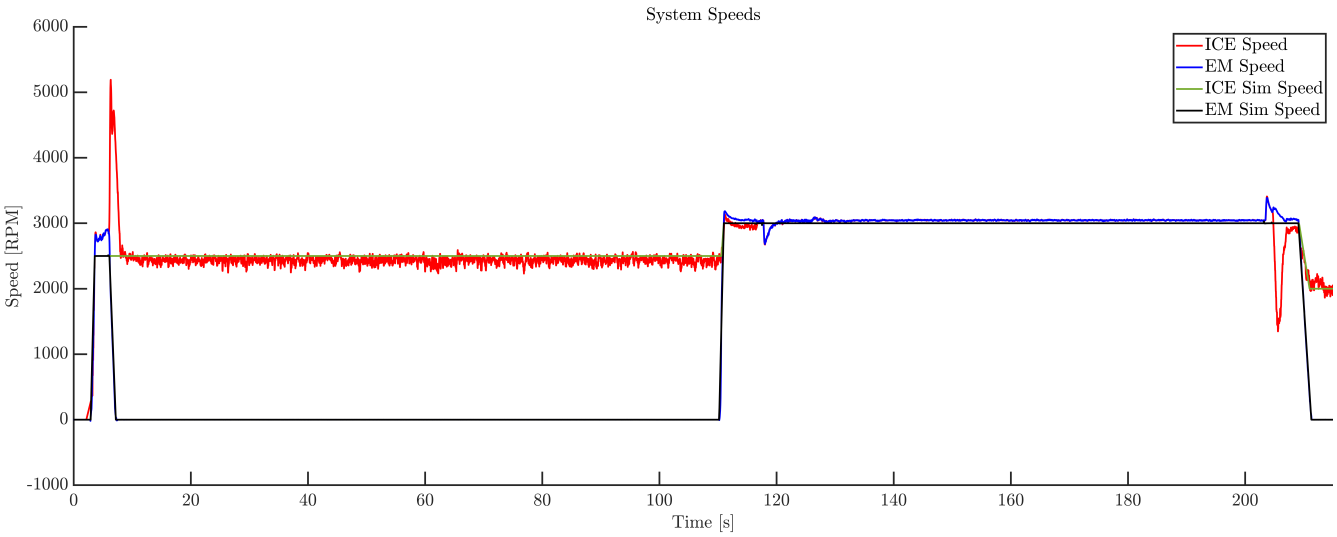

Figure 54: Speed response of the system

After the loading phase of the test the load was disengaged followed by the clutch. This sequence caused a rapid acceleration of the electric motor and deceleration of the combustion engine. The rise in electric motor speed upon clutch/load disengagement was caused by the PMSM providing more current during clutch engagement. The additional current draw is required to smooth the operation of the combustion when there is no load. When there is a load, the electric motor provides the required power to overcome the torque from the dynamometer. When both scenarios are occurring, the EM will provide substantially more power than if it was spinning on its own. Thus, in this test when the clutch and load were disengaged the electric motor was still providing far more current than required to maintain the commanded speed which caused it to accelerate. The opposite occurs for the combustion engine, it cuts fuel when the PMSM is regulating its speed. This reduces the combustion load on the engine itself, hence when the clutch is disengaged the controller does not provide enough fuel and throttle for the commanded speed. Again, because of the ECUs propeller designed control scheme the recovery from this change state is much slower compared to the electric motor. The simulation outputs for the electric motor response show a small change in speed in these scenarios but are nearly instantaneous and less severe.

5.1.3 ICE Response

During this test the combustion engine throttle decreased slightly over time as the cylinder head temperature increased. The throttle value is directly connected to the fuel flow of the engine, which is used to determine fuel consumption along with speed.

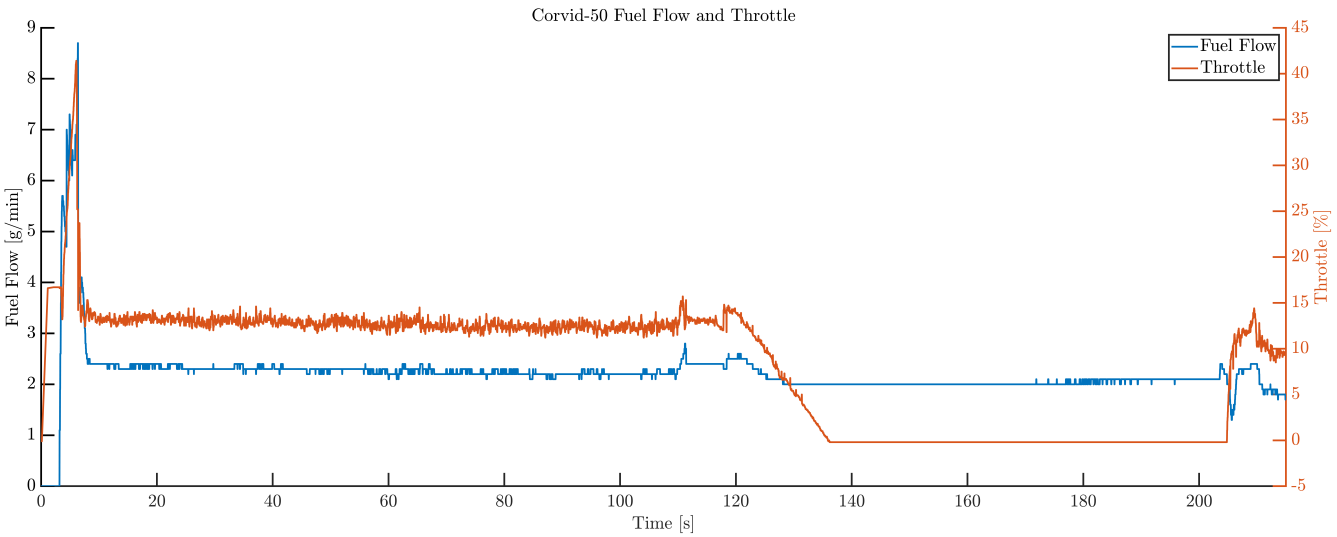

Figure 55: Fuel and throttle response

The torque provided by the combustion engine has three specific regions during this test, starting, idle, and speed governed. During the startup phase fuel was injected into the cylinder to promote combustion and once the first ignition occurred there was a large torque spike. The spike at startup for this test was just over 1.5Nm which dropped almost immediately to the value determined by the speed and throttle values. As the motor spun at 2500RPM to warm up the throttle command remained unchanged, but the torque dropped slightly due to less internal resistance as the temperature increased. When the electric motor is engaged and smooths the operation of the combustion engine fuel injection was reduced. This was caused by the electric motor supplementing power and reducing the inertial load of the ICE. This is further exaggerated when the speeds are synchronized and the load applied, in this state torque is further reduced by the ECU.

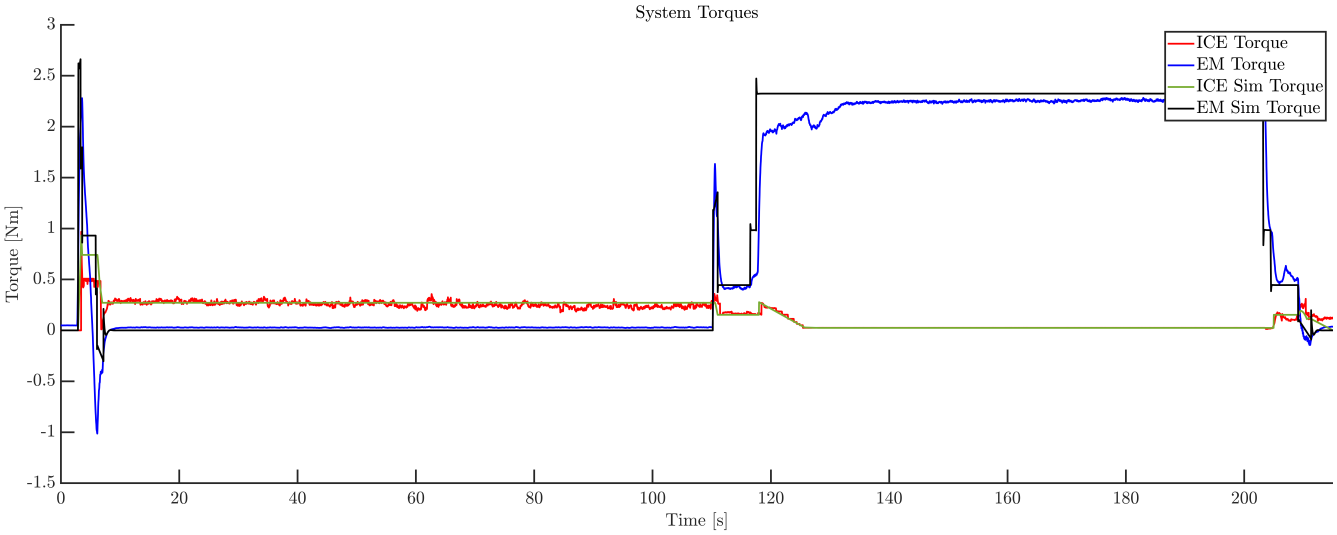

Figure 56: Torque response during Mode 1 30A test

In Mode 1 this response only occurs when the speeds are synchronized, if the ICE is commanded a speed higher than the PMSM by over 200RPM the roles reverse and the combustion engine supplements power. However, if the speed differential is too high the controllers will interfere with

each other causing an unstable system response that can damage the test bench. This mode is designed for synchronous speeds and other operating modes are suggested when wanting better control over the system.

5.1.4 PMSM Response

Under startup the PMSM produced a large current spike to start the combustion engine and the power supplementation required to govern the speed of the system occurred. Simulation results for this test demonstrated a strong electric motor model. The current, torque, and speed outputs of the simulation followed the same profiles as the experimental results and closely matched the values determined from drivetrain characterization during the modelling phase.

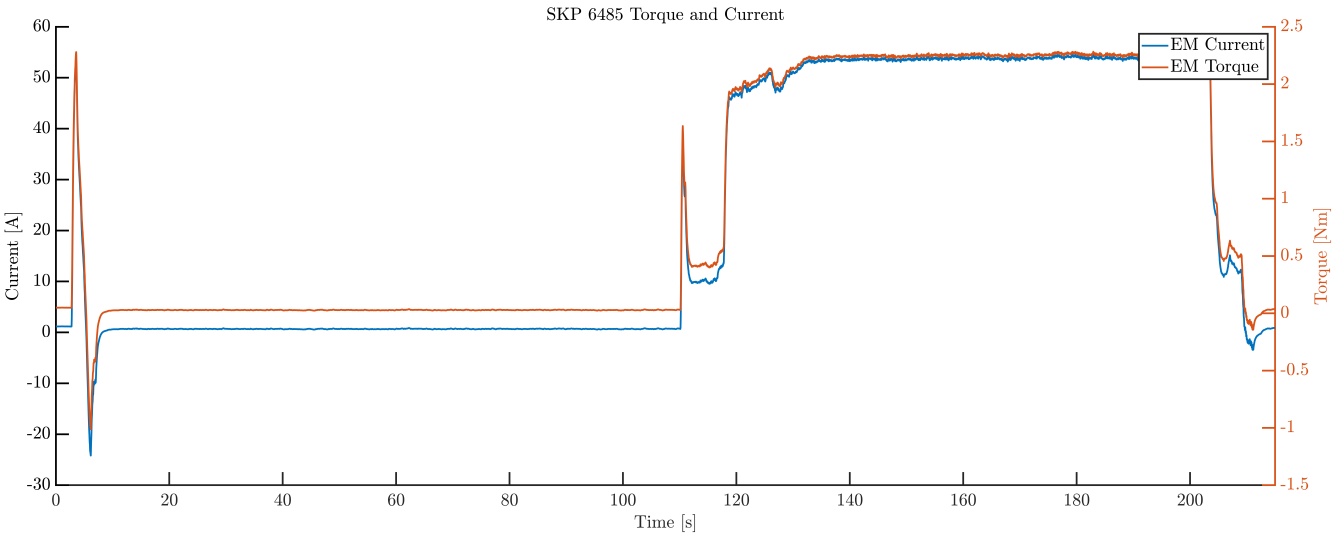

Figure 57: Current and torque response from the PMSM

Unfortunately, as stated above the change in speed and torque caused by the load and clutch disengagement is not captured in the simulation. There are visual indications that a state change has occurred, but the magnitude of this change is not representative of the system's response. To improve this response a new controller would need to be designed to behave similar to the VESC. Despite this, the component and system responses in simulation closely represent the real-world operation.

5.2 Throttle and Speed Command (Mode 2)

The second test performed on the test bench and in simulation includes the same speed, clutch, and load profile as Mode 1 but has a change to the command scenario. For this mode the electric motor governed the speed when the clutch was engaged while the combustion engine was commanded a throttle without the ECU governor enabled. When the governor is disabled the throttle command is not mapped to a speed curve, which means that the commanded throttle is the received value for the ICE. This direct throttle command allows the operator to directly control the torque output of the combustion engine.

The first two minutes of the test run matched the first test in Mode 1 where the electric motor starts the ICE, followed by clutch disengagement and combustion engine warm up. With the ECU

governor disabled the engine ran at a constant throttle during warm up instead of a constant speed. Once the combustion engine was at 100°C the electric motor was spun up to match the ICE speed, the clutch engaged, followed by the load being applied at thirty amps.

During the loaded sequence this test demonstrated the direct torque control of the combustion engine via throttle manipulation. Unlike Mode 1 the power split between the two power units is not determined by the controllers and which power unit was commanded a higher speed. In this operating mode the torque output was directly controlled by the throttle request. The electric motor still drew additional current to smooth combustion operation and govern speed. However, the current output was inversely proportional to the torque output of the combustion engine. The summation of torque from the combustion engine and electric motor must always equal the torque demanded from the system and load. This summation rule meant that as the throttle command increased the current draw from the EM decreased and vice versa. The throttle command during this test was increased until the electric motor was drawing two amps of current. If the throttle was increased further the electric motor would start to produce current that could be used for regeneration, this was avoided due to safety concerns since the batteries during testing were fully charged and regeneration limits were not set in the VESC software.

The simulation model for this operating mode is far more challenging to create and does not match the accuracy of Mode 1. However, the overall response of the simulation closely follows the trends of the experimental data with minimal error.

5.2.1 Inputs

The inputs for this test included the same PMSM speed command, clutch state, and load value as the previous test. However, in this test the combustion engine was commanded a throttle value that directly controlled its torque output with the ECU governor disabled.

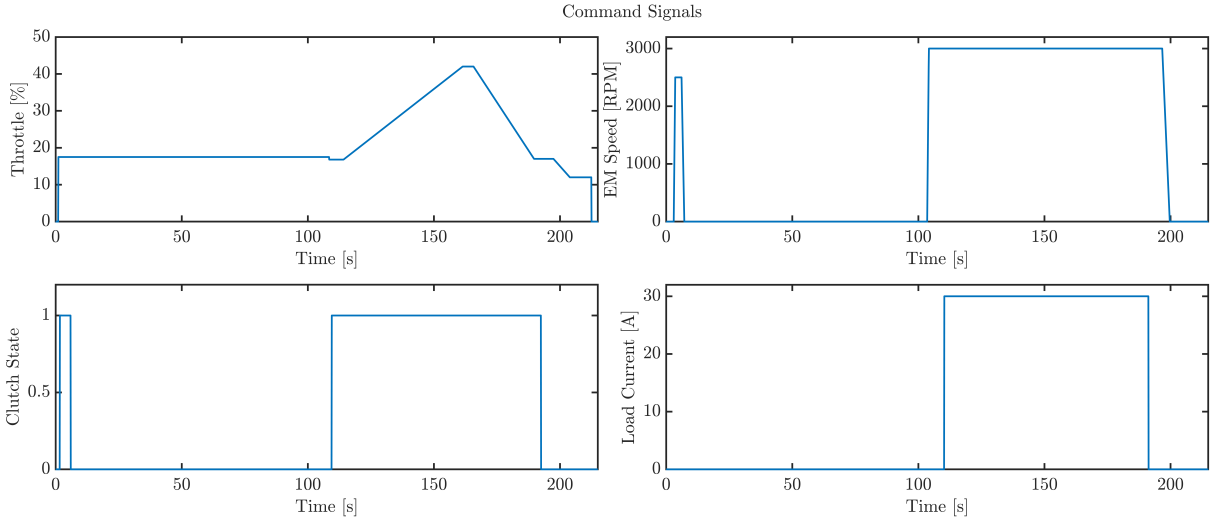

Figure 58: Input signals for Mode 2 low power test

The same passive inputs were used for this test: which included the same batteries fully charged, power supply for telemetry components, and fuel with oil mixture.

5.2.2 System Response

The system response during startup was the same as the dual speed commanded simulation where the electric motor experiences a torque spike between two and three Newton meters to promote initial combustion. However, once the clutch was disengaged the combustion response was drastically different from Mode 1 because of its throttle command scheme. During the idle sequence the rotational speed changed constantly because it was not given a setpoint by the ECU governor. Once the clutch was engaged the speed immediately matched the commanded value of the PMSM at 3000RPM. The load was activated at thirty amps and the same speed decrease spike and recovery occurred due to the instantaneous torque request and the ECU not being designed for the scenario. While loaded the ICE throttle was commanded a throttle curve from 17 to 44.5 percent and back down to 14 percent. This profile caused the combustion engine torque to increase to nearly the entire required value from the system.

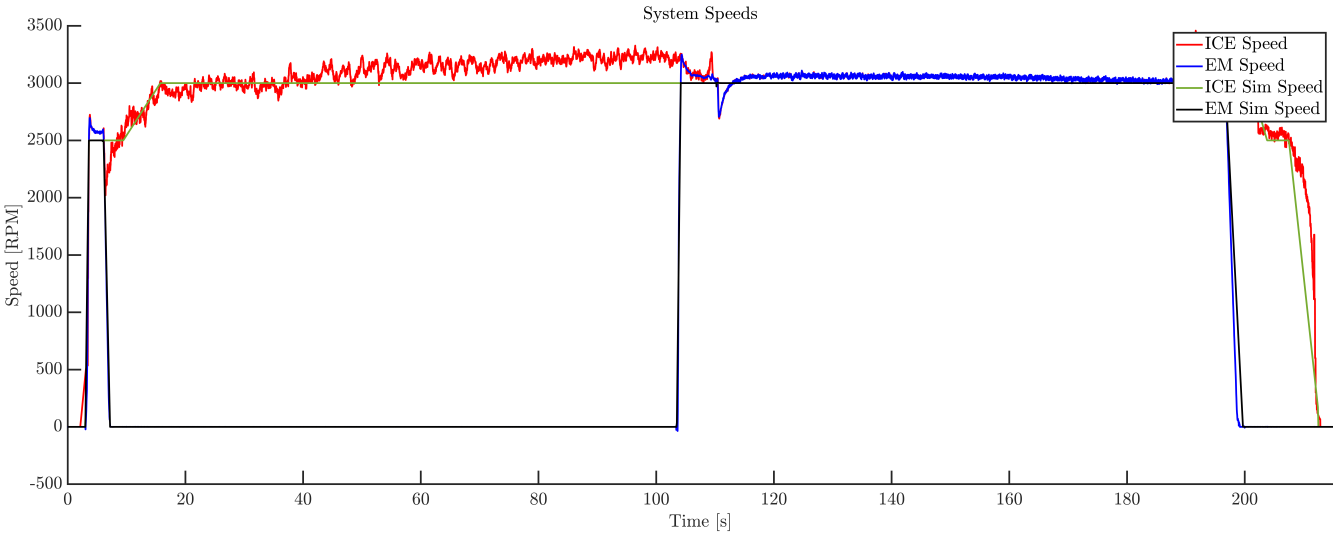

Figure 59: System torque response for Mode 2

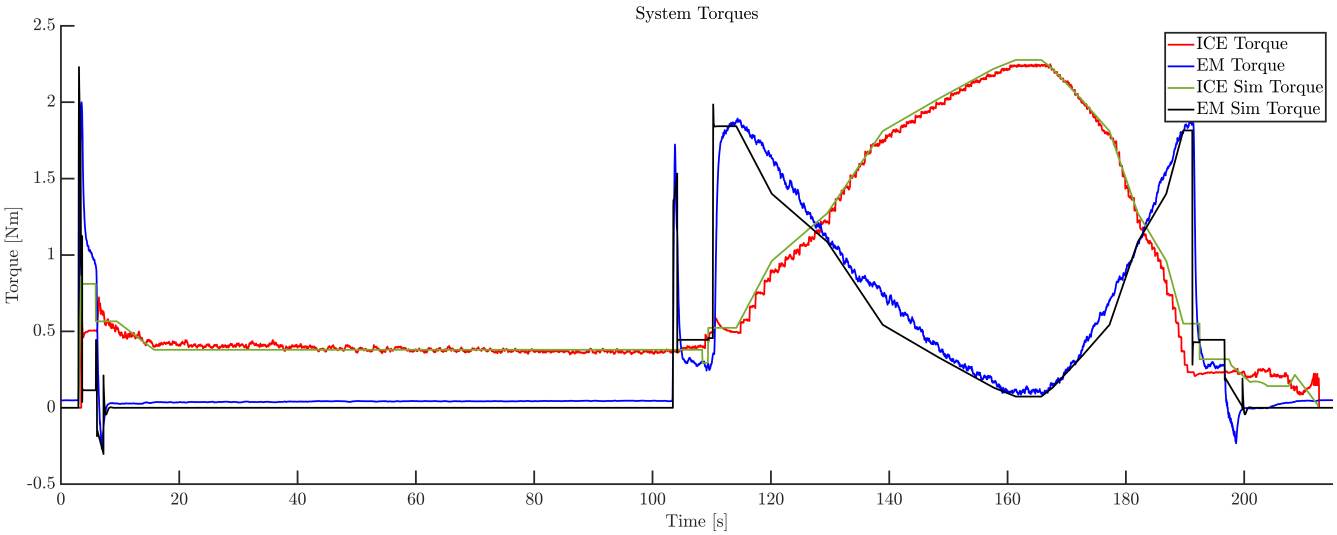

Figure 60: System torque response for Mode 2

This curve also demonstrated that the torque output of the electric motor decreases with throttle increase. The electric motor had a current range between 45 and 2 amps during the loaded section of the test. Load and clutch disengagement followed the same sequence as Mode 1 testing with a resulting speed spike from load disengagement.

5.2.3 ICE Response

During the idle period of the test profile, it was extremely difficult to model the engine behavior under throttle command without speed governor. The data provided from the ECU represents operation once the cylinder head is up to temperature. With the lack of temperature, air, and pressure inputs for the combustion engine model it is near impossible to produce an accurate ICE response during the early stages of operation. Once the system was at temperature the fuel and throttle data showed better responses in simulation. There were still discrepancies caused by the governor not being enabled in the ECU but this was required to operate correctly in Mode 2.

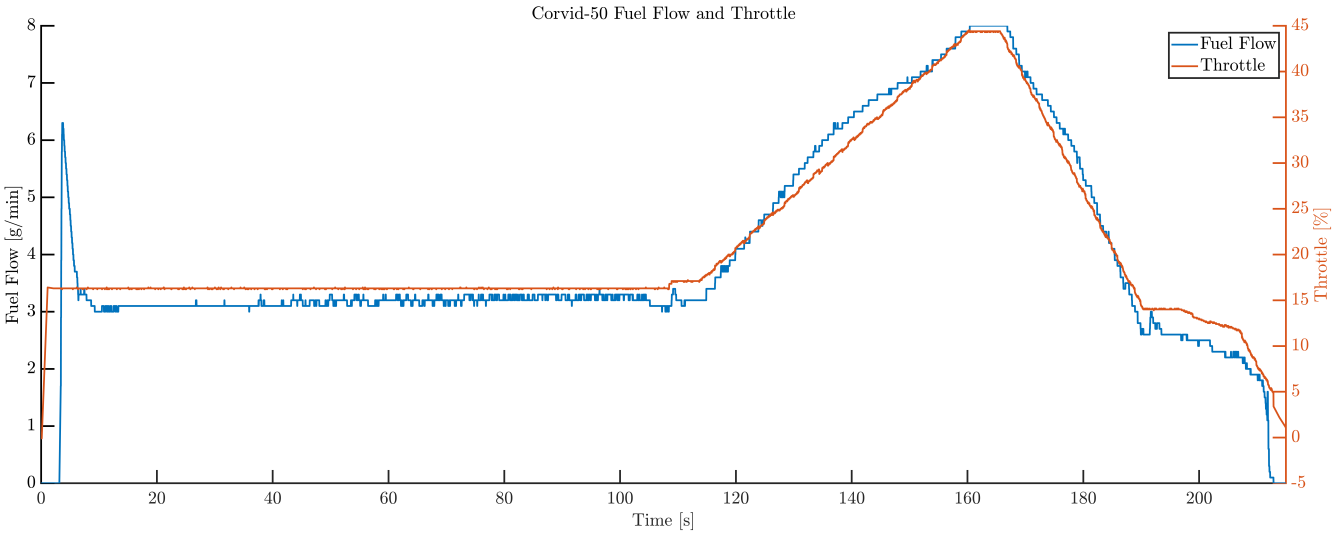

Figure 61: Fuel and throttle profile for Mode 2

The fuel flow during operation is directly connected to the throttle and speed of the combustion engine. During the throttle curve segment of the test fuel flow matched the same profile as the torque output, this indicates the possibility of selecting throttle based on the most efficient fuel flow for a required power. Other than the direct throttle speed prediction challenges the combustion engine response closely matches the predictions made by the simulation model.

5.2.4 PMSM Response

The outputs from the electric motor were similar to the dual speed commanded simulation for combustion start up. The electric motor produced the same torque spike on combustion startup between two and three newton meters. Once the clutch was engaged the PMSM increased its current draw as expected to regulate the speed of the combustion engine while also smoothing its operation. The primary difference in this operating mode was that the torque output of the electric motor was controlled by the throttle of the ICE.

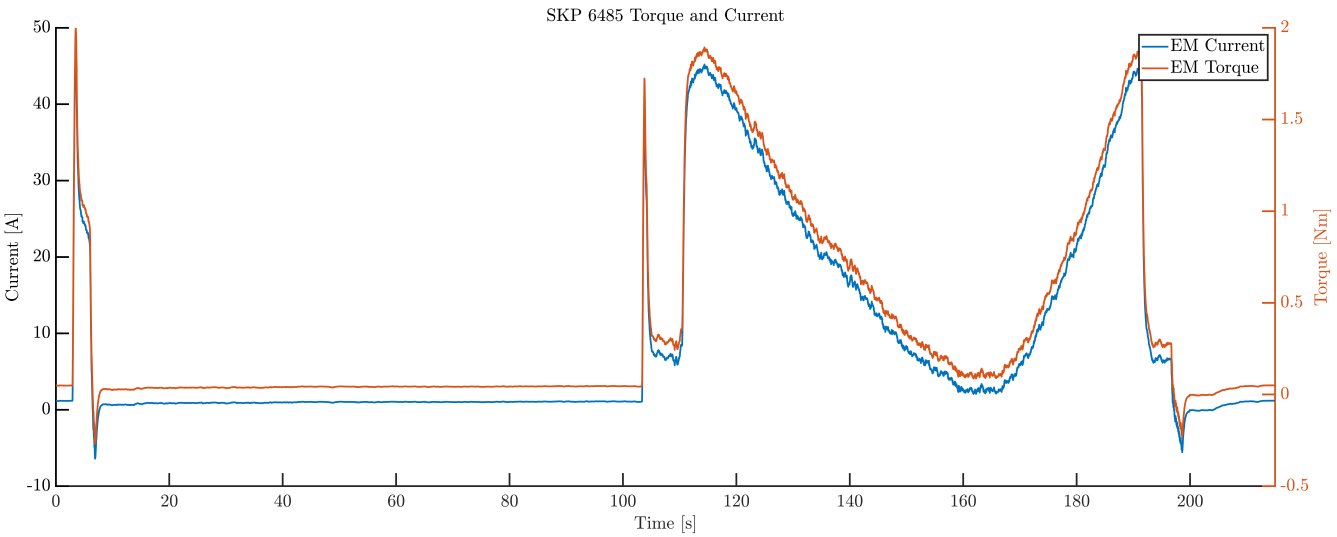

Figure 62: Current and torque response from the EM for Mode 2

During the loaded section of the test the current of the electric motor decreased overtime as the throttle was increased. The torque sum of both power units constantly equaled the demand of the system and load, which was also demonstrated in simulation. There was a constant torque difference in simulation when compared to the experimental output. This was caused by using the theoretical throttle input to the system, which is much smoother and more stable compared to the experimental signal. Using the real-world throttle values would increase the throttle accuracy and synchronize signals better. However, using the experimental signal does not test the accuracy of the model compared to using full theoretical inputs. The magnitude, effect, and cause for these discrepancies will be discussed in the results section.

5.3 Speed and Current Command (Mode 3)

The final test run was for Mode 3 operation where the combustion engine governed speed and the torque output of the PMSM was directly controlled via a current command. The test followed the same startup, speed, and load profile as the previous two tests. This test replication provides the ability to compare all three modes against each other with minimal discrepancy in operation. The startup sequence for this test was vastly different compared to Mode 1 and 2 because the electric motor was no longer speed controlled. To start the combustion engine the PMSM was commanded a current curve instead of a 2500RPM curve. This created a different start profile and torque spike. Combustion took longer to initiate, and the torque response was not a spike but a short-sustained value. Once combustion occurred the same process followed with the clutch being disengaged and combustion engine running at 2500RPM to reach operating temperature. The electric motor speed was synchronized with the combustion engine and the clutch engaged.

The loading sequence saw the same current demand from the programmable load as the previous two tests. During this segment of the test the current command for the electric motor was increased from 0 to 27 amps in the same profile as the throttle in Mode 2. The Mode 2 test could have been replicated from 0 to 44 amps to show that mode two and three are similar to each other but with a torque control swap. However, this lower current range was selected to see the response of the ICE speed governor. Commanding higher current draw at the same climb rate caused the

IntelliJect control algorithm to struggle maintaining the requested speed. The shutdown sequence of the test follows the same process as mode one and two.

5.3.1 Inputs

For this test configuration the required inputs were the combustion engine speed, clutch state, load current, and electric motor current. Adjusting the current of the PMSM directly increased or decreased the torque output of the motor proportionally.

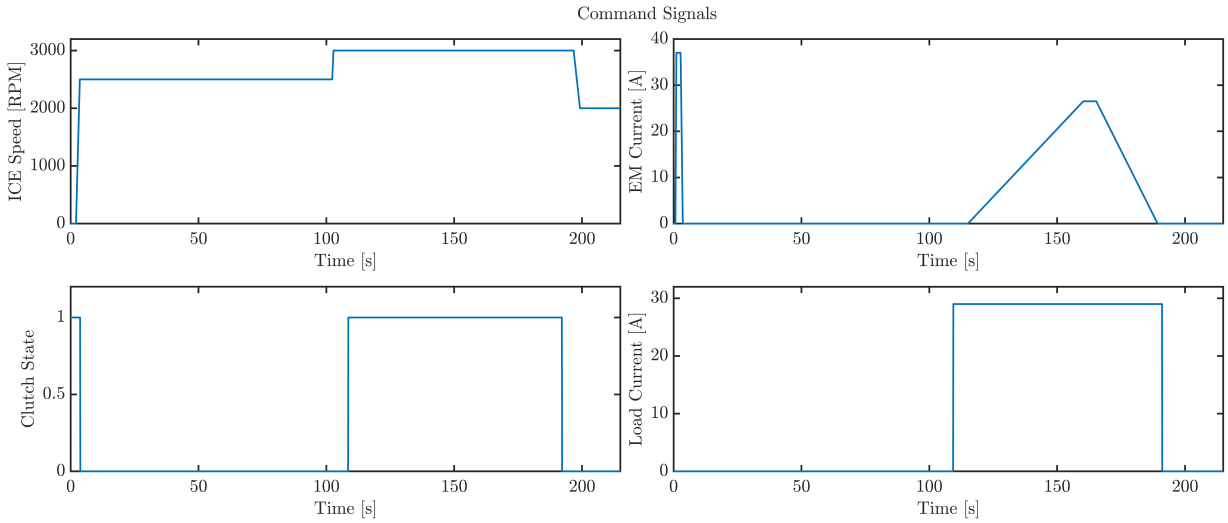

Figure 63: Input signals for the Mode 3 test

5.3.2 System Response

The starting sequence produced a sustained torque band of just over 1.5Nm for approximately three seconds because of the current commanded start sequence. This varies from the torque spike produced by a speed commanded start which were used in Mode 1 and 2. The combustion engine held its speed command during the idle sequence. When the clutch was engaged the PMSM maintained its current output while matching the combustion engine speed. Once the 30-amp load was applied the torque from the combustion engine spiked to keep the requested speed while the current command for the electric motor remained the same.

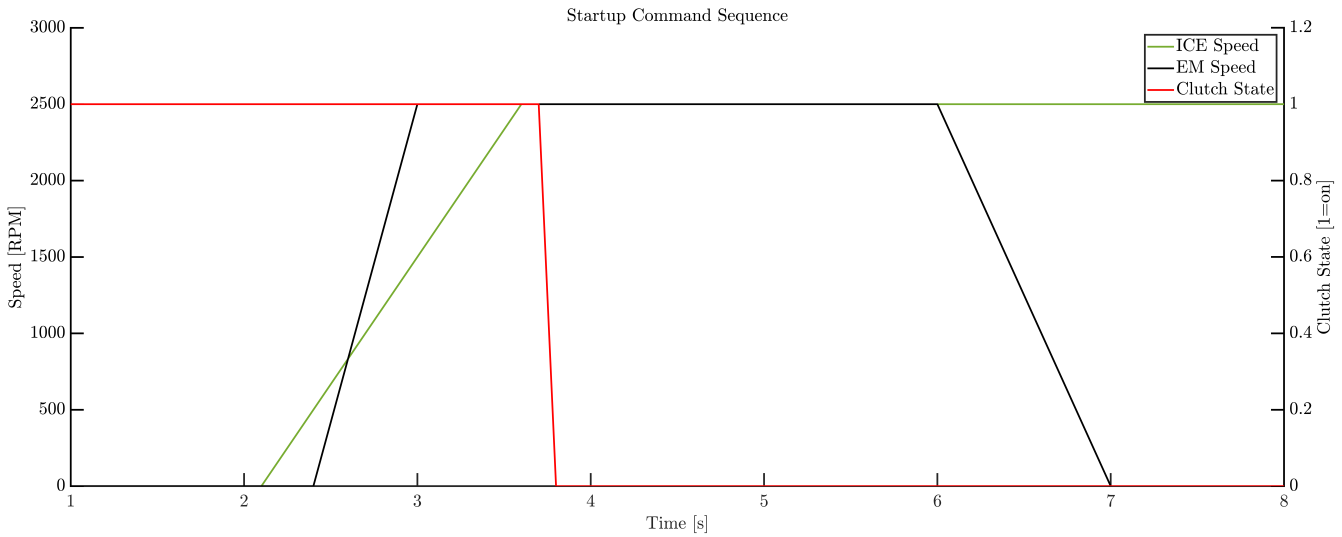

Figure 64: Starting inputs for the Mode 3 test

As the current draw was increased for the electric motor the torque output produced by the ICE decreased. This behaved in the same manner as Mode 2 where the torque sum matched the torque load and system losses. Compared to Mode 2 the response from the EM was quicker and linear compared to the ICEs throttle response, this meant the current increase for the PMSM was the straight triangular profile that was requested. The speed profile under load suffers from the IntelliJect PID weakness, this meant that when the load was engaged there was a substantial speed drop of nearly 1300RPM. A similar response occurred when the load was disabled causing the ICE to climb by approximately 1000RPM. These abrupt speed changes were not captured in simulation because the mapped combustion model is far more stable and does not have the abrupt transient response data required. The experimental response from the ICE showed that the PMSM is a much better speed controller and that the ICE's PID gains needs to be tuned further to improve ECU response.

5.3.3 ICE Response

The behavior of the combustion engine is far more predictable and stable at a commanded speed when the clutch was disengaged compared to a throttle command. The speed was maintained during idle while the torque dropped with engine temperature increase. The abrupt load activation caused the ECU governor to lose control of the setpoint for a significant amount of time allowing the ICE to drop or increase speed substantially. This was caused by the ECU control scheme being designed for gradual load responses. The simulation results for the loaded segment of the test show a similar torque curve to the experimental outputs. There was a larger error in the simulation results that could not be remedied because of the PID challenges of the IntelliJect. In theory the combustion torque would follow the same profile as the PMSM but inverted. Unfortunately, this was not the experimental result because of the added torque deviations that occur when the speed control of the combustion engine needs to make a correction. This can be observed in the speed profile of the system as the two power units lose speed over time when the load was applied. This shows that the ECU controller becomes less capable of reaching its setpoint as torque load was applied to the combustion engine.

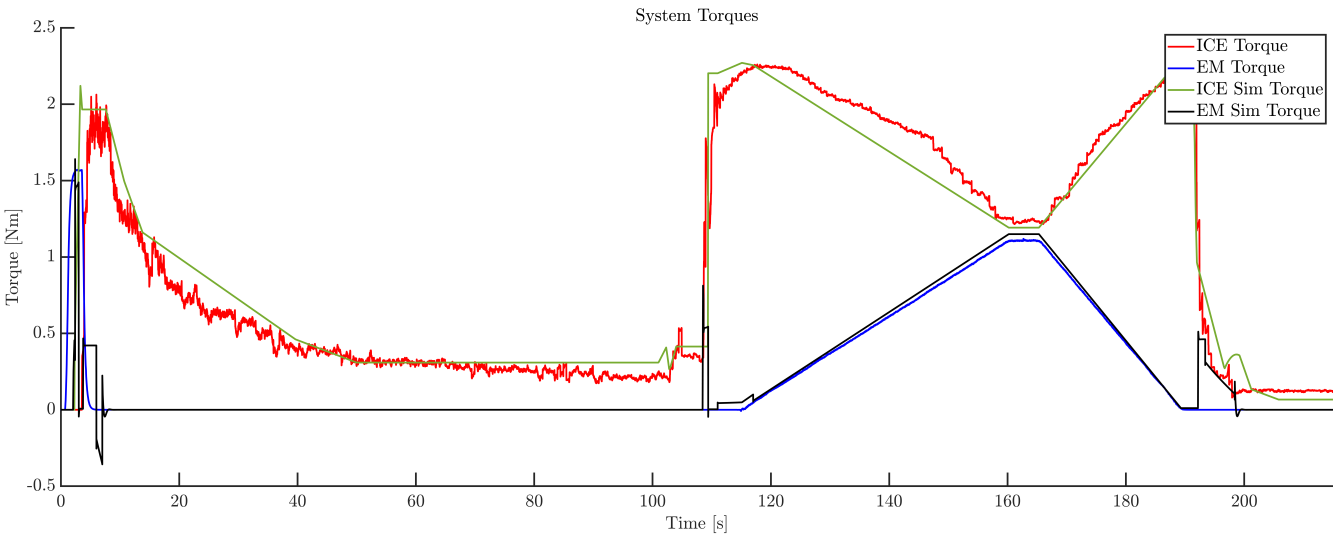

Figure 65: Combustion engine torque output and fuel flow

The fuel and throttle response from the combustion engine represented the throttle governor manipulation required to maintain the speed setpoint. As the current in the loaded segment increased the throttle and fuel flow decreased, inversely similar to Mode 2 operation. The shutdown sequence for the combustion engine in this mode changed compared to the throttle commanded mode since the RPM governor has stall protection. This meant that the throttle was not allowed to reach zero and was maintained at 8.5 percent to keep the engine spinning; the ECU disable button was used to shut down the engine.

5.3.4 PMSM Response

The startup response from the electric motor varied drastically compared to the other starting modes, this was caused by the commanded current. When a speed commanded start occurs the PID of the ESC is in control of the current and aims to reach the setpoint quickly. In a current commanded start mode the user is under control of the current draw. This resulted in a slower and weaker starting sequence with a starting torque of approximately 1.5Nm that lasted nearly three seconds.

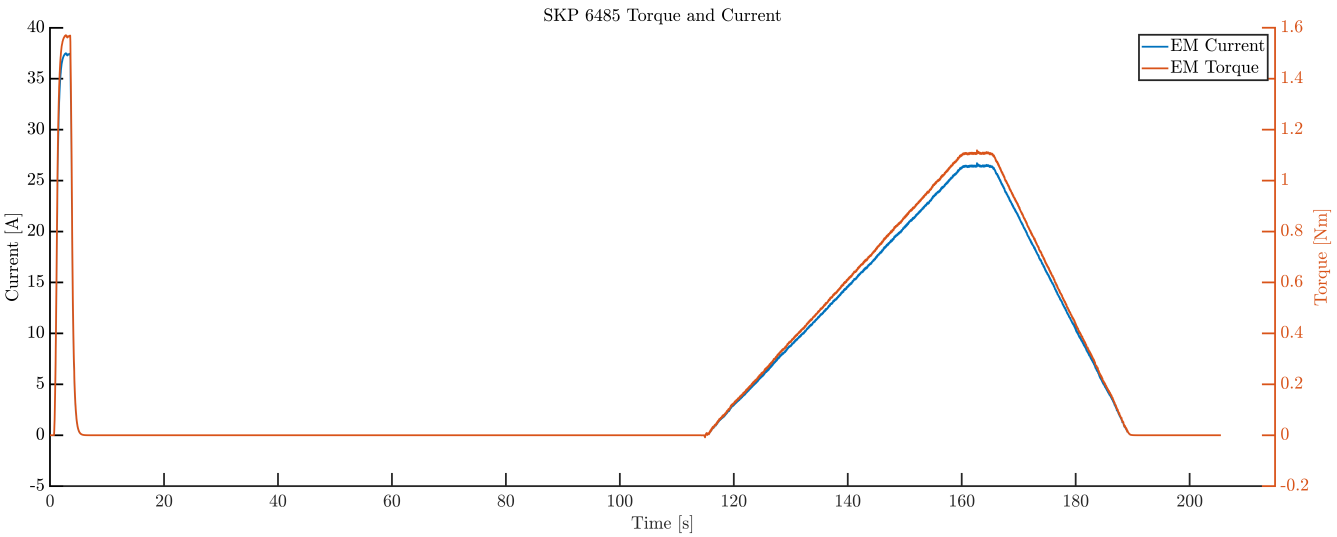

Figure 66: Electric motor current draw and torque output for Mode 3

When the load was applied to the system the electric motor had no reaction to the event because it was commanded zero current; essentially making it spin passively. The current command was sent to the PMSM and the response nearly matched the sent values. This torque response from the electric motor was far more stable and responsive compared to the combustion engine throttle in Mode 2. The simulation for this sequence closely matched the experimental results and shows that the accuracy of the PMSM model is greater than that of the combustion engine in Mode 2.

5.4 Flight Mission

The three different operating modes verified that the simulation model works under the most common power splitting scenarios and that the parallel test bench was capable of operating in said modes. To further solidify the simulations real-world application capabilities a theoretical flight mission was created to determine how accurate the model and test bench are for real applications. This flight mission was executed in Mode 2, all-electric, and combustion-only operation to determine the accuracy of each power units' model and compare the performance of parallel hybrid configuration to conventional propulsion systems.

5.4.1 Inputs

The virtual flight mission for the test was a simple VTOL profile that includes vertical climb, cruise, dash, and descent. This profile was selected to operate the system at a much higher power compared to previous tests. In future mission profiles the propulsion system operating points and the dynamometer load will be determined based on the airframe and mission. These missions will represent a higher degree of accuracy which includes air speed, payload, weather conditions, and other real world factors. All of these factors will be assessed by the flight science and airframe departments to provide a set of propulsion system speeds and dynamometer loads for the test.

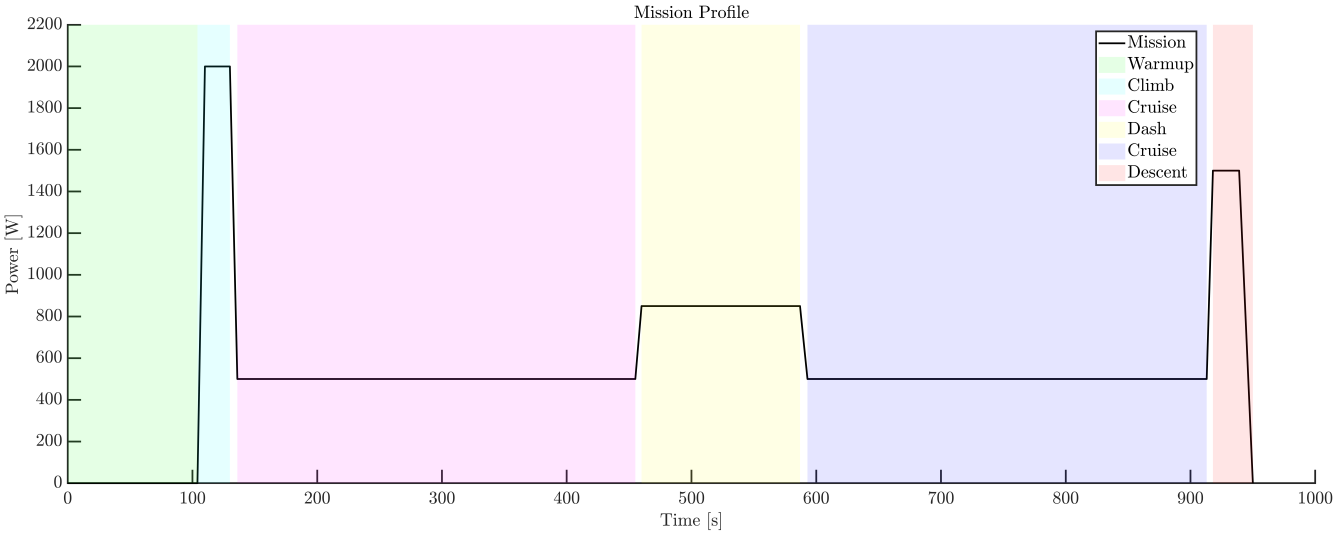

Figure 67: Virtual flight mission profile

For the hybrid mission the simulation was set to Mode 2 where the electric motor controls the speed of the system when the clutch is engaged. The propulsion system reached a maximum speed of 6100 RPM during the mission, this speed was selected for the power availability of the combustion engine during the ICE only testing. The mission could have been completed at 6000 RPM but that speed value is a dedicated breakpoint. Using a breakpoint value does not test the full extent (interpolation, regressions, extrapolation, etc.) of the model and could operate perfectly if there are parameters that were explicitly written at breakpoint intervals.

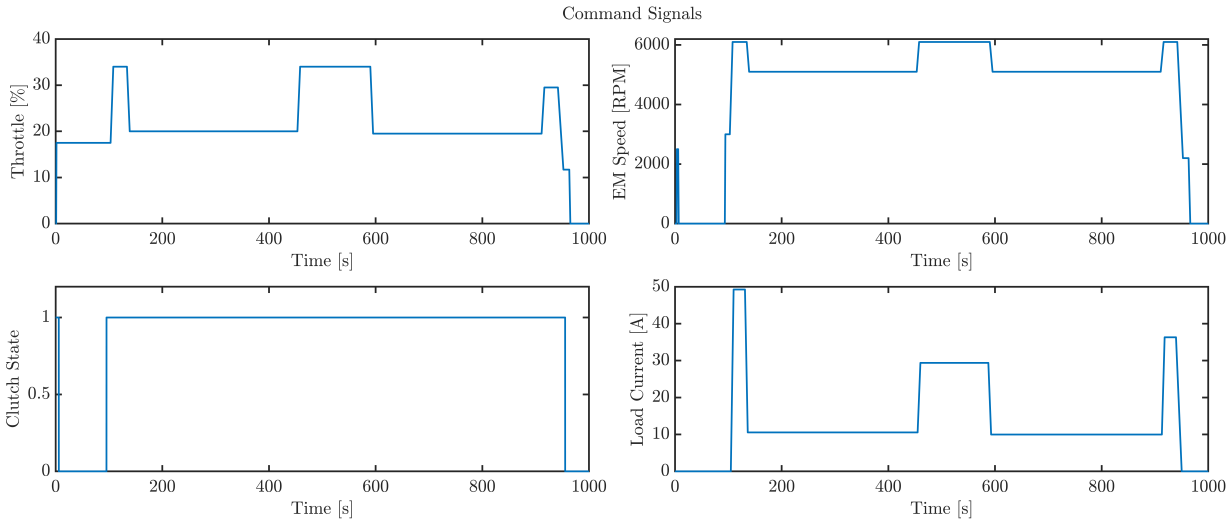

Figure 68: Mode 2 hybrid virtual flight mission commands

Segment	Speed[RPM]	Power [W]	Time [s]
Idle	3200	0	90
Climb	6100	2000	25
Cruise	5100	187	320
Dash	6100	800	120
Cruise	5100	187	320
Descent	6100	1400	25

Table 26: Flight mission description

The combustion engine was provided a throttle curve that determines the torque at all operating points throughout the test. This throttle curve will also be used to determine the speed of the ICE when the clutch is disengaged. The clutch and programmable load inputs are the state and current respectively, where the load current is the torque required to generate the mission power at operating speed. Unlike the previous tests the load is applied progressively, reducing rapid torque spikes on the system. This represents the load curve of a propeller during flight and should improve the performance of the combustion engine since its ECU control scheme is designed for these kinds of load profiles.

5.4.2 System Response

The flight mission responded in a similar manner to the low power Mode 2 test discussed earlier. Unlike the thirty amp tests the throttle was not adjusted during a given segment, the throttle and speed were held during each individual flight segment. The ICE startup sequence was the same as the shorter simulation tests in Mode 2 where a speed was commanded to the PMSM to promote initial combustion. The same torque spike range as before occurred. The combustion engine speed slowly increased as the temperature rose during idle; this was caused by the speed governor being disabled in the ECU.

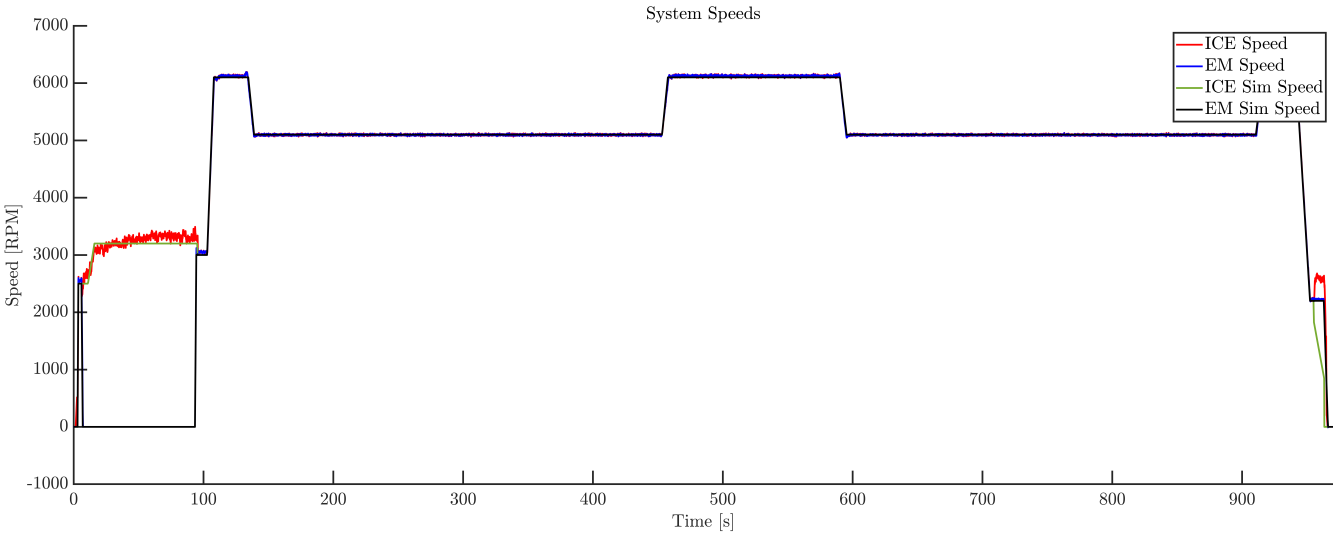

Figure 69: Speed response for the Mode 2 virtual flight mission

Once the combustion engine was at operating temperature the electric motor was spun to 3000 rpm and the clutch engaged. The system sped up to 6100RPM as the load was activated to execute the mission profile shown above. The power splitting during the loaded segments of this test followed

the same rules and behaviors as experienced in the Mode 2 initial test. With the progressive load applications there were no drastic speed or torque responses from the ECU or ESC which meant the experimental results were more stable.

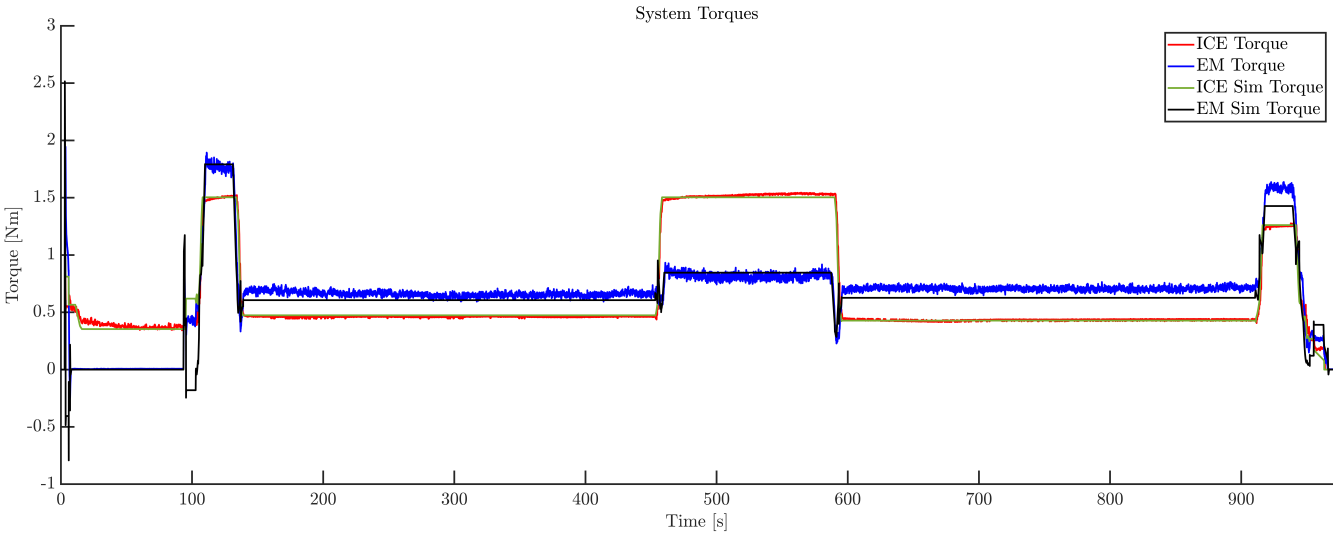

Figure 70: Torque response for the Mode 2 virtual flight mission

During the climb, dash, and descent segments the electric motor provided more power than the combustion engine because it controls speed, is already in the power transition state, and due to the throttle command at the given speed provides more than half the loaded power. There was more noise in the electric motor speed and current during this test because the operating speeds used exposed some mechanical weaknesses in the mounting system. The simulated results closely match the experimental values thanks to the more progressive loading profile, demonstrating that the accuracy of the model is higher when there are fewer drastic transient requests.

5.4.3 ICE Response

The simulated startup sequence still cannot replicate the fuel spike and initial power strokes of the combustion engine, but once in steady-state the model behaves well. During all mission segments the combustion engine response followed the maps and parameters provided from the IntelliJect. This includes expected speed, fuel flow, fuel consumption, and power. The overall response of the ICE matched what is to be expected from the Mode 2 control scheme.

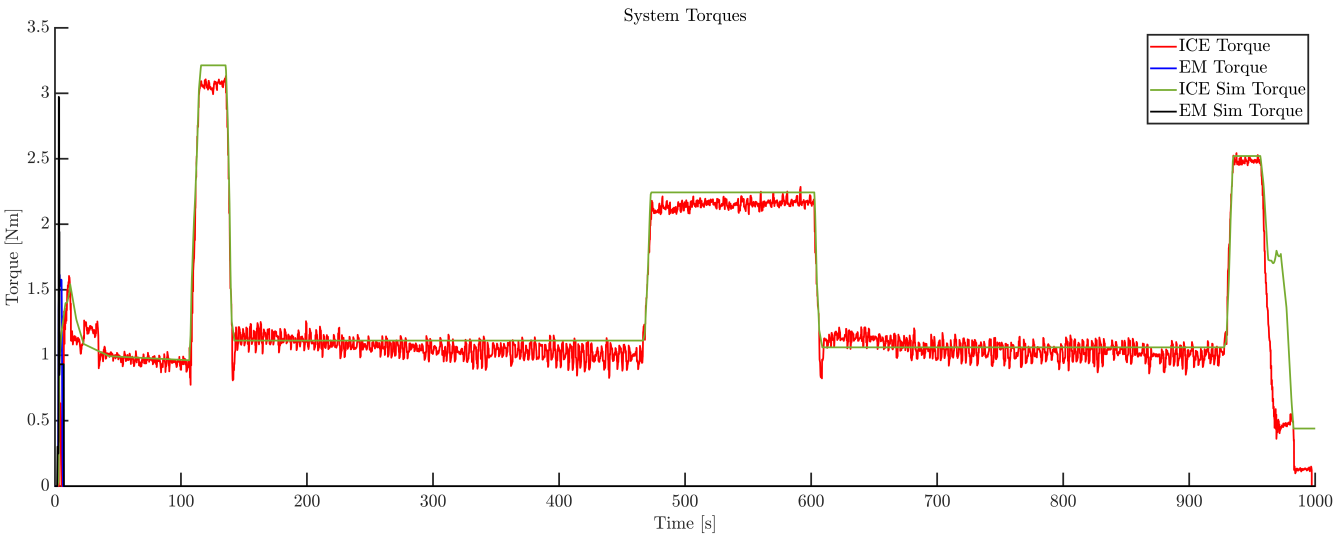

Figure 71: Torque response for the combustion-only virtual flight mission

During the combustion-only test of the mission profile the engine was responsible for full power output. For this test the RPM governor needed to be enabled so that the speed commands could be met by the ECU. The throttle and torque outputs of the combustion engine were then determined by the system load during each segment. The overall power limit of the mission profile was dictated by the combustion engine since it has the lower maximum power and the weaker PID gains for the scenario. The experimental and simulated responses were closer matched compared to the previous thirty-amp hybrid tests because of the simplicity of the power distribution and the activation of the speed governor. These two parameters make speed and torque prediction much simpler.

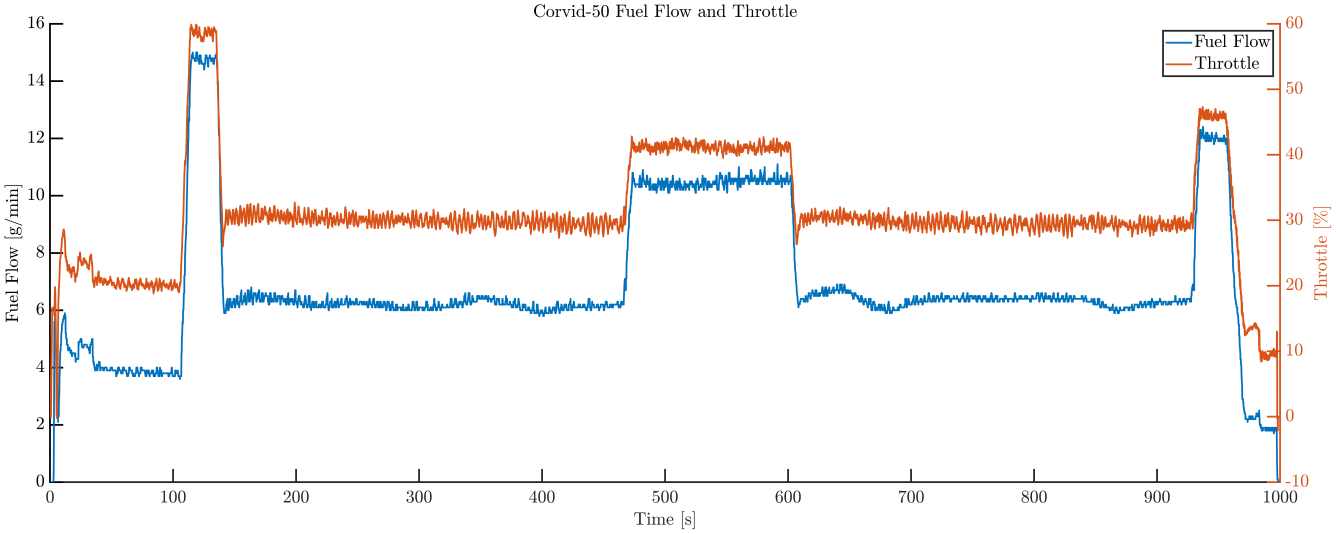

Figure 72: Fuel flow during combustion-only virtual flight mission

The primary goal of running the mission in combustion-only mode was to obtain the amount of fuel required. As expected, the throttle values, fuel flow, and overall consumption increased when the mission was run without electric assistance. The comparison between electric, hybrid, and combustion will be discussed in the results section.

5.4.4 PMSM Response

For the Mode 2 virtual hybrid flight test the electric motor behaved in the same manner as the lower powered thirty-amp test discussed before. The PMSM produced more torque under clutch engagement same as before since the motor must maintain speed and smooth combustion vibration. The torque output from the electric motor was the difference between the torque provided by the ICE and the amount requested by the system. The simulation results for this test provided a good representation of the experimental response. Compared to the first test run in Mode 2 the simulation and experimental results had lower error rates thanks to the progressive loading profile of the dynamometer.

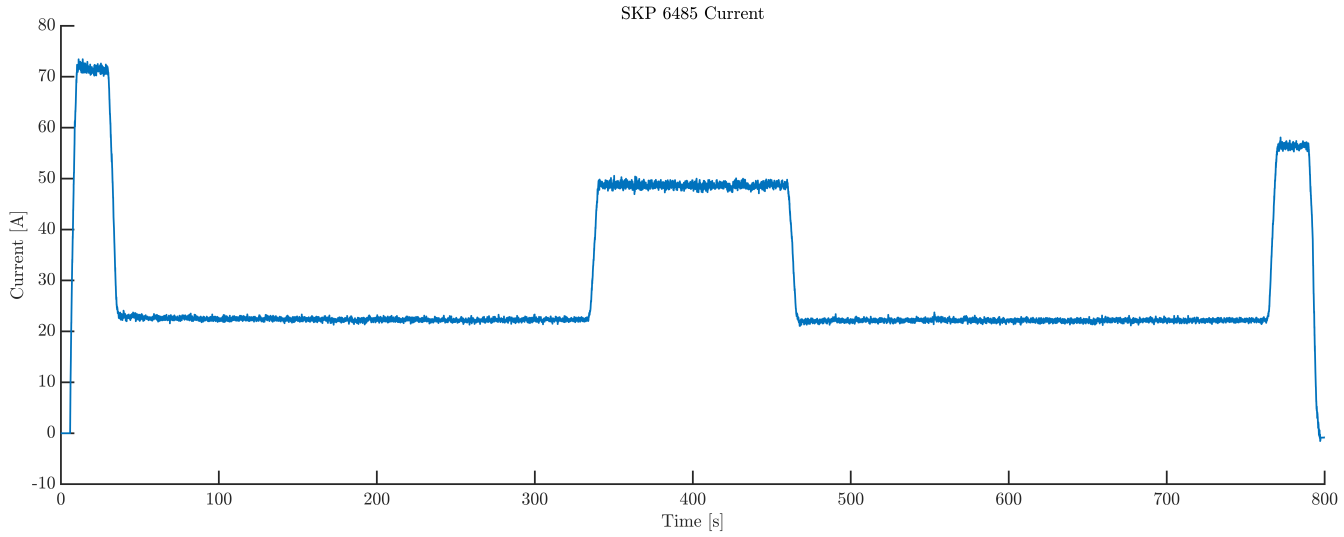

Figure 73: Current draw during electric-only virtual flight mission

The electric motor was also run separately for the entire flight mission to determine the response of the electric motor, and the energy used. For the electric-only mission, the motor was required to produce all the power requested by the system. The speed and torque responses were nearly instantaneous and far more responsive compared to the combustion-only mission. Simulation results for this test were nearly identical to the experimental outputs. This predictable performance can be attributed to there being no power splitting and the drivetrain dynamics being well characterized in the simulation model. The performance of the PMSM will be discussed in the next section and compared to the hybrid and combustion-only flight missions.

The six tests performed and described in this section were used to test the ability of the test bench and simulation model. The initial tests in modes 1-3 were ran at a lower power and speed to check stability of the controllers. In addition, the lower speed and power allowed for an initial mechanical test of the new components that were installed on the test bench throughout the year. Once the thirty-amp tests were completed the test bench was proven operational and capable of further testing. During these low power tests, the experimental data provided the insight required to improve the simulation model. Each test exposed errors and weaknesses in the modelling of various components and logic blocks. The Simulink model improved as testing progressed until the outputs resembled that of the experimental tests. The virtual flight mission was then chosen to run the test bench at operational speeds and loads. This final test scheme further substantiated the test bench's ability to operate within the limits of the power units. Initial results from the

simulation model for flight missions generated results that closely matched the real response of the system. Small changes to the ramps, timing, and efficiencies were required to improve the simulation results. This modification requirement to the model can be attributed to the fact that the entire model was created based on previous tests that experienced half the power and that neither the PMSM nor ICE behave exactly the same between tests. Detailed analysis of the experimental and simulation results are discussed in the next section.

6 Results

The previous section described the tests executed on both the test bench and in simulation from a high level perspective. In this section the results of these tests will be discussed in detail to provide a deeper understanding of the system responses, simulation accuracy, and the differences between the operating modes. In addition to these operating modes the performance of the hybrid system will be compared to conventional propulsion methods. The results from these discussions aim to answer the questions posed at the beginning of this thesis to support the legitimacy of parallel hybrid-electric propulsion systems for small-scale UAVs.

6.1 Mode 1, Dual Speed Command

Each mode will be analyzed in order of operation, beginning with the startup sequence and ending with shut off. During the startup sequence in Mode 1 the electric motor was used to start the combustion engine via a speed command with the clutch engaged. This aspect of the test bench operation was difficult to model accurately compared to steady-state operation once the system is rotating and up to temperature. Modelling the startup sequence was difficult for two reasons, firstly the combustion engine model is a mapped design which is intended for steady-state operation. This means the transient responses of initial combustion is not possible with the currently used model. Using a more complex model would require substantially more modelling which could be its own thesis because of the complexity of combustion and thermodynamics. The second reason that startup was challenging to model is because the starting state of the test bench is never the same. Some of the variables that attribute to this deviation in startup state were the engine temperature, starting crank angle, oil presence in the cylinder, electric motor angle, and environment. For these reasons the main goal for the startup sequence in simulation was to model the EM starting torque spike well. Predicting the starting torque range for the electric motor provides the insight and tolerance required to correctly select an electric motor for a hybrid-electric system.

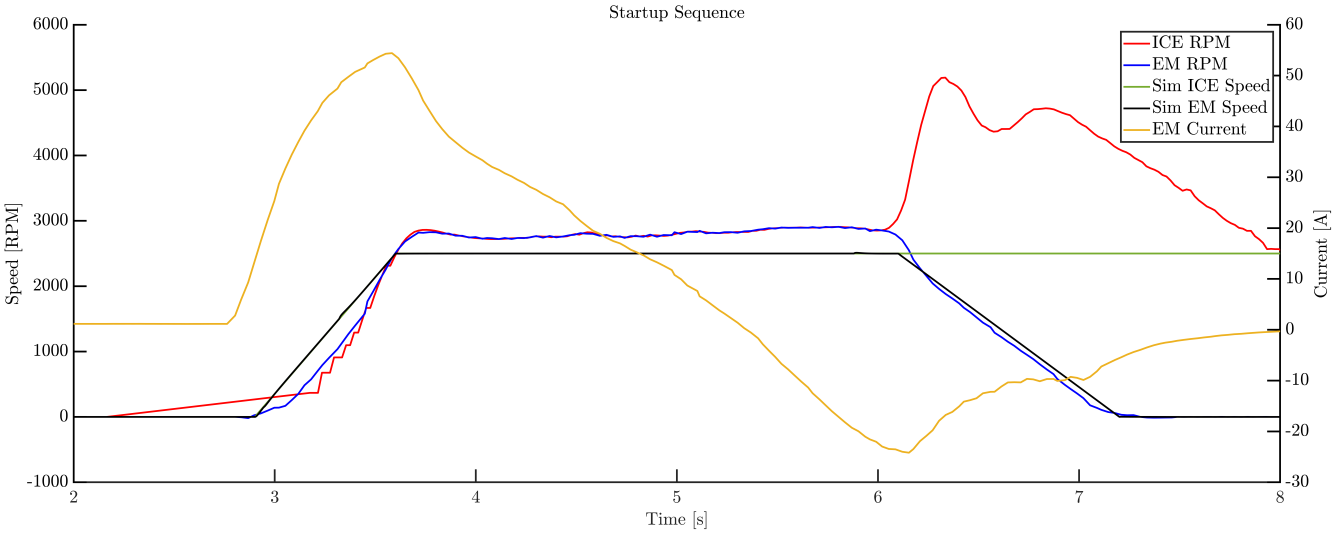

Figure 74: Startup response from the system during simulation and experimental testing

Based on extensive testing of the propulsion system the starting torque requirement of the electric motor for the Corvid-50 engine has a range between 2-3Nm for a speed commanded cold start. The

difficulty of predicting combustion start means this segment of simulation has strong uncertainty and aims to over-predict starting torque to guarantee that electric motor selection is capable of starting the combustion engine. In the Mode 1 thirty-amp test the simulated electric motor starting torque was 2.658Nm while the experimental torque during testing yielded 2.280Nm. For the specific test this represents a 16.59% error between simulated and experimental measurements of the starting PMSM torque. This magnitude of error was common for the starting torque sequence across the different modes and tests.

For the remaining segments of the test the mean torque and speed values were collected to quantify the accuracy of the model compared to experimental results under operation. The mean values were collected over each time range of the different segments of the mission, for the 30A test there are three segments; startup, idle, and loaded. The speed data quantifies the ability of the controllers in simulation and on the test bench to maintain a setpoint. While the simulated and experimental mean torque describes the accuracy of the torque splitting logic in the Simulink model.

Segment	Mean Speed [RPM]	Error [%]	Mean Torque [Nm]	Error [%]	Unit
Startup	2776.2	-3.60	2.279	-16.59	EM
Loaded	3039.6	-1.32	2.073	6.06	EM
Startup	2781.0	-5.76	0.967	4.61	ICE
Idle	2442.8	2.29	0.256	5.69	ICE
Loaded	3034.0	-1.13	0.049	-3.05	ICE

Table 27: Mean torque and speed values for the 30A Mode 1 test

For Mode 1 in the low power test the speed prediction of the simulation model was fairly accurate with the highest error being 5.76% under startup for the combustion engine. During the other two mission segments the accuracy of the simulation was under 3% with error being attributed to the nature of real world PID speed control and combustion vibration. Mean values can often be misleading and therefore should be paired with more detailed analysis. For the idle and loaded sections the error in torque and speed prediction for both power units were calculated. This provides a description of the error between simulated and experimental data throughout the specific time frame.

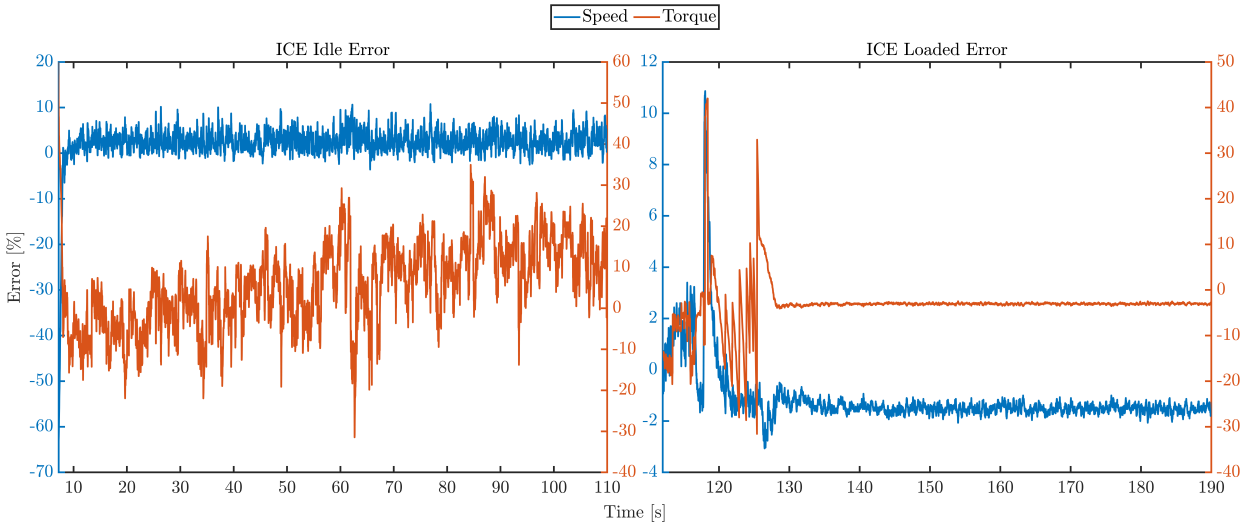

Figure 75: Error between experimental and simulated responses of the ICE

As Figure 75 above shows there are error value spikes during both segments of the mission, demonstrating the importance of accurate data visualization. During idle both the ICE speed and torque error was higher than the mean and was caused by the vibration of the combustion as well as the variation in temperature as it warms up. Speed error oscillates with peaks of just over 10% while torque increases in error up to approximately 35% because of the decrease in torque as the engine warms. The highest errors during the loaded sequence reached over 40%. This large error was caused by the abrupt speed drops that occurred when the load was activated. As stated in the previous section these responses are not experienced in the simulation because of the PIDs used in the power unit models.

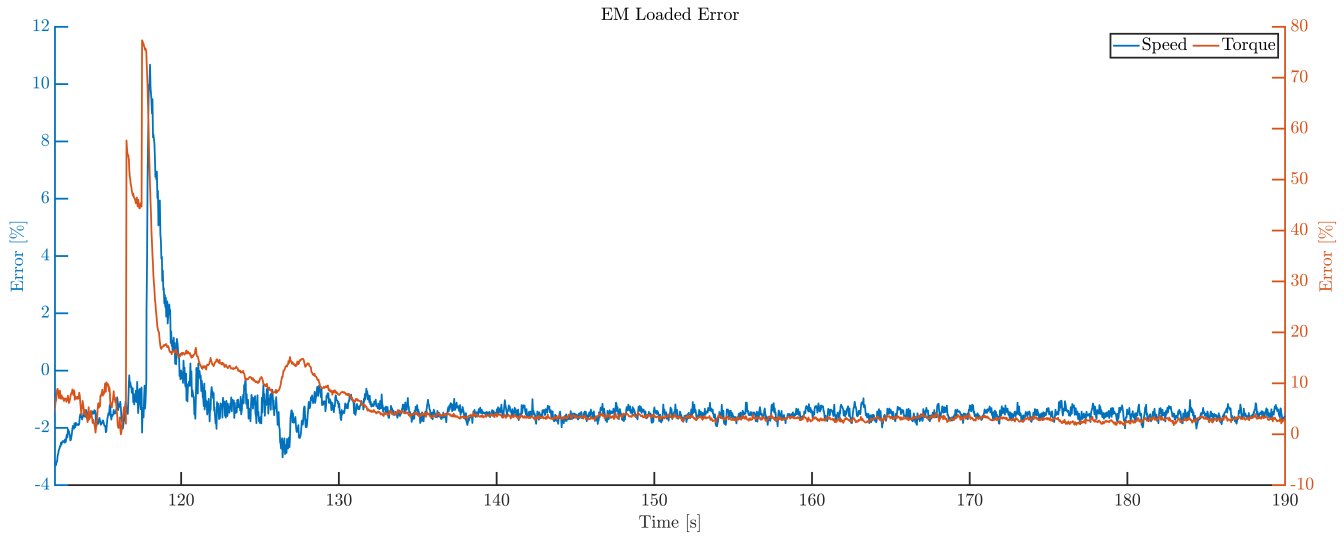

Figure 76: Error between experimental and simulated responses of the EM

The electric motor during the same loaded segment demonstrated the same behavior. The error in both speed and torque predication increased dramatically with the ECU spike response during load activation on the test bench. However, for both the ICE and the PMSM once the system recovered from this excitation the steady-state error was below 5%.

Comparing the simulation and experimental results from a macro perspective shows a strong representation of real-world response from the Simulink model. Despite large errors caused by controller PID weakness on the test bench the operating envelope of the system was well represented by the simulation tool.

6.2 Mode 2, Throttle and Speed Command

Using the same approach as the previous test, Mode 2 yielded similar results for both the simulated and experimental data. For this mode the combustion engine torque was directly controlled by the throttle command sent by the operator. During startup the responses from the combustion engine and electric motor were similar to Mode 1. The speed commanded startup yielded a maximum torque of 1.999Nm from the electric motor while the simulation predicted a value of 2.217Nm. These two values resulted in a starting torque error of roughly 10.91%. Again, the error in starting torque for the electric motor was caused by the same discrepancies and sensitivities described for Mode 1. The lower starting torque during this test was caused by the combustion engine not

fighting against the electric motor speed command. In Mode 1 both controllers are fighting each other to maintain their respective commanded speeds even if they are sent the same setpoint.

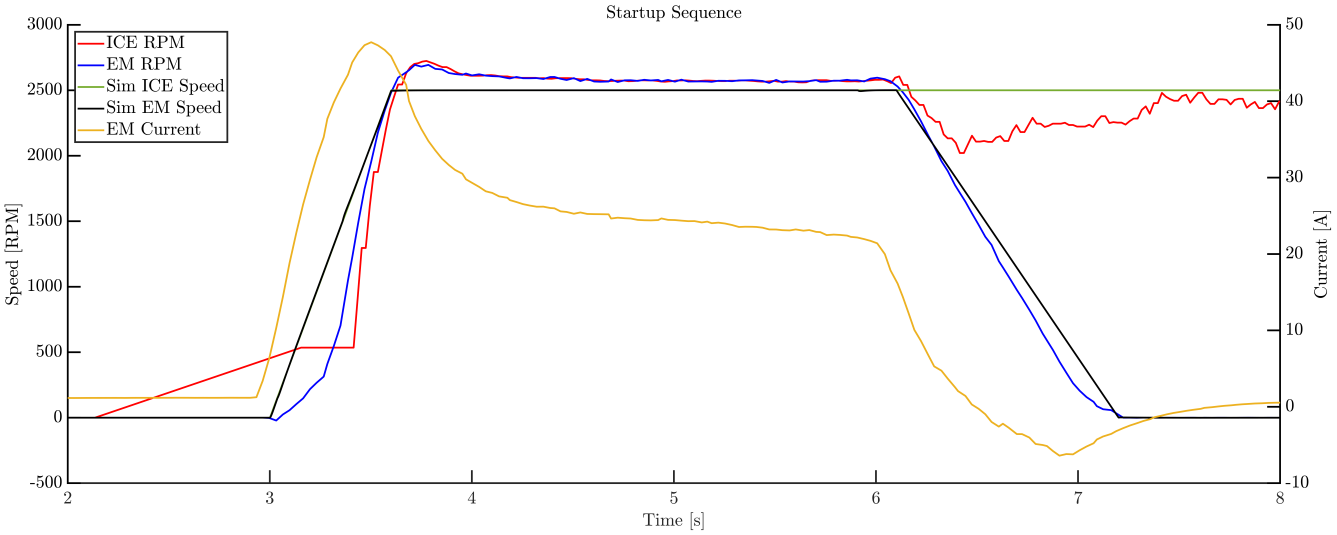

Figure 77: Startup response for Mode 2

During the idle sequence of the test the throttle was held at a constant value of 16.5%. This throttle value provided enough speed for the combustion engine to run smoothly as it reached operating temperature. During this operating mode the combustion engine speed error was caused by the lack of command sent to the combustion engine to regulate speed since the throttle governor was disabled. The speed error would have increased further had the combustion engine not been warm from previous tests. As the temperature difference between start and loading sequence increases so does the error in torque and speed since the internal load of the combustion changes further.

Segment	Mean Speed [RPM]	Error [%]	Mean Torque [Nm]	Error [%]	Unit
Startup	2574.7	6.73	1.999	-10.91	EM
Loaded	3045.9	-1.53	0.837	-15.69	EM
Startup	2574.0	-0.69	1.128	12.00	ICE
Idle	3076.8	-3.50	0.394	-1.10	ICE
Loaded	3046.0	-1.53	1.565	1.94	ICE

Table 28: Mean torque and speed values for the 30A Mode 2 test

During the loaded segment of this test the mean torque error for the electric motor increased substantially compared to the Mode 1 test. The mean error of 15.69% represents the difficulty of modelling the torque logic for this specific operating mode. When both power units were commanded a speed (Mode 1) the torque distribution between the ICE and EM was nearly nonexistent; the power unit that was commanded a higher speed or has the more robust controller takes the full load of the system up to its maximum capacity. This made torque logic in Mode 1 much simpler to predict. When the ICE was commanded a throttle in Mode 2 the torque prediction model became more complicated. Predicting the torque output of the combustion engine in Mode 2 was fairly simple; using the speed and throttle values during operation the torque could be determined using the power map. Because of the direct availability of the torque value the error in prediction for the combustion engine was much lower at 1.94%. To calculate the electric motor torque the logic

became much more complex; to find the torque output of the electric motor both the torque of the combustion engine, load, torque required to govern speed, and smoothing torque needed to be known. Therefore, the deviation in torque prediction was much higher because of stacking error from those various parameters which resulted in a higher electric motor torque error. The full mathematical model of how the PMSM torque is found in Mode 2 can be seen in the modelling section.

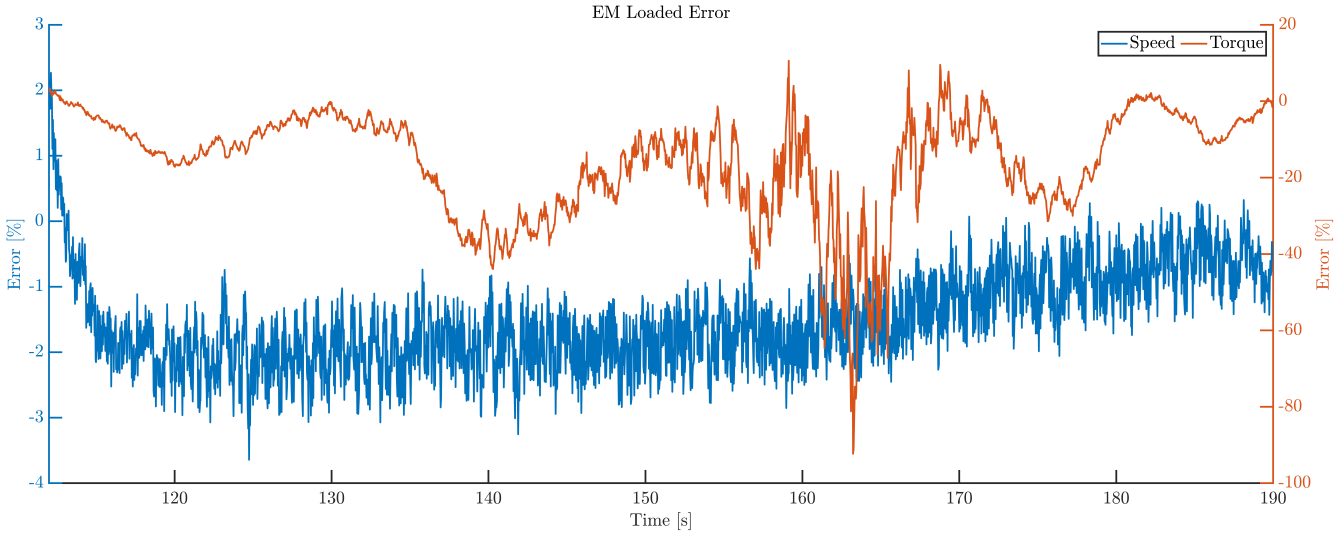

Figure 78: Error between experimental and simulated responses of the EM

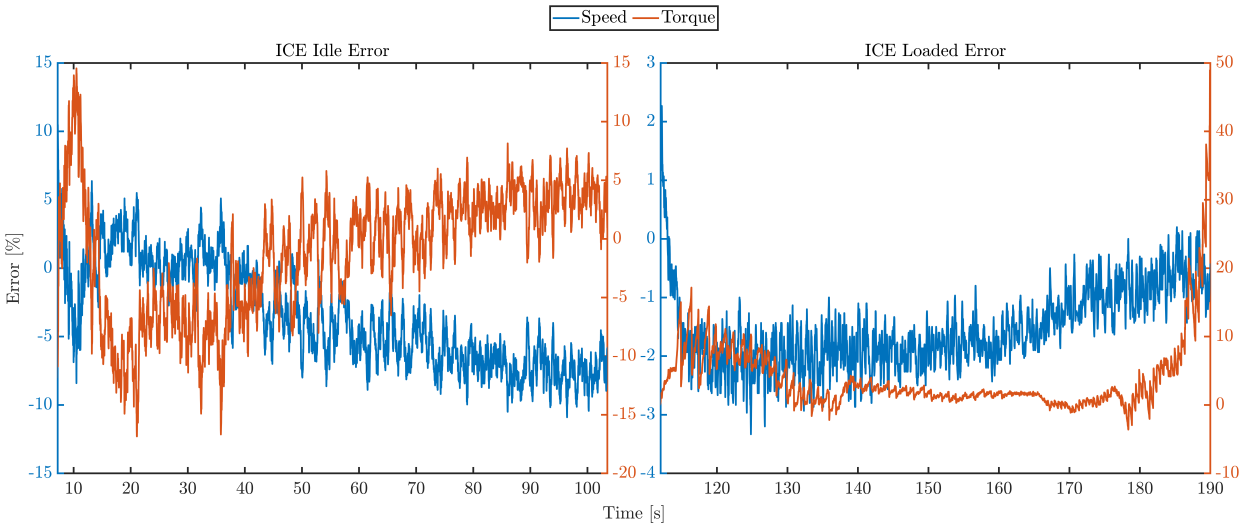

Figure 79: Error between experimental and simulated responses of the ICE

While these mean torque, speed, and error values provided a broad understanding of how well the simulation predicted the experimental response further detail was required. During the idle and loaded phases the error in simulated versus experimental data fluctuated constantly. Plotting this error behavior provided a deeper understanding of the simulations ability and what events exposed weaknesses in the test bench and/or simulation model. In the same manner as Mode 1 there was a large error spike during the loaded phase when the programmable load was activated. This torque spike caused an abrupt drop in system speed resulting in a large error, the same event

occurred in Mode 1. For this specific test there was another large error occurrence for the electric motor at maximum throttle from the ICE. At this point the torque prediction error was 92.31% which was caused by the magnitude of the operating torque which was 0.14Nm experimentally. At low power the simulation prediction becomes inaccurate because of the inability to characterize the drivetrain at that power level. The characterization process of the drivetrain described in the modelling section explained that the system was spun from 1000 to 6000 rpm to collect the required data to find inertia, damping, and static friction. The test bench was not capable of spinning slow enough to characterize the low power operation of the system. Additionally, the 0.14Nm torque value at the bottom of the torque curve was a large spike caused by the combustion engine, further amplifying the error during the segment. While the error was quite large at this segment of the test the torque difference between prediction and experimental was only 0.067Nm which is inconsequential for a motor capable of 5.53Nm.

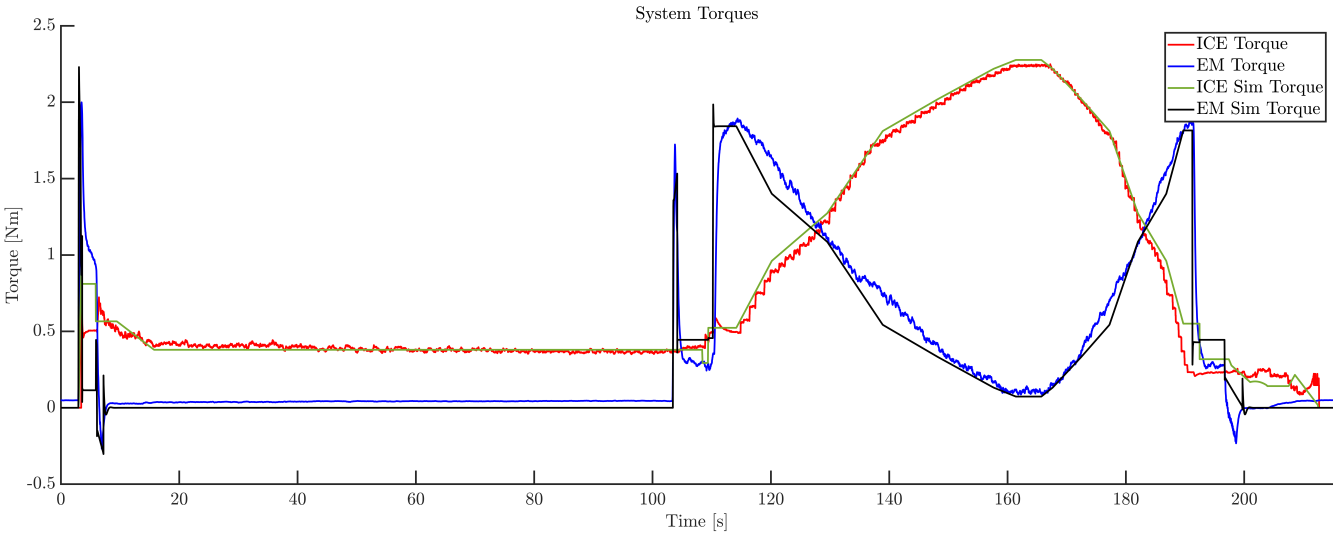

Figure 80: Torque response in Mode 2

Looking at the overall simulated results compared to the experimental data provides a stronger understanding of the Simulink models ability to predict the tests benches response. During startup the system dynamics and results provide the torque requirement to start the combustion engine with an electric motor. The idle process is by far the least important segment in the simulation model since this is an unloaded segment required by the ICE to reach a operational state before it can be used in the hybrid propulsion system. The loaded segment of the Mode 2 test represents legitimate power split control and is critical in hybrid-electric propulsion development. This section of the simulation model must be accurate as it will be used to optimize operation of the system and determine the limitations of the propulsion system. The overall response of the model compared to the test bench results provides a well-represented operating envelope that can be used to predict mission performance, influence component selection, and increase propulsion system optimization.

6.3 Mode 3, Speed and Current Command

The last thirty-amp test for the test bench was the combustion engine speed regulated test with electric motor current control. This operating mode was the most unique scenario out of the three modes since neither the speed nor torque had been controlled with their respective power unit before. In the previous two tests the speed was held steady by the electric motor; this meant the feedback PID control for speed was handled by the VESC which is designed for these load cases. Using the ECU to control speed in this test proved challenging since the gains in the IntelliJect were tuned for propeller profiles. The electric motor for this test was controlled via current command which is directly proportional to torque. Since the electric motor was in current command mode the startup sequence was also different.

To start the combustion engine in Mode 3 a current curve was needed to provide enough torque and speed to promote initial combustion. The current curve was created using the maximum current experienced during warm startup with a ramp speed and hold length to keep the ICE spinning without damaging the ESC because of high current draw. Over the span of 1.5 seconds the current rose to 37 amps and held for the same period. This current curve executed a starting cycle that was much slower and less reliable compared to the 2500rpm speed commanded start in Mode 1 and 2. However, once the combustion engine was self-sustaining from the current command the ICE ran smoothly at the requested 2500rpm from the throttle governor.

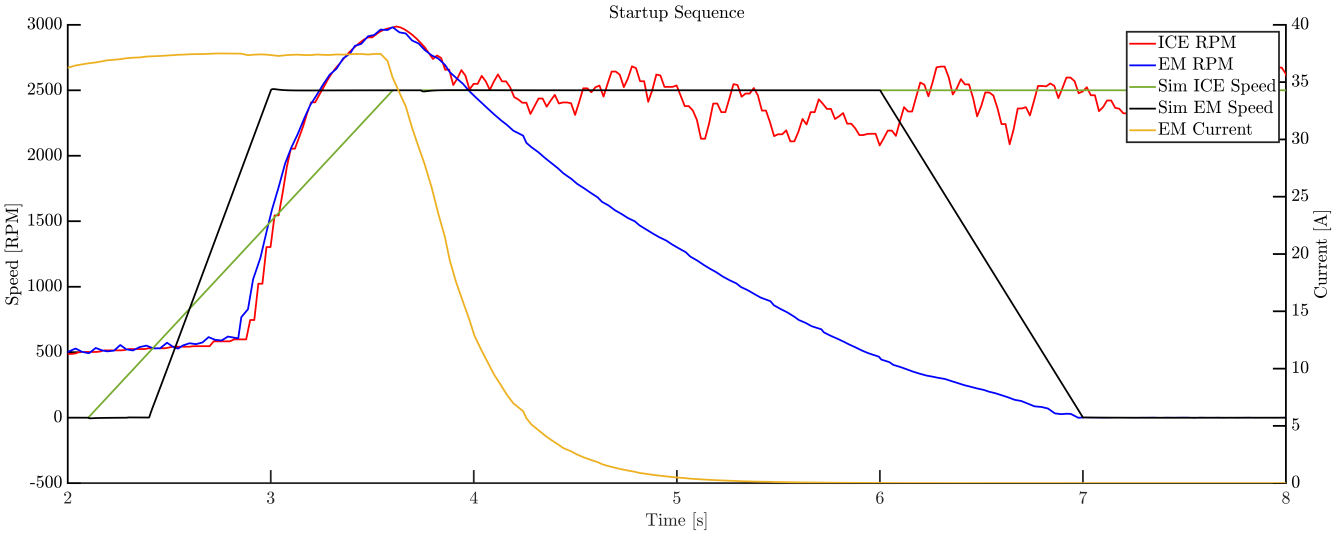

Figure 81: Current commanded startup sequence in Mode 3

The idle process of the combustion engine during this test was essentially the same as the Mode 1 test. Using the throttle governor to command speed of the combustion engine provided a consistent speed with fluctuations caused by the vibration of the engine and PID gains. For this test another variable was added to challenge the capability of the simulation model. In Mode 1 when the combustion engine had the throttle governor enabled the engine was already warm from previous tests, for this Mode 3 test it was not. The engine was started from cold to see how drastically torque changed with temperature during the idle phase. This challenging scenario caused an error of 14.14% for ICE torque prediction during idle. The torque upon startup was 2.063Nm and dropped to 0.180Nm after operating for 90 seconds, right before the clutch was engaged. This large

torque variance was difficult to predict and is directly connected to the throttle map, governor, and startup multipliers that are in the ECU.

Following the trend of the previous tests the mean speed and torque values fell within a reasonable error range that provided confidence in the simulation's performance. However, because the IntelliJect was in control of maintaining speed for the system through the combustion engine there were some abrupt speed spikes. When the electronic load was activated on the dynamometer at 30A the speed of the system dropped by approximately 1200rpm, over twice the decrease that occurred with the electronic speed controller when it governed speed in Mode 2. The ICE controller took roughly eleven seconds to reach the commanded 3000rpm after the spike event which was over three times longer than what the electric motor took to recover during the Mode 2 test. The same behavior occurred when the electronic load was deactivated and the speed spiked to 4228rpm. This test demonstrated the weakness of the combustion engine controller who's gains and control scheme need to be modified if it is to be used further on the test bench. Due to these large spikes during the test the time frames in which they occur were omitted from mean error calculation and real-time error visualization since their magnitude would make the rest of the errors imperceptible.

Segment	Mean Speed [RPM]	Error [%]	Mean Torque [Nm]	Error [%]	Unit
Startup	2718.3	-4.20	1.570	5.34	EM
Loaded	2928.2	0.60	0.542	14.33	EM
Startup	2449.5	-1.07	2.063	-2.69	ICE
Idle	2482.5	1.83	0.456	14.14	ICE
Loaded	2928.9	2.37	1.834	-5.03	ICE

Table 29: Mean torque and speed values for the 30A Mode 3 test

The errors shown in Figures 82 and 83 represent the real error during the time spans of the two major test segments. As stated earlier the large spikes in speed and torque from the ICE controller were omitted from these graphs, however, the remnants of recovery can be seen. The simulation does not have the capability to predict spikes caused by the controller which explains the high error on either side of the graphs. One important aspect of this error profile is the response from the electric motor versus the combustion engine. The graphs represent the same time period for both power units; however, the electric motor responds quicker to the spikes while also reaching steady-state faster. These graphs provided a strong visualization of how much better the ESC responds to system changes compared to the ECU, further demonstrating the ICE should not be used as the speed governor until the ECU is improved.

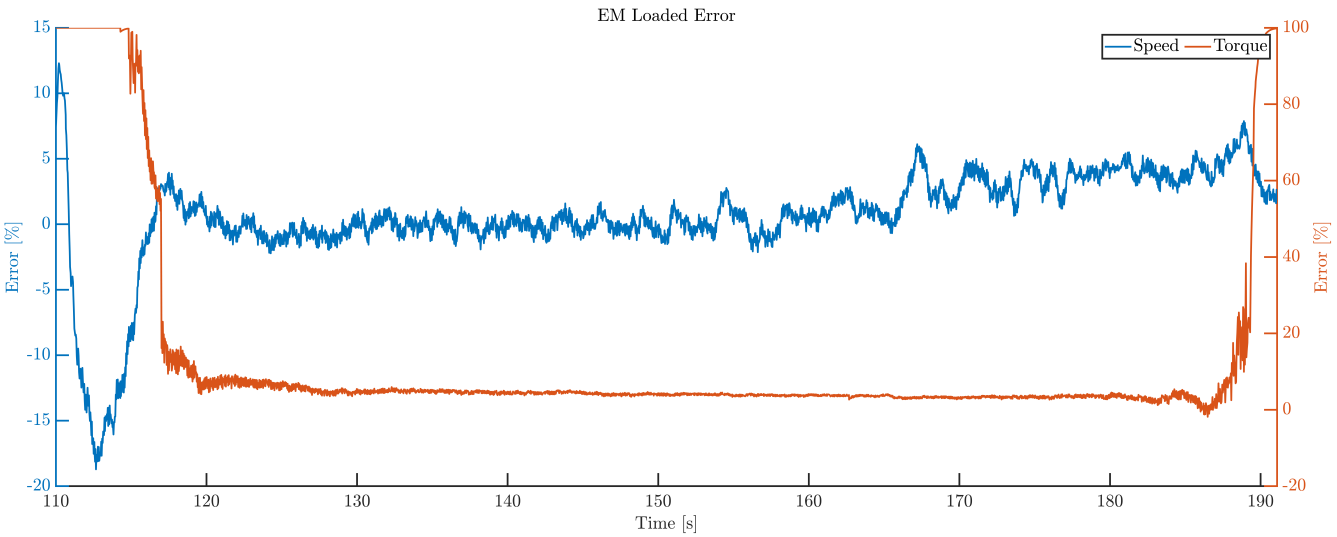

Figure 82: Error between experimental and simulated responses of the EM

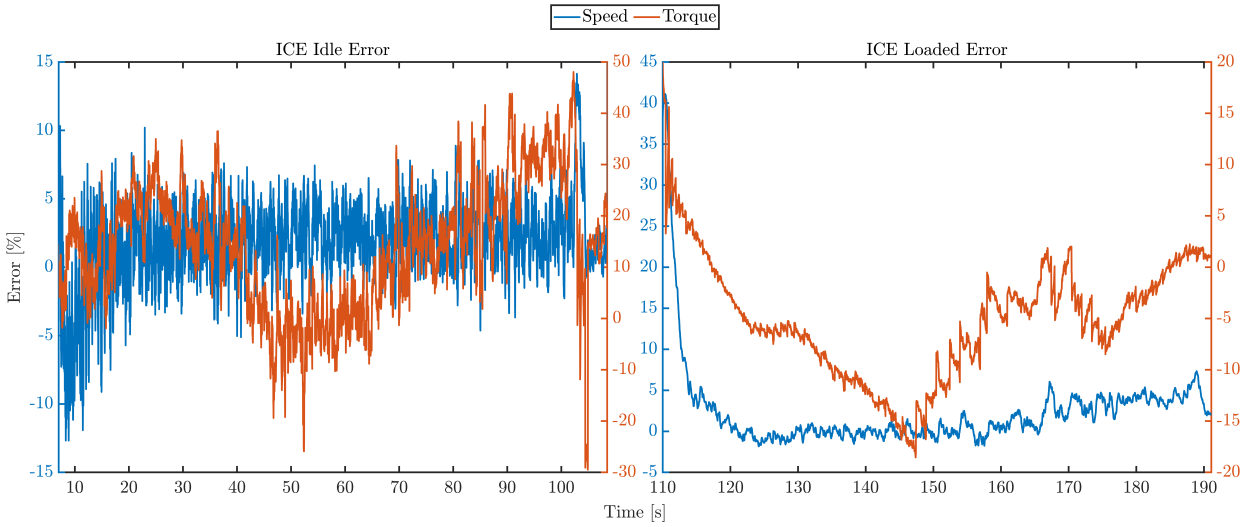

Figure 83: Error between experimental and simulated responses of the ICE

Looking past the sections affected by the speed/torque spikes, the system response is very strong and sits within a similar error region as the previous two modes. The electric motor torque error was much lower during the current curve thanks to its stable response that closely matched the commands sent. When the ICE was commanded a throttle in Mode 2 the commanded throttle signal was the same shape as the one seen in Mode 3. However, the combustion engines response rounded the throttle response causing a slower and less controlled output. This rounding effect can be seen in the combustion engines response to the current increase in Mode 3. During the current curve segment, the PMSM error was less than 10% for both speed and torque while the combustion engine error range was higher at less than 18.55%.

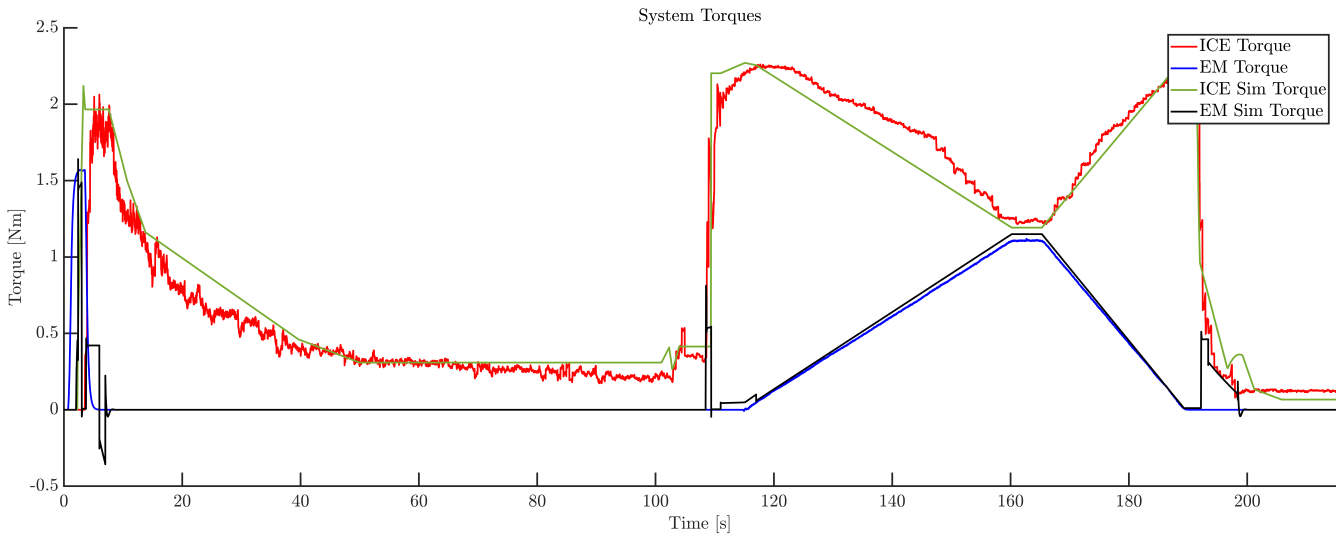

Figure 84: Full test torque response in Mode 3

Despite the large spikes caused by the ECUs control algorithm the system response as a whole represents what occurred on the test bench with reasonable accuracy. The starting sequence was drastically different from previous tests because of the current command state. This starting mode is not recommended but does work if required for a specific mission. The loaded segment of the test (omitting the spikes) shows a responsive torque curve from the PMSM that closely matches the commanded values sent. The combustion engine responds to the electric motor as expected with some added deviation caused by the ECU. The total outcome of this test demonstrated that Mode 3 in theory behaves the same as Mode 2 but with torque and speed control swapped between the ICE and EM. However, in practice Mode 3 is not ideal for use on the test bench with the current engine control unit.

6.4 Electric

The next three tests ran on the test bench and in simulation were the virtual flight mission described in the previous section. The goal of this flight mission was to challenge the mechanical capabilities of the new components on the test bench, verify simulation results at higher power, and collect telemetry to compare conventional propulsion methods to parallel hybrid-electric.

For the first flight mission test the experimental bench was configured in an all-electric configuration to determine the response of the system based on electric motor only power. For electric propulsion there is no combustion startup sequence or idle segment, which means the test begins with the PMSM spinning up to operating speed. For this mission the dynamometer is applied at a ramp speed to represent the propeller load that would occur during flight operations. The startup segment of the electric motor for this mission was smooth, predictable, and matched the command almost identically. During ramp up the error between simulated and experimental speed was 1.82%, while the initial torque spike had an error of 19.69%. This starting torque error is caused by the reaction time of the simulation and the test bench being different which either decreases or increases the torque response of the PMSM at startup.

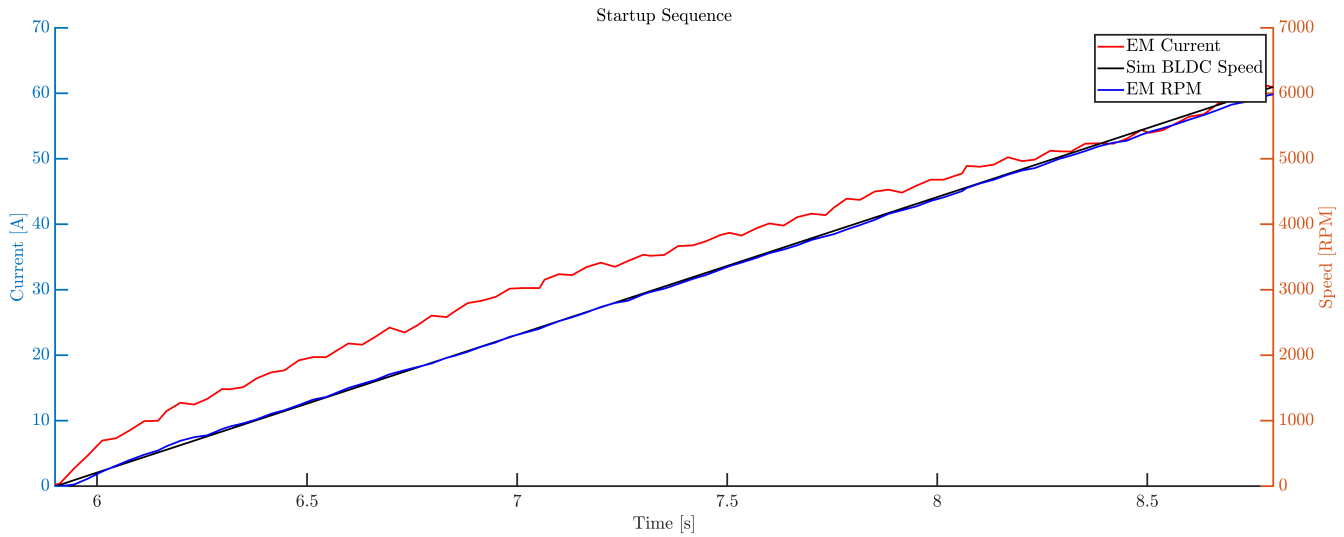

Figure 85: Startup sequence for all-electric virtual flight mission

The first segment of the flight mission was the climb sequence, this represents a high power region required to lift the aircraft off the ground. During this segment the speed and torque predicted by the simulation has a mean error of 0.35% and 1.8% respectively. This high level of accuracy compared to the previous tests is caused by the simplicity of electric-only operation. There are essentially two loads on the PMSM and does not require any distribution to the combustion engine. This means the torque required from the electric motor is from the drivetrain and dynamometer. The following three different segments, cruise, dash, and descent, follow a similar magnitude of mean error with a maximum of 4.31% for torque and 0.35% for speed.

Segment	Mean Speed [RPM]	Error [%]	Mean Torque [Nm]	Error [%]	Unit
Startup	3039.6	1.82	2.562	-19.69	EM
Climb	6121.3	-0.35	2.903	-1.80	EM
Cruise	5099.3	0.01	0.937	-4.31	EM
Dash	6121.2	-0.35	2.032	-0.47	EM
Descent	6120.9	-0.34	2.3017	-1.54	EM

	Experimental [%]	Simulated [%]	Error [%]
SOC	9.97	10.24	-2.74

Table 30: Mean torque and speed values with SOC for the electric virtual flight mission

Building on the mean error values of the electric motor data and simulation results the real-time error is shown in Figure 86. This visualization of the error per flight segment shows how the system reacts to small changes in system operation. The climb sequence had a larger error spike of 20.67% in torque prediction at the end of the climb segment where the PMSM began to decelerate to maintain speed. This trend of having larger torque errors at transition periods continued throughout the flight mission while speed error remained below 1.64%. The error between test data and simulation remained below 10% with the majority of error fluctuating below 5% during the steady-state segments of each section. The noise found in the experimental data was caused by the mechanical mounting solution for the electric motor not being built for high-speed testing. A better rigid mount for the PMSM would result in much lower errors since the model could be tuned with less vibrational uncertainty.

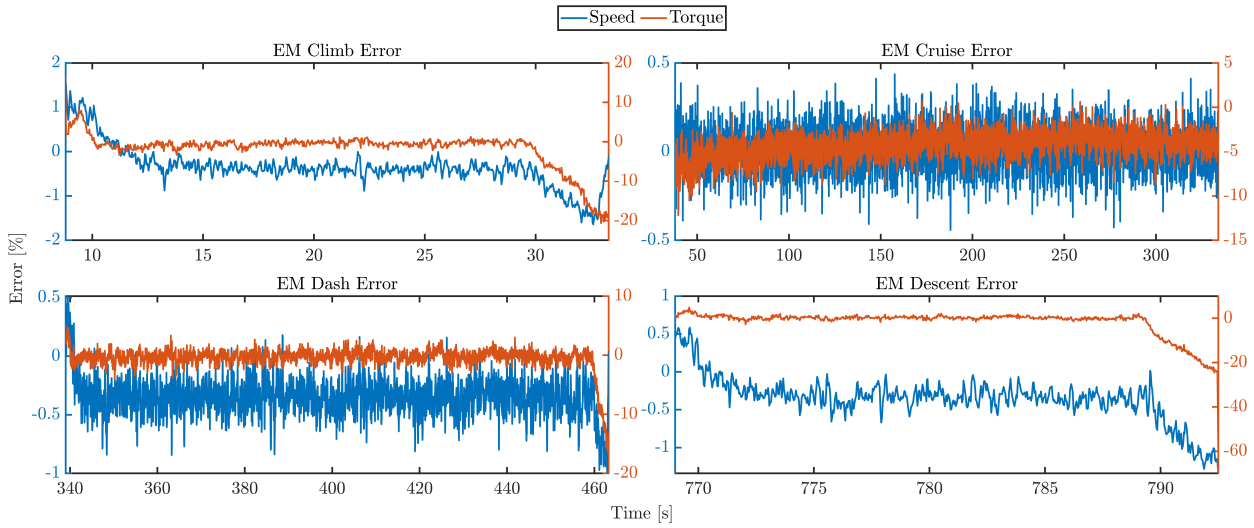

Figure 86: Error between experimental and simulated responses of the EM

Arguably the most important set of data for the electric-only flight mission was the amount of battery energy used to complete the mission profile. Being able to predict the amount of battery use for a given mission provides the ability to estimate battery weight, endurance, and power limitations of the propulsion system. The simulation model's ability to predict energy consumption is paramount in justifying the validity of hybrid propulsion and in what modes the system should operate for mission success. For the electric-only flight mission, the test bench ended with 9.97% state of charge while the Simulink model predicted 10.24% which is an error of 2.74%.

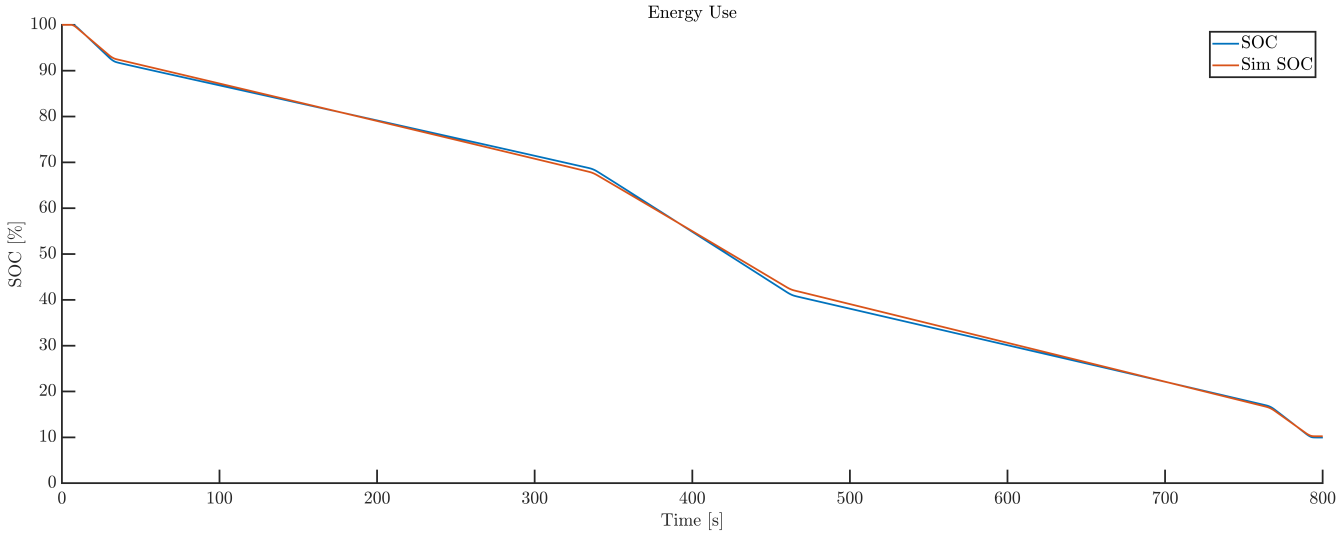

Figure 87: State of charge profile for the electric virtual flight

The results of this test displayed the strength of the electric motor model and how well it predicts the real-world operation of the SKP 6485. As indicated in the previous tests the speed control of the ESC is capable of withstanding changes in load quite well. The electric flight mission test also verified that the electric motor is capable of providing the required power for the flight profile with a 4000mAh battery.

6.5 Combustion

The same flight mission was used in a combustion-only test to determine if the Corvid-50 was capable of the power requirements and to determine how much fuel was required. For this test the electric motor was required to start the combustion engine, once self-sustaining the electric motor was not used for the remainder of the test. The starting sequence for this test was the same as the Mode 1 test described earlier in this section. The electric motor was commanded a speed of 3000RPM and spun until combustion occurs, which was then followed by the clutch being disabled and PMSM turned off. The startup torque error for the PMSM was 23.88% due to the combustion engine being warm from previous tests throughout the day. As stated before, the simulation was designed to predict cold start torque, therefore a warm 1.707Nm starting torque was relatively low.

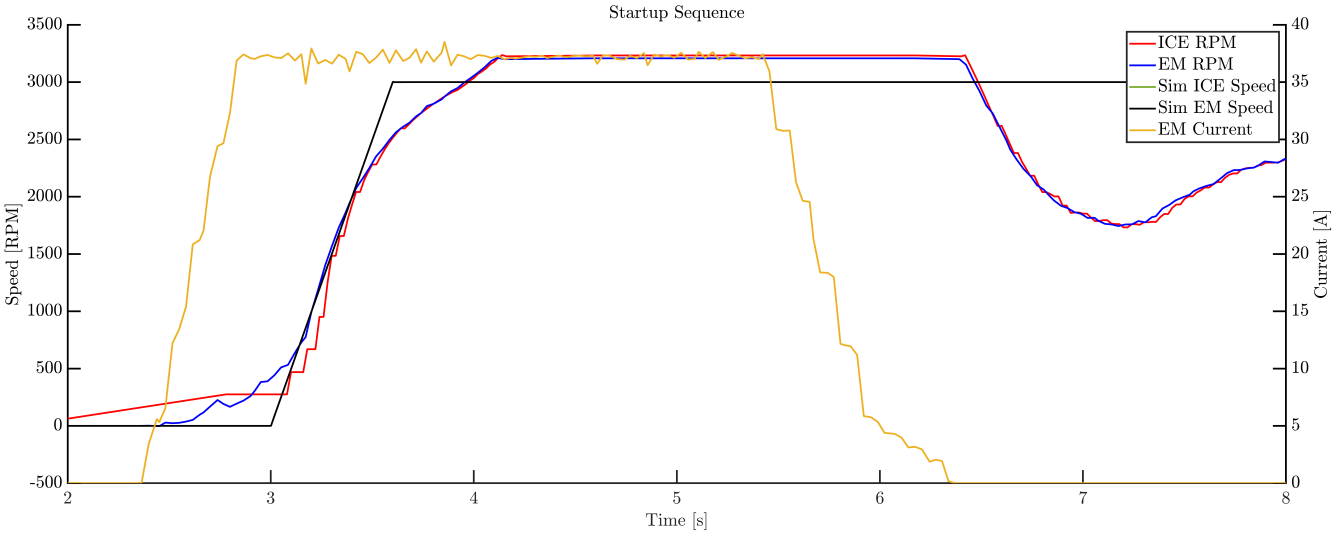

Figure 88: Startup sequence for the combustion virtual flight test

During idle the speed and torque of the ICE was predicted with accuracy; the experimental speed of 2970.2RPM was predicted with 0.99% error while the mean torque error was 0.34%. For each flight segment the combustion engine response in simulation was favorable. The climb segment saw a mean speed error of 0.04% while the mean torque error for the same segment was 4.57%. These values demonstrated a strong model of the ICE thanks to the accuracy of the Simulink maps based on the ECU values. This trend continued throughout the flight mission with cruise having the largest mean speed and torque error of 1.05% and 5.18% respectively.

Segment	Mean Speed [RPM]	Error [%]	Mean Torque [Nm]	Error [%]	Unit
Startup	2900.3	0.39	1.707	23.88	ICE
Idle	2970.2	0.99	1.017	-0.34	ICE
Climb	6102.6	-0.04	2.999	4.57	ICE
Cruise	5046.7	1.05	1.054	5.18	ICE
Dash	6071.9	0.46	2.147	4.09	ICE
Descent	6080.2	0.33	2.467	1.72	ICE

	Experimental [%]	Simulated [%]	Error [%]
Fuel Consumed [g]	114.0	110.9	2.74

Table 31: Mean torque and speed values with fuel consumption from combustion flight mission

The mean error values provided in Table 31 deliver a base level understanding of how the simulated mission corresponds to the experimental data. Plotting the error of the two against each other provided a better picture of how the system responded in real-time from perturbations. Similar to previous tests error values increased on the boundaries of each flight segment as the system transitioned to a different section. The increase in error was a combination of poor value prediction but also time synchronization. This was present in all tests performed for this thesis work, having the test bench and the simulation data perfectly synchronized was not possible. Despite these challenges the maximum errors experienced during any flight segment for the combustion test was 25.54% for torque predication during cruise.

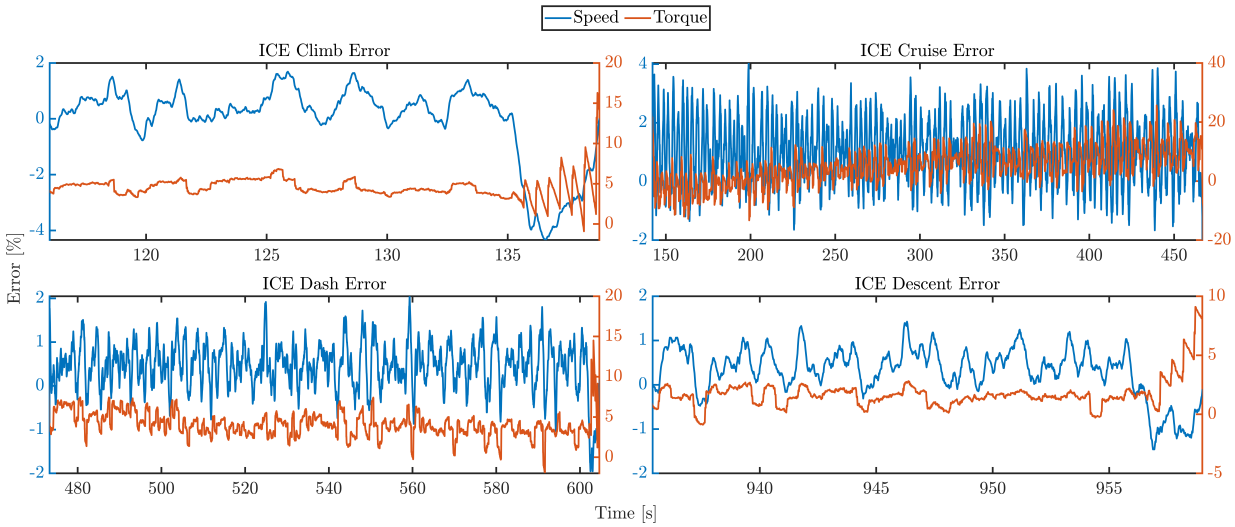

Figure 89: Error between experimental and simulated responses of the ICE

Similar to the electric-only test the energy used for the flight mission was an important parameter to determine. For this specific flight mission, the combustion engine consumed 114 grams of fuel to startup, warm, and complete the mission. The simulation model predicted a consumption value 110.9 grams which is an error of 2.74%. Knowing the fuel consumption of the mission allows for the prediction of fuel weight, endurance, and what limits the Corvid-50 produces.

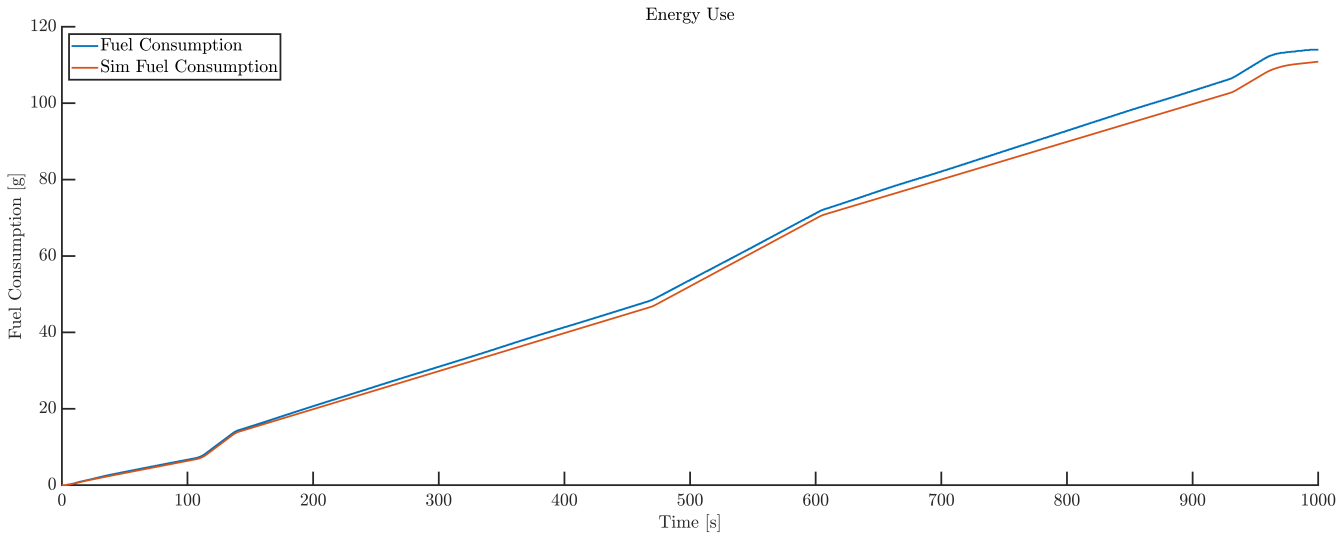

Figure 90: Fuel consumption of the ICE during combustion virtual flight mission

The execution of the combustion engine test showed that the ICE was capable of handling the power requirements of the mission profile while also responding quickly to changes in speed and load. The response from the system in this test compared to the previous tests demonstrated how sensitive the ECU is to rapid load activation. The combustion engine was able to maintain speed throughout the entire mission without any drops or spikes. Combustion power has been available at the small-scale for a while now, however the noise, vibration, and safety requirements of the system make them less common compared to electric propulsion in recent years.

6.6 Hybrid

The final flight mission test for both the test bench and simulation was in hybrid operating mode. This test was used to determine how well the parallel hybrid-electric propulsion system reacted to a longer, higher power test. The data from this mission would also provide tangible information on the benefits and disadvantages of hybrid power compared to the other two conventional tests.

For this hybrid test Mode 2 was selected as the test benches operating mode to provide the best opportunity for clean data. As discussed in the previous thirty-amp tests, Mode 1 is not capable of direct torque control while Mode 3 speed control is not stable enough to use in the current configuration. Using Mode 2 the speed was smoothed by the electric motor and responded quickly with the ESC PID control. Direct throttle commands were used to control the torque output of the combustion engine while the electric motor filled the remaining torque requirement.

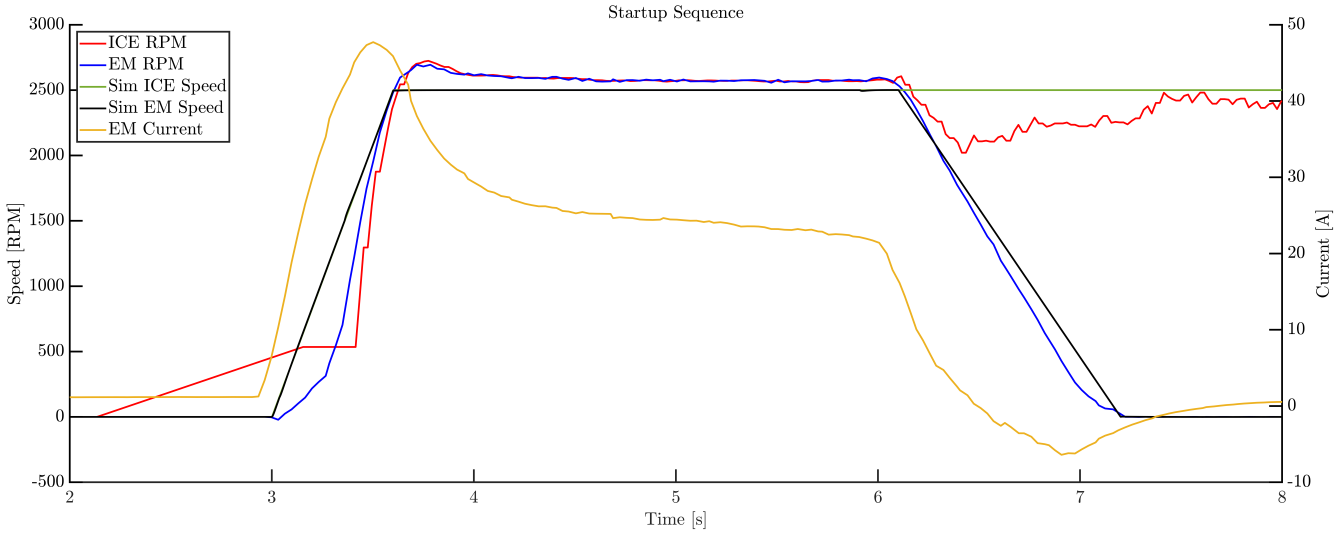

Figure 91: Startup sequence for the Mode 2 virtual flight mission

The startup sequence for this test followed the pattern that has been recognized throughout the testing period of the project. A 2500RPM starting speed was commanded by the electric motor while the clutch was engaged and the combustion engine primed. The torque spike experienced by the electric motor to turn over the ICE was 1.944Nm while the simulation predicted a starting torque of 2.507Nm, this results in an error of 28.94%. This discrepancy, as stated before, was caused by the simulation predicting cold starting torques and the test bench having been ran throughout the day. The mean speed error for this segment was much lower than the torque prediction at 6.05%. These errors represent a standard starting sequence that has been observed during months of testing. The combustion engine idle segment for this test experienced a torque decrease over

time as the combustion engine temperature increased which resulted in a mean torque error of 8.04%; mean speed error during the same time period was much lower at 1.87%.

Segment	Mean Speed [RPM]	Error [%]	Mean Torque [Nm]	Error [%]	Unit
Startup	2299.3	-6.05	1.944	-28.94	EM
Climb	6118.7	-0.31	1.691	-0.90	EM
Cruise	5097.3	0.05	0.660	-8.93	EM
Dash	6122.0	-0.36	0.812	2.86	EM
Descent	6114.3	-0.23	1.551	-11.58	EM
Startup	2387.1	0.34	0.977	-1.29	ICE
Idle	3259.7	-1.87	0.382	-8.04	ICE
Climb	6118.8	-0.31	1.496	0.37	ICE
Cruise	5097.4	0.05	0.460	2.90	ICE
Dash	6122.1	-0.36	1.519	-1.05	ICE
Descent	6114.3	-0.23	1.244	1.32	ICE

	Experimental [%]	Simulated [%]	Error [%]
SOC	39.33	41.13	-4.56
Fuel Consumed [g]	86.8	83.3	3.98

Table 32: System mean responses from the Mode 2 virtual flight test

During the climb sequence both the combustion engine and the electric motor increased speed to 6100RPM while the load trailed by two seconds to prevent stalling and represents the power profile of a propeller powered aircraft. The PMSM mean speed and torque error for this segment were 0.31% and 0.90% respectively, which demonstrated the accuracy of the ESC performance and how predictable torque outputs were when the load was progressively loaded. The combustion engine mean speed error during climb was 0.31% while the torque for the same segment was 0.37%; the mean values for the entire flight profile are shown in Table 32. The PMSM/ICE errors were greater than the electric and combustion-only tests but lower than the previous Mode 2 test. This observation showed that error prediction from the simulation model is not only dependent on the hybrid mode but also the mission profile.

Building on the mean error for each segment the real time error was also found for each flight segment. This parameter provided perspective of how representative the mean values were and why high values occurred during testing. The highest errors for the electric motor occurred at the limits of each flight segment as the test bench transitioned. At these junctions both power units experienced maximum errors of approximately 27% for torque prediction while speed had a much lower maximum error of 1.53%. Looking at the steady-state range of each segment the maximum error for torque oscillated around 10% while speed was near 0.3%. The errors in the same segments for the combustion engine were noticeably lower, the real-time error for both power units are shown in Figure 92 and 93 below.

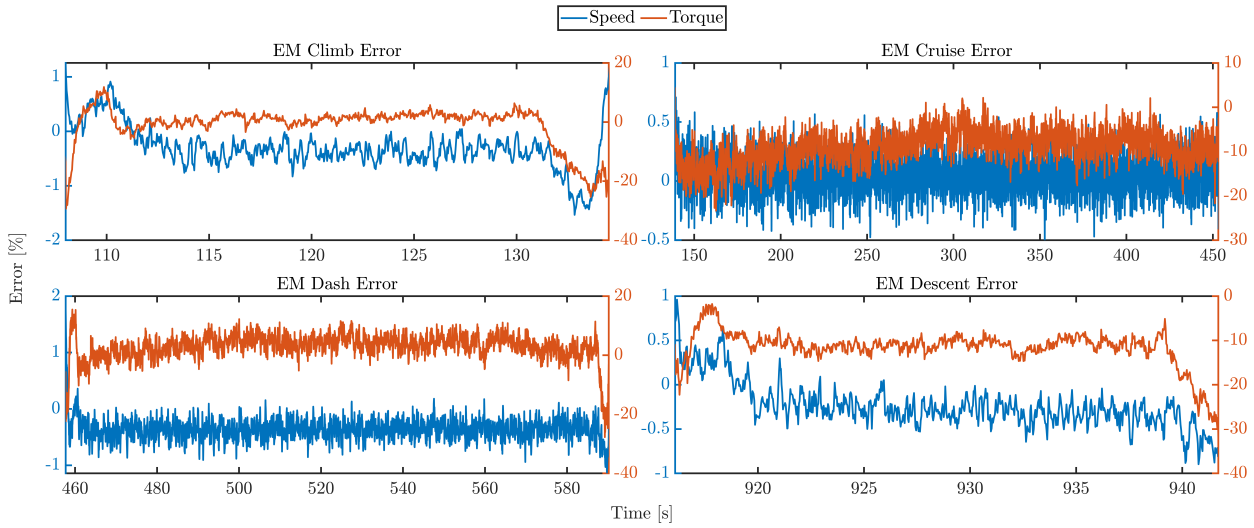

Figure 92: Error between experimental and simulated responses of the EM

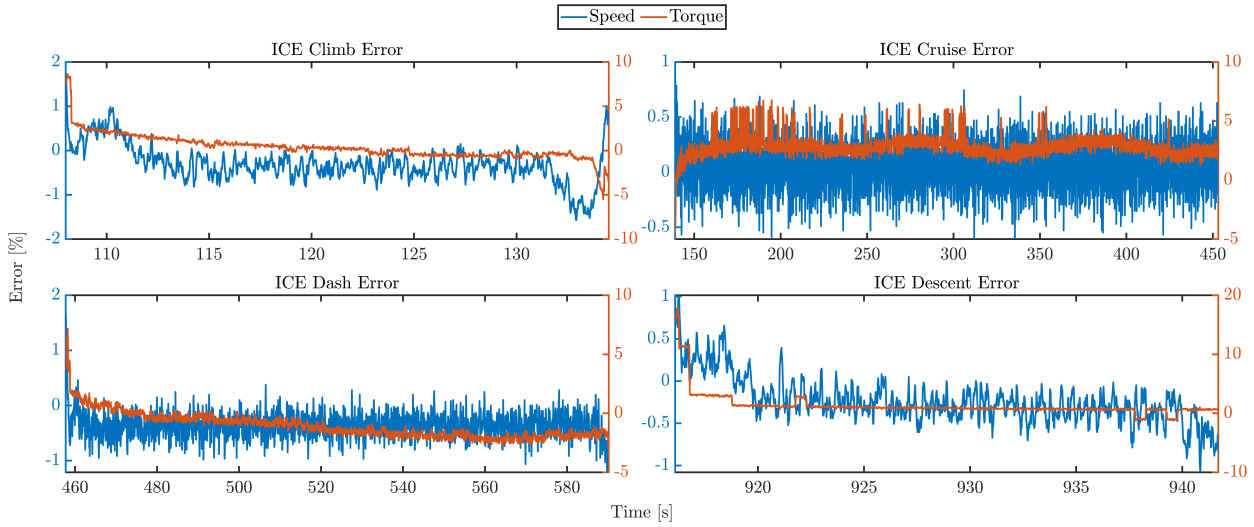

Figure 93: Error between experimental and simulated responses of the ICE

The energy used by the test bench was another key aspect of this test and was required to properly compare this test bench configuration to the conventional combustion and electric-only tests. For this Mode 2 hybrid flight mission the combustion engine throttle was commanded half the value from the combustion-only test. This provided the opportunity for the electric motor to fill the remaining required power during the entire mission. The clutch and electric motor remained active during the entire test to simplify the operation of the test bench which also reduced risk of stalling either power unit. Upon successful completion of the mission profile the combustion engine consumed 86.8g of fuel and the electric motor battery had 39.33% battery charge remaining. The simulation predicted a fuel consumption of 83.3g with battery charge remaining at 41.13%. These two values represent an error of 3.98% for fuel predication and 4.56% for state of charge.

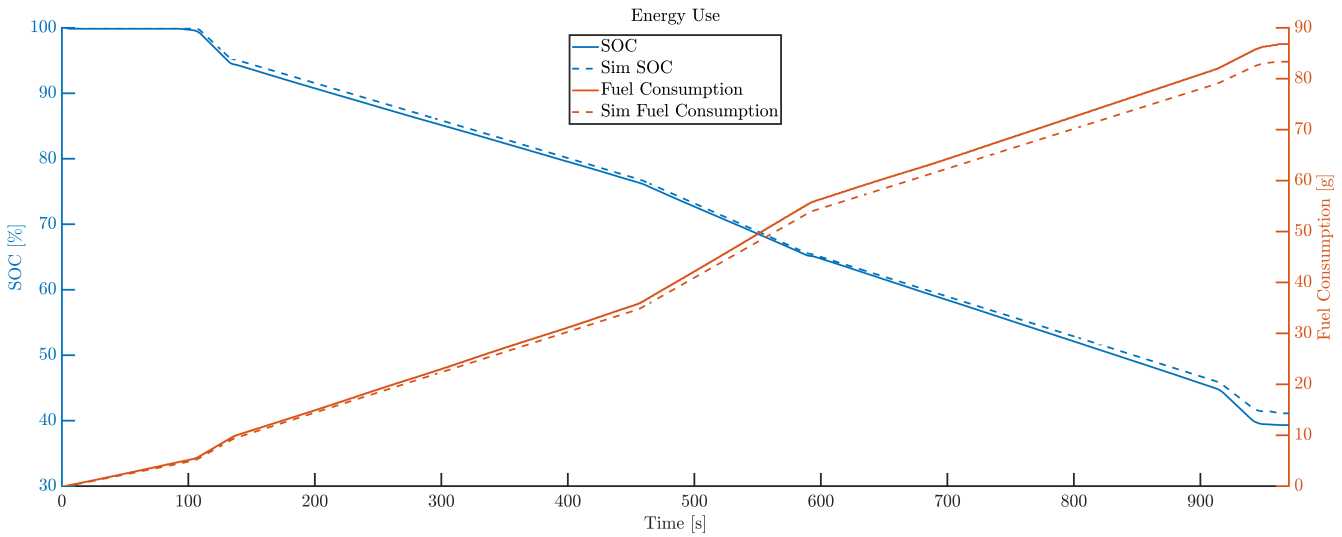

Figure 94: Fuel consumption and SOC from Mode 2 virtual flight mission

This relatively simple hybrid control scheme resulted in an experimental test that tested the capabilities of the test bench at high power while also splitting power between the two power units. This test showed how Mode 2 operation was able to fill in the power gaps with electric power while maintaining a steady speed and torque throughout each flight segment. While the command scheme was simple for this first hybrid flight profile on the parallel test bench it provided the verification required to further progress testing and development.

6.7 Comparison

The data from the three flight mission tests provides an opportunity to compare electric, combustion, and hybrid propulsion to outline the benefits/drawbacks of each technology. Starting with energy consumption, the hybrid configuration allowed for a 23.86% reduction in fuel consumption along with a 29.37% increase in remaining battery charge. This was accomplished by reducing the commanded throttle of the ICE by approximately 50%.

	Fuel Consumption [g]		SOC [%]	
	Experimental	Simulated	Experimental	Simulated
Electric	-	-	9.97	10.235
Combustion	114.0	110.872	-	-
Hybrid	86.8	83.343	39.33	41.125
Difference	23.86	24.83	29.37	30.89

Table 33: Fuel consumption and SOC for each virtual flight mission

The control scheme for this test was far from ideal and was not designed to minimize energy consumption to the fullest. Adding regeneration segments to the mission would allow for the battery to recharge, further reducing the electric energy requirement. The throttle and speed command of the combustion engine was set to test the capabilities of the test bench, not to reduce fuel consumption. There are opportunities to optimize the command profile to minimize mass required to complete the mission based on the energy densities of the fuel and batteries. With data from this hybrid test the mass reduction of the energy sources were relatively low at 27.2g for fuel and 373g for batteries.

For conventional propulsion systems the combustion configuration had the lowest system weight because of the energy density of the fuel. The energy density of a fuel powered propulsion system is why they have been the ruling technology since the inception of aircraft. These systems provide the best endurance and range for a given weight. The electric-only system has a lower mass value but the range and endurance of the system is substantially reduced because of the energy density of current battery technology. The hybrid propulsion system has the heaviest mass as it is the combination of both technologies with additional components. These mass and energy comparisons are shown in Table 34 below.

	Combustion	Electric	Hybrid
Available Energy [MJ]	5.06	0.91	5.98
Mass [kg]	4.33	2.60	8.43
Energy Density [MJ/kg]	1.170	0.351	0.709

Table 34: Mass and energy comparison between combustion, electric, and hybrid propulsion

Using the specific energy of gasoline and lithium polymer batteries the operating mass of the hybrid system could be optimized to a lower weight penalty. However, with current technology a combustion-only propulsion system will always weigh less than either electric or hybrid systems with equivalent energy storage. Using the current components of the hybrid test bench the energy density of the system and overall mass can be parametrically analyzed. Gasoline has a specific energy of 44.4MJ/kg [86] and LCO lithium polymer batteries have an energy density of 200Wh/kg (Table 1). These two energy values were used to determine the energy of the hybrid system at various fuel and battery configurations which are shown in Figure 95.

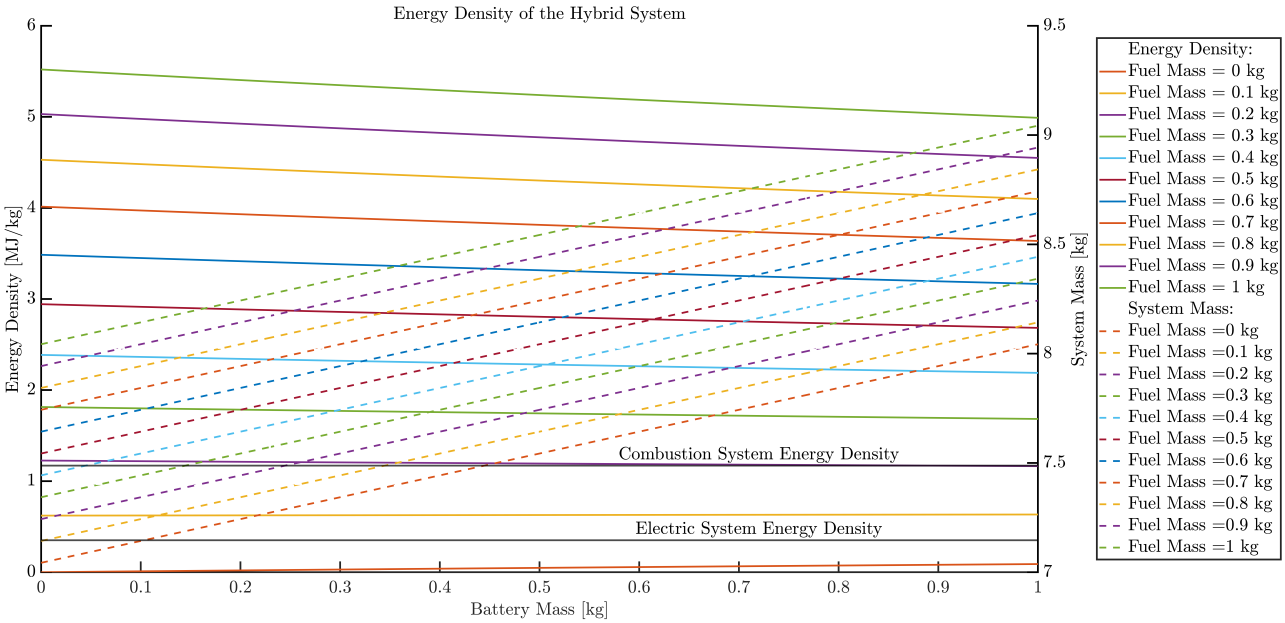

Figure 95: Energy density of the current hybrid system at various energy masses

The graph above shows how the energy density of the hybrid-electric system changes with battery and fuel mass. This plot also visualizes the total system mass for the same range of configurations. The energy density of the system has a noticeable trend that indicates the increase in fuel mass also increases the energy density of the system. This parametric study showed that the battery,

fuel, and system mass must be optimized to increase energy availability without excessive mass penalty. An important consideration when optimizing the mass and energy of the system is to account for the required power increase of the propulsion system with the added weight to match the same aircraft performance of a combustion-only configuration.

Generally speaking, hybrid propulsion systems are used when emissions are a concern and/or an all-electric solution does not meet the requirements of the application. Unfortunately, emission data is not currently available for the parallel test bench which means the reduction of pollutants cannot be quantified in this report. Further optimizations to the power distribution, energy masses, and component selection can create a hybrid system with a stronger benefit ratio than the current configuration. However, from these experimental results the hybrid-electric technology reduces fuel and battery consumption compared to the convention propulsion systems. In addition, the parallel system benefits from the quick response of electric power while having the range and endurance of combustion systems.

Looking at the simulation results outlined throughout this section the model performed well considering the complexity of development. The system was capable of producing system responses that followed the same reaction and curves as the experimental data. This visual comparison of the experimental and simulated system responses was further supported with error ranges per test. The mean torque and speed errors across both the 30A tests and flight missions in Tables 36 and 35 show the accuracy of the simulation for those parameters.

Segment	Mean Speed Error [%]	Mean Torque Error [%]	Unit
Startup	3.94	24.32	EM
Climb	0.33	1.35	EM
Cruise	0.03	6.62	EM
Dash	0.35	1.67	EM
Descent	0.29	6.56	EM
Startup	0.36	12.58	ICE
Idle	1.43	4.19	ICE
Climb	0.18	2.47	ICE
Cruise	0.55	4.04	ICE
Dash	0.41	2.57	ICE
Descent	0.28	1.52	ICE
	Error [%]		
Fuel	3.36	-	ICE
SOC	3.65	-	ICE

Table 35: Mean errors for all virtual flight tests per segment

Segment	Mean Speed Error [%]	Mean Torque Error [%]	Unit
Startup	4.84	10.95	EM
Loaded	1.74	12.03	EM
Startup	2.51	6.43	ICE
Idle	2.54	6.98	ICE
Loaded	1.68	3.34	ICE

Table 36: Mean errors for all 30A tests per segment

The simulation had the highest error in predicting starting torque for the electric motor with a value of ±24.32% on average for all tests. This error was caused by engine temperature, crank angle, and oil presence since the mathematical model only predicts cold engine starts. The speed error for the simulation model never exceeded ±5% while the torque error for all segments remained between 1-13%. There are numerous errors spikes throughout each test that occur from transient responses that were difficult to represent in the Simulink model.

During the simulation process there were a number of parameters that were extremely sensitive and affected the system response substantially. The ramp speed of the electric motor had a direct effect on the torque load of the PMSM, when the speed and ramp time were not well matched the electric motor model became unstable. The speed and torque outputs of the model would oscillate at higher frequencies with extremely large magnitudes. Changing the ramp time by 0.05s for a 3000RPM command could be the difference needed to make the model response stable. This time sensitivity was also important for clutch engagement close to state changes. If the clutch was engaged too closely to a large torque or speed change the system would lose stability. These reactions from the electric motor model were attributed to the PMSM controller model not having the control parameter variety that the ESC has on the test bench.

The EM controller in Simulink has a speed and current controller which aims to meet the speed request of the operator while keeping the current response within the required operating range of the motor. Conversely, the VESC used on the test bench has both those controllers plus numerous other control parameters such as; hall effect sensors, phase filters, ramp speed, and position controller. These added features prevent the motor from overspinning, becoming unstable, and overreacting to torque changes. If these features were implemented in the modelled controller the electric motor stability would be greatly improved.

The torque distribution logic created for the model has numerous parametric variables that currently work well based on testing. However, this section of the model may need more testing and updating if the system response becomes inaccurate for different tests in the future. The logic in its current configuration provides a good representation of how torque is handled based on load, speed, and command mode. The simulation predicted the experimental results of the flight mission with high accuracy before the test bench was run. However, drastically different mission profiles may expose some weakness in the logic.

Throughout this section torque and speed have been discussed extensively as the two driving parameters of the hybrid system. These two values combine to create power which connects to nearly every variable in the system. Parameters such as current, voltage, fuel flow, three-phase power, and throttle value were also modelled extensively. The values of these variables needed to be accurate to generate the responses discussed so far. Details on these parameters and how they responded during testing can be found in the appendix. Each modelled parameter of the system contributed to the Simulink model's ability to predict system responses and will continue to improve with further development.

7 Conclusions

7.1 Achievements

Hybrid-electric technology has matured over the past 20 years as land-based vehicles have continued to develop these kinds of systems in the pursuit of better fuel economy, performance, and carbon neutrality. Aircraft hybrid systems are in their infancy which provides significant opportunity in research and development for possible new solutions to the emission challenges in aviation. The work completed during this thesis provides an analysis of parallel hybrid-electric propulsion for small-scale UAVs.

The first few months of this thesis began with the development of a parallel test bench capable of harnessing combustion power. A previous version of the test bench was redesigned to handle the demands of a combustion engine which includes more power, strong vibrations, and fueling. The design process included increasing the strength of the drivetrain by adding keyways to the timing pulleys while also increasing the belt widths. This was paired with stronger and better machined belt tensioners that were capable of maintaining belt tension during high power tests. The electromagnetic clutch was significantly upgraded to a unit that is capable of eight times more torque than the previous. This upgrade was the most important since the old clutch was unable to harness system torque at any power level. These test bench upgrades were completed with some electrical and software improvements that made the test bench capable of completing the tests needed for this thesis. The parallel hybrid bench was also fitted with analog inputs to provide better control over the combustion engine and electric motor. Preprogrammed missions and serial communication with the programmable load were the last two test bench upgrades that allowed for fully automatic testing.

These test bench upgrades were required to begin the bulk of the project work; creating a simulation model of the propulsion system. The process of modelling the current hybrid-electric propulsion system began with collecting as many parameters as possible for the power units, clutch, drivetrain, load, and controllers. The modelling process was an iterative exercise where component level models were created and tested. First the electric motor model was selected as the PMSM block in Simulink paired with a matching controller. The various motor parameters for the electric motor were collected and used to populate the model block. Simulations for this PMSM model were run and compared to the experimental results of the SKP 6485 motor. This process was repeated for the ICE, clutch, and drivetrain. As each model was verified it was added to the larger system model which was developed using a logical layout based on power flow.

Once the system model was operating relatively well logic for speed determination and torque distribution was developed. The initial algorithms were determined using theoretical principles but further modelling was required using experimental data. The test bench was operated in three different modes: dual speed, throttle and speed, speed and current. These three modes represent the distinct command mode combinations that the test bench is capable of performing. Each mode executed a test with the same load and speed requests. This collection of data provided the system responses required to create a robust and representative model block that determines system speed and torque.

With the model well developed a simulated flight mission was created to further test the capability of the test bench and Simulink model. These flight mission tests paired with a set of lower power

tests formed the data set used to characterize the accuracy of the model. The low power tests demonstrated that the simulation model was capable of predicting speed and torque well. The simulated error for the electric motor speed in these tests had a mean value of 3.29% while torque was predicted with a mean error of 11.49%. The combustion engine for the same two responses had an error of 2.24% and 5.58% respectively. While the mean error values are favorable, larger errors occurred during transient sections and the model does not include vibration caused by the combustion engine.

The virtual flight mission developed for testing was executed in combustion, electric, and hybrid configurations. The simulation model was able to predict speed and torque with less error deviation; the mean speed and torque error were 0.745% and 6.17% respectively. These tests also provided an opportunity to predict fuel consumption and SOC. The fuel consumption error for these tests was 3.36% while SOC was 3.65%. Speed and torque are the two values discussed in depth during this research because they combine to make power. Other parameters such as current, fuel flow, load voltage, and throttle value were modelled extensively. These smaller values are all driving factors of power and therefore must be accurate to produce the results seen from the model. The model at this stage of the project was well developed and predicted system response both graphically and numerically.

Using the experimental and simulation data the benefits of hybrid-electric propulsion were analyzed. The tests executed throughout this paper demonstrated some key aspects of each propulsion technology. Combustion powered propulsion remains the lightest and most energy dense solution. For the current component selection this meant the combustion system weighed twice that of the electric system but had five times the energy. The batteries required to complete the simulated flight mission weighed 1.27kg while 114g of fuel was capable of the same mission. The main benefits of electric propulsion are zero emissions and the quick response time of electric power. Combining the two technologies into hybrid-electric propulsion created a system that weighed more than both systems combined but provided some benefits.

The hybrid configuration was able to complete the same simulated mission profile as the other two conventional systems while using 23.86% less fuel and 29.37% less battery. These experimental results were confirmed with simulated predictions of the same test yielding 24.83% and 30.89% reduction in fuel and battery consumption. Improving the current hybrid-electric propulsion system can be optimized to increase the energy density of the system. This optimization should include increasing the complexity of the command scheme while also balancing the system mass and energy. Adding regeneration, clutch disengagement, and throttle tuning would greatly increase the benefits of the hybrid system. Overall, the hybrid testing and simulation showed that the test bench is capable of parallel hybrid operation while also providing telemetry to further develop and study the technology. The simulation model created during this project can be used for MBD to predict system performance, virtually assess new component options, and test optimization schemes for future experimental applications. Combining the test bench and simulation tool provides a well-rounded approach to hybrid development that will greatly benefit future projects.

7.2 Future Work

While the results of both the simulation model and test bench were accurate enough to open up new possibilities at CfAR for future projects there are still numerous areas for improvement. The first and maybe the most obvious is to continue developing the Simulink model. The current version of the model can be considered a first revision with the minimum required amount of testing. More testing and research will further increase the robustness and accuracy of the model. Currently the model requires small modifications per test to guarantee it represents the current run. This includes modifying ramp speeds, adjusting timing, and selecting the command mode. With more development some of these adjustments could become automatic with better logic blocks. Running more unique and challenging test profiles will also benefit the model greatly since it increases the probability of exposing model errors.

The test bench system has quite a few small areas for improvement that will be worked on in the near future. Mounting solutions for the electric motor and combustion engine currently work but the output shafts of both units experience strenuous vibration. The vibration in the electric motor noticeably affected the data collected by the ESC and load cells. New mounting setups should be developed that better constraint each power unit while reducing shaft wear and data noise. These upgrades should also be combined with a better pulley ratio pairing to try and reduce the possibility of preload on the load cells between motor poles. There are a few electrical upgrades that need to be addressed to make the test bench more reliable and user friendly. The current control panel needs to be designed into a PCB to improve voltage stability for the analog inputs and reduce the possibility of disconnecting. Additionally, the potentiometers used for analog control should be upgraded to make small adjustments easier for the user.

From a software perspective the test bench has made leaps and bounds since the start of this research project. The test bench is now capable of analog control, automatic runs, and serial communication with the programmable load; none of which was possible at the begin of the project. With this rapid development there are a few bugs with the current configuration. The first improvement that needs to be made is with the automatic runs, the current software configuration loses synchronization as the test progresses. Improvements to the hardware timing and software logic needs to be made to maintain timing between the commanded value and hardware outputs. The current setup does not loose/skip command values, but the sequence gradually shortens or lengthens in execution time. These software improvements would also greatly benefit from a custom controller that can control both the ECU and ESC. This addition would allow both control units to communicate with each other greatly improving the system operation.

The future work for theoretical research has a large opportunity for hybrid optimization. The small parametric study shown in this report is just the beginning of what is possible. There are many different aspects of the hybrid system that can be improved. The first and maybe simplest is to optimize the throttle and speed commands of the system for the virtual flight missions. This study could greatly increase the performance. Looking at the system from a broader sense the fuel mass, battery size, ICE, and EM class could all be optimized to create a system of adequate power with a significantly lower mass.

The final goal for this hybrid project outside of the test bench and Simulink model is to develop a package for aircraft integration using MBD. This next stage aims to create a parallel hybrid-electric propulsion system for small-scale UAVs. The propulsion package will be a single unit that can be

dropped into an existing airframe for integration. If successful, the system would provide all the possibilities of the test bench in a significantly smaller and lighter envelope. This integrated power unit is nearing a reality because of the research done in this thesis and the knowledge gained.

References

[1] Porsche, *Taycan history*, 2023. [Online]. Available: https://newsroom.porsche.com/en/products/taycan/history-18563.html.

[2] Toyota, *Toyota canada releases february sales results*, 2023. [Online]. Available: https://www.toyota.ca/toyota/en/about/news/toyota-canada-releases-february-sales-results.

[3] S. Kanal, *How f1 technology has supercharged the world*. [Online]. Available: https://www.formula1.com/en/latest/article/how-f1-technology-has-supercharged-the-world.6Gtk3hBxGyUGbNH0q8vDQK.

[4] Reuters, *Jsx orders 330 hybrid electric regional airplanes*, 2023. [Online]. Available: https://www.reuters.com/business/aerospace-defense/jsx-orders-up-330-hybrid-electric-regional-airplanes-2023-12-19/.

[5] F. B. Insights, *Uav market*. [Online]. Available: https://www.fortunebusinessinsights.com/industry-reports/unmanned-aerial-vehicle-uav-market-101603.

[6] O. Liang, *Flightradar24: Live flight tracker*, https://www.flightradar24.com/, Accessed: 2024-10-22, 2024.

[7] O. W. in Data, *Global aviation emissions*. [Online]. Available: https://ourworldindata.org/global-aviation-emissions.

[8] M. T. Review, *All about alternative jet fuels (safs)*, 2023. [Online]. Available: https://www.technologyreview.com/2023/05/24/1073568/all-about-alternative-jet-fuels-safs/.

[9] Toyota Canada, *Toyota celebrates 10 years of prius in canada*, https://media.toyota.ca/en/releases/2010/toyota-celebrates-10-years-of-prius-in-canada.html, Accessed: 2024-10-22, 2010.

[10] J. Dawes, *Flying taxi startup lilium burned through $1 billion. now it's facing bankruptcy*, https://skift.com/2024/10/25/flying-taxi-startup-lilium-burned-through-1-billion-now-its-facing-bankruptcy/, Accessed: 2024-11-07, 2024.

[11] *Renault 2014 engine*. [Online]. Available: https://f1framework.blogspot.com/2014/01/renault-2014-engine.html.

[12] R. Y. Dahham, H. Wei, and J. Pan, "Improving thermal efficiency of internal combustion engines: Recent progress and remaining challenges," *Energies*, vol. 15, no. 17, 2022. DOI: 10.3390/en15176222. [Online]. Available: https://www.mdpi.com/1996-1073/15/17/6222.

[13] C. Engineering, *Cortex series*. [Online]. Available: https://www.currawongeng.com/cortex-series/.

[14] *Pegasus aerospace*, https://www.pegasusaero.ca/, Accessed: 2024-10-22, 2024.

[15] *Lowe heiser*, https://www.loweheiser.com/, Accessed: 2024-10-22, 2024.

[16] P. F. Technologies, *Parallel flight product*. [Online]. Available: https://www.parallelflight.com/product-1.

[17] T. Rotramel, "Optimization of hybrid-electric propulsion systems for small remotely-piloted aircraft," *Air Force Institute of Technology*, p. 152, Mar. 2011.

[18] R. Glassock, J. Hung, L. Gonzalez, and R. Walker, "Design, modelling and measurement of a hybrid powerplant for unmanned aerial systems," *Australian Journal of Mechanical Engineering*, vol. 6, 2007. DOI: 10.1080/14484846.2008.11464559. [Online]. Available: https://doi.org/10.1080/14484846.2008.11464559.

[19] *Ampaire*, 2023. [Online]. Available: https://www.ampaire.com/.

[20] *Ampaire eco caravan*. [Online]. Available: https://www.ampaire.com/vehicles/eco-caravan.

[21] S. Magazine, *The hybrid electric evolution*. [Online]. Available: https://skiesmag.com/features/the-hybrid-electric-evolution/.

[22] Heart Aerospace, *Heart aerospace unveils new airplane design, confirms air canada and saab as new shareholders*, https://heartaerospace.com/heart-aerospace-unveils-new-airplane-design-confirms-air-canada-and-saab-as-new-shareholders/, Accessed: 2024-10-22, 2024.

[23] NRC, *Nrc status update*. [Online]. Available: https://x.com/NRC_CNRC/status/1511690026932965381.

[24] S. Flying, *Ge, rolls-royce, and pratt and whitney: A look at the big three engine manufacturers*, https://simpleflying.com/ge-rolls-royce-pratt-whitney/, Accessed: 2024-10-22, 2024.

[25] NASA, *Nasa ge complete historic hybrid electric propulsion tests*, 2023. [Online]. Available: https://www.nasa.gov/aeronautics/nasa-ge-complete-historic-hybrid-electric-propulsion-tests/.

[26] Airbus, *Hybrid and electric flight*, 2023. [Online]. Available: https://www.airbus.com/en/innovation/low-carbon-aviation/hybrid-and-electric-flight.

[27] Airbus, *Ecopulse aircraft demonstrator makes first hybrid electric flight*, 2023. [Online]. Available: https://www.airbus.com/en/newsroom/press-releases/2023-12-the-ecopulse-aircraft-demonstrator-makes-first-hybrid-electric.

[28] A. Kuśmierek, C. Galiński, and W. Stalewski, "Review of the hybrid gas - electric aircraft propulsion systems versus alternative systems," *Progress in Aerospace Sciences*, vol. 141, 2023. DOI: https://doi.org/10.1016/j.paerosci.2023.100925. [Online]. Available: https://www.sciencedirect.com/science/article/pii/S0376042123000416.

[29] J. Leite and M. Voskuijl, "Optimal energy management for hybrid-electric aircraft," *Aircraft Engineering and Aerospace Technology*, vol. 92, 2020. DOI: https://doi.org/10.1108/AEAT-03-2019-0046. [Online]. Available: https://www.emerald.com/insight/content/doi/10.1108/AEAT-03-2019-0046/full/pdf?title=optimal-energy-management-for-hybrid-electric-aircraft.

[30] C. Martinez, X. Hu, D. Cao, E. Velenis, and M. Wellers, "Energy management in plug-in hybrid electric vehicles: Recent progress and a connected vehicles perspective," *IEEE Transactions on Vehicular Technology*, vol. 66, 2016. DOI: 10.1109/TVT.2016.2582721. [Online]. Available: https://ieeexplore.ieee.org/abstract/document/7496906.

[31] T. Lei, Z. Yang, Z. Lin, and X. Zhang, "State of art on energy management strategy for hybrid-powered unmanned aerial vehicle," *Chinese Journal of Aeronautics*, vol. 32, 2019. DOI: https://doi.org/10.1016/j.cja.2019.03.013. [Online]. Available: https://www.sciencedirect.com/science/article/pii/S1000936119301268.

[32] Y. Xie, A. Savvarisal, A. Tsourdos, D. Zhang, and J. Gu, "Review of hybrid electric powered aircraft, its conceptual design and energy management methodologies," *Chinese Journal of Aeronautics*, vol. 34, 2021. DOI: https://doi.org/10.1016/j.cja.2020.07.017. [Online]. Available: https://www.sciencedirect.com/science/article/pii/S1000936120303368.

[33] T. Wall and R. Meyer, "Hybrid electric aircraft switched model optimal control," *Journal of Propulsion and Power*, vol. 36, no. 4, pp. 488–497, 2020. DOI: 10.2514/1.B37419. [Online]. Available: https://doi.org/10.2514/1.B37419.

[34] J. Ribeiro, F. Afonso, I. Ribeiro, and B. Ferreira, "Environmental assessment of hybrid-electric propulsion in conceptual aircraft design," *Journal of Cleaner Production*, vol. 247, p. 119 477, 2020, ISSN: 0959-6526. DOI: https://doi.org/10.1016/j.jclepro.2019.119477. [Online]. Available: https://www.sciencedirect.com/science/article/pii/S0959652619343471.

[35] N. Thonemann, K. Saavedra-Rubio, E. Pierrat, *et al.*, "Prospective life cycle inventory datasets for conventional and hybrid-electric aircraft technologies," *Journal of Cleaner Production*, vol. 434, p. 140 314, 2024, ISSN: 0959-6526. DOI: https://doi.org/10.1016/j.jclepro.2023.140314. [Online]. Available: https://www.sciencedirect.com/science/article/pii/S0959652623044724.

[36] C. Pornet and A. Isikveren, "Conceptual design of hybrid-electric transport aircraft," *Progress in Aerospace Sciences*, vol. 79, 2015. DOI: https://doi.org/10.1016/j.paerosci.2015.09.002. [Online]. Available: https://www.sciencedirect.com/science/article/pii/S0376042115300130.

[37] L. Trainelli, C. Riboldi, F. Salucci, and A. Rolando, "A general preliminary sizing procedure for pure-electric and hybrid-electric airplanes," *Aerospace Europe Conference*, 2020. [Online]. Available: https://re.public.polimi.it/bitstream/11311/1133484/1/TRAIL01-20.pdf.

[38] C. E. Riboldi, F. Gualdoni, and L. Trainelli, "Preliminary weight sizing of light pure-electric and hybrid-electric aircraft," *Transportation Research Procedia*, vol. 29, 2018. DOI: https://doi.org/10.1016/j.trpro.2018.02.034. [Online]. Available: https://www.sciencedirect.com/science/article/pii/S2352146518300383.

[39] C. Riboldi and F. Gualdoni, "An integrated approach to the preliminary weight sizing of small electric aircraft," *Aerospace Science and Technology*, vol. 58, 2016. DOI: https://doi.org/10.1016/j.ast.2016.07.014. [Online]. Available: https://www.sciencedirect.com/science/article/pii/S1270963816303601.

[40] D. F. Finger, C. Braun, and C. Bil, "An initial sizing methodology for hybrid-electric light aircraft," *American Institute of Aeronautics and Astronautics*, 2018. DOI: 10.2514/6.2018-4229. [Online]. Available: https://arc.aiaa.org/doi/abs/10.2514/6.2018-4229.

[41] D. F. Finger, R. de Vries, R. Vos, C. Braun, and C. Bil, "A comparison of hybrid-electric aircraft sizing methods," *AIAA Scitech*, 2020. DOI: 10.2514/6.2020-1006. [Online]. Available: https://arc.aiaa.org/doi/abs/10.2514/6.2020-1006.

[42] R. de Vries, M. F. M. Hoogreef, and R. Vos, "Range equation for hybrid-electric aircraft with constant power split," *Journal of Aircraft*, vol. 57, no. 3, pp. 552–557, 2020. DOI: 10.2514/1.C035734. [Online]. Available: https://doi.org/10.2514/1.C035734.

[43] A. Batra, R. Raute, and R. Camilleri, "An endurance equation for hybrid-electric aircraft," *Aerospace*, vol. 11, no. 9, 2024. DOI: 10.3390/aerospace11090698. [Online]. Available: https://www.mdpi.com/2226-4310/11/9/698.

[44] T. Donateo, C. L. De Pascalis, and A. Ficarella, "Synergy effects in electric and hybrid electric aircraft," *Aerospace*, vol. 6, no. 3, 2019. DOI: 10.3390/aerospace6030032. [Online]. Available: https://www.mdpi.com/2226-4310/6/3/32.

[45] D. F. Finger, C. Braun, and C. Bil, "Comparative assessment of parallel-hybrid-electric propulsion systems for four different aircraft," *Journal of Aircraft*, vol. 57, no. 5, pp. 843–853, 2020. DOI: 10.2514/1.C035897. [Online]. Available: https://doi.org/10.2514/1.C035897.

[46] J. Ausserer, "Integration, testing and validation, of a small hybrid-electric remotely-piloted aircraft," M.S. thesis, Air Force Institute of Technology, 2012.

[47] J. Schoemann and M. Hornung, "Modeling of hybrid electric propulsion systems for small unmanned aerial vehicles," *12th AIAA Aviation Technology, Integration, and Operations (ATIO) Conference*, 2012. DOI: 10.2514/6.2012-5610. [Online]. Available: https://arc.aiaa.org/doi/abs/10.2514/6.2012-5610.

[48] A. S. Saeed, A. B. Younes, C. Cai, and G. Cai, "A survey of hybrid unmanned aerial vehicles," *Progress in Aerospace Sciences*, vol. 98, pp. 91–105, 2018, ISSN: 0376-0421. DOI: https://doi.org/10.1016/j.paerosci.2018.03.007. [Online]. Available: https://www.sciencedirect.com/science/article/pii/S0376042117302233.

[49] L. Boggero, S. Corpino, A. De Martin, G. Evangelista, M. Fioriti, and M. Sorli, "A virtual test bench of a parallel hybrid propulsion system for uavs," *Aerospace*, vol. 6, p. 77, Jul. 2019. DOI: 10.3390/aerospace6070077.

[50] J. Matlock, "Evaluation of hybrid-electric propulsion systems for unmanned aerial vehicles," *University of Victoria*, 2019, Accessed: 2024-10-22.

[51] C. Mi and A. Masrur, "1.4," in *Hybrid Electric Vehicles. Principles and Applications with Practical Perspectives* (Automotive Series), 2nd, Automotive Series. Wiley, 2017, pp. 11–16.

[52] AutoTrader, *What was the last car in america sold with a carburetor?* https://www.autotrader.com/oversteer/what-was-last-car-america-sold-carburetor-260855, Accessed: 2024-10-22, 2024.

[53] LowbrowCustoms, *Jrc 26mm carburetors*. [Online]. Available: https://www.lowbrowcustoms.com/products/british-standard-jrc-26mm-carburetors-pwk-keihin-replace-amal-626.

[54] Lubrizol, *Pfi vs gdi engines*. [Online]. Available: https://360.lubrizol.com/Resources/How-It-Works/How-it-Works---PFI-vs-GDI-Engines.

[55] Electrical4U, *Series wound dc motor or dc series motor*, https://www.electrical4u.com/series-wound-dc-motor-or-dc-series-motor/, Accessed: 2024-10-22, 2024.

[56] I. Motor, *Bldc motor specifications: About motor selection*, https://ican-motor.com/bldc-motor-specifications-about-motor-selection/, Accessed: 2024-10-22, 2024.

[57] S. Sidda, R. Kiranmayi, and P. Nagaraju, *A study on industrial motor drives comparison and applications of pmsm and bldc motor drives*, Aug. 2017. DOI: 10.1109/ICECDS.2017.8390224.

[58] A. P. Society, "Back page: The evolution of the modern laboratory," *APS News*, 2012, Accessed: 2024-10-22.

[59] B. University, *Types of lithium-ion*. [Online]. Available: https://batteryuniversity.com/article/bu-205-types-of-lithium-ion.

[60] Redeweb, *Principles and uses of edlc*. [Online]. Available: https://www.redeweb.com/en/present/principles-and-uses-of-edlc/.

[61] A. Kumar, *Different types of gear*, https://themechanicalengineering.com/types-of-gear/, Accessed: 2024-10-28, 2021.

[62] I. Directory, *Planetary gears*. [Online]. Available: https://www.iqsdirectory.com/articles/gear/planetary-gears.html.

[63] A. Dynamics, *Planetary gearbox introduction*, https://www.apexdyna.nl/en/gearboxes/planetary-gearbox-introduction, Accessed: 2024-10-22, 2024.

[64] O. Ordering, *Your manual transmission deserves better*. [Online]. Available: https://oilordering.com/your-manual-transmission-deserves-better/.

[65] *Engine component image*. [Online]. Available: https://m.media-amazon.com/images/I/81j05th5+ML.jpg.

[66] Turbomotori, *Automatic transmission ratio*, 2022. [Online]. Available: https://turbomotori.com/wp-content/uploads/2022/04/che-cosa-e-il-rapporto-di-trasmissione-automatico.png.

[67] C. Garage, *R8 huracan transmission power handling*. [Online]. Available: https://www.colabgarage.com/blog/how-much-power-can-the-r8-huracan-dl800-dct-transmission-handle.

[68] HowStuffWorks, *How continuously variable transmissions work*, https://auto.howstuffworks.com/cvt.htm, Accessed: 2024-10-22, 2024.

[69] M. Prislusenstvo, *Centrifugal clutch for atv/quad*. [Online]. Available: https://www.moto-prislusenstvo.sk/CENTRIFUGAL-CLUTCH-ATV-QUAD-70-110-125-CC-automaticka-d173186.htm#googtrans(sk).

[70] O. A. Cylinders, *Basic parts of a vehicle clutch assembly*, 2024. [Online]. Available: https://www.onallcylinders.com/2024/09/13/tech-101-basic-parts-of-a-vehicle-clutch-assembly-how-to-measure-for-a-replacement-clutch-disc/.

[71] O. Clutch, *Electromagnetic clutch*. [Online]. Available: https://ogura-clutch.com/electromagnetic_clutch.php.

[72] A. Tech, *Clutch assembly image*. [Online]. Available: https://www.ariat-tech.com/upfile/images/4f/20240709162237734.png.

[73] M. P. Systems, *Buck converters*, https://www.monolithicpower.com/en/learning/mpscholar/power-electronics/dc-dc-converters/buck-converters, Accessed: 2024-10-22, 2024.

[74] M. P. Systems, *Boost converters*, https://www.monolithicpower.com/en/learning/mpscholar/power-electronics/dc-dc-converters/boost-converters, Accessed: 2024-10-22, 2024.

[75] M. P. Systems, *Buck-boost converters*, https://www.monolithicpower.com/en/learning/mpscholar/power-electronics/dc-dc-converters/buck-boost-converters, Accessed: 2024-10-22, 2024.

[76] M. P. Systems, *Cuk converters*, https://www.monolithicpower.com/en/learning/mpscholar/power-electronics/dc-dc-converters/cuk-converters, Accessed: 2024-10-22, 2024.

[77] E. Bureau, *Testing automotive mcu – an overview*, https://www.electronicsforu.com/market-verticals/testing-automotive-mcu-overview, Accessed: 2024-11-06, 2022.

[78] O. Liang, *Electronic speed controller*. [Online]. Available: https://oscarliang.com/esc/.

[79] MathWorks, *Surface mount permanent magnet synchronous motor*, https://www.mathworks.com/help/mcb/ref/surfacemountpmsm.html, Accessed: 2024-10-22, 2024.

[80] M. Tursini, F. Parasiliti, and D. Zhang, "Real-time gain tuning of pi controllers for high-performance pmsm drives," *Industry Applications, IEEE Transactions on*, vol. 38, pp. 1018–1026, Aug. 2002. DOI: 10.1109/TIA.2002.800564.

[81] MathWorks, *Pmsm controller block diagram*, 2023. [Online]. Available: https://www.mathworks.com/help/autoblks/ref/block_pmsm_controller_over.png.

[82] MathWorks, *Bldc motor speed control with cascade pi controllers*, 2023. [Online]. Available: https://www.mathworks.com/help/slcontrol/ug/bldc-motor-speed-control-with-cascade-pi-controllers.html.

[83] MathWorks, *Mapped si engine*, https://www.mathworks.com/help/vdynblks/ref/mappedsiengine.html, Accessed: 2024-10-22, 2024.

[84] MathWorks, *Battery data sheet*, https://www.mathworks.com/help/autoblks/ref/datasheetbattery.html, Accessed: 2024-10-22, 2024.

[85] C. Voisin, F. Renard, and J.-R. Grasso, "Long term friction: From stick-slip to stable sliding," *Geophysical Research Letters*, vol. 34, Jul. 2007. DOI: 10.1029/2007GL029715.

[86] W. N. Association, *Heat values of various fuels*, https://world-nuclear.org/information-library/facts-and-figures/heat-values-of-various-fuels, Accessed: 2024-11-06, 2020.

8 Appendix

8.1 Experimental Results

8.1.1 Mode 1 Test

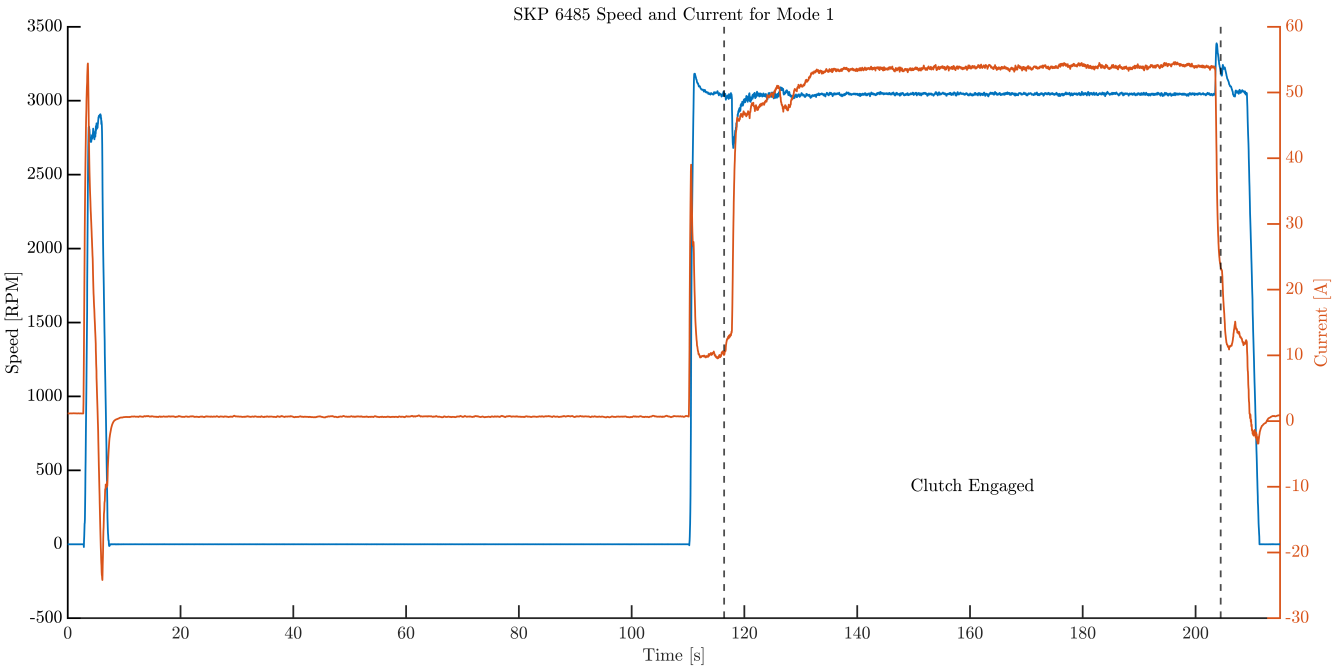

Figure 96: Experimental SKP speed and current in Mode 1 30A test

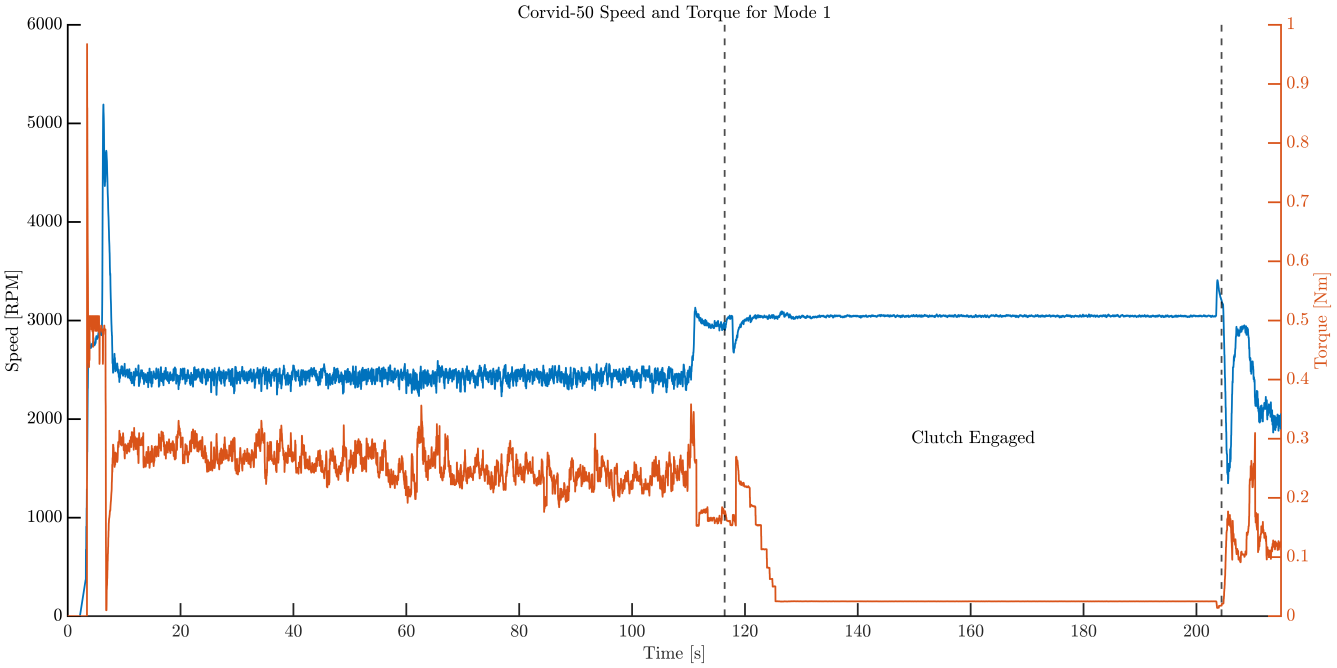

Figure 97: Experimental Corvid-50 speed and torque in Mode 1 30A test

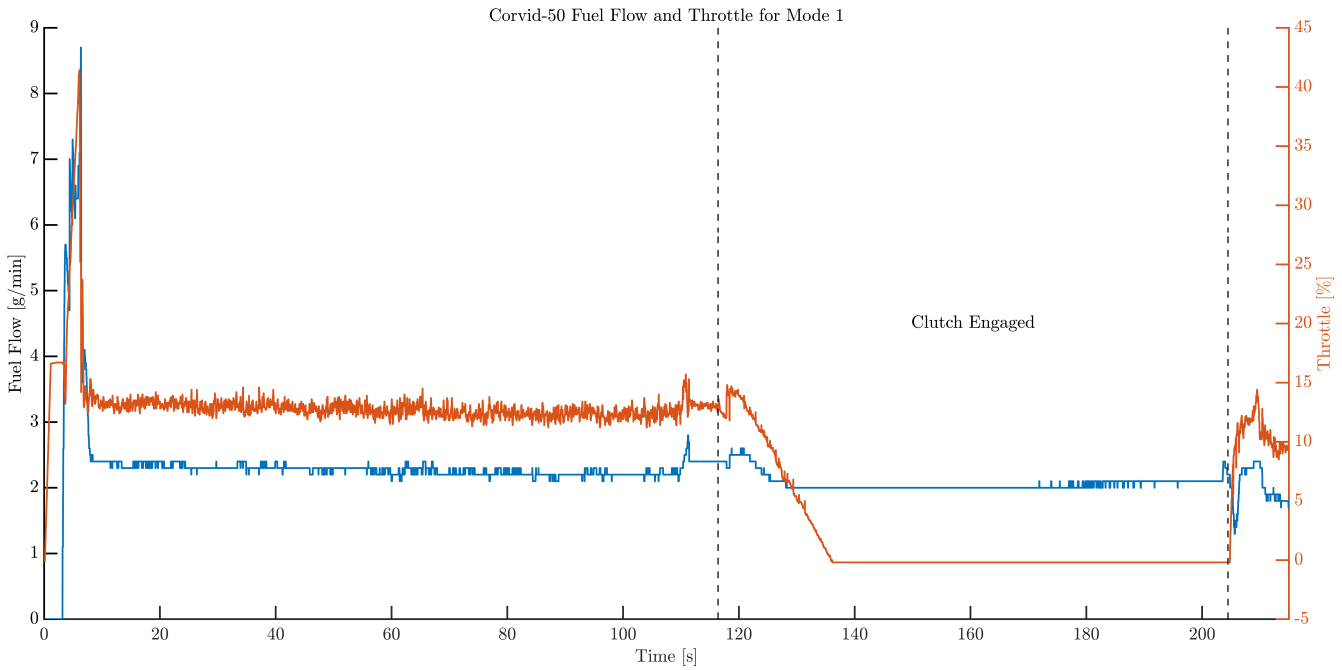

Figure 98: Experimental fuel and throttle in Mode 1 30A test

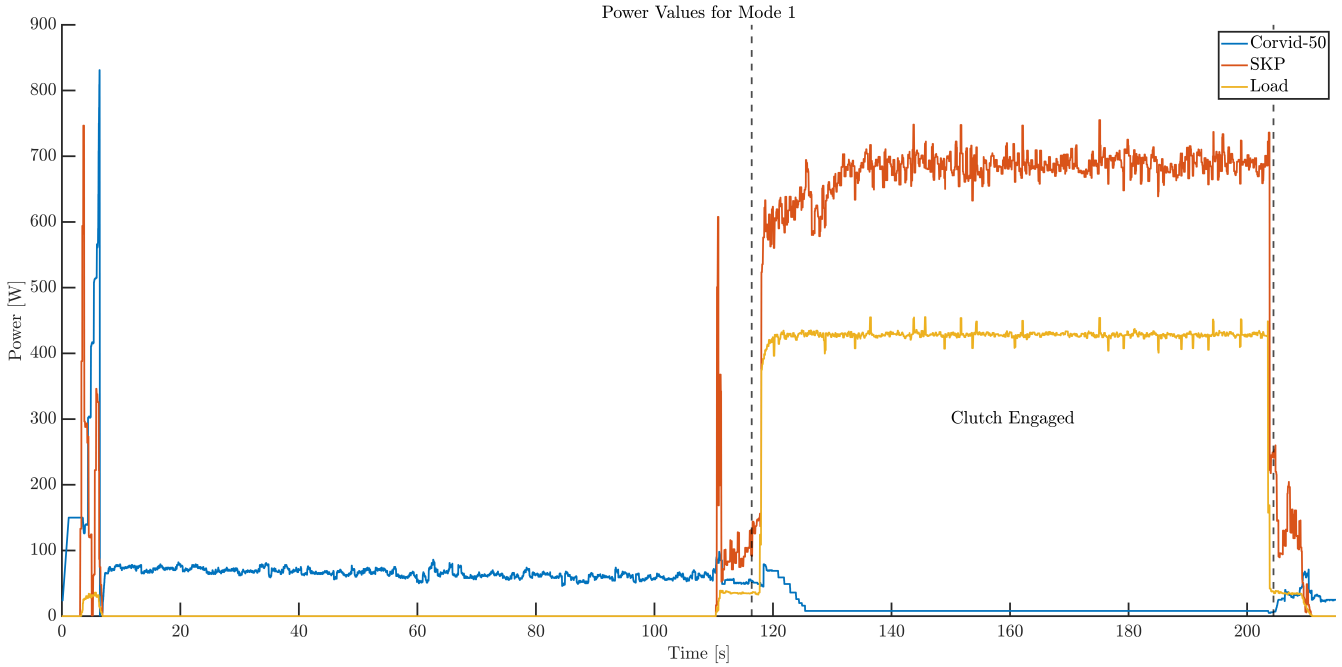

Figure 99: Experimental power values in Mode 1 30A test

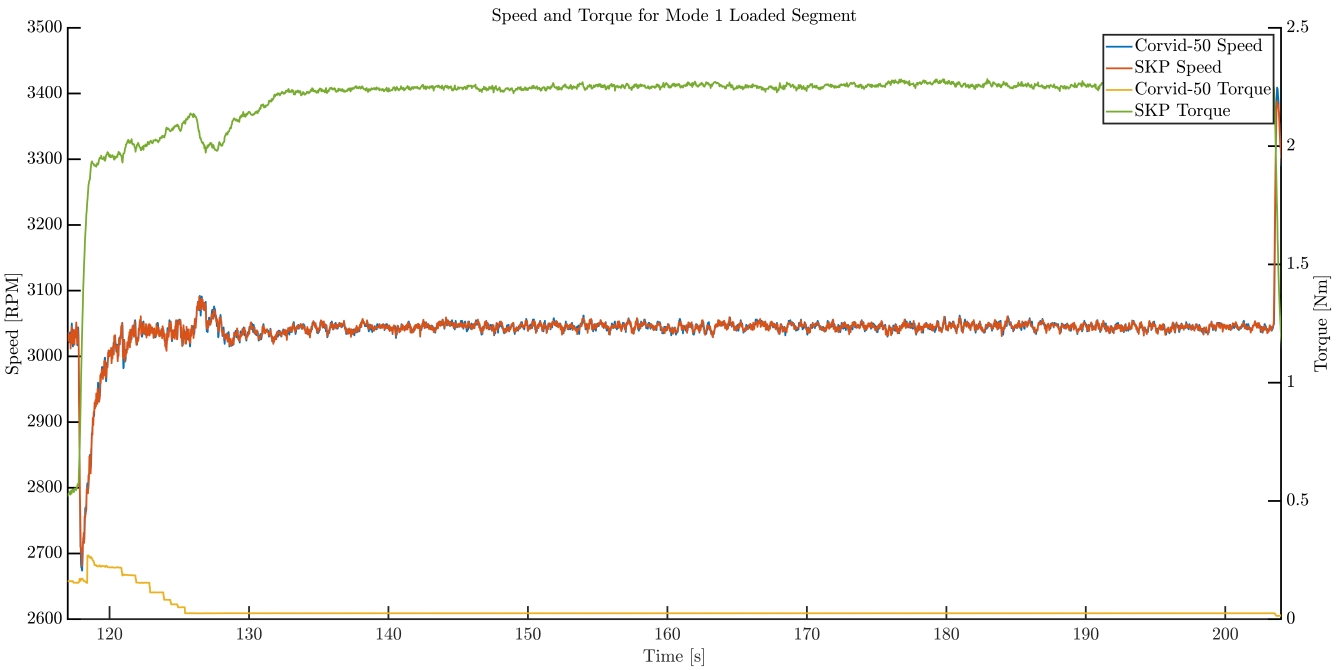

Figure 100: Experimental speed and torque in loaded segment of Mode 1 30A test

8.1.2 Mode 2 Test

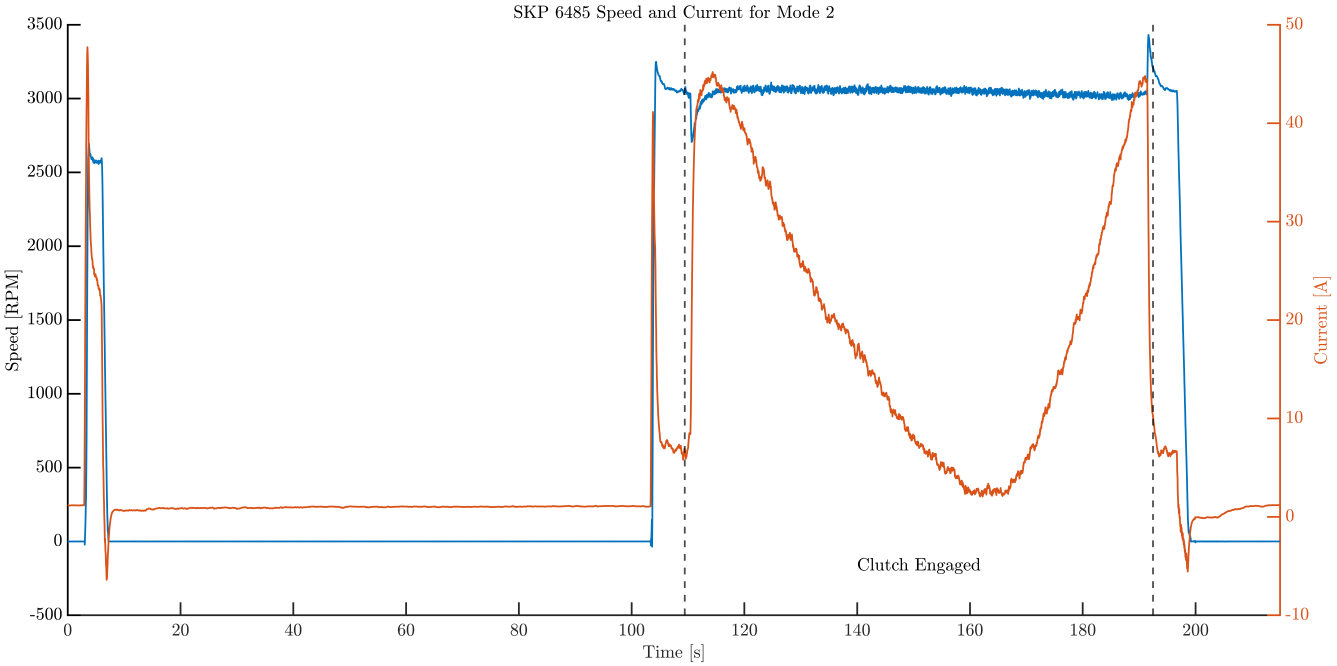

Figure 101: Experimental SKP speed and current in Mode 2 30A test

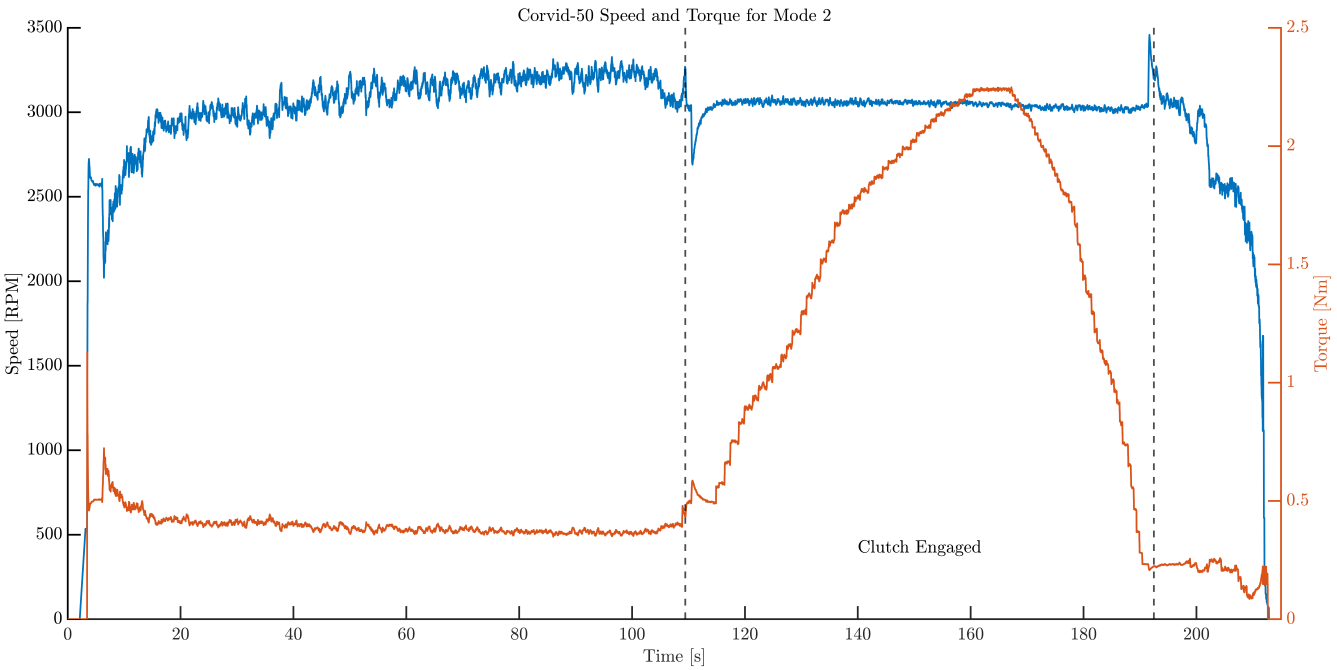

Figure 102: Experimental Corvid-50 speed and torque in Mode 2 30A test

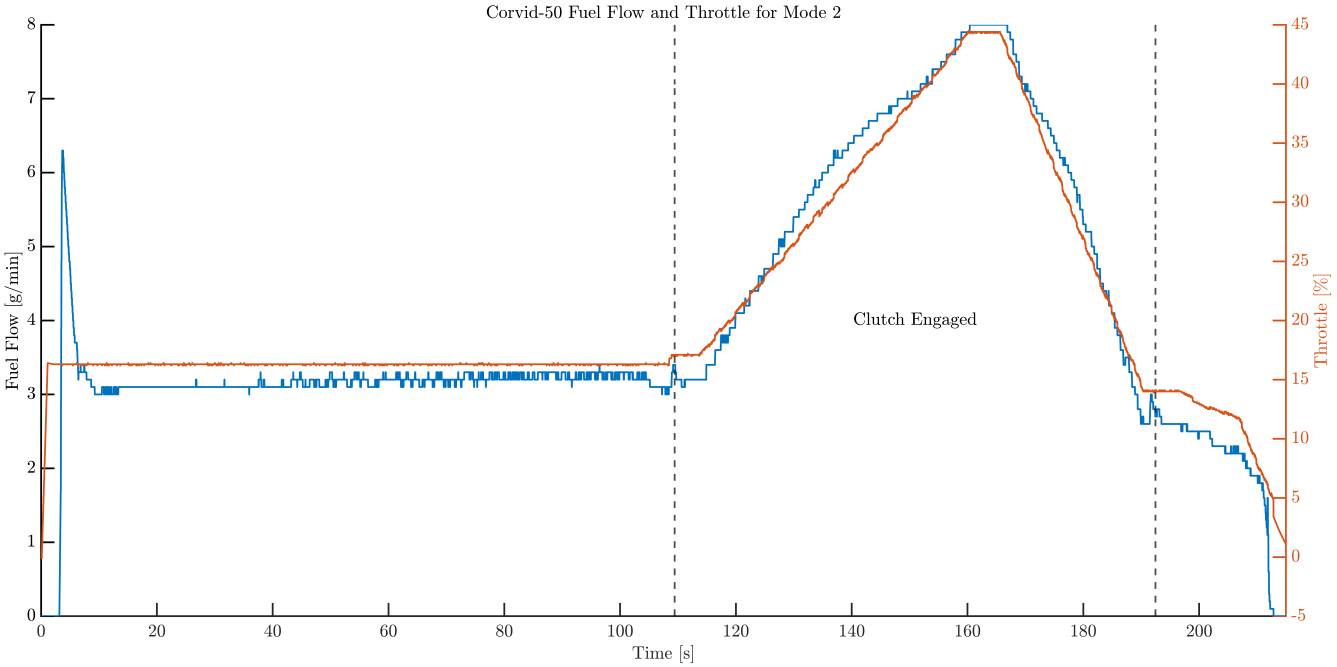

Figure 103: Experimental fuel and throttle in Mode 2 30A test

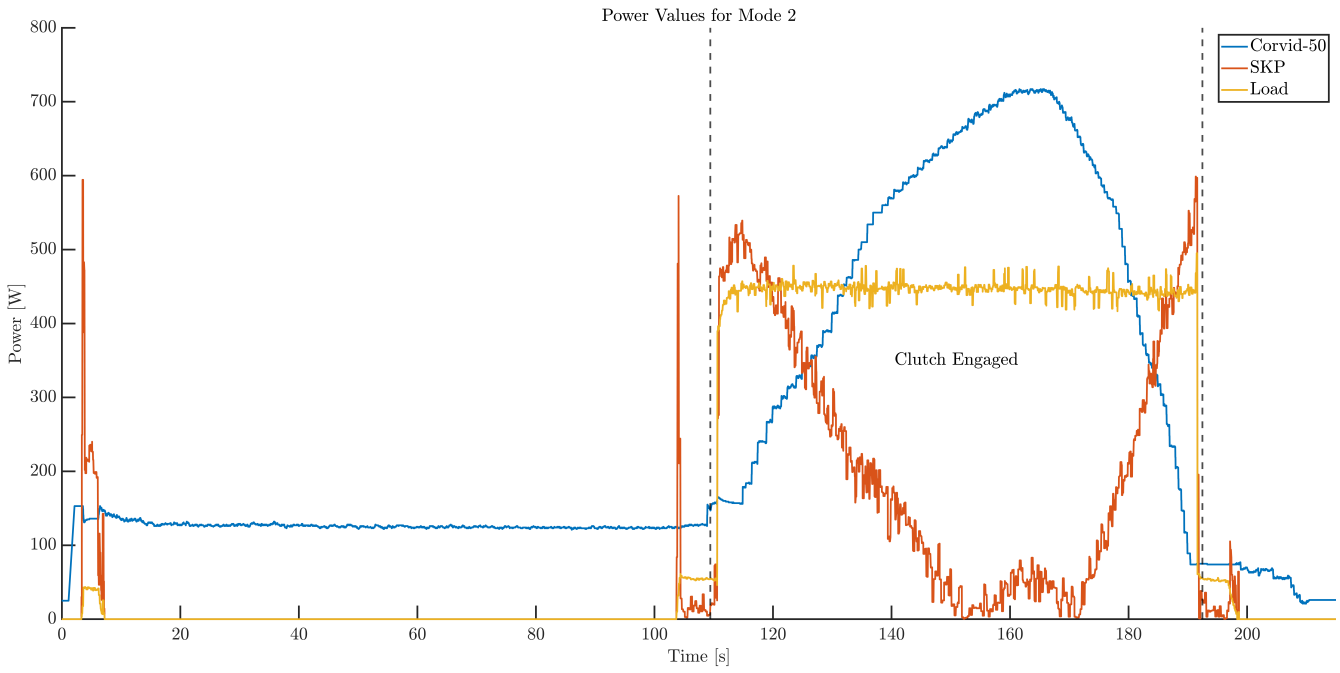

Figure 104: Experimental power values in Mode 2 30A test

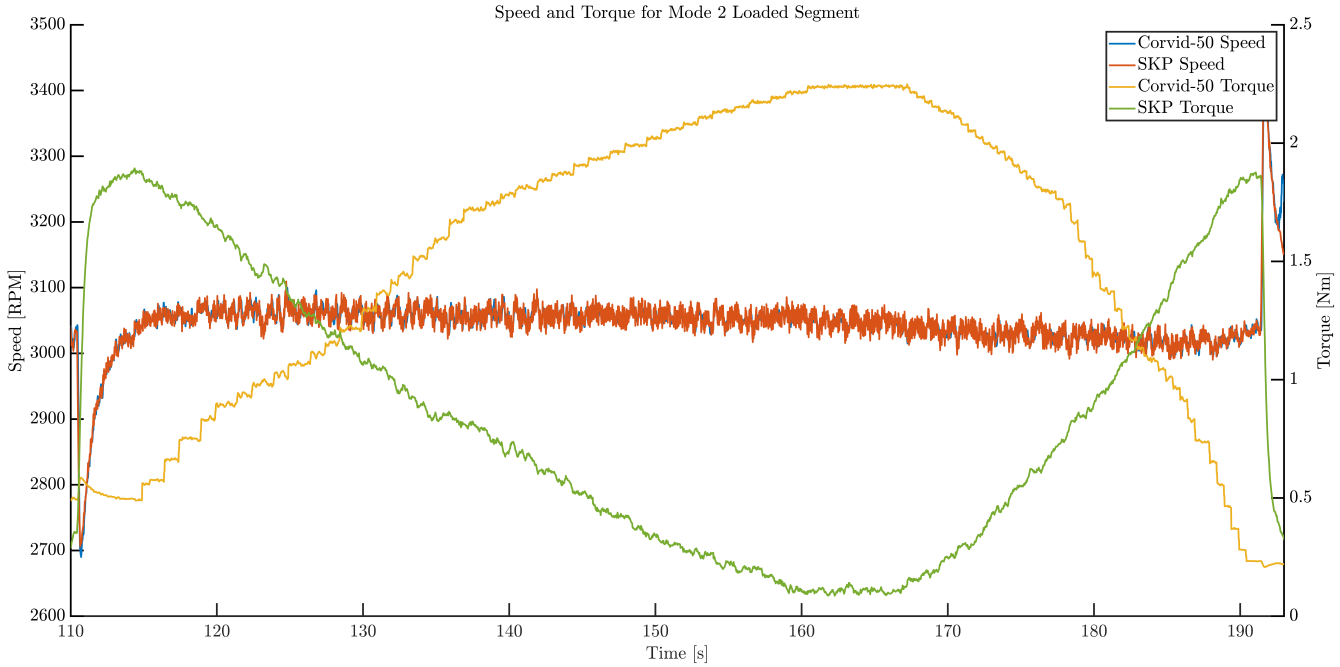

Figure 105: Experimental speed and torque in loaded segment of Mode 2 30A test

8.1.3 Mode 3 Test

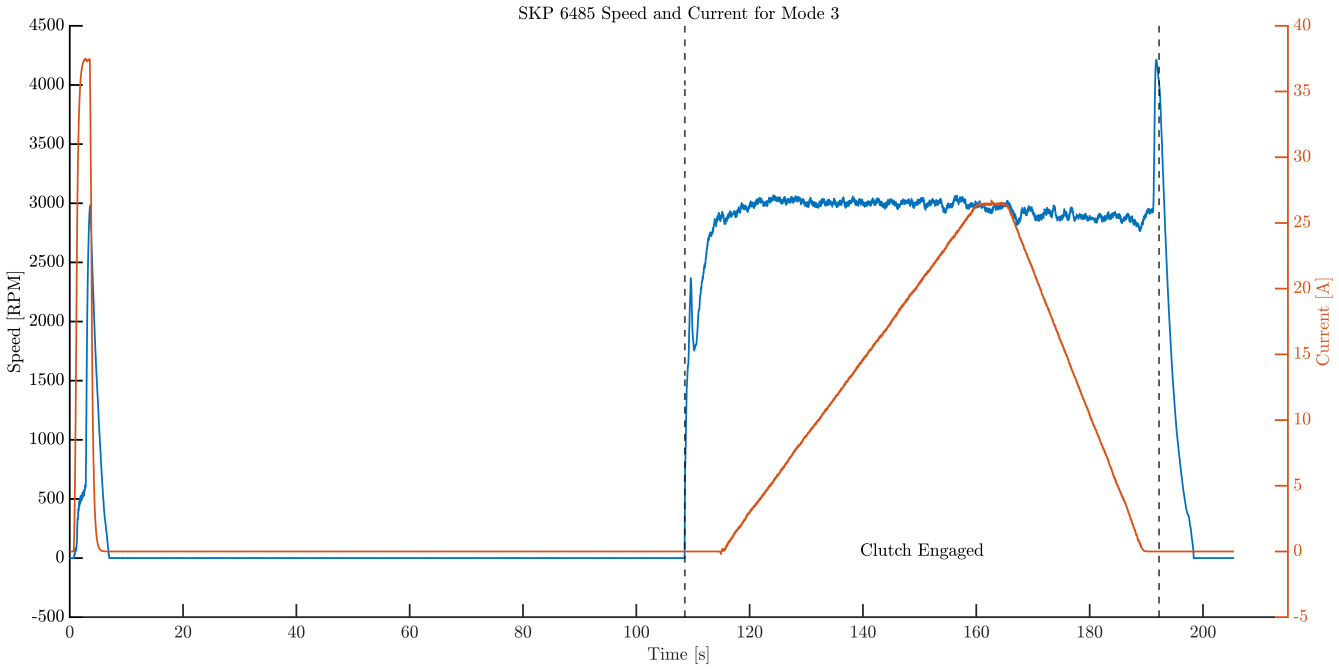

Figure 106: Experimental SKP speed and current in Mode 3 30A test

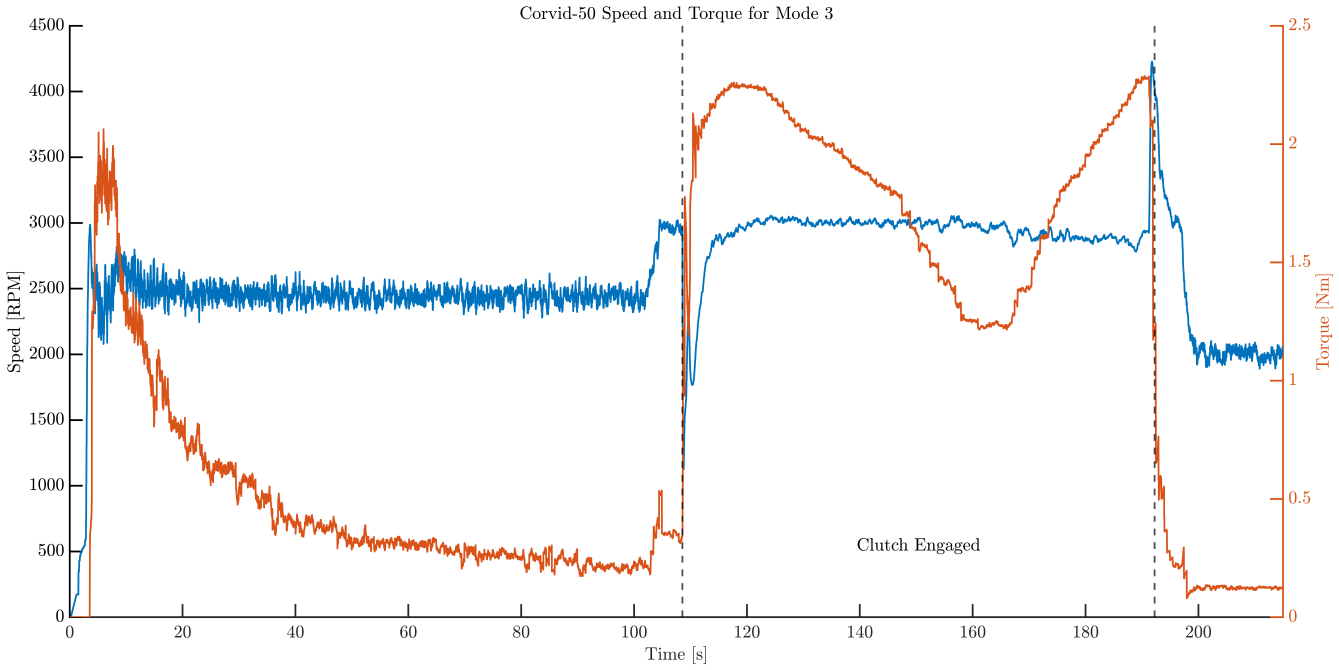

Figure 107: Experimental Corvid-50 speed and torque in Mode 3 30A test

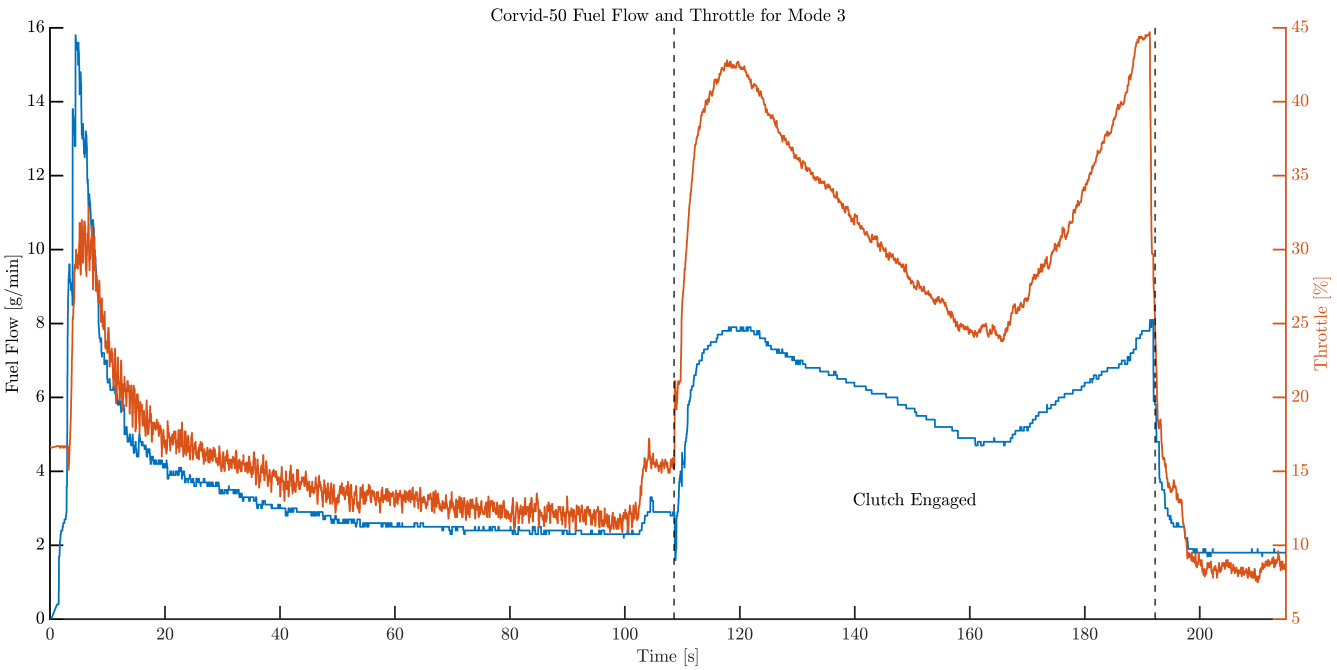

Figure 108: Experimental fuel and throttle in Mode 3 30A test

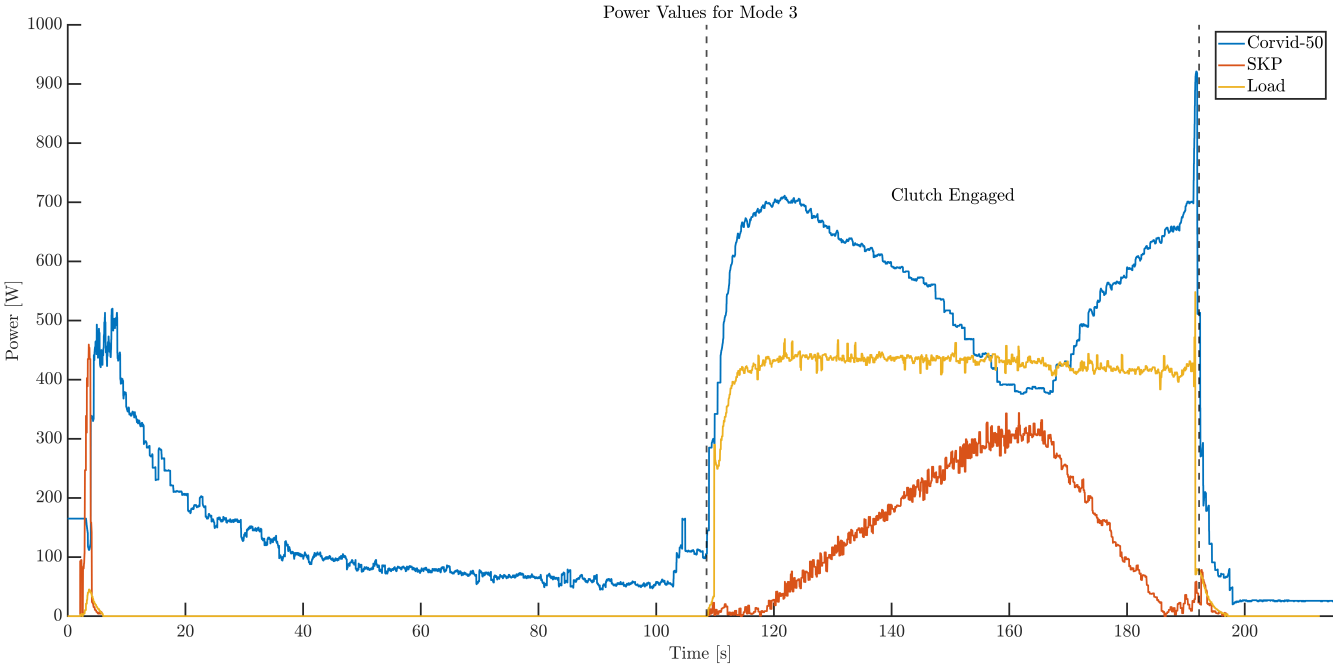

Figure 109: Experimental power values in Mode 3 30A test

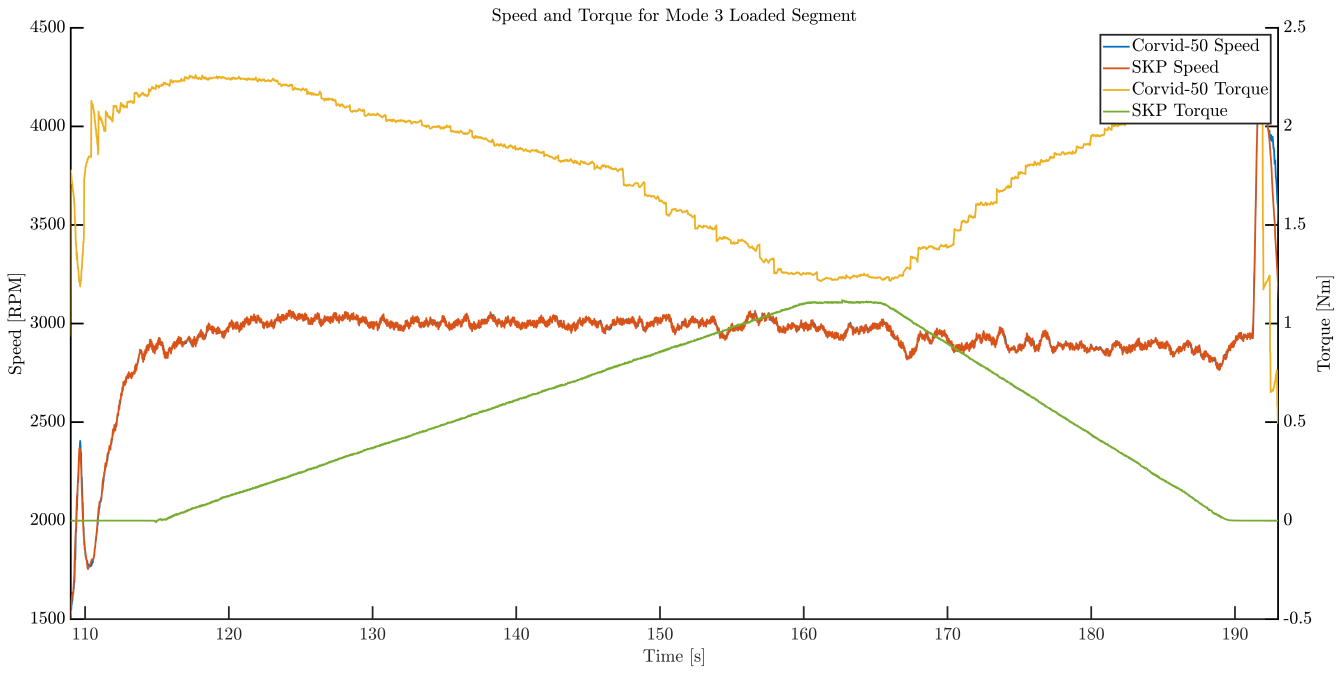

Figure 110: Experimental speed and torque in loaded segment of Mode 3 30A test

8.1.4 Electric Virtual Flight Mission

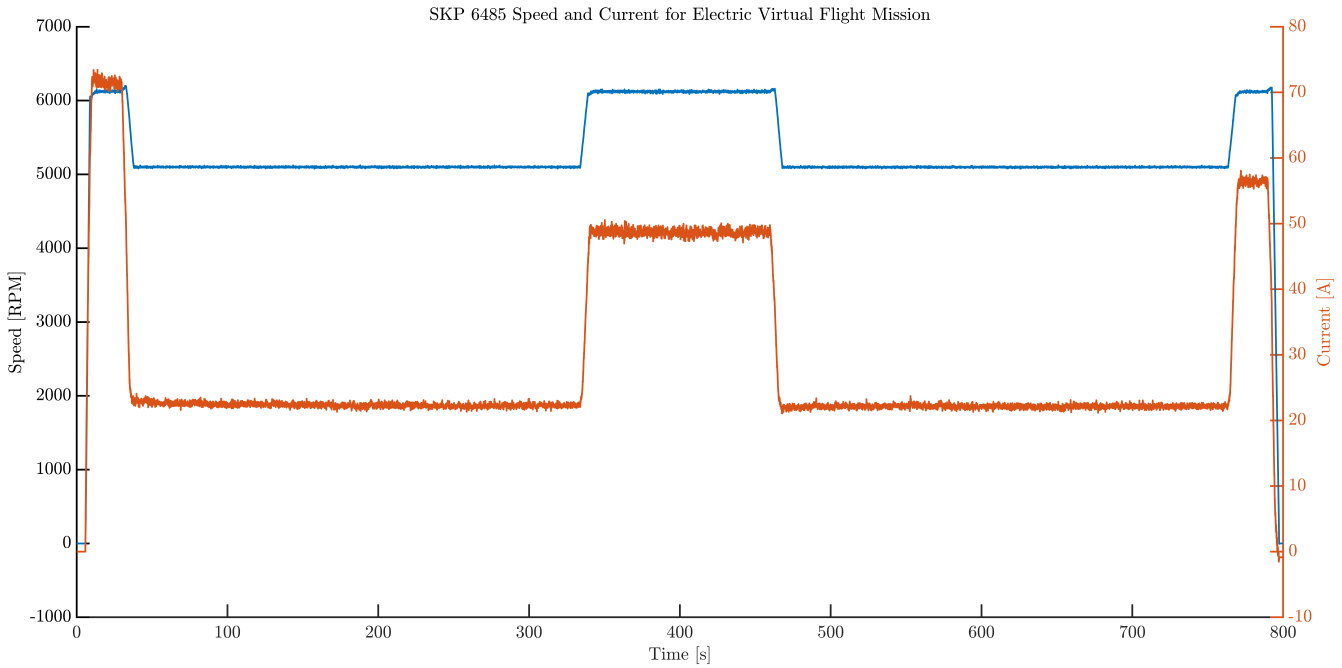

Figure 111: Experimental SKP speed and current in electric-only virtual flight mission

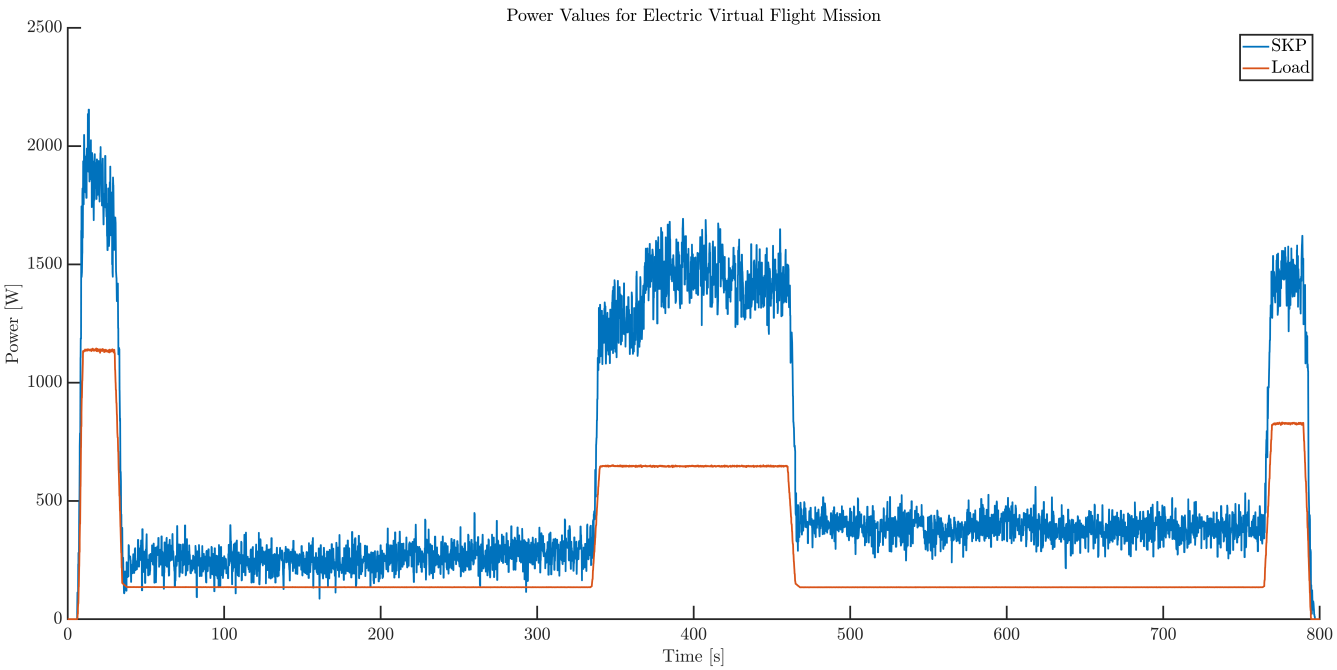

Figure 112: Experimental power values in electric-only virtual flight mission

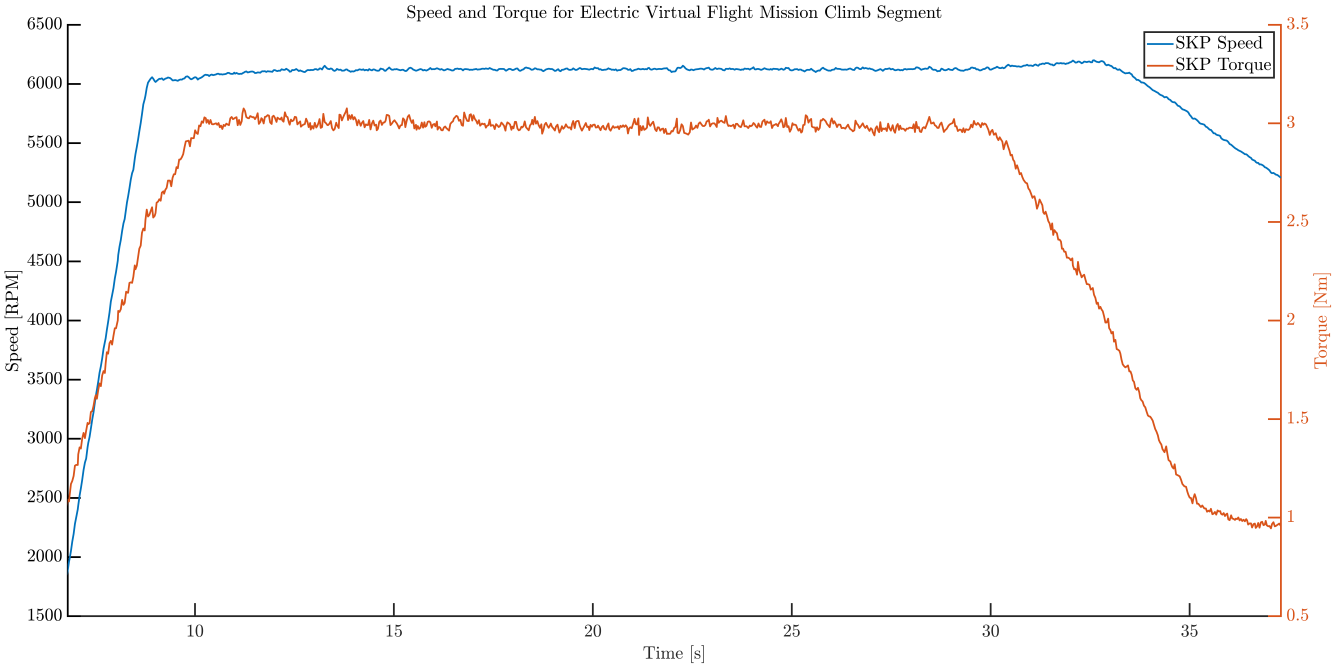

Figure 113: Experimental speed and torque in electric-only climb segment

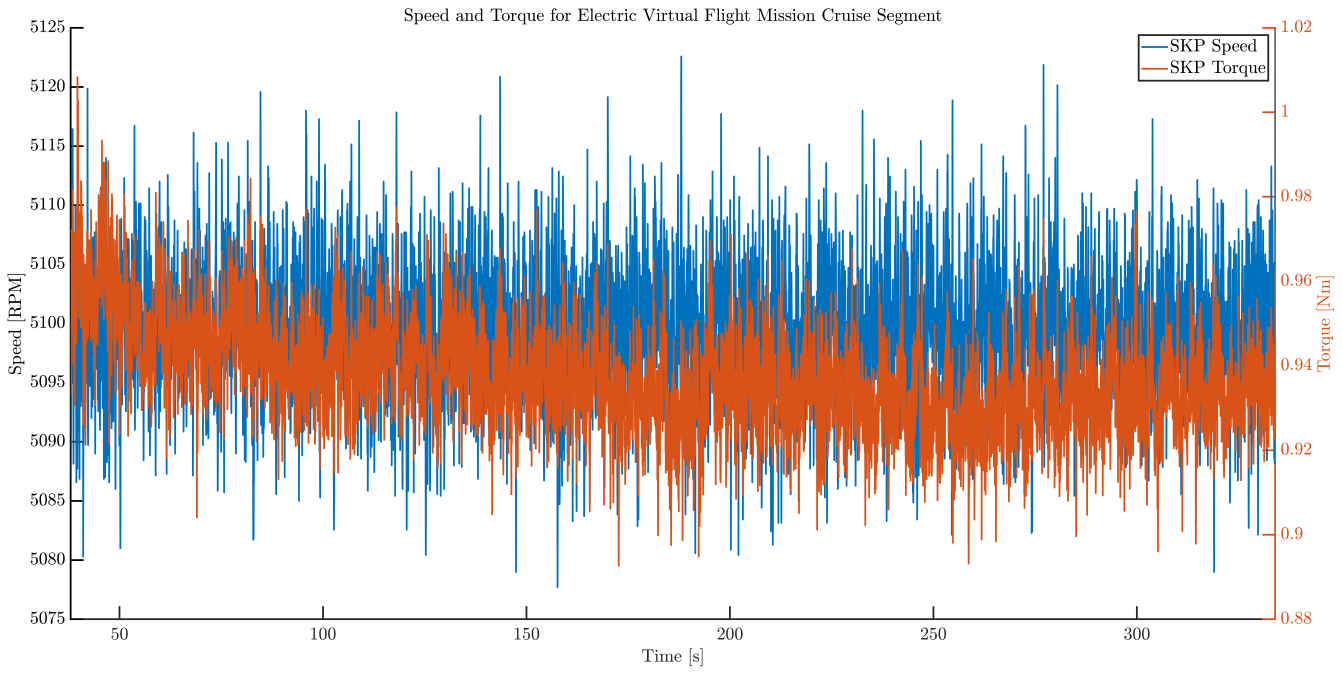

Figure 114: Experimental speed and torque in electric-only cruise segment

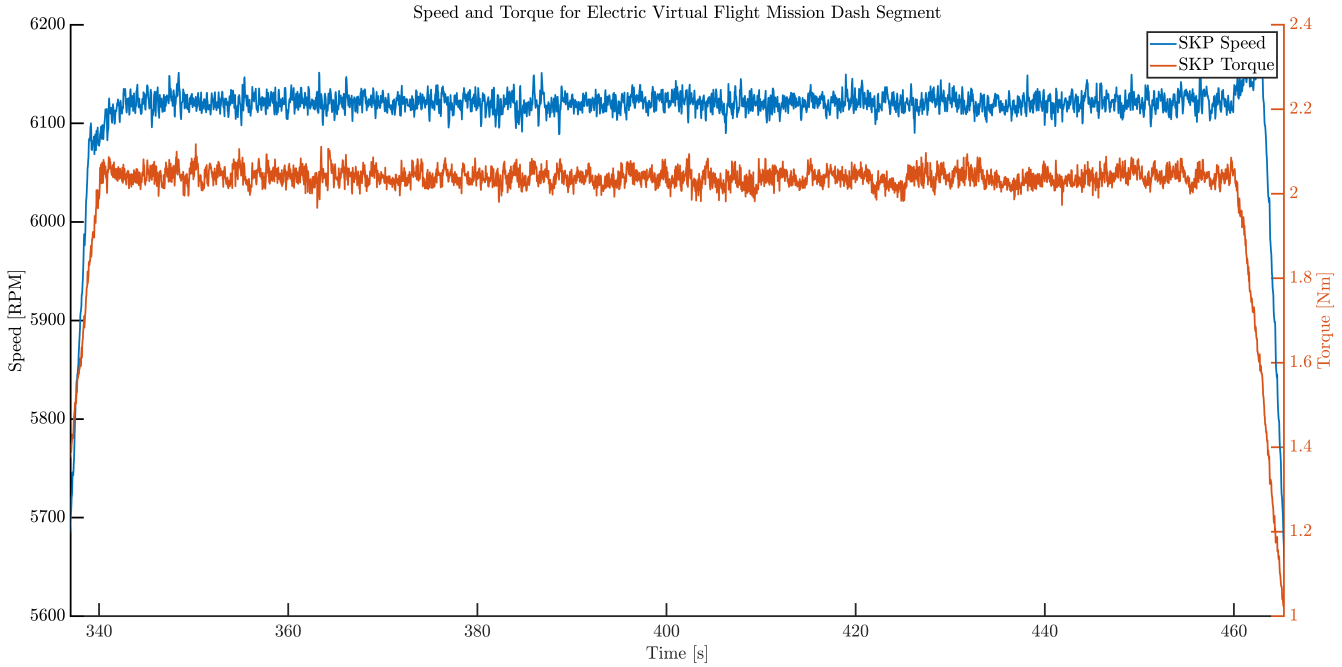

Figure 115: Experimental speed and torque in electric-only dash segment

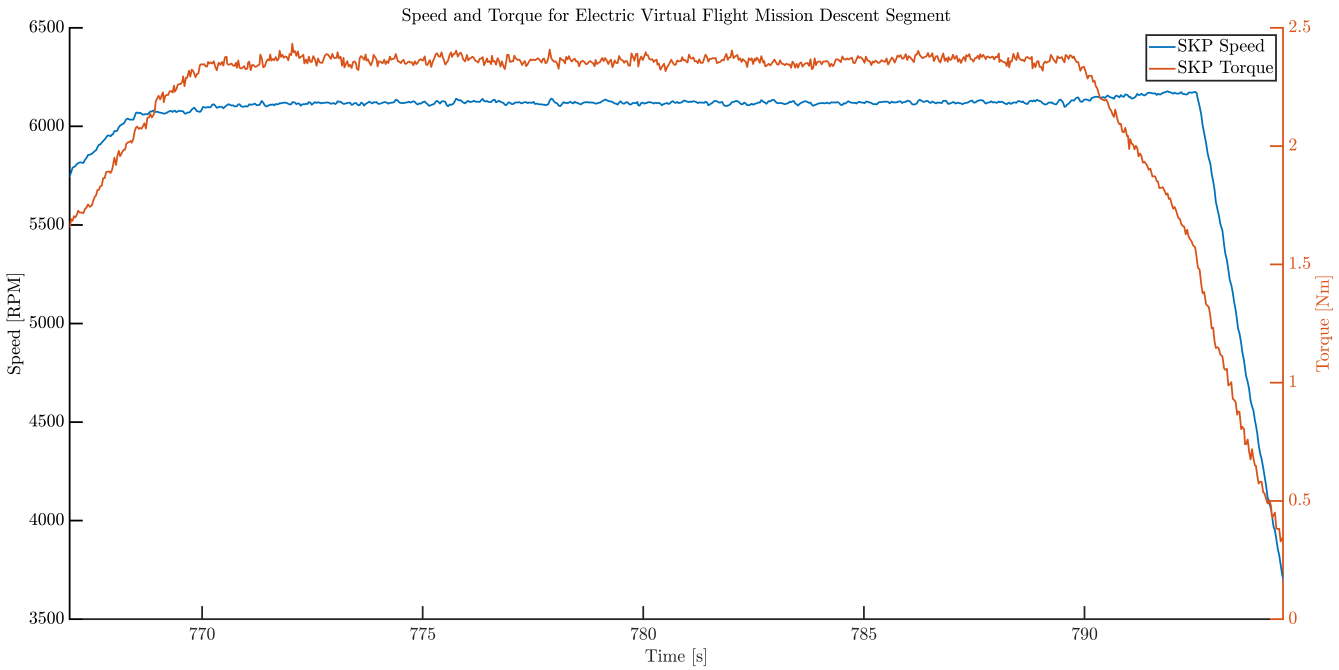

Figure 116: Experimental speed and torque in electric-only descent segment

8.1.5 Combustion Virtual Flight Mission

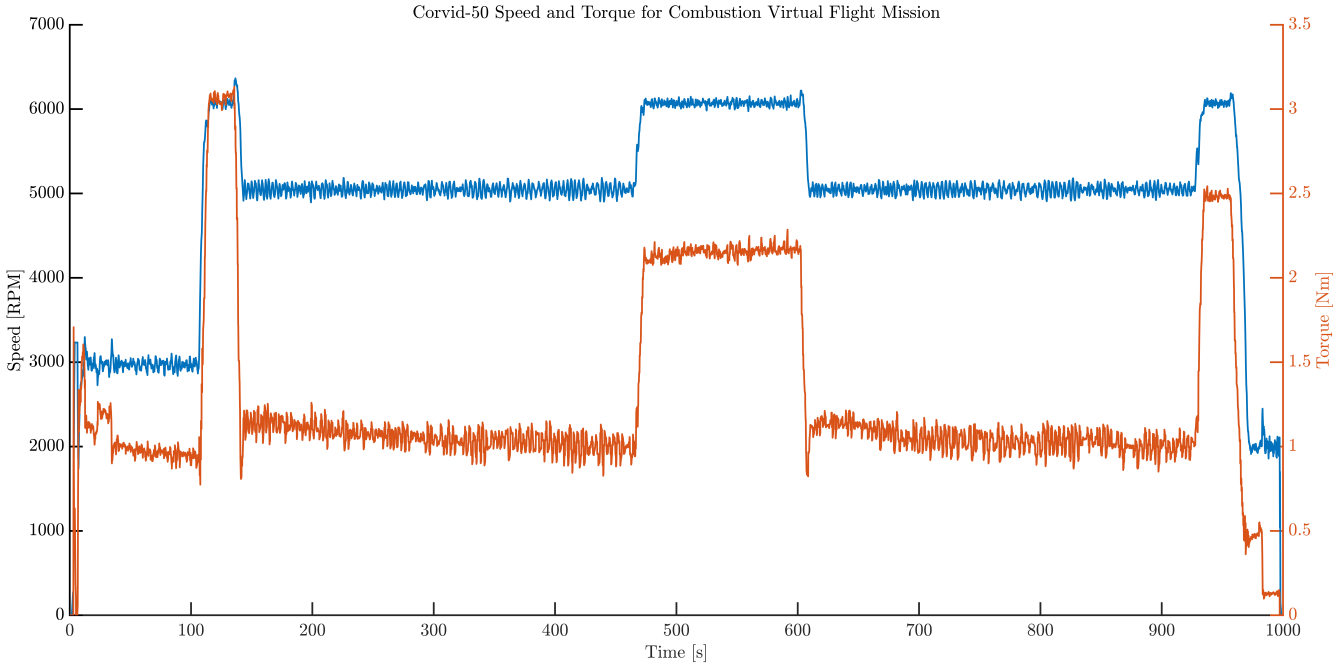

Figure 117: Experimental Corvid-50 speed and torque in combustion-only virtual flight mission

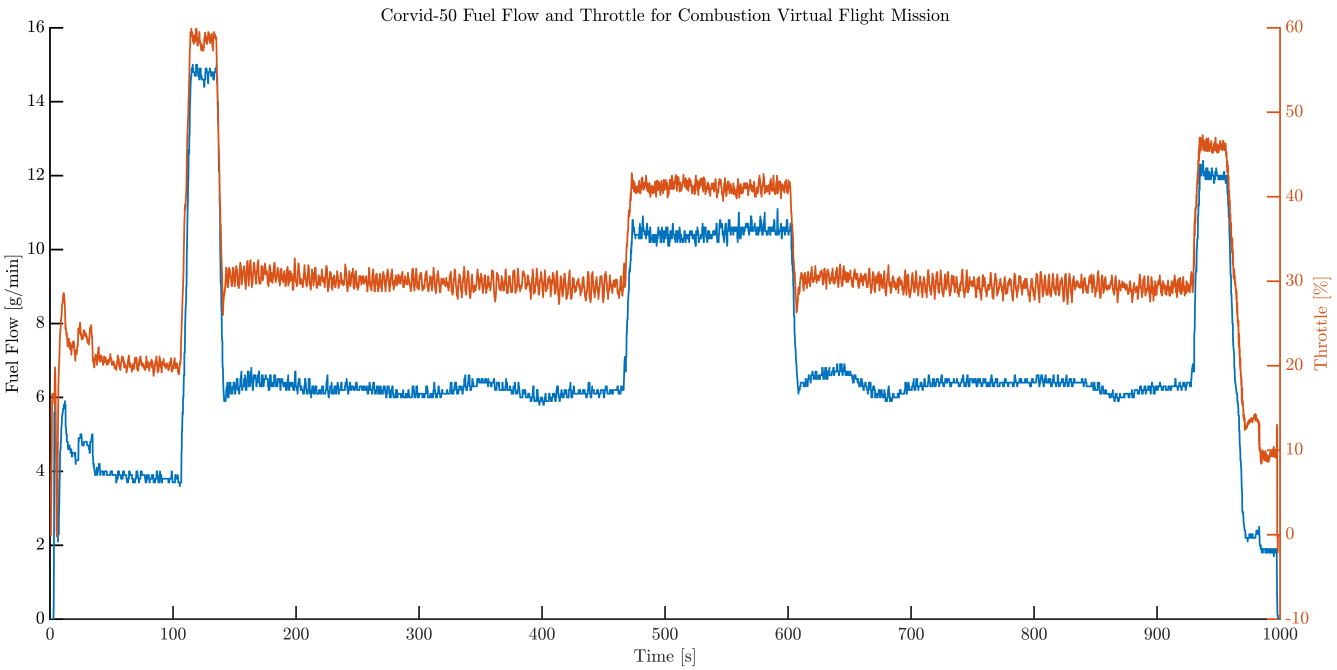

Figure 118: Experimental fuel and throttle in combustion-only virtual flight mission

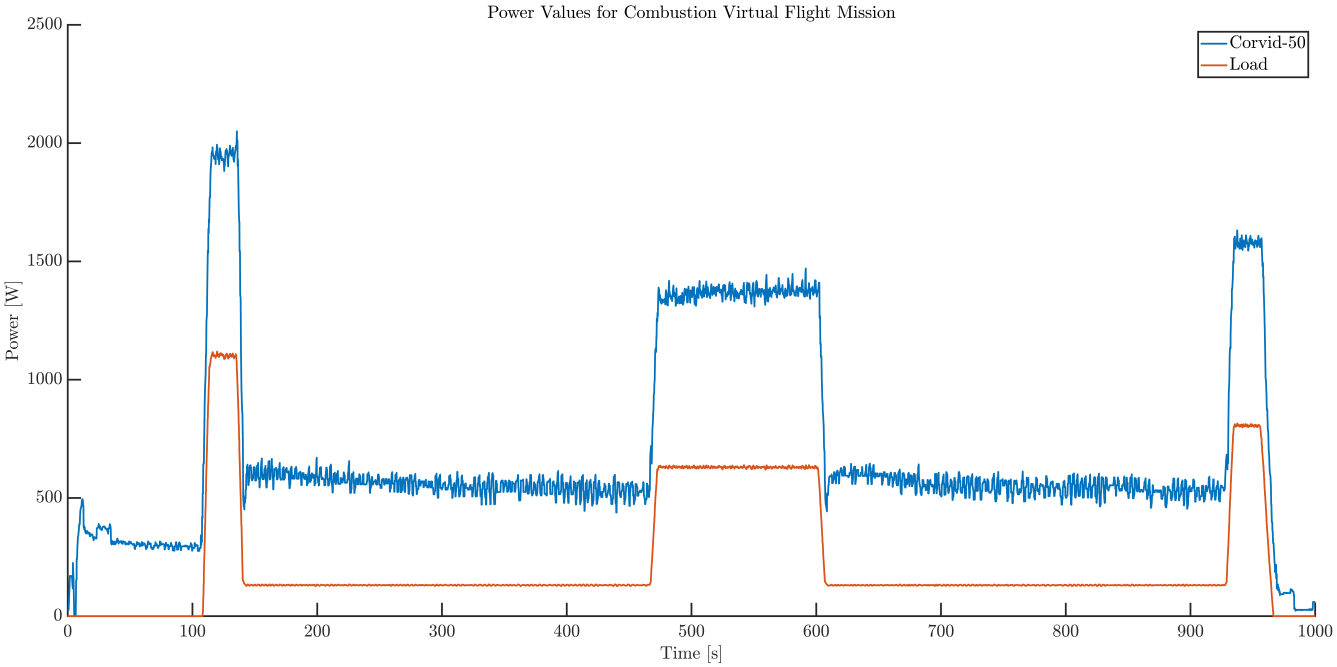

Figure 119: Experimental power values in combustion-only virtual flight mission

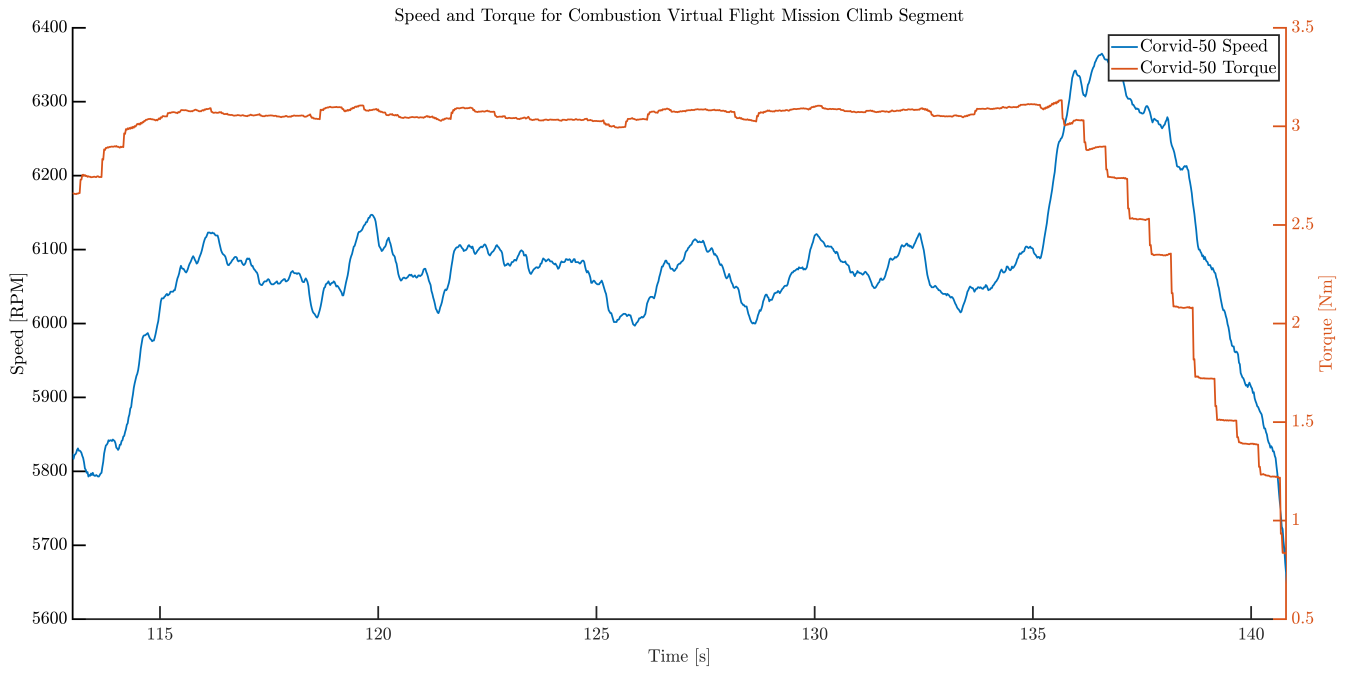

Figure 120: Experimental speed and torque in combustion-only climb segment

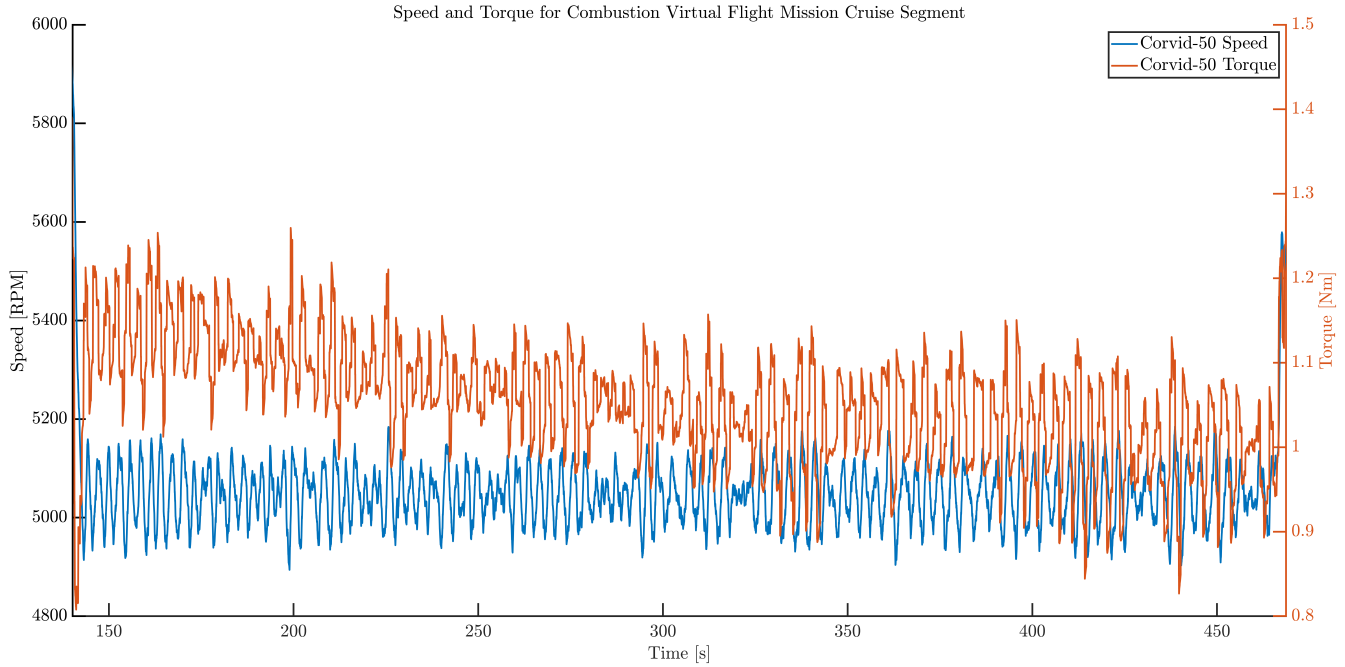

Figure 121: Experimental speed and torque in combustion-only cruise segment

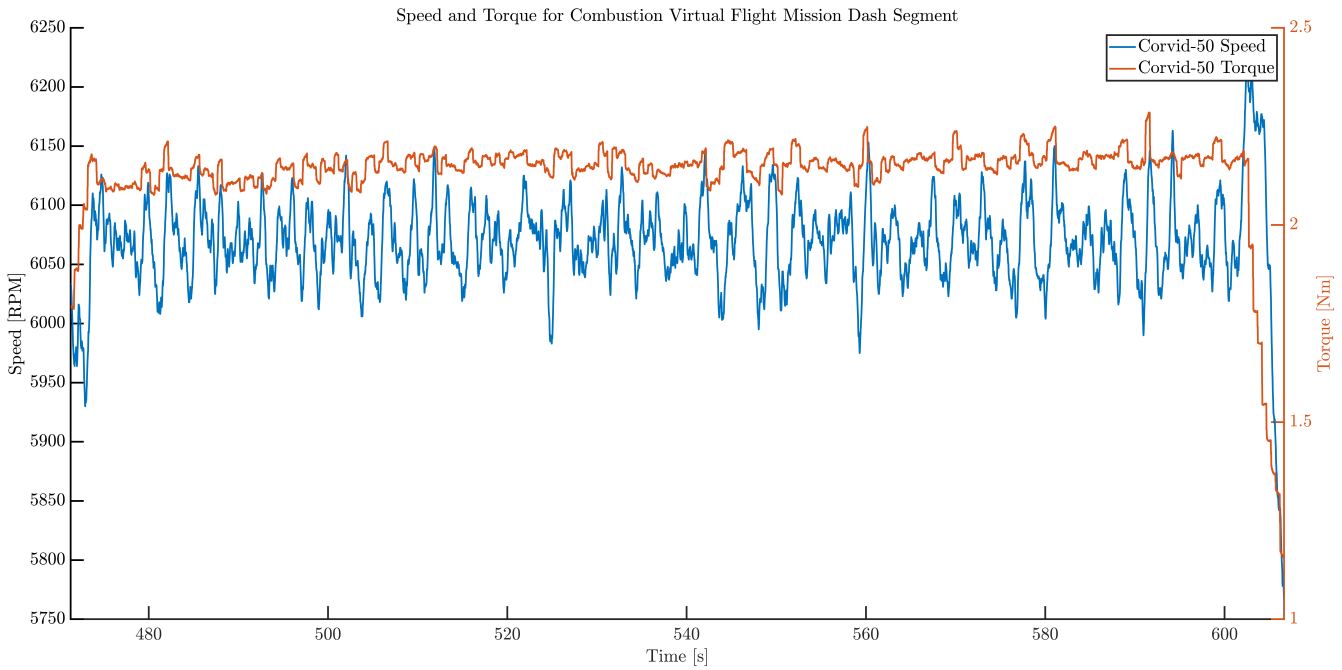

Figure 122: Experimental speed and torque in combustion-only dash segment

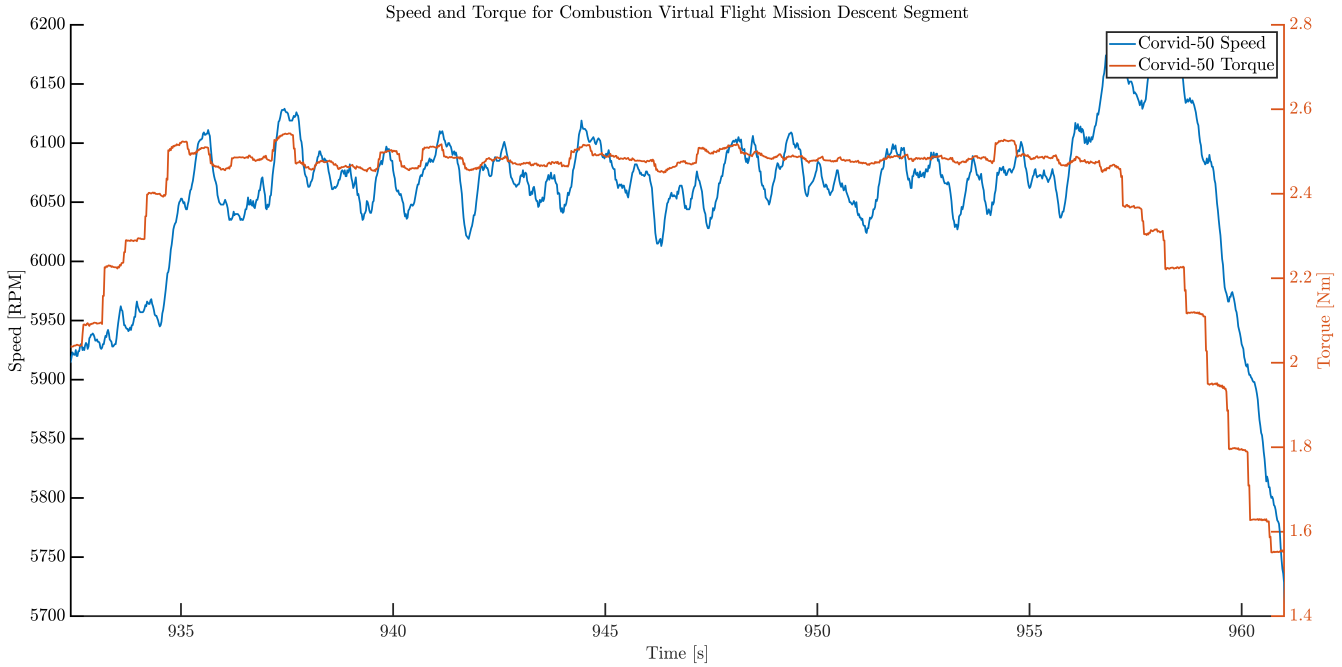

Figure 123: Experimental speed and torque in combustion-only descent segment

8.1.6 Hybrid Virtual Flight Mission

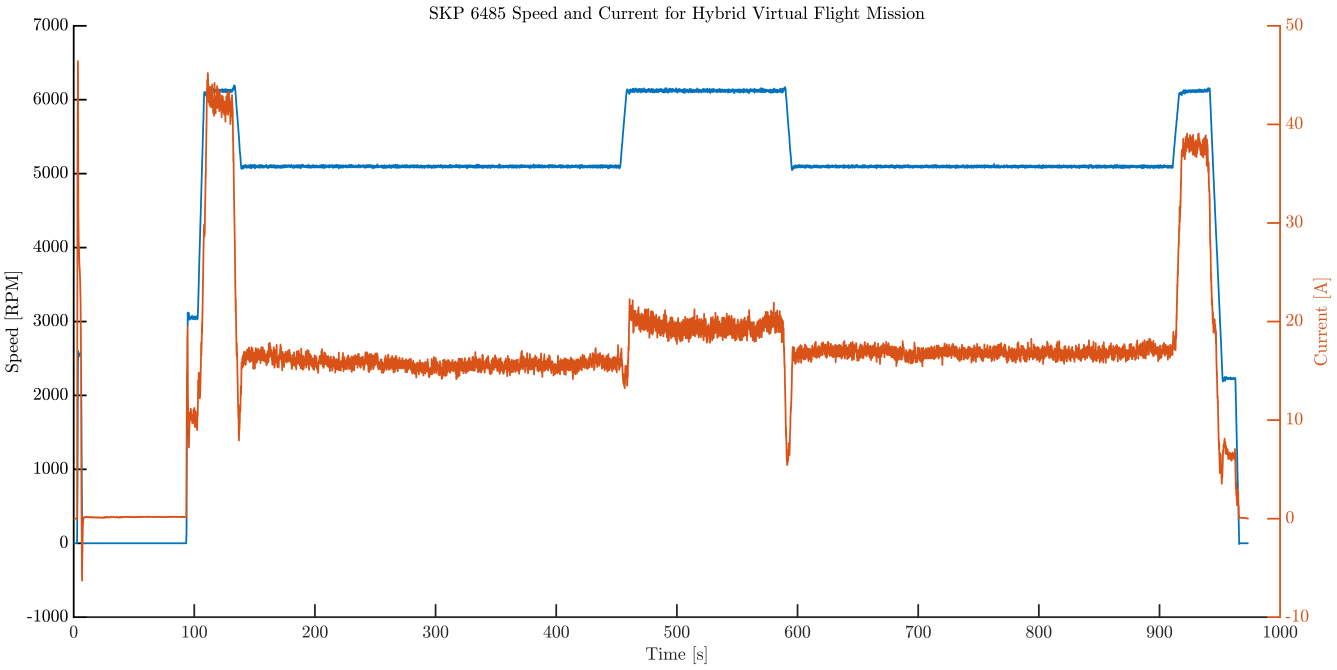

Figure 124: Experimental SKP speed and current in hybrid virtual flight mission

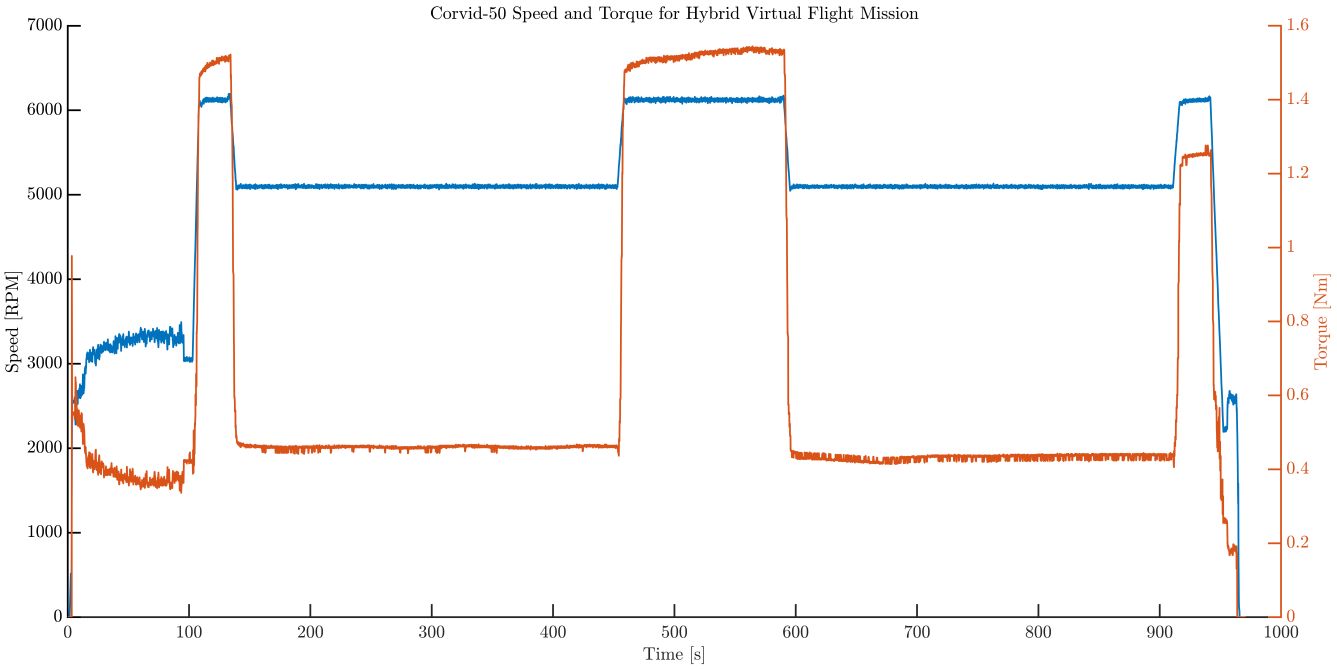

Figure 125: Experimental Corvid-50 speed and torque in hybrid virtual flight mission

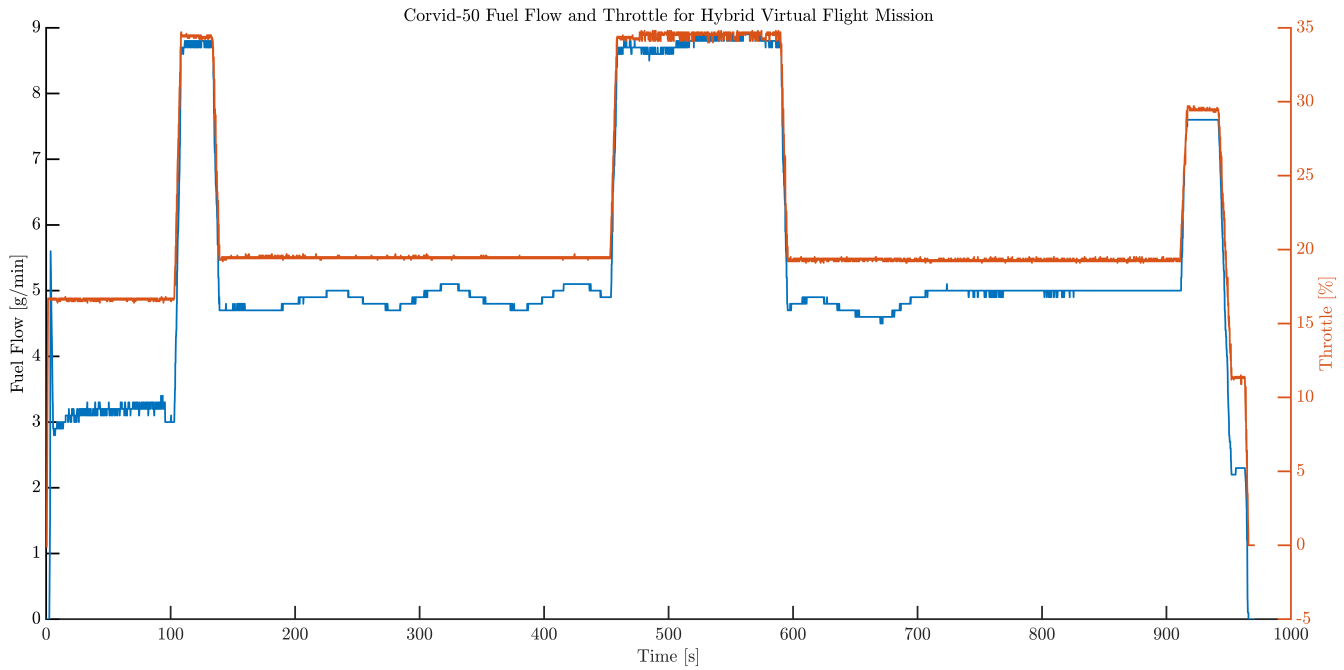

Figure 126: Experimental fuel and throttle in hybrid virtual flight mission

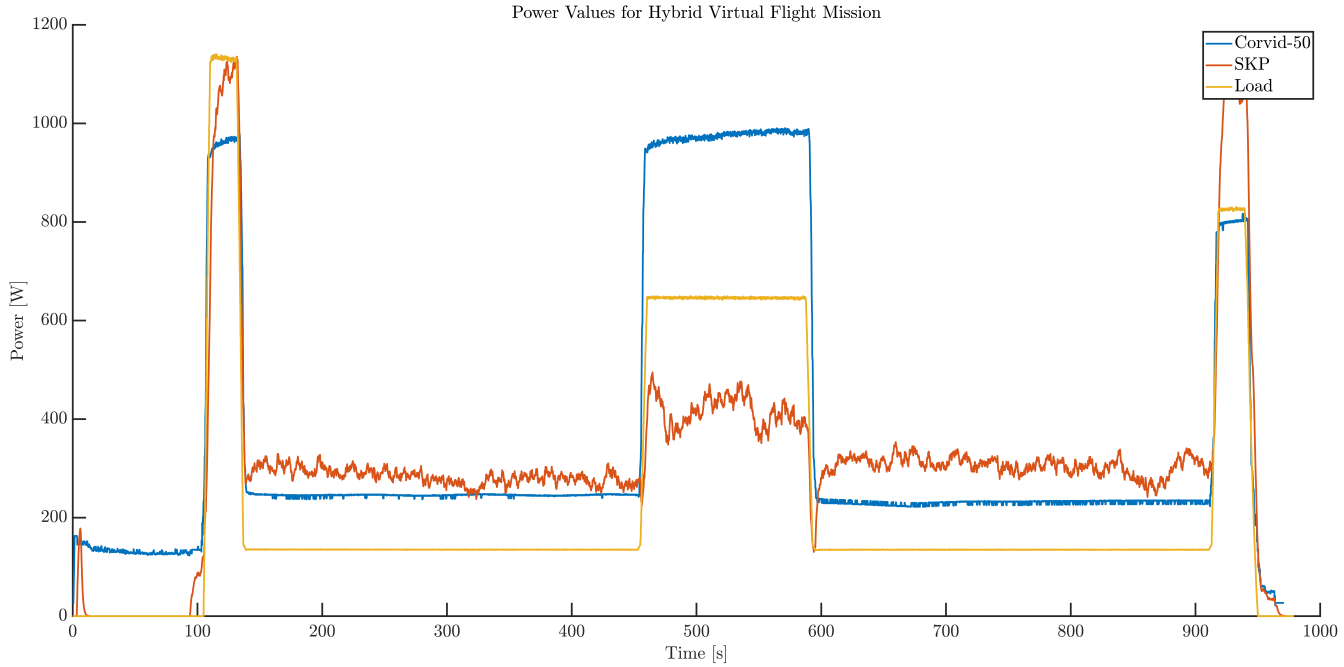

Figure 127: Experimental power values in hybrid virtual flight mission

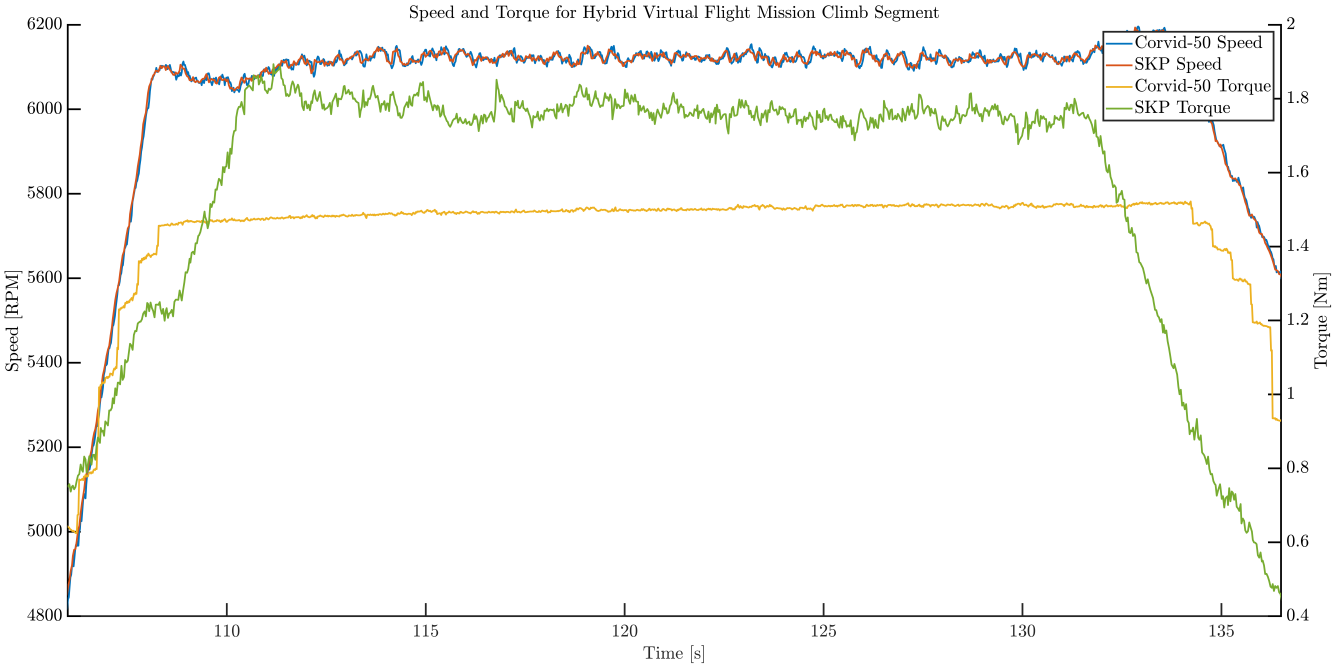

Figure 128: Experimental speed and torque in hybrid climb segment

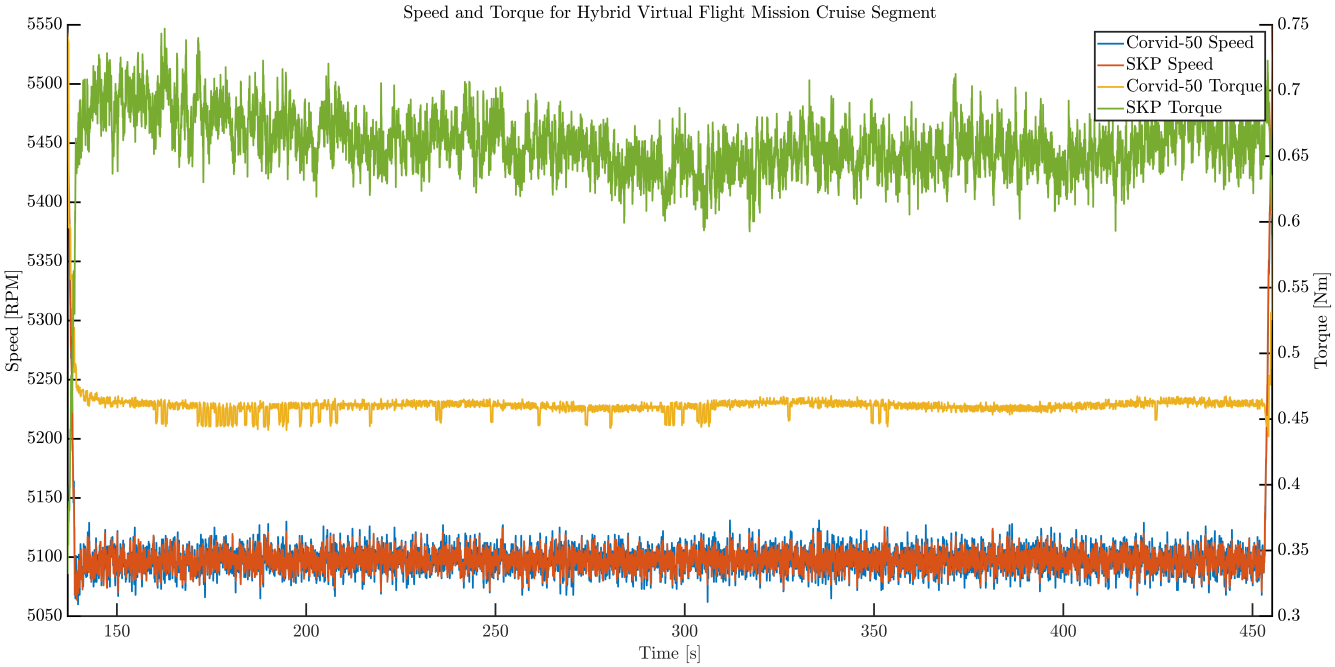

Figure 129: Experimental speed and torque in hybrid cruise segment

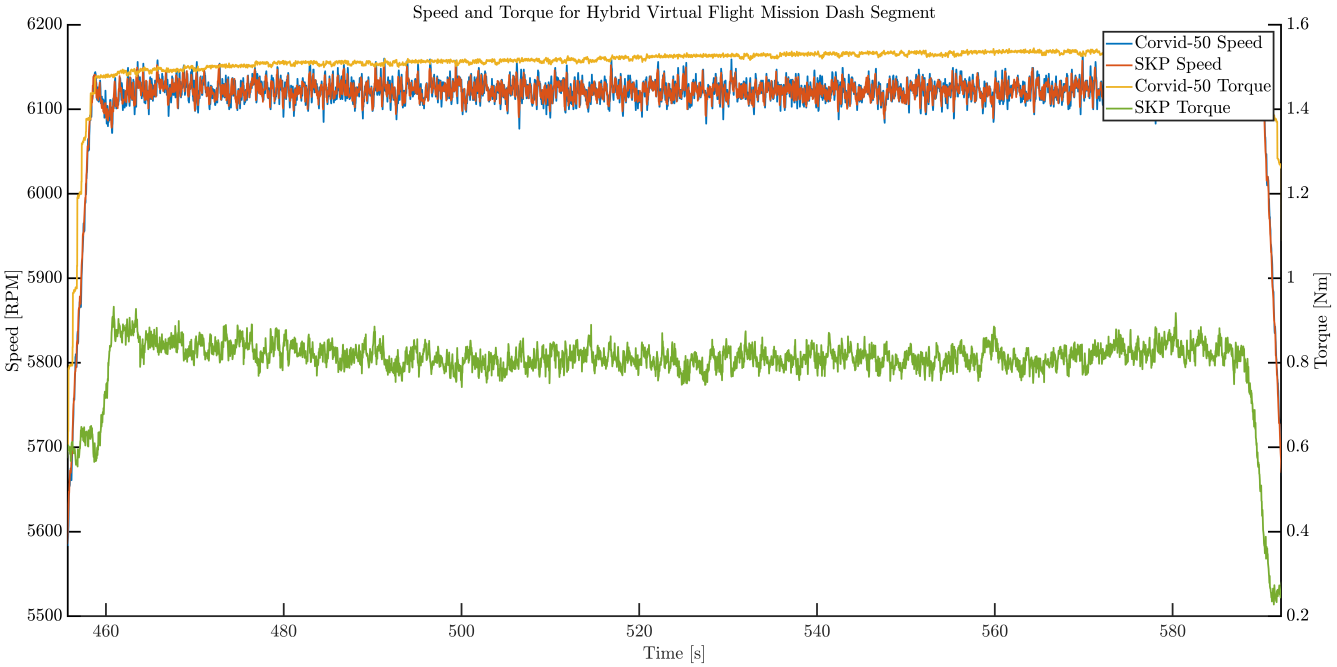

Figure 130: Experimental speed and torque in hybrid dash segment

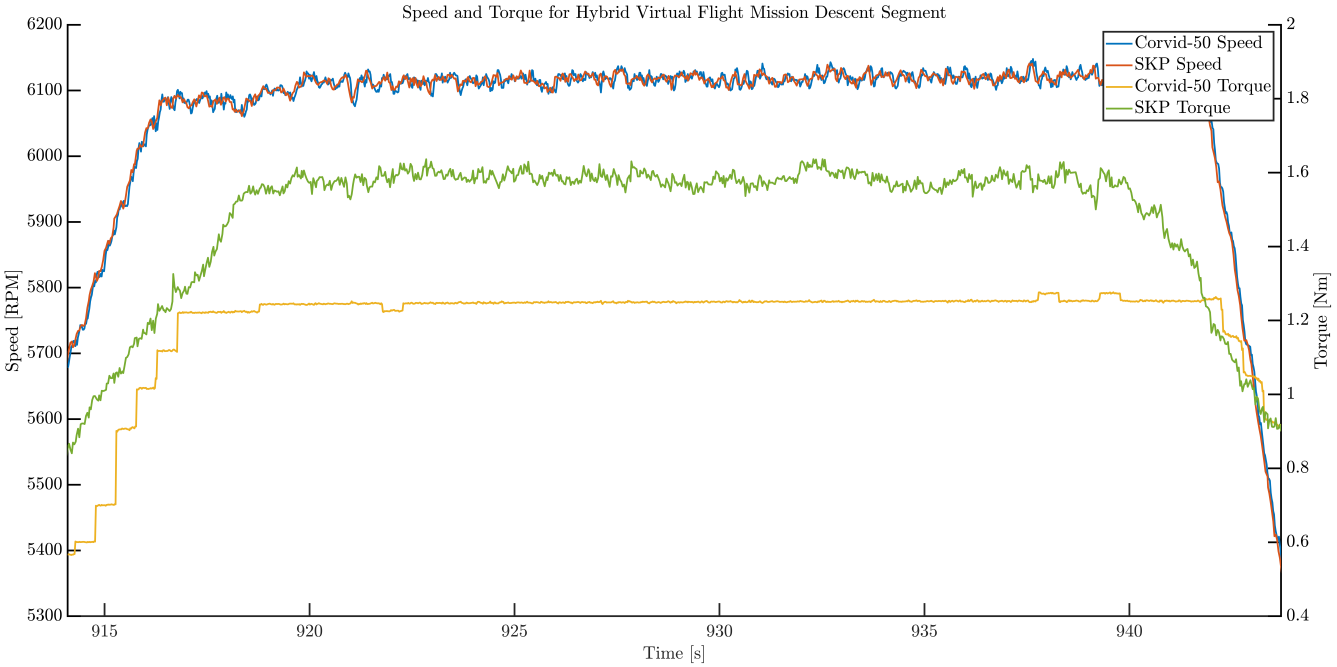

Figure 131: Experimental speed and torque in hybrid descent segment

8.2 Simulation Results

8.2.1 Mode 1 Test

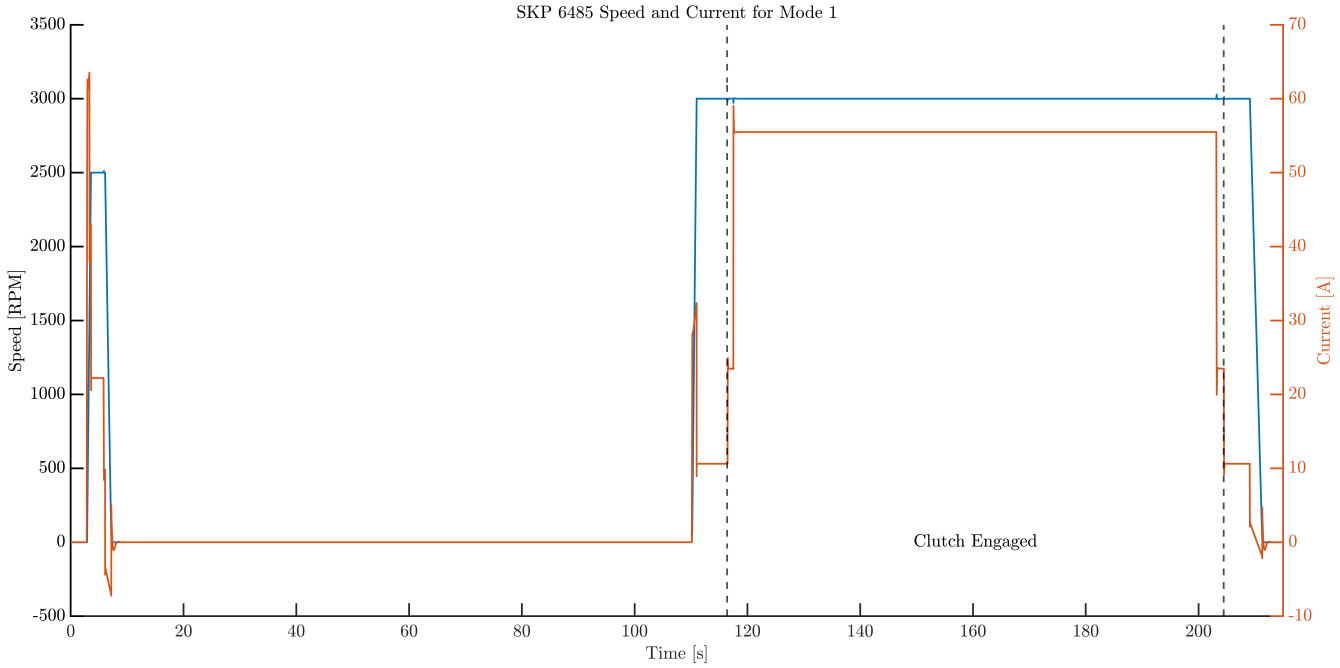

Figure 132: Simulated SKP speed and current in Mode 1 30A test

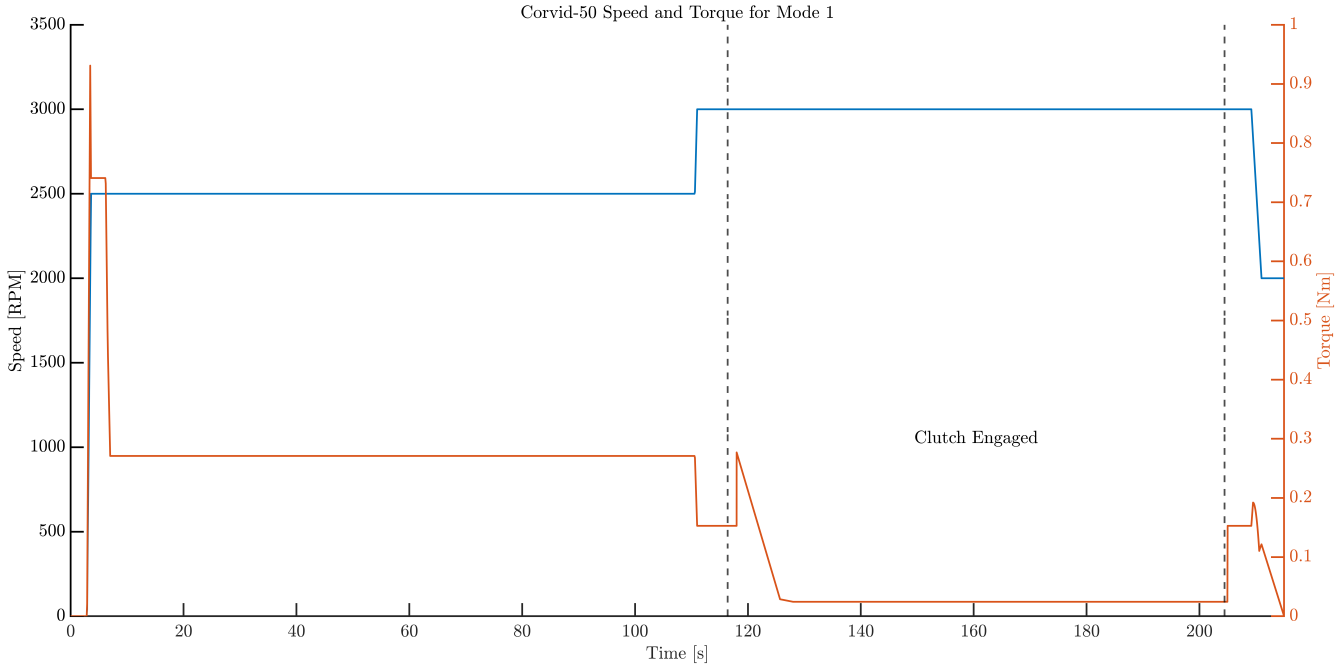

Figure 133: Simulated Corvid-50 speed and torque in Mode 1 30A test

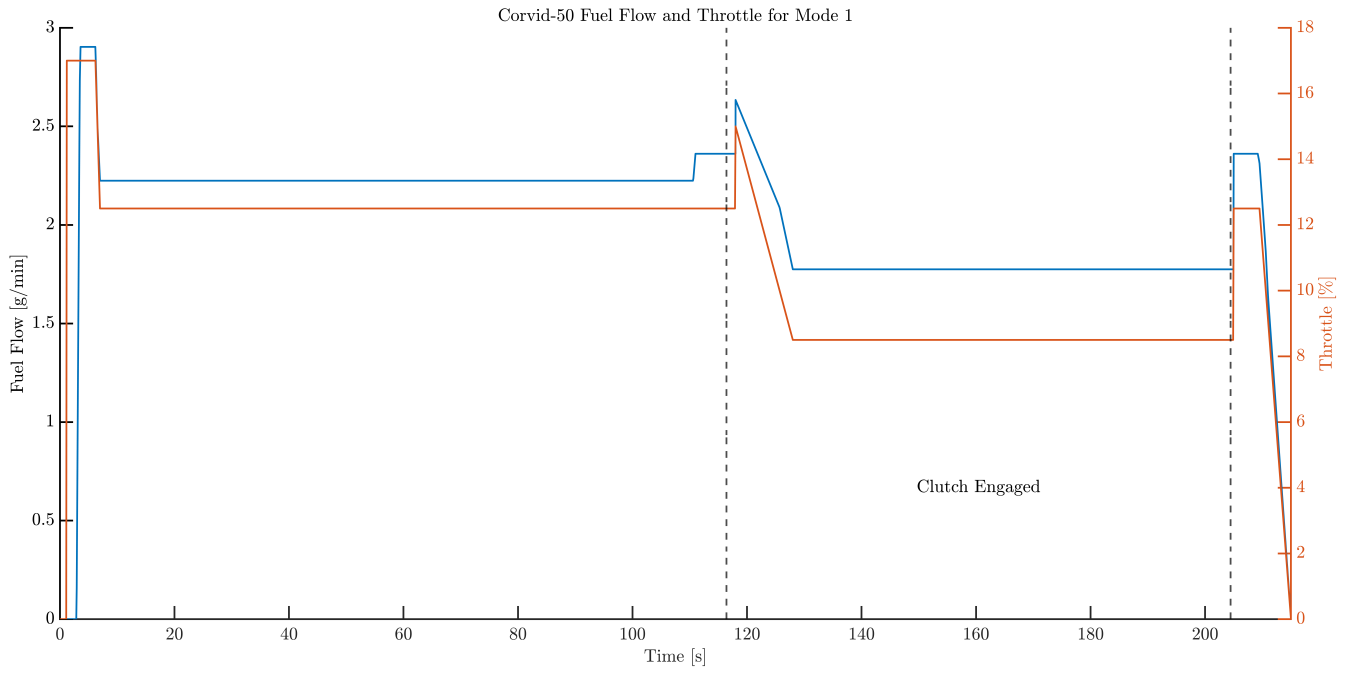

Figure 134: Simulated fuel and throttle in Mode 1 30A test

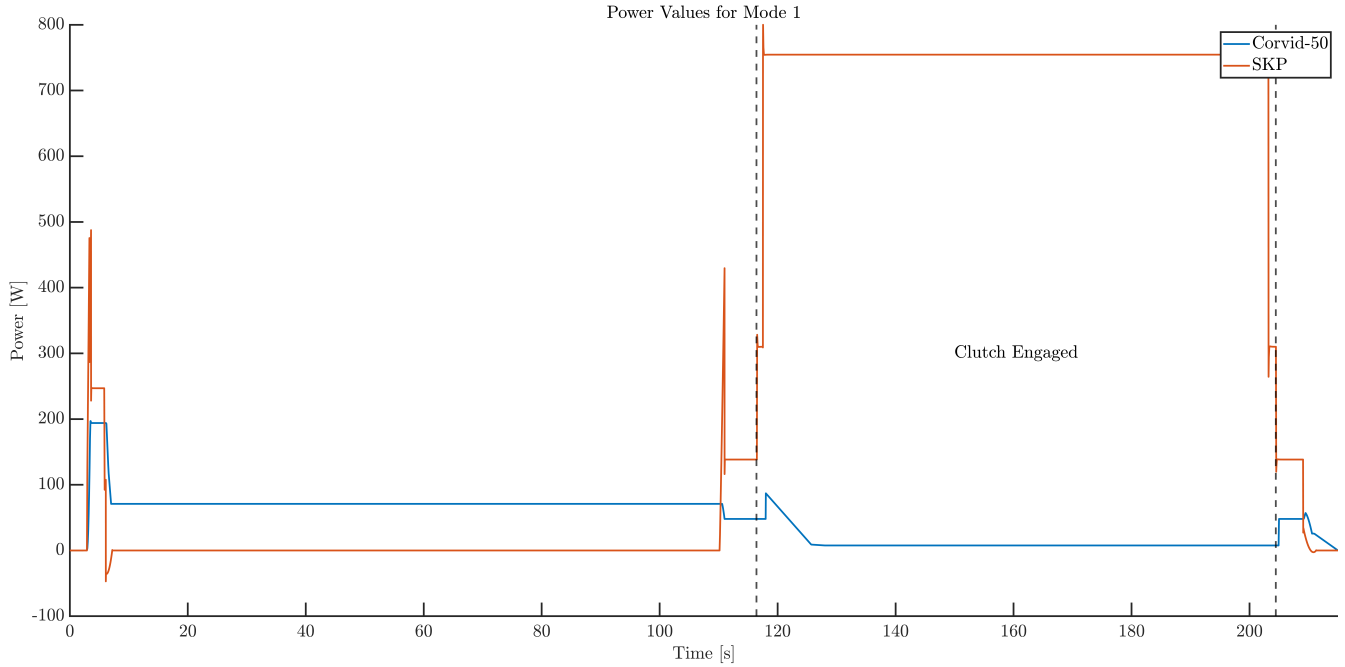

Figure 135: Simulated power values in Mode 1 30A test

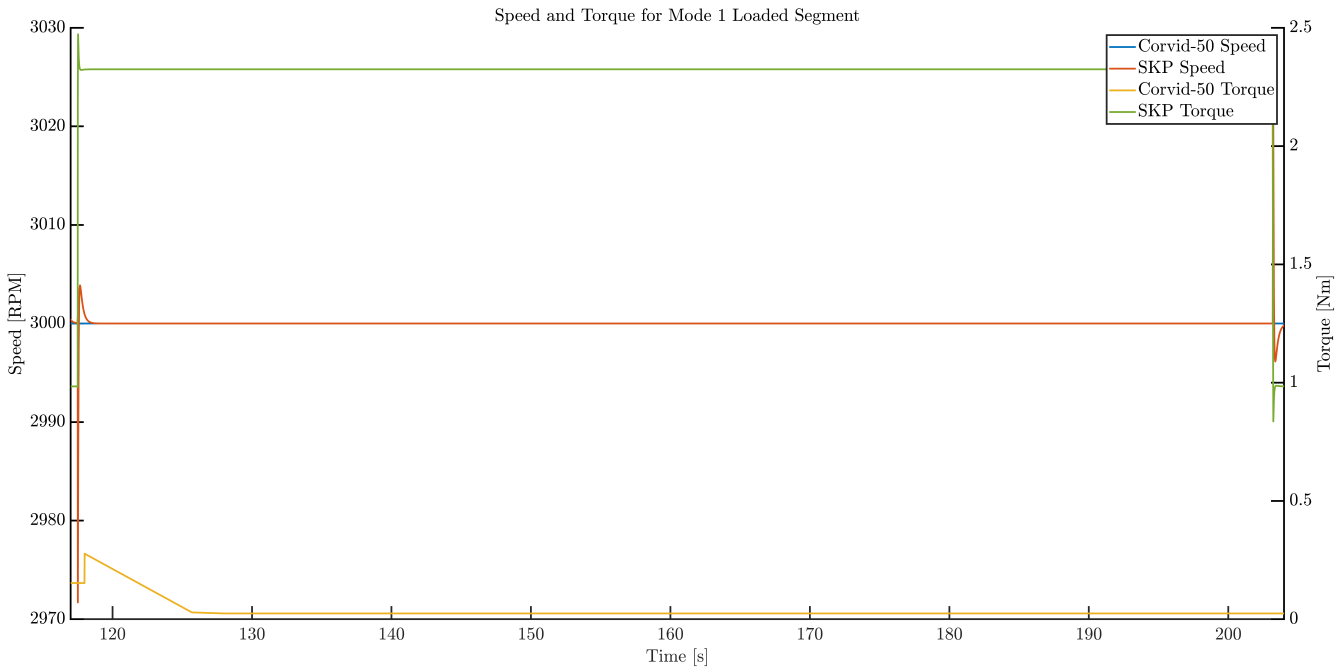

Figure 136: Simulated speed and torque in loaded segment of Mode 1 30A test

8.2.2 Mode 2 Test

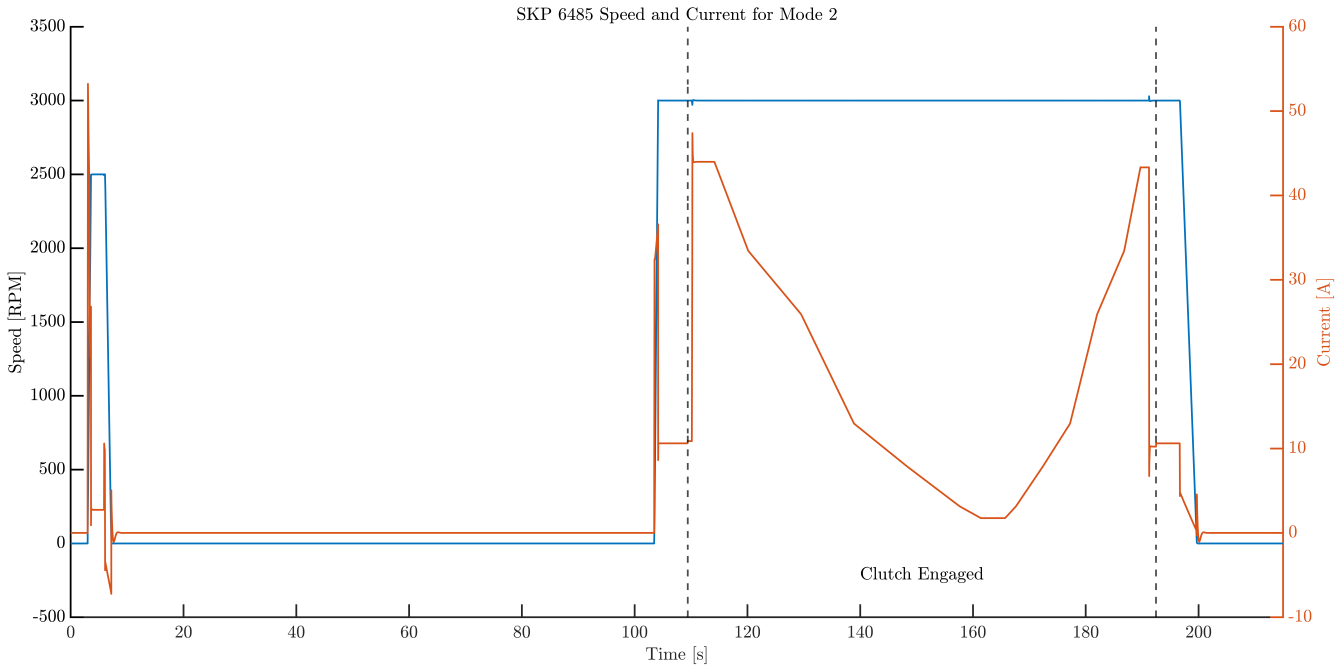

Figure 137: Simulated SKP speed and current in Mode 2 30A test

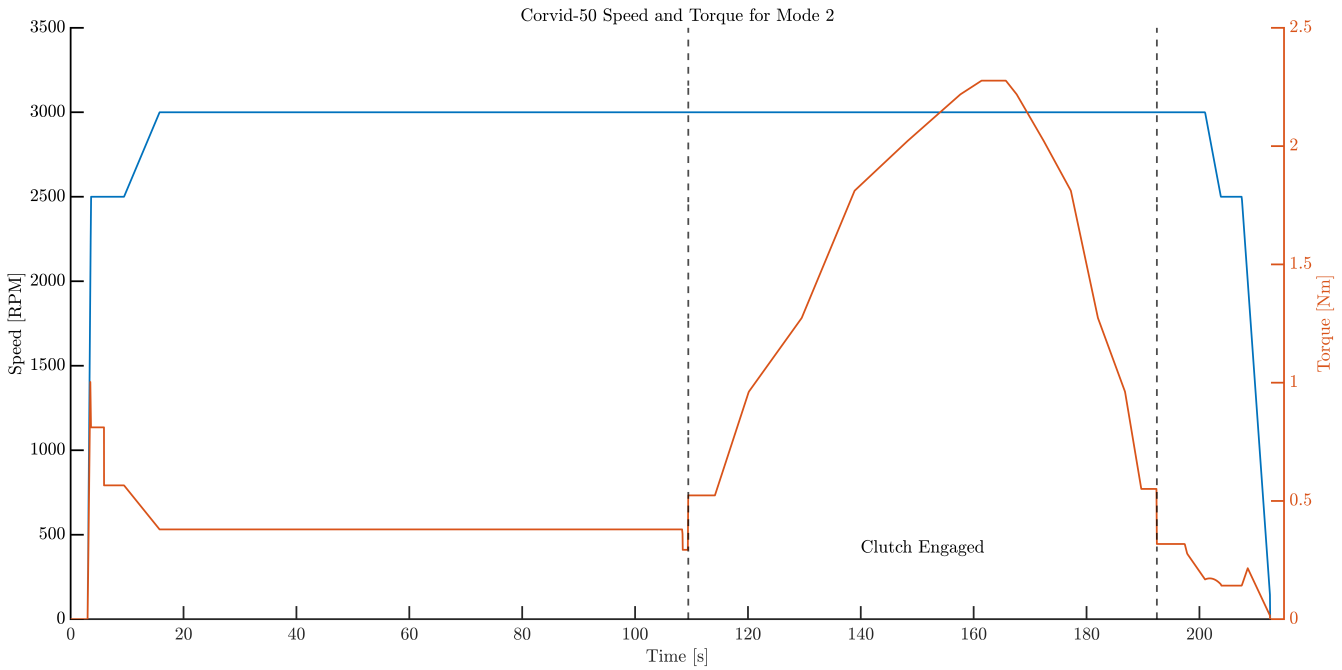

Figure 138: Simulated Corvid-50 speed and torque in Mode 2 30A test

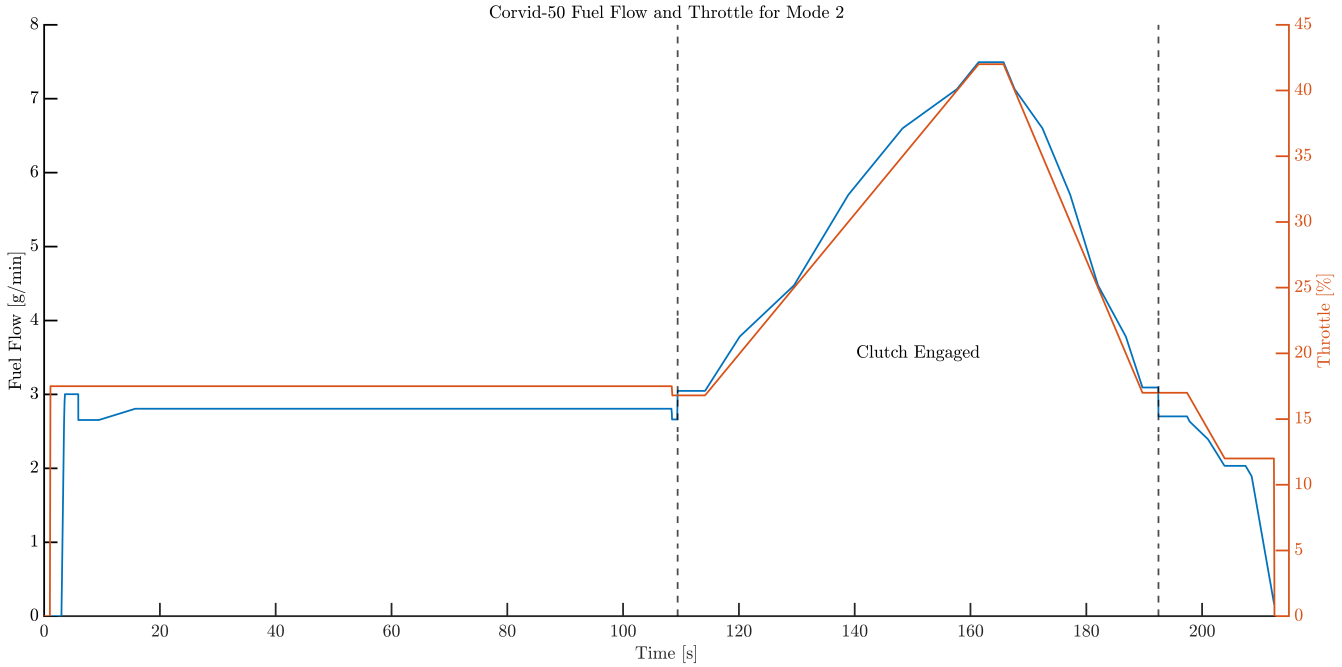

Figure 139: Simulated fuel and throttle in Mode 2 30A test

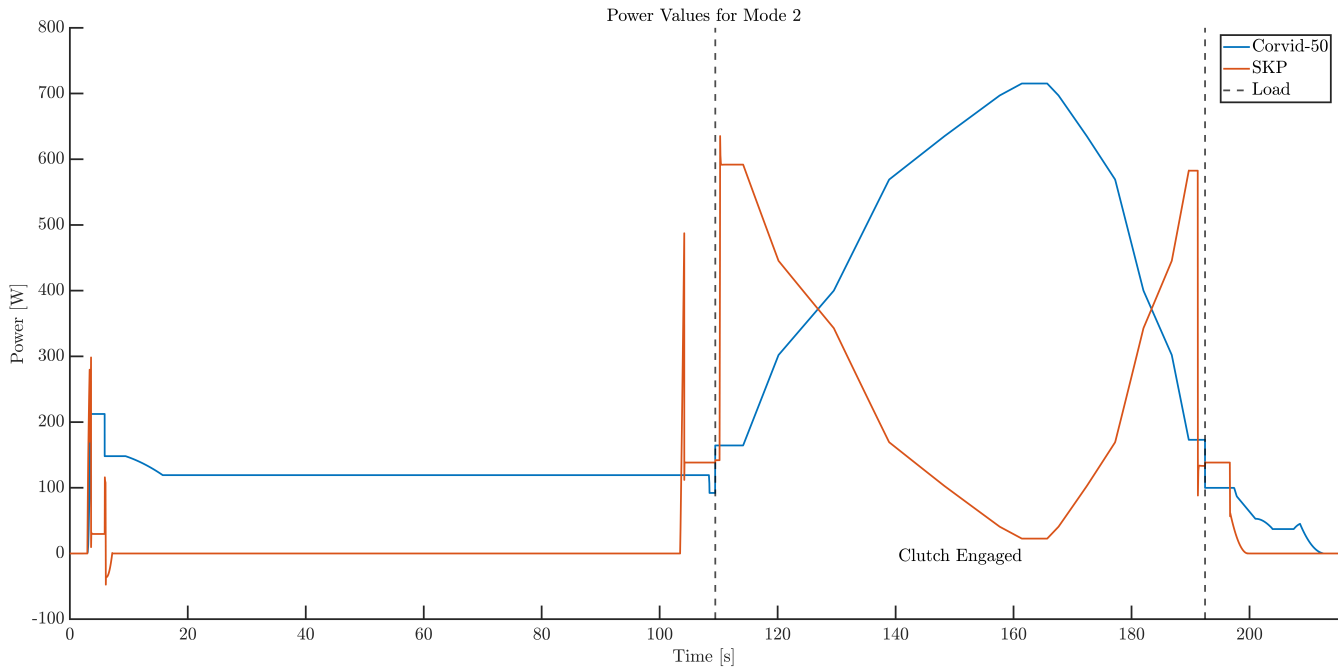

Figure 140: Simulated power values in Mode 2 30A test

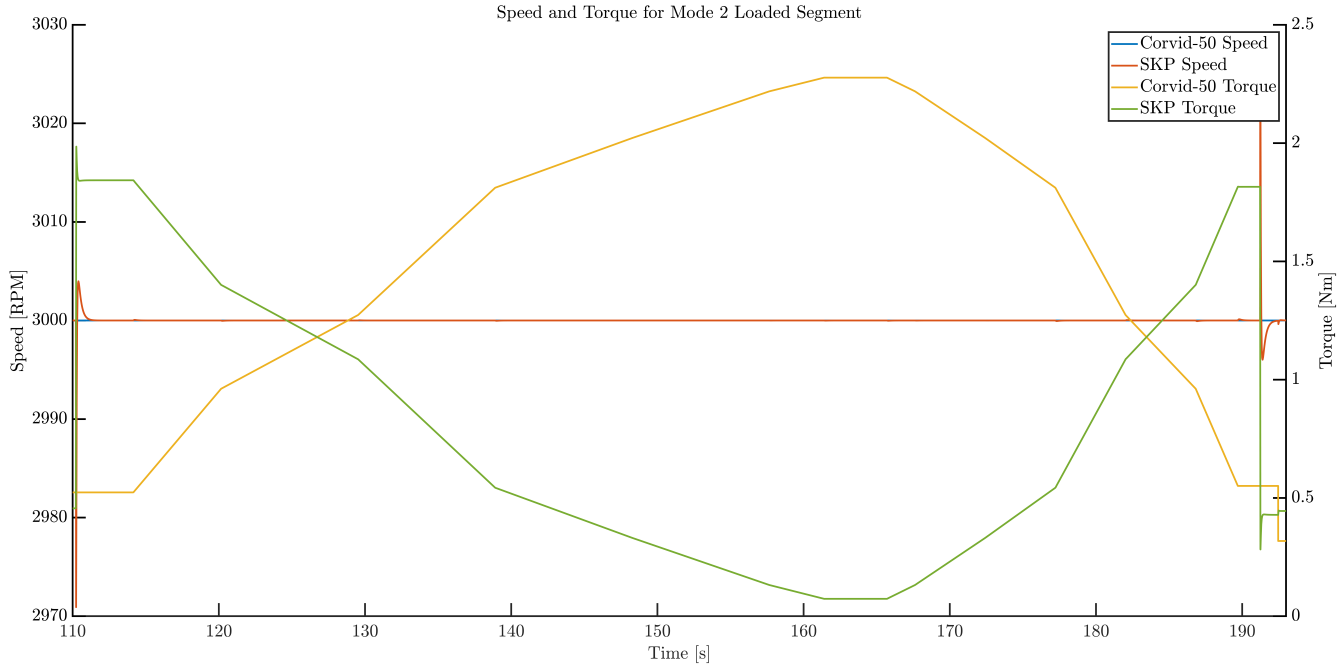

Figure 141: Simulated speed and torque in loaded segment of Mode 2 30A test

8.2.3 Mode 3 Test

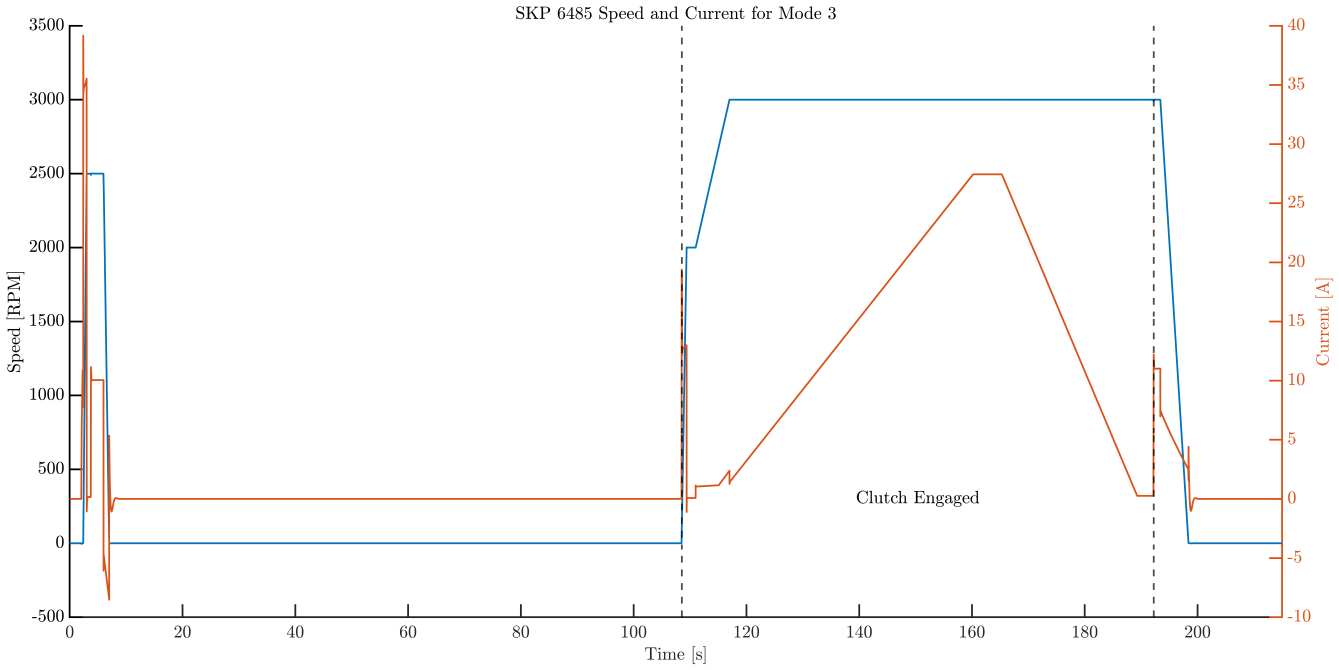

Figure 142: Simulated SKP speed and current in Mode 3 30A test

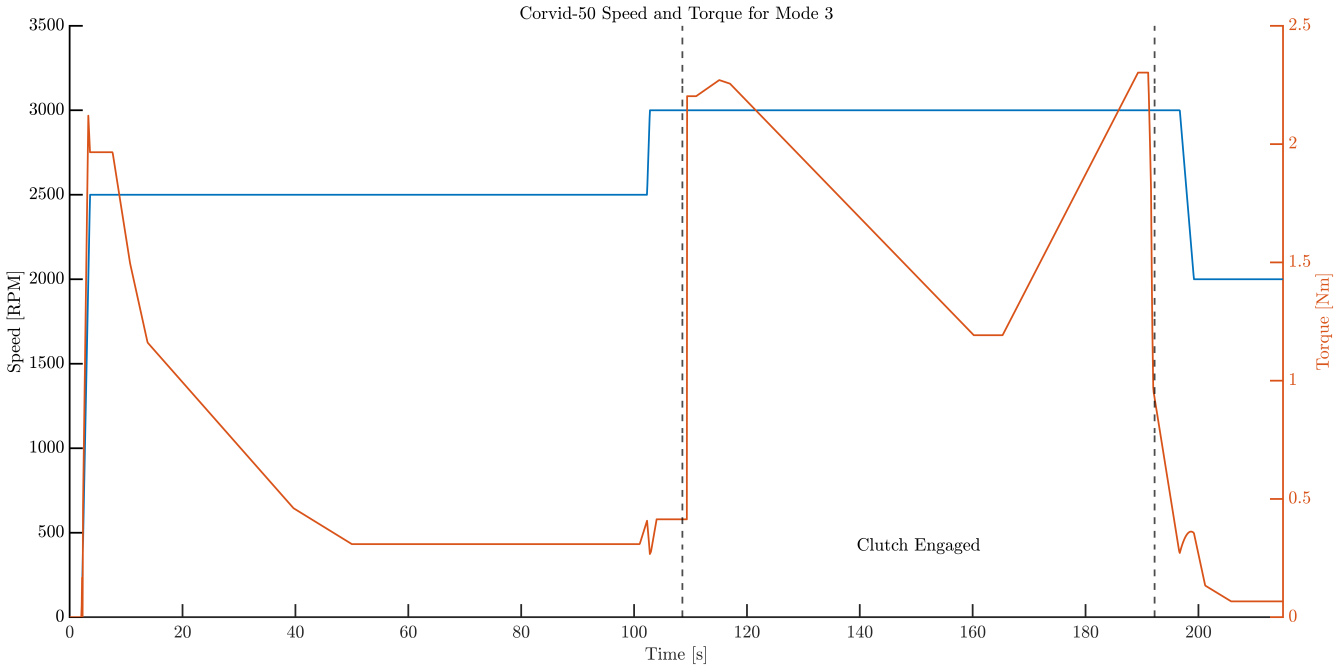

Figure 143: Simulated Corvid-50 speed and torque in Mode 3 30A test

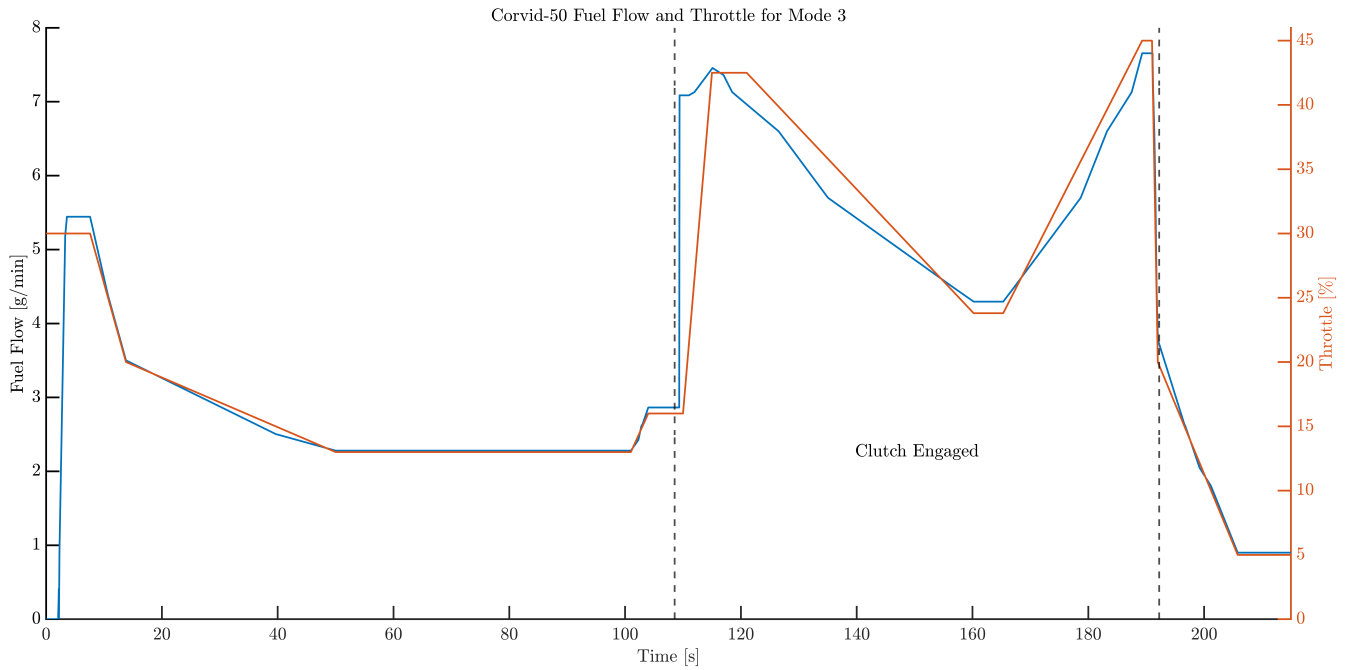

Figure 144: Simulated fuel and throttle in Mode 3 30A test

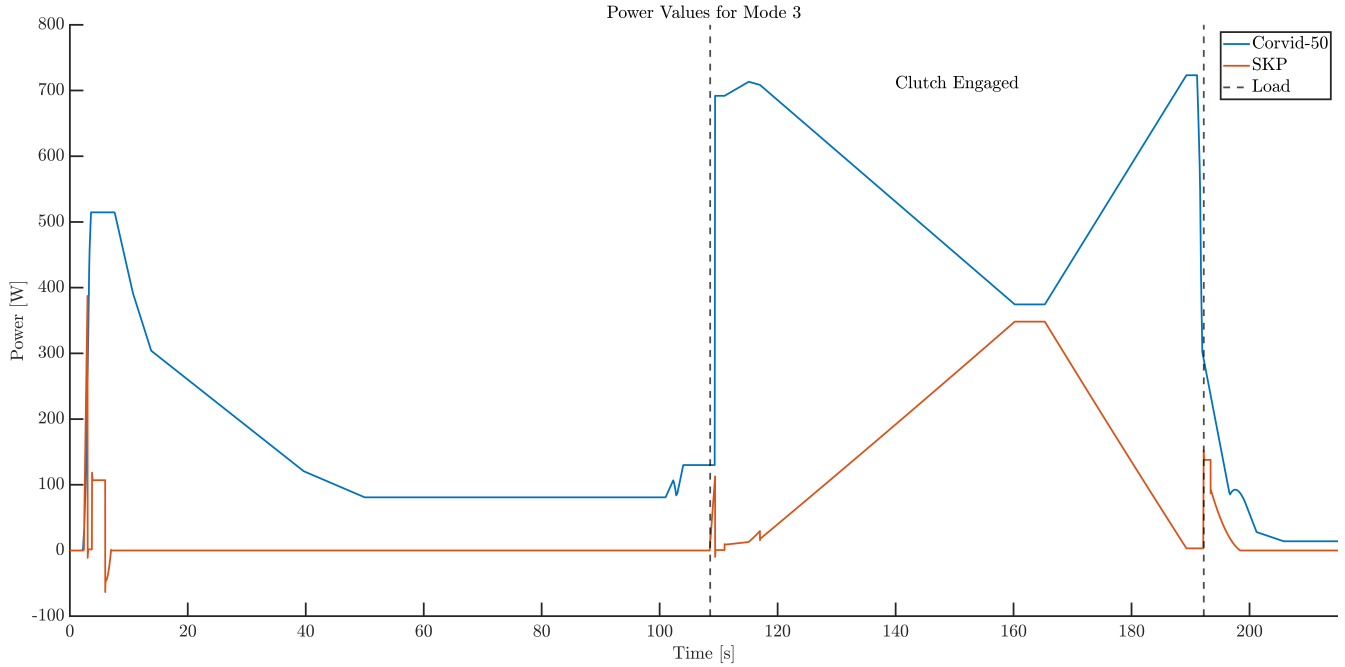

Figure 145: Simulated power values in Mode 3 30A test

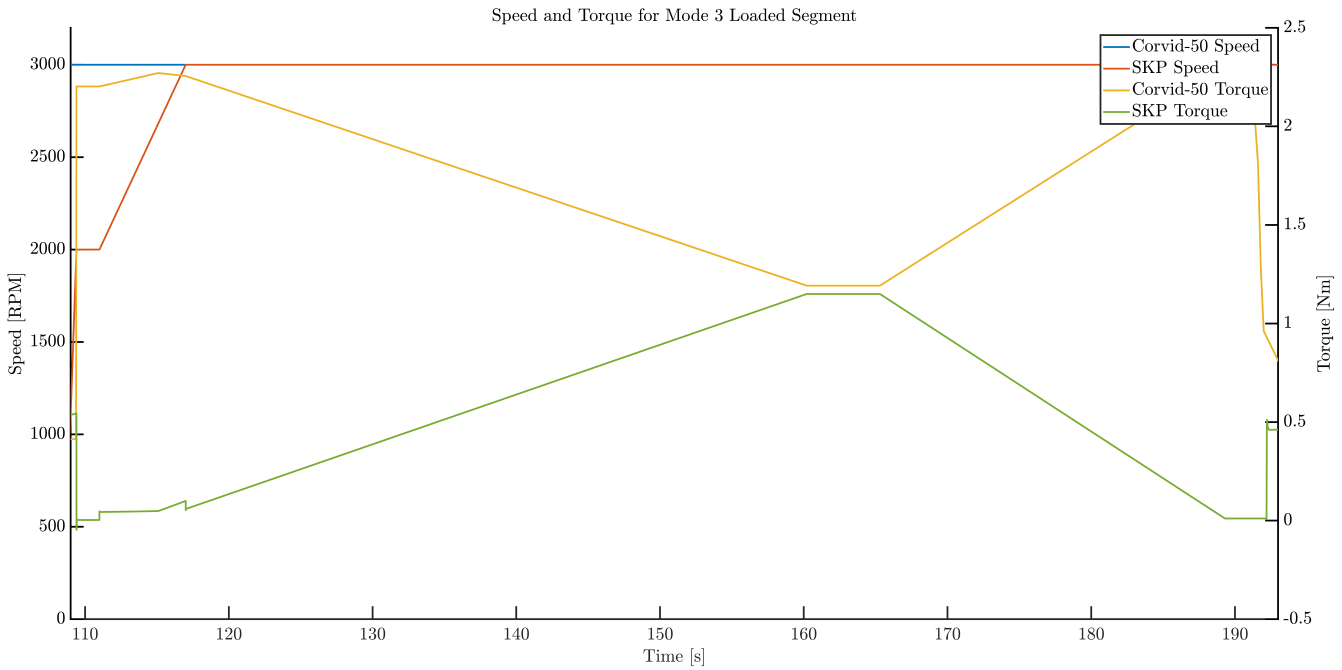

Figure 146: Simulated speed and torque in loaded segment of Mode 3 30A test

8.2.4 Electric Virtual Flight Mission

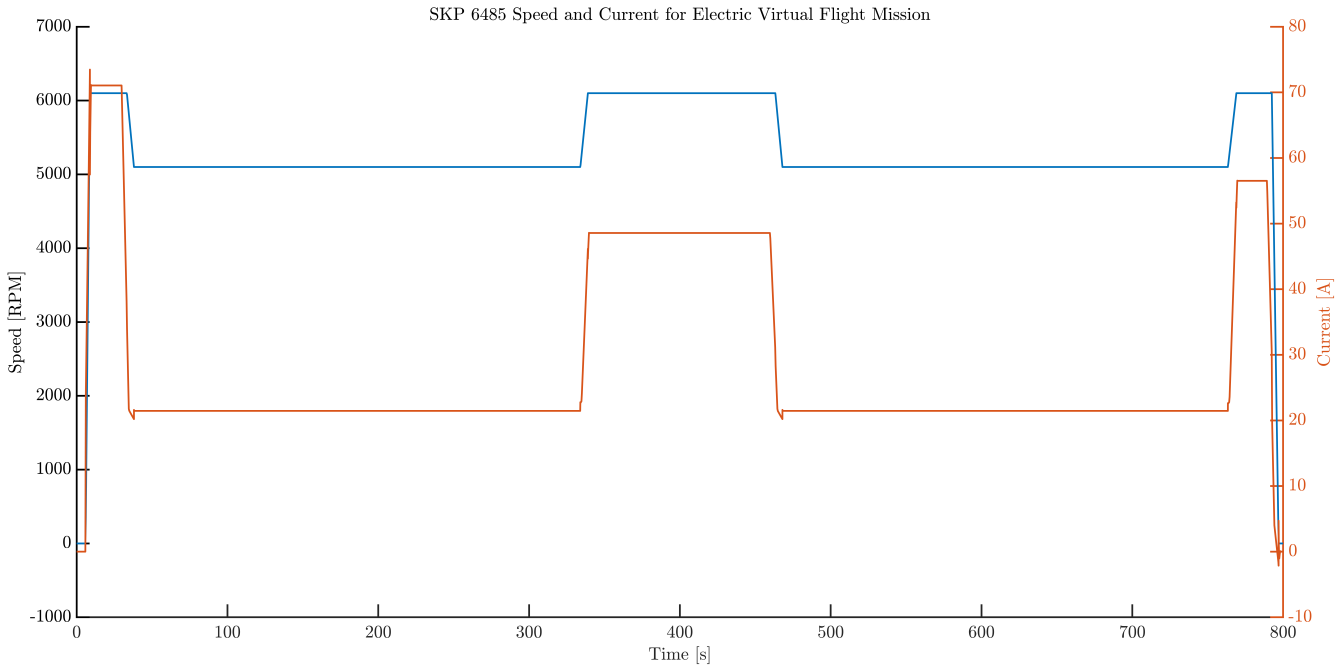

Figure 147: Simulated SKP speed and current in electric-only virtual flight mission

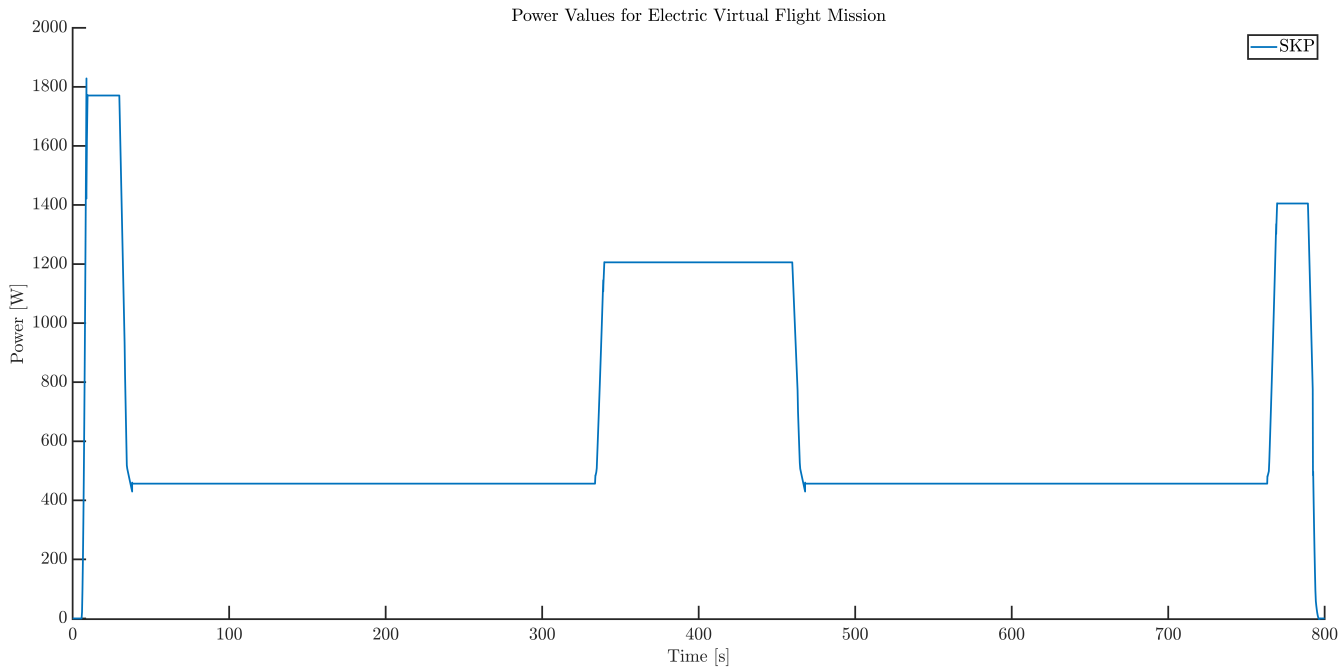

Figure 148: Simulated power values in electric-only virtual flight mission

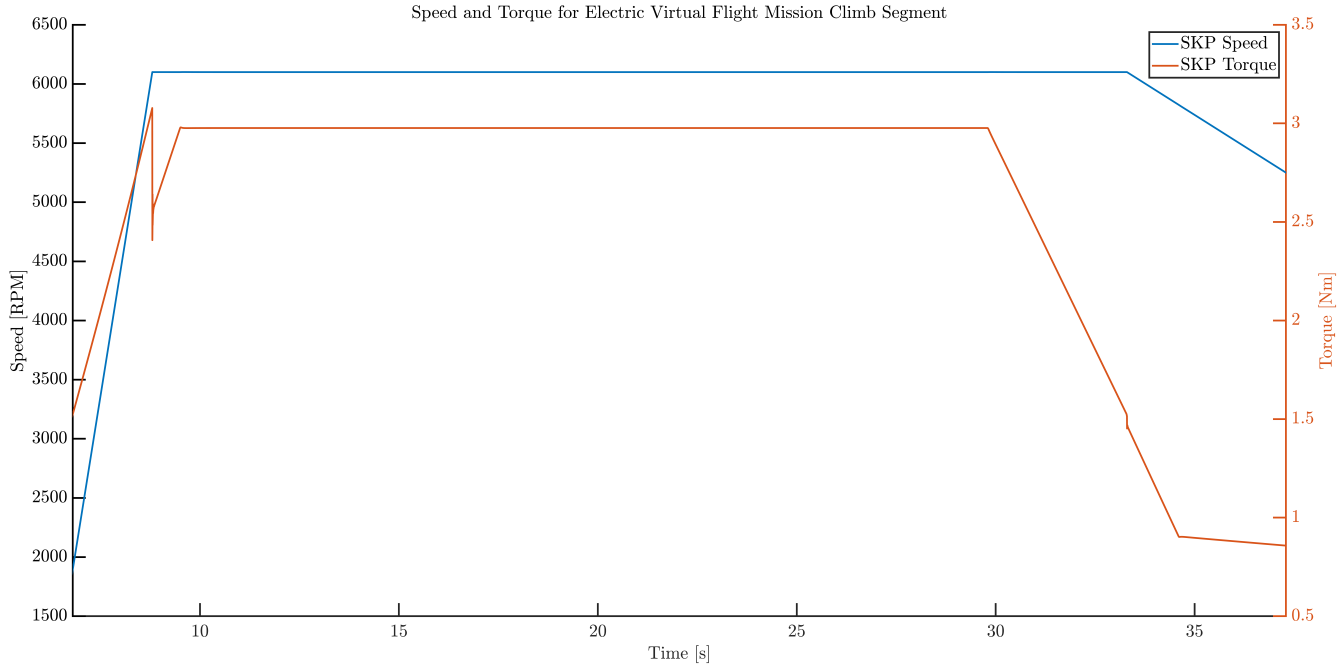

Figure 149: Simulated speed and torque in electric-only climb segment

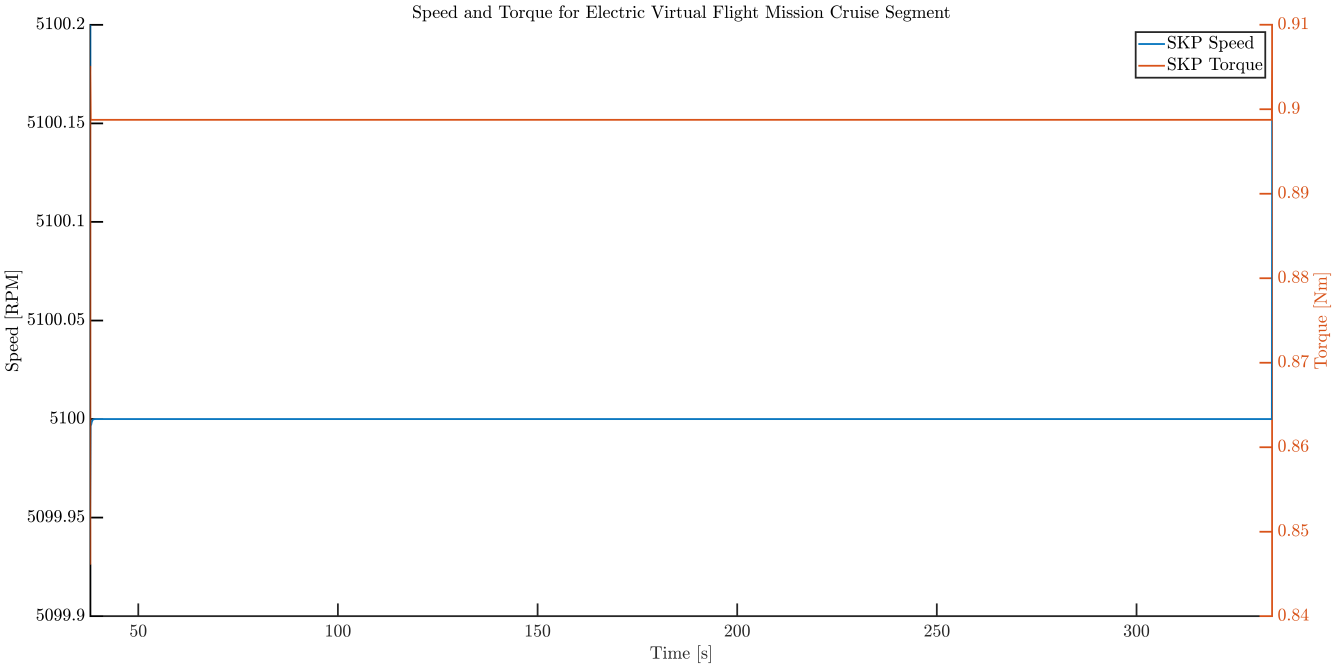

Figure 150: Simulated speed and torque in electric-only cruise segment

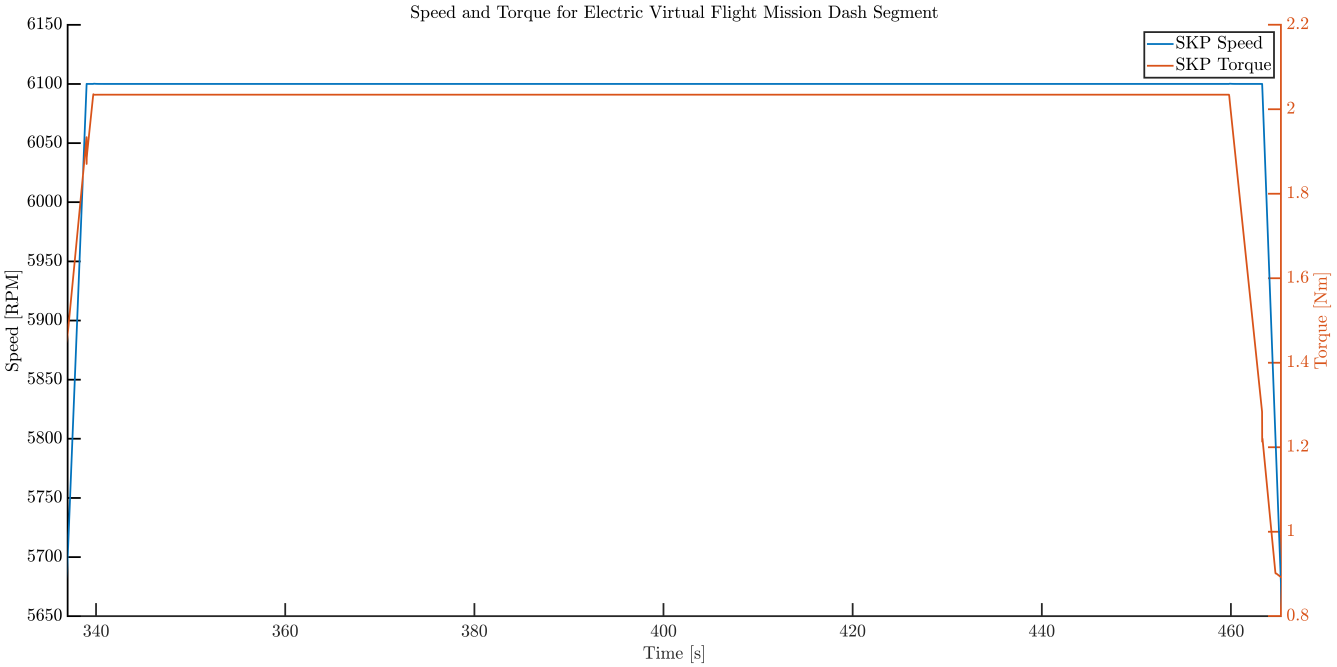

Figure 151: Simulated speed and torque in electric-only dash segment

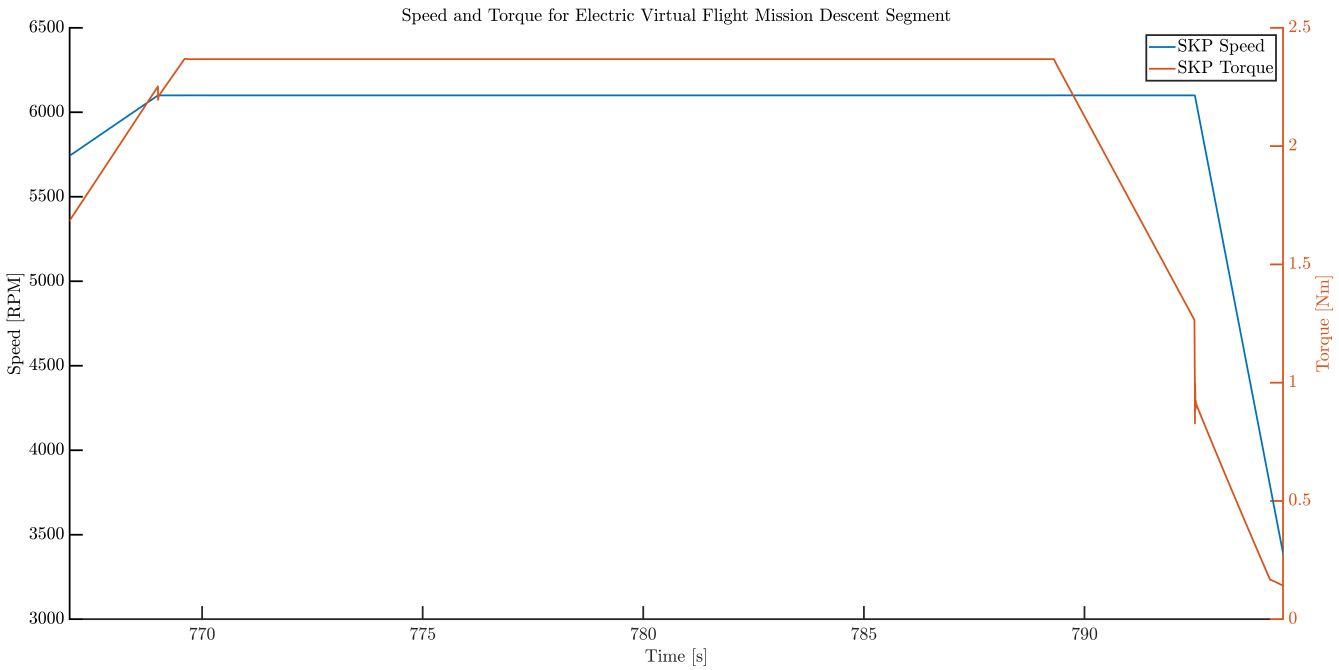

Figure 152: Simulated speed and torque in electric-only descent segment

8.2.5 Combustion Virtual Flight Mission

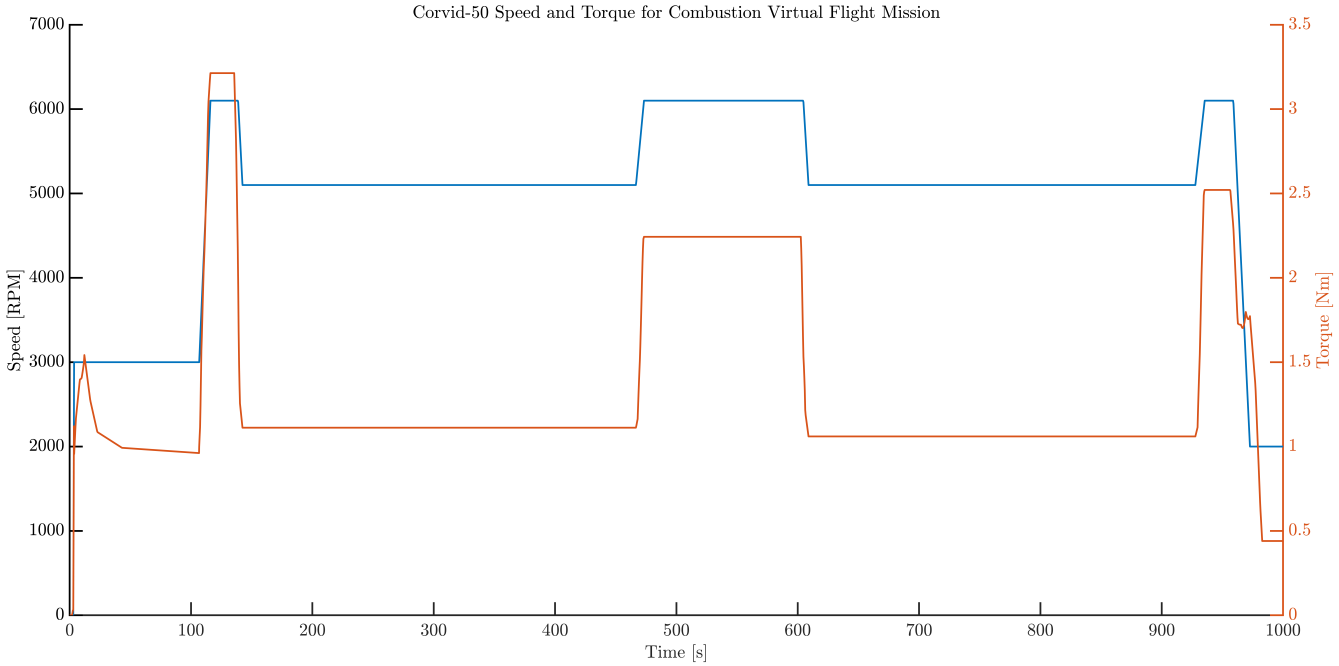

Figure 153: Simulated Corvid-50 speed and torque in combustion-only virtual flight mission

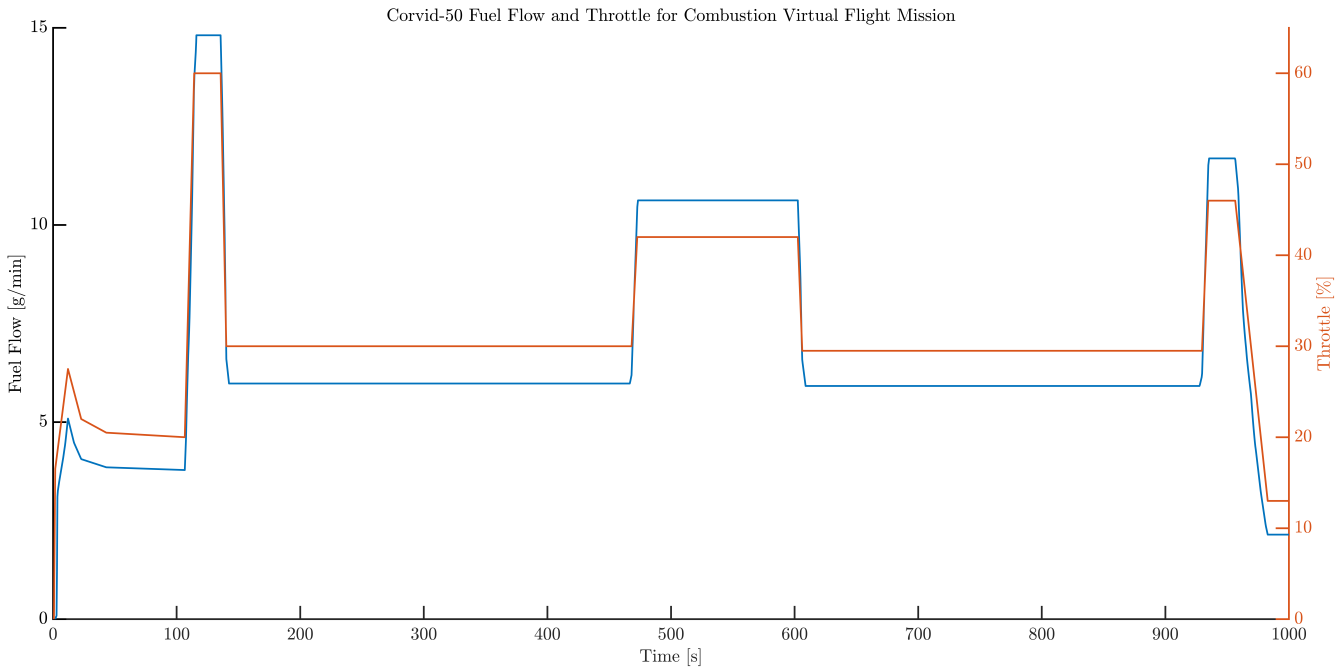

Figure 154: Simulated fuel and throttle in combustion-only virtual flight mission

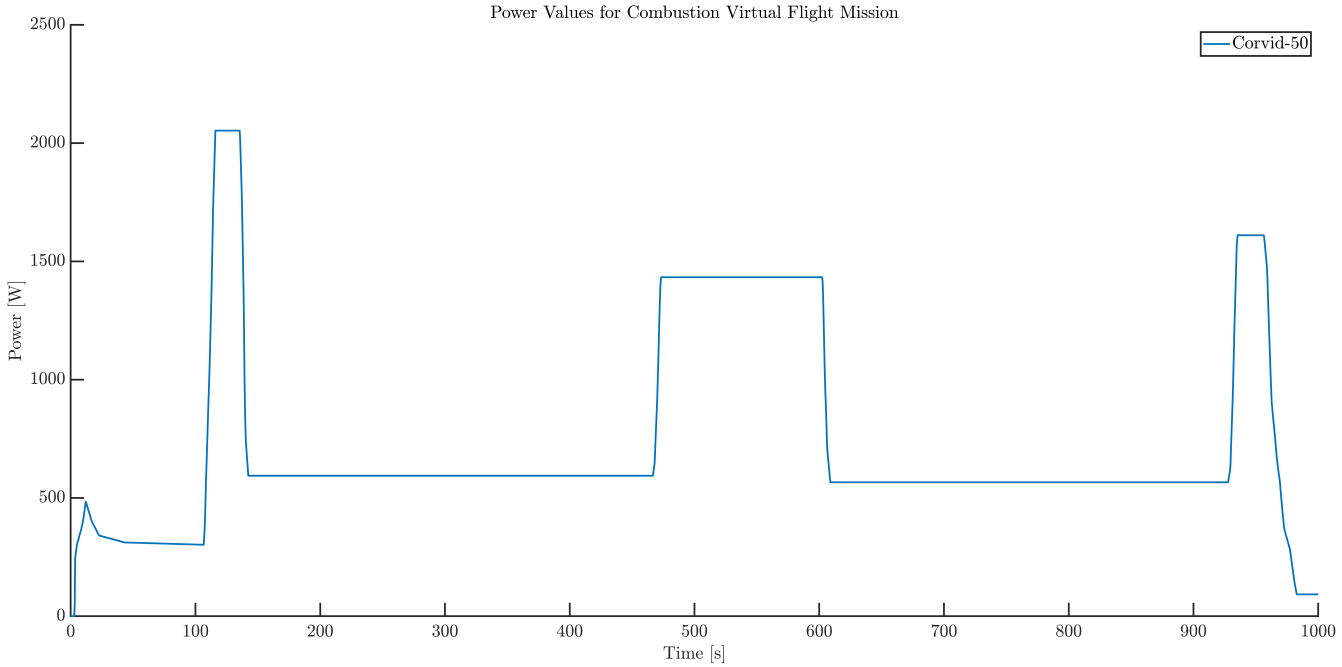

Figure 155: Simulated power values in combustion-only virtual flight mission

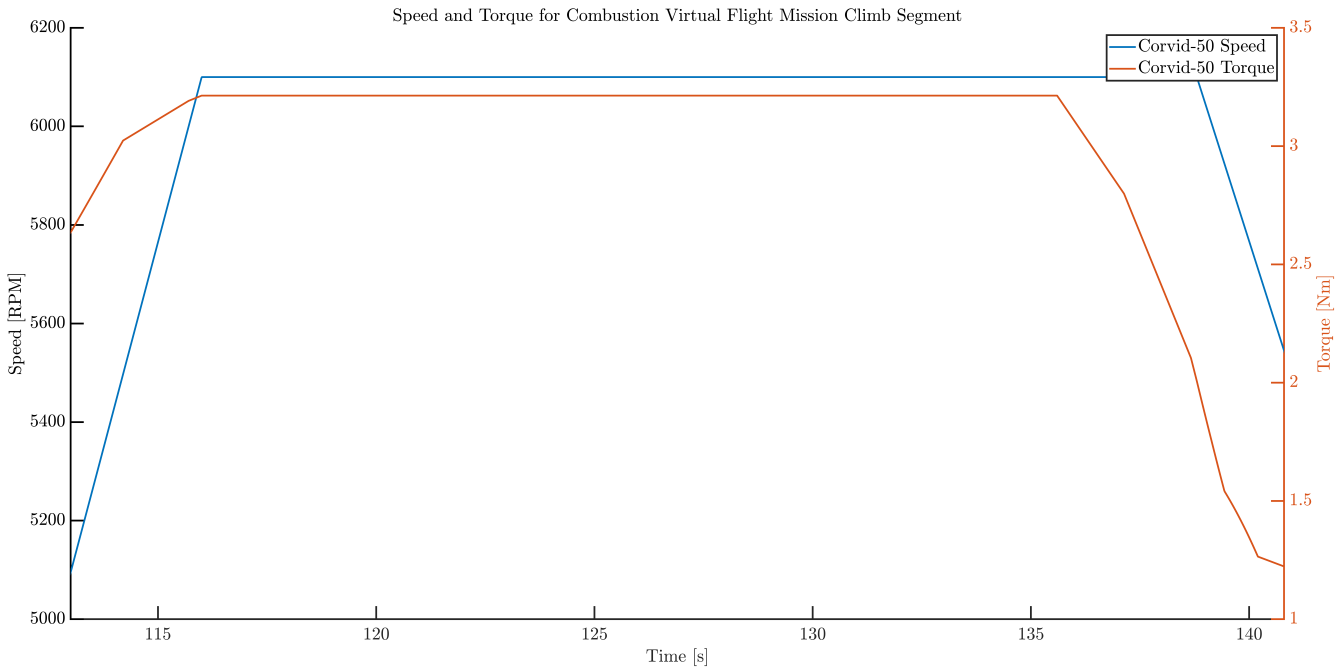

Figure 156: Simulated speed and torque in combustion-only climb segment

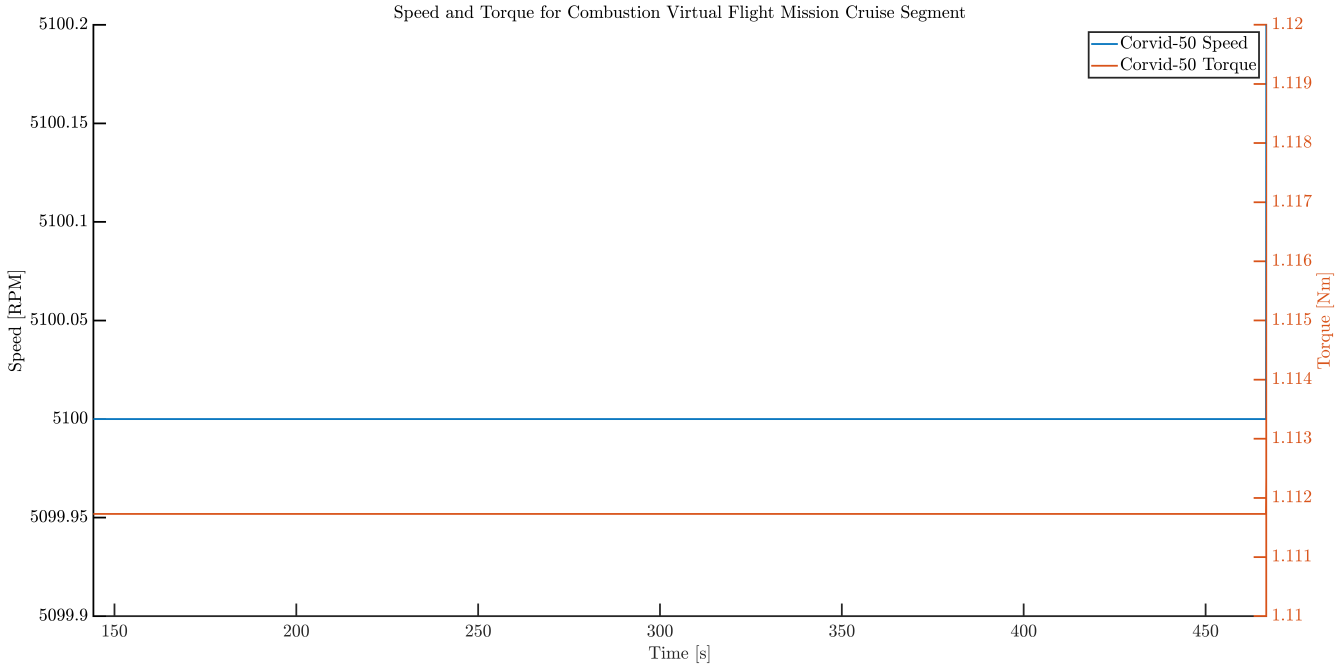

Figure 157: Simulated speed and torque in combustion-only cruise segment

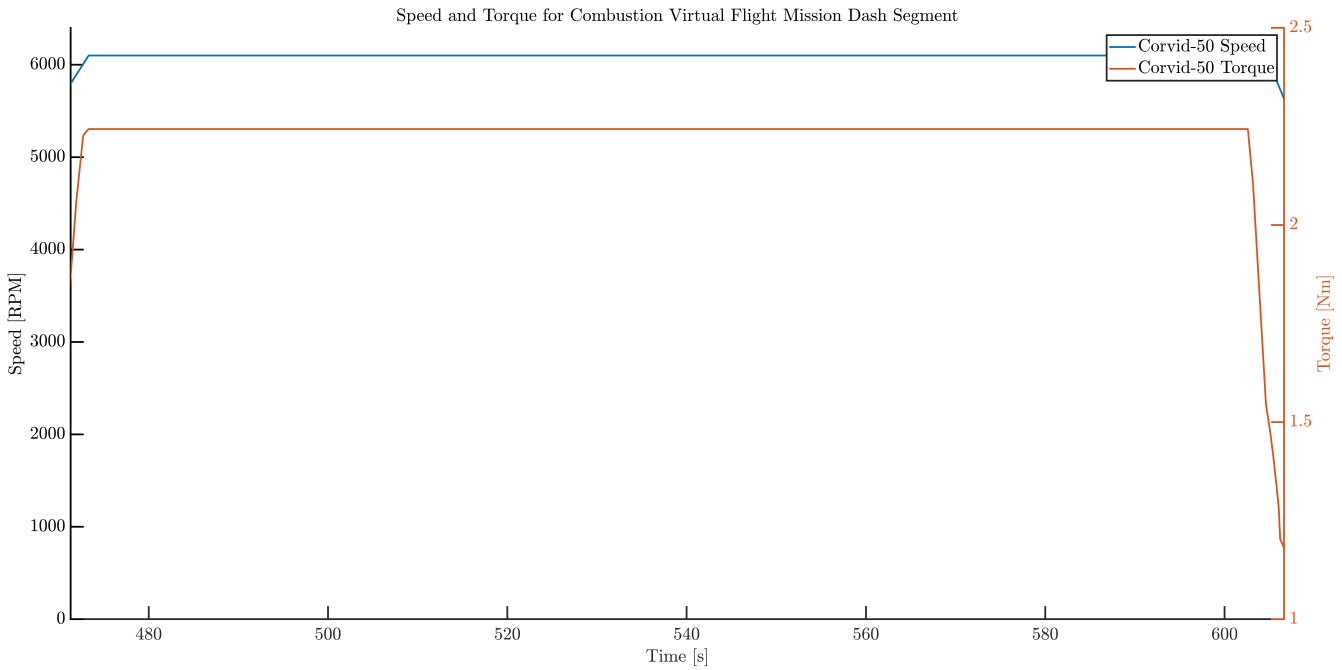

Figure 158: Simulated speed and torque in combustion-only dash segment

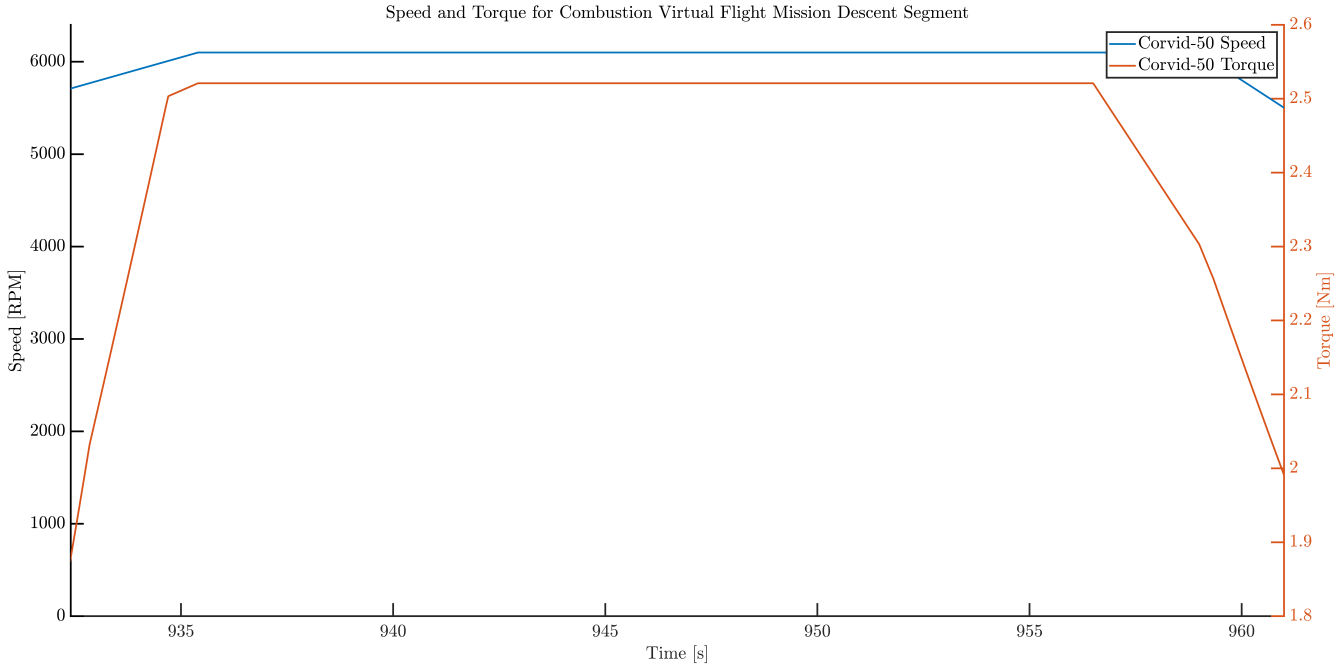

Figure 159: Simulated speed and torque in combustion-only descent segment

8.2.6 Hybrid Virtual Flight Mission

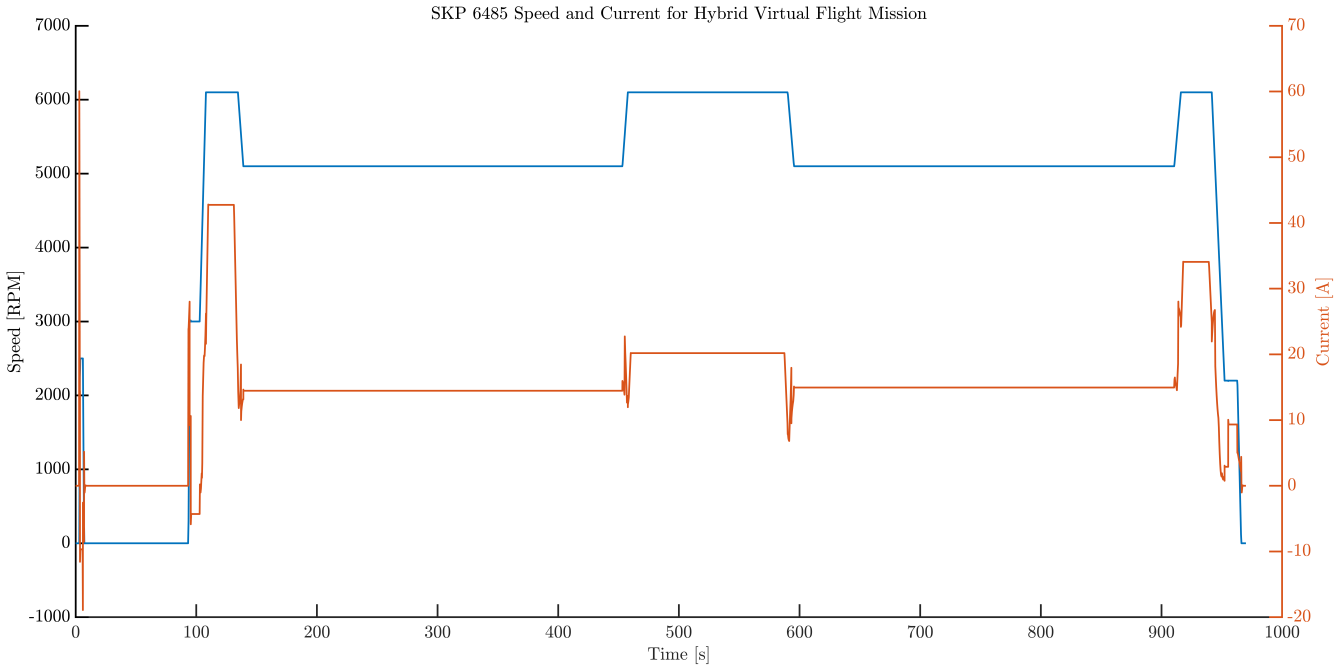

Figure 160: Simulated SKP speed and current in hybrid virtual flight mission

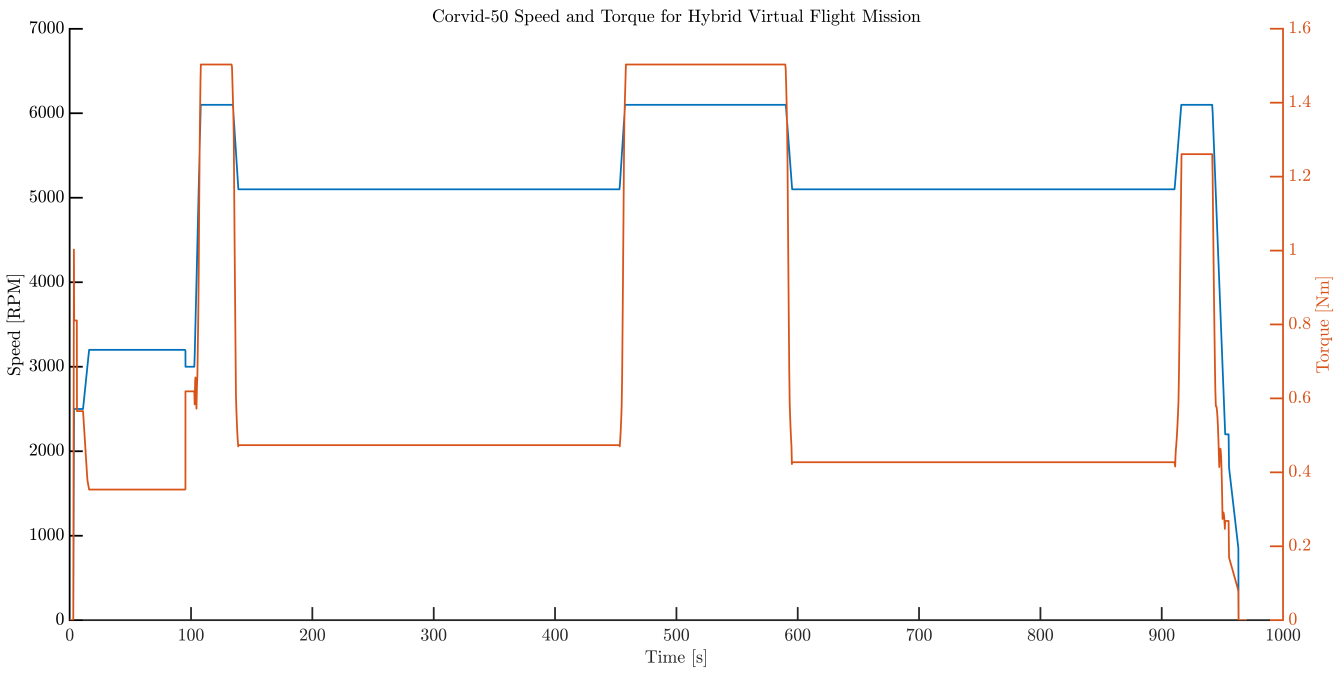

Figure 161: Simulated Corvid-50 speed and torque in hybrid virtual flight mission

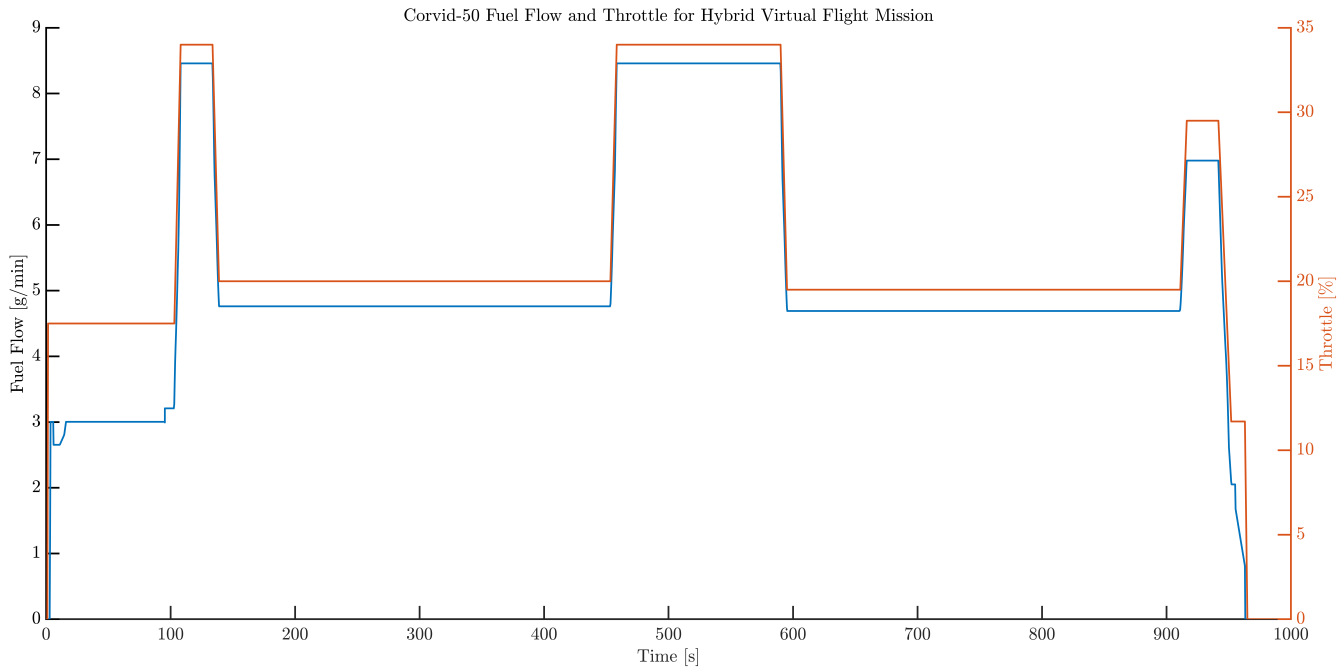

Figure 162: Simulated fuel and throttle in hybrid virtual flight mission

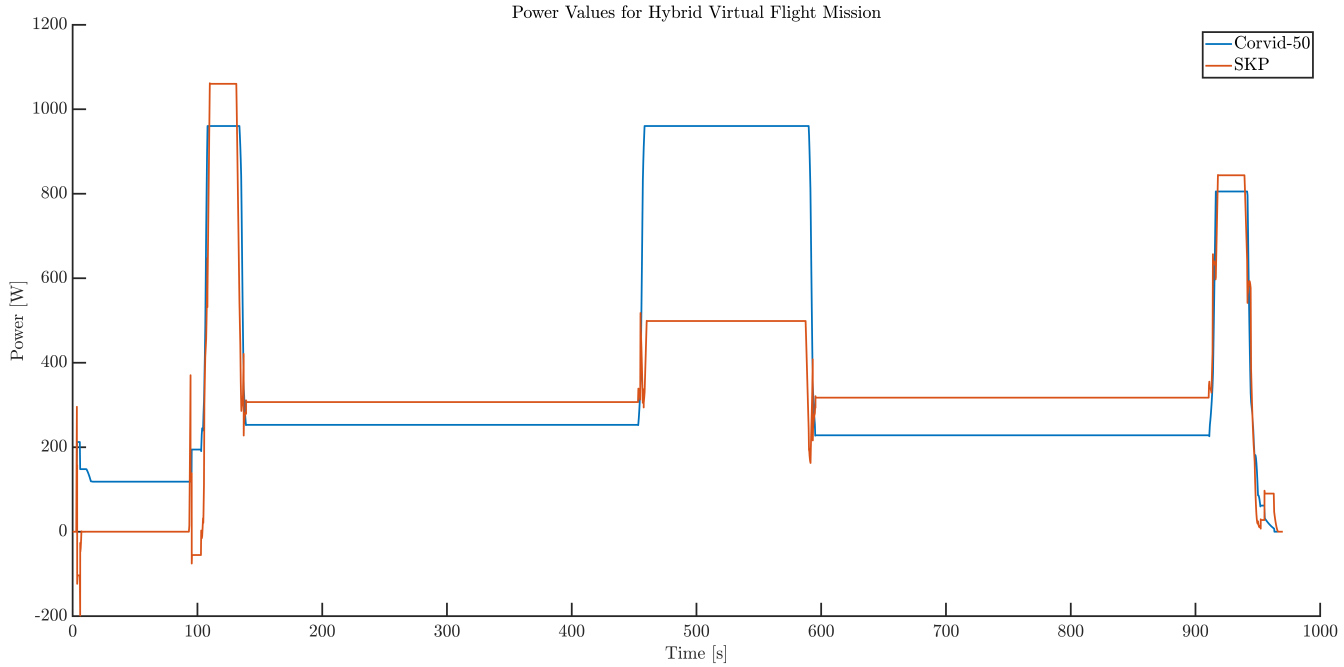

Figure 163: Simulated power values in hybrid virtual flight mission

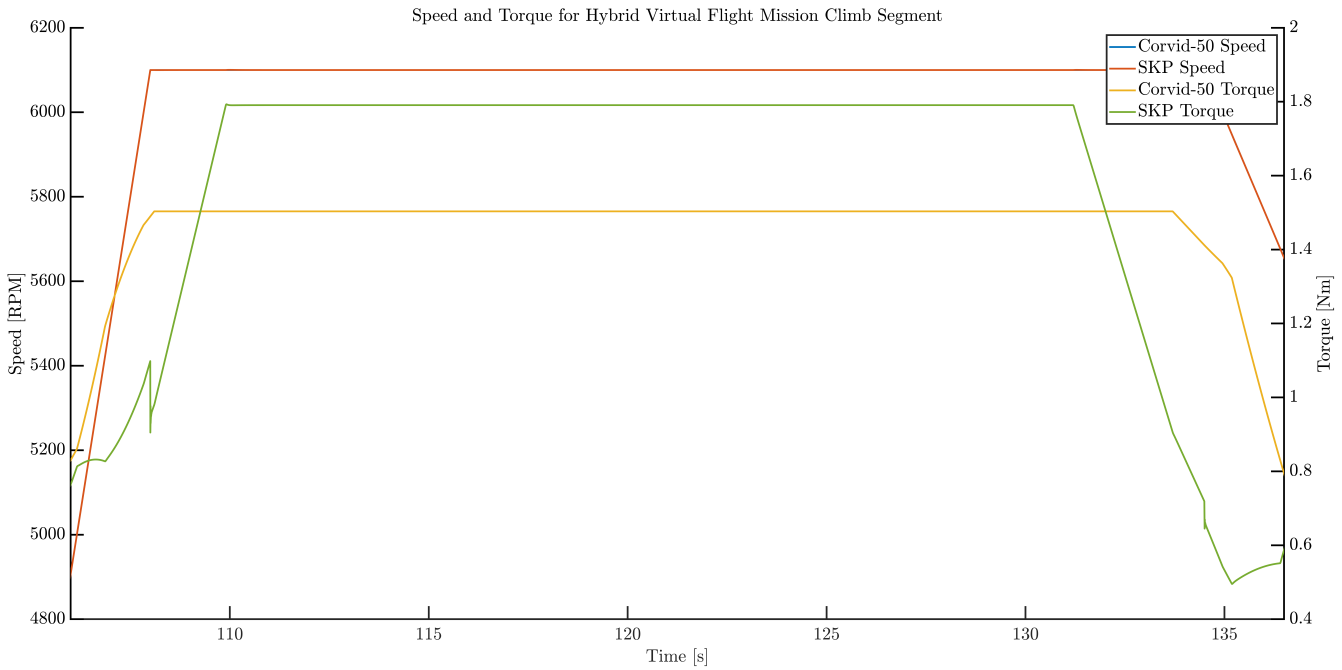

Figure 164: Simulated speed and torque in hybrid climb segment

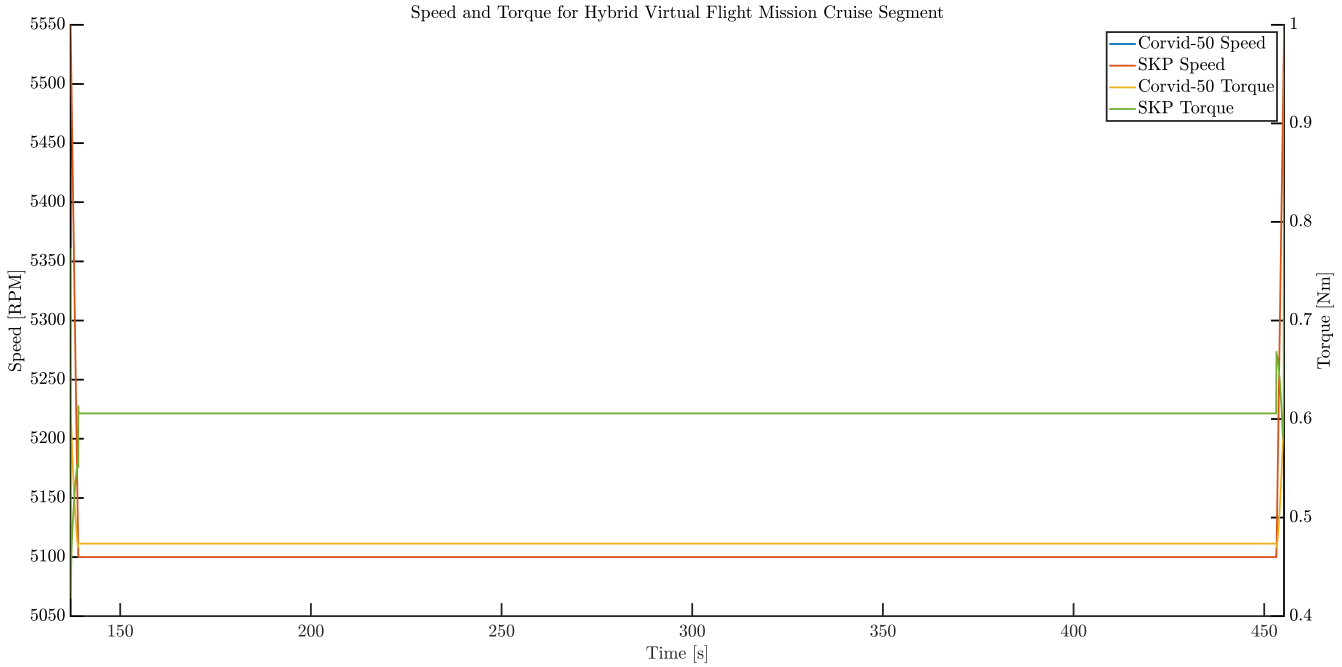

Figure 165: Simulated speed and torque in hybrid cruise segment

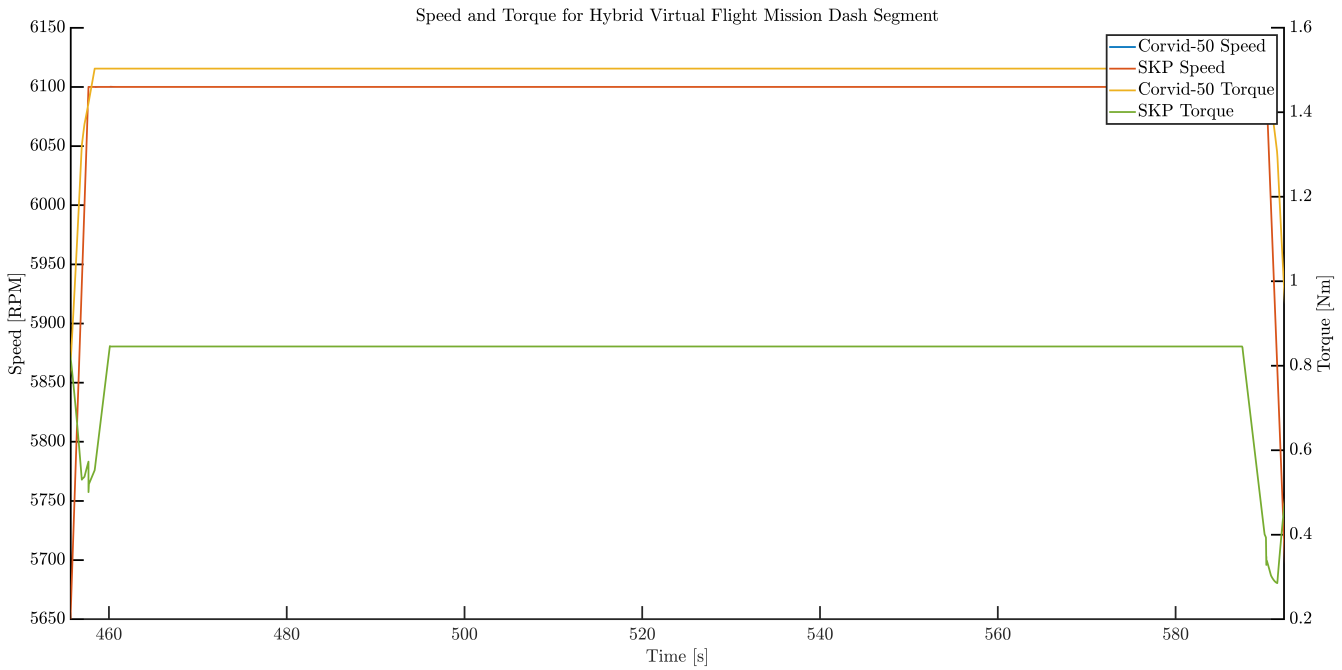

Figure 166: Simulated speed and torque in hybrid dash segment

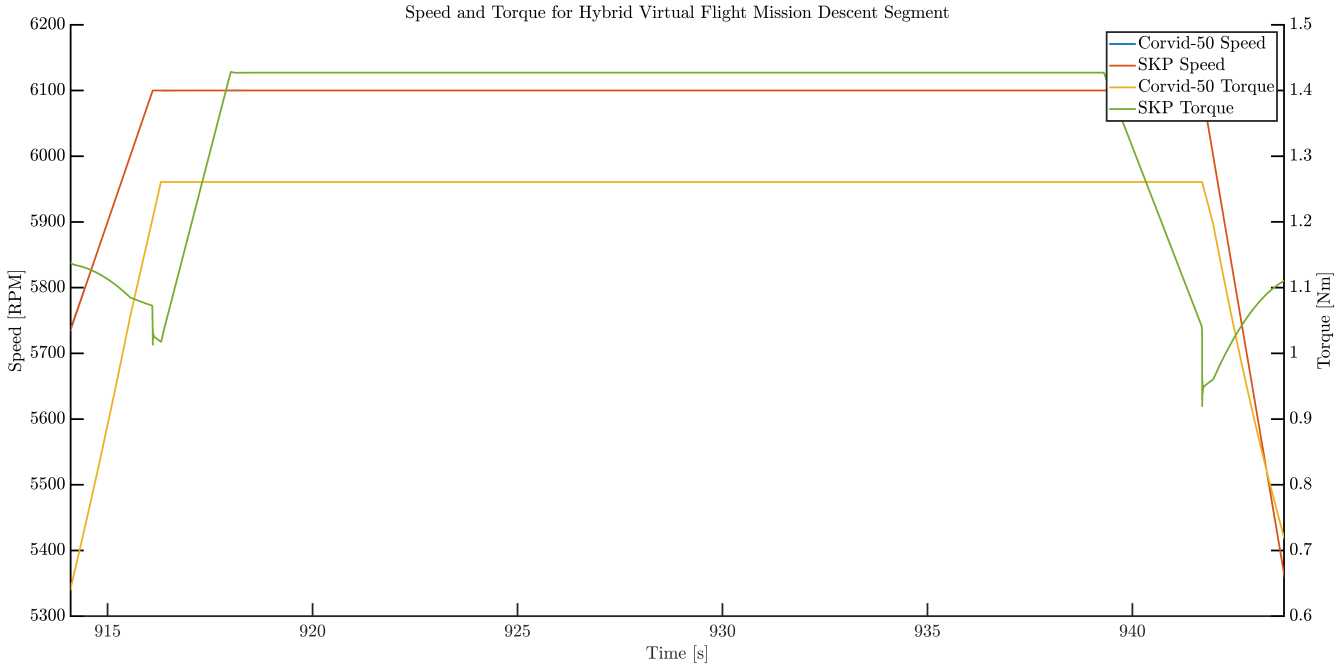

Figure 167: Simulated speed and torque in hybrid descent segment